

**CARDIFF  
UNIVERSITY**

**PRIFYSGOL  
CAERDYDD**

**ELUCIDATING RYANODINE RECEPTOR DOMAIN  
INTERACTIONS IN SUDDEN CARDIAC DEATH:  
TOWARDS THE DEVELOPMENT OF NOVEL  
THERAPEUTIC STRATEGIES**

**Hala Jundi**

*A thesis submitted in candidature for the degree of  
Philosophiae Doctor*

2009

**Wales Heart Research Institute  
School of Medicine  
Cardiff University**



**CARDIFF  
UNIVERSITY**

**PRIFYSGOL  
CAERDYDD**

**ELUCIDATING RYANODINE RECEPTOR DOMAIN  
INTERACTIONS IN SUDDEN CARDIAC DEATH:  
TOWARDS THE DEVELOPMENT OF NOVEL  
THERAPEUTIC STRATEGIES**

**Hala Jundi**

*A thesis submitted in candidature for the degree of  
Philosophiae Doctor*

2009

**Wales Heart Research Institute  
School of Medicine  
Cardiff University**

UMI Number: U585495

All rights reserved

INFORMATION TO ALL USERS

The quality of this reproduction is dependent upon the quality of the copy submitted.

In the unlikely event that the author did not send a complete manuscript and there are missing pages, these will be noted. Also, if material had to be removed, a note will indicate the deletion.



UMI U585495

Published by ProQuest LLC 2013. Copyright in the Dissertation held by the Author.  
Microform Edition © ProQuest LLC.

All rights reserved. This work is protected against  
unauthorized copying under Title 17, United States Code.



ProQuest LLC  
789 East Eisenhower Parkway  
P.O. Box 1346  
Ann Arbor, MI 48106-1346

## DECLARATION

This work has not previously been accepted in substance for any degree and is not concurrently submitted in candidature for any degree.

Signed ..... *H. Dandi* ..... (candidate) Date ..... *20/5/09* .....

## STATEMENT 1

This thesis is being submitted in partial fulfilment of the requirements for the degree of Philosophiae Doctor

Signed ..... *H. Dandi* ..... (candidate) Date ..... *20/5/09* .....

## STATEMENT 2

This thesis is the result of my own independent work/investigation, except where otherwise stated.

Other sources are acknowledged by explicit references.

Signed ..... *H. Dandi* ..... (candidate) Date ..... *20/5/09* .....

## STATEMENT 3

I hereby give consent for my thesis, if accepted, to be available for photocopying and for inter-library loan, and for the title and summary to be made available to outside organisations.

Signed ..... *H. Dandi* ..... (candidate) Date ..... *20/5/09* .....

## STATEMENT 4

I hereby give consent for my thesis, if accepted, to be available for photocopying and for inter-library loans **after expiry of a bar on access previously approved by the Graduate Development Committee.**

Signed ..... *H. Dandi* ..... (candidate) Date ..... *20/5/09* .....

## **Acknowledgements**

I would like to thank some people, without whom the work in this thesis would never have been completed.

Firstly, I would like to thank Professor Tony Lai for giving me the opportunity to work as part of his group at the Wales Heart Research Institute.

I am especially grateful to Dr Chris George, for his patience, guidance and occasional constructive sarcasm, throughout every stage of my PhD, from helping me out in the lab when I first started, to helping me see beyond the mountain of spreadsheets that needed analysis at the end.

Also thanks to Debra Fry for kindly supplying some figures for this thesis, and to Steve Barberini, the original designer of SALVO, without which my data analysis would have been unbearable!

I would also like to thank everyone on the 2<sup>nd</sup> floor for making my time here so enjoyable, particularly Debbi Fry for sharing my many moments of hysteria, and helping me through them by introducing me to Wii boxing. Thanks also to Lowri Thomas for her friendship and advice, and to Laila Guzadhur for making everything a little bit more fun!

Thank you to all my family and friends for putting up with my absence and my constant complaining during my writing up, especially to Claire Raisin for putting up with thesis-related phonecalls and making everything seem a bit brighter (most of the time), to my parents for their endless love and support, and to the rest of my family for their continuing interest in my progress, despite being thousands of miles away. Thanks especially to Chris Saunders for providing endless moral support while I moaned about my thesis day after day, and for always being there and believing that I could do it – even when I didn't!

## **Publications**

### **Full papers**

- George CH, **Jundi H**, Fry DL, Thomas NL and Lai FA (2007) Ryanodine receptors and ventricular arrhythmias: emerging trends in mutations, mechanisms and therapies. *J. Mol. Cell. Cardiol.* **42** 34-50.
- George CH, **Jundi H**, Walters N, Thomas NL, West RR and Lai FA (2006) Arrhythmogenic mutation-linked defects in ryanodine receptor auto-regulation reveal a novel mechanism of Ca<sup>2+</sup> release dysfunction. *Circ. Res.* **98** 88-97.
- George CH, **Jundi H**, Thomas NL, Walters N, Scoote M, Williams AJ and Lai FA (2004) Ryanodine receptor regulation by intramolecular interaction between cytoplasmic and transmembrane domains. *Mol. Biol. Cell* **15** 2627-2638.

### **Abstracts**

- **Jundi H**, Lai FA, George CH (2009) Targeted stabilisation of the RyR2 I-domain restores Ca<sup>2+</sup> handling and intercellular synchrony in ouabain-disrupted cardiac cell monolayers. *Biophys J.*
- **Jundi H**, Fry DL, Barberini SR, Lai FA and George CH (2008) Suppression of arrhythmogenic Ca<sup>2+</sup> fluxes in cardiac cells using fragments of human RyR2. *Biophys J. Suppl.* 428a
- Fry DL, **Jundi H**, Thomas NL, Lai FA and George CH (2007) Modulating intracellular Ca<sup>2+</sup> signalling using recombinant fragments of the human cardiac ryanodine receptor (RyR2). *Biophys. J. Suppl.* S 260a.
- **Jundi H**, Lai FA, George CH (2007) Targeting the RyR2 I-domain as a novel strategy to correct mutation linked Ca<sup>2+</sup> release channel dysfunction. *Biophys. J. Suppl.* S 262A-262A
- George CH, Barberini SR, Bloise R, Higgs GV, **Jundi H**, Fry DL, Priori SG and Lai FA (2006) Exercise-induced factors in human serum trigger abnormal Ca<sup>2+</sup> release via cardiac ryanodine receptor (RyR2) mutations. *Biophys. J. Suppl.* 263-264a.
- George CH, **Jundi H**, Thomas NL and Lai FA (2004) Altered intra-RyR interaction associated with stress-induced ventricular tachycardia. *Biophys. J.* 86 49a.

## **Summary**

Interdomain interactions within the complex three-dimensional architecture of the cardiac ryanodine receptor (RyR2) are pivotal in channel regulation. Acquired or genetic abnormalities that perturb these stabilising intra-molecular interactions are pathogenic. This laboratory identified the interacting- or I-Domain of human RyR2 that mediated interaction between cytoplasmic and transmembrane (TM) assemblies. To further elucidate the precise roles of functional motifs within the I-Domain, three contiguous fragments spanning RyR2 amino acid residues 3722-4610 were synthesised using a cell-free system. One fragment termed ID<sup>B</sup> (amino acid residues 4353-4499) profoundly modulated cellular Ca<sup>2+</sup> cycling and resulted in the remarkable normalisation of intercellular synchrony following its microinjection into ouabain-treated cardiomyocyte monolayers. These phenomena were linked to ID<sup>B</sup>-mediated stabilisation of RyR2 and were fully corroborated using ID<sup>B</sup> purified from a bacterial expression system. Bioinformatic analysis revealed striking structural homology between sub-fragments of the RyR2 I-Domain and I-Domain-like regions of inositol 1,4,5-trisphosphate receptors (IP<sub>3</sub>R). Recombinant expression of I-domain sub-fragments in RyR-null human embryonic kidney (HEK) cells remodelled carbachol-evoked Ca<sup>2+</sup>-responses and suppressed homeostatic Ca<sup>2+</sup> signalling events indicating that ID<sup>B</sup> also modulated IP<sub>3</sub>R signalling mechanisms. In both HL-1 and HEK cells, ID<sup>B</sup>-dependent Ca<sup>2+</sup> modulation extended to surrounding cells that were not microinjected with recombinant protein. This so-called 'bystander effect' was mediated by the transfer of signalling molecules via direct cell-to-cell coupling (gap junctions) and also by the extracellular transmission of diffusible effectors. This thesis supports the concept that RyR2 stabilisation rescues pathogenic Ca<sup>2+</sup> dysregulation and suggests that there is substantial merit in developing further epitope-targeting strategies for the therapeutic normalisation of Ca<sup>2+</sup> cycling in cardiac disease.



<b>LIST OF ABBREVIATIONS .....</b>	<b>19</b>
<b>CHAPTER 1    GENERAL INTRODUCTION .....</b>	<b>25</b>
1.1    CALCIUM SIGNALLING IN THE HEART .....	26
1.1.1 <i>The cardiac action potential</i> .....	28
1.1.2 <i>The cardiac myocyte</i> .....	29
1.1.3 <i>Cardiac excitation-contraction (EC) coupling</i> .....	32
1.1.3.1 <i>Tuning EC coupling by phosphorylation</i> .....	34
1.2    EC COUPLING IN CARDIAC DISEASE .....	36
1.2.1 <i>Heart failure</i> .....	37
1.2.2 <i>Sudden Cardiac Death (SCD)</i> .....	38
1.2.3 <i>Cardiac arrhythmia</i> .....	39
1.3    THE RYANODINE RECEPTOR.....	41
1.3.1 <i>Molecular cloning of RyR isoforms and their tissue distribution</i> .....	43
1.3.2 <i>Structure of the RyR</i> .....	44
1.3.3 <i>Correlating the linear sequence to the three-dimensional structure using recombinant RyR</i> .....	47
1.3.4 <i>Topology of RyR transmembrane domains</i> .....	50
1.3.5 <i>Regulation of RyR by the macromolecular complex</i> .....	52
1.3.5.1 <i>Regulators of RyR2 phosphorylation - PKA, CaMKII and phosphatases</i> .....	54
1.3.5.2 <i>FK-binding proteins (FKBP)</i> .....	56
1.3.5.3 <i>Calsequestrin</i> .....	58
1.3.6 <i>Regulation of the RyR macromolecular complex by endogenous factors</i> .....	58
1.3.6.1 <i>Cytosolic Ca<sup>2+</sup></i> .....	59
1.3.6.2 <i>Luminal Ca<sup>2+</sup></i> .....	59
1.3.7 <i>Functional interactions within the RyR</i> .....	60
1.3.7.1 <i>Inter-channel interaction</i> .....	60
1.3.7.2 <i>Inter-domain interaction within the RyR tetramer</i> .....	63
1.3.8 <i>The RyR2 I-Domain</i> .....	63
1.4    RYR2 AND PATHOLOGY .....	66
1.4.1.1 <i>RyR2 in Heart Failure</i> .....	67
1.4.1.2 <i>ARVC2 / CPVT</i> .....	70
1.4.1.3 <i>The 'hot-spot' nature of RyR2 mutational loci</i> .....	71
1.5    DEFECTIVE INTER-DOMAIN INTERACTIONS AND CHANNEL DESTABILISATION IN MUTATION-LINKED RYR2 DYSFUNCTION .....	72
1.6    TREATING CARDIAC ARRHYTHMIAS .....	74
1.6.1 <i>Intracellular targets for anti-arrhythmics</i> .....	75

1.6.1.1	Targeting the RyR2 I-Domain .....	76
1.7	AIMS OF THIS THESIS.....	77
1.8	GENERAL HYPOTHESIS .....	77
<b>CHAPTER 2</b>	<b>MATERIALS AND METHODS.....</b>	<b>79</b>
2.1	GENERAL MATERIALS AND METHODS .....	80
2.2	MOLECULAR BIOLOGY .....	80
2.2.1	<i>Molecular biology reagents</i> .....	80
2.2.2	<i>Oligonucleotides</i> .....	81
2.2.3	<i>Propagation of recombinant DNA constructs</i> .....	82
2.2.4	<i>Generating frozen stocks of bacterial cells</i> .....	83
2.2.5	<i>Small-scale plasmid DNA isolation ('mini-prep')</i> .....	83
2.2.6	<i>Agarose gel electrophoresis</i> .....	84
2.2.7	<i>Large-scale plasmid isolation ('maxi-prep')</i> .....	85
2.2.8	<i>Spectrophotometric DNA quantification</i> .....	86
2.2.9	<i>DNA Sequencing</i> .....	86
2.2.10	<i>PCR amplification of DNA</i> .....	87
2.2.11	<i>Cloning of DNA fragments</i> .....	88
2.3	PROTEIN BIOCHEMISTRY .....	90
2.3.1	<i>Protein biochemistry reagents</i> .....	90
2.3.2	<i>Antibodies</i> .....	90
2.3.3	<i>SDS-Polyacrylamide gel electrophoresis (SDS-PAGE)</i> .....	91
2.3.4	<i>Staining proteins on an SDS-PAGE gel</i> .....	92
2.3.5	<i>Electro-transfer of proteins onto a membrane</i> .....	93
2.3.6	<i>Immunoblot analysis</i> .....	93
2.3.7	<i>Purification of histidine-tagged proteins using a Ni<sup>2+</sup> affinity technique</i> .....	94
2.3.8	<i>Purification of S-tagged proteins by S-protein affinity</i> .....	95
2.3.9	<i>Densitometric analysis</i> .....	96
2.3.10	<i>Determination of protein concentration</i> .....	97
2.4	MAMMALIAN CELL CULTURE .....	97
2.4.1	<i>Mammalian cell culture reagents</i> .....	97
2.4.2	<i>Mammalian cell lines</i> .....	98
2.4.3	<i>Culture of Human Embryonic Kidney (HEK) 293 cells</i> .....	98
2.4.4	<i>Culture of HL-1 cardiomyocytes</i> .....	99
2.4.5	<i>Generating frozen stocks of mammalian cell lines</i> .....	100
2.5	COMPUTER SOFTWARE AND DATA ANALYSIS .....	101
2.6	HEALTH AND SAFETY .....	101

<b>CHAPTER 3</b>	<b>IN VITRO EXPRESSION AND PURIFICATION OF I-DOMAIN PROTEINS .....</b>	<b>103</b>
3.1	INTRODUCTION .....	104
3.1.1	<i>The RyR2 I-Domain</i> .....	104
3.1.2	<i>Cell-free protein expression</i> .....	105
3.1.3	<i>Objectives of this chapter</i> .....	107
3.2	METHODS.....	108
3.2.1	<i>Preparation of hRyR2 I-Domain expression plasmids</i> .....	108
3.2.2	<i>Cell-free protein expression</i> .....	109
3.2.3	<i>Autoradiography</i> .....	111
3.2.4	<i>Antibody purification using affinity strategies</i> .....	111
3.2.5	<i>Zn<sup>2+</sup>-affinity purification of recombinant proteins</i> .....	112
3.3	RESULTS.....	113
3.3.1	<i>Generation of truncated I-Domain constructs</i> .....	113
3.3.2	<i>In vitro expression of I-Domain fusion proteins</i> .....	115
3.3.2.1	<i>Selection of an appropriate cell-free expression system</i> .....	115
3.3.2.2	<i>Quantification of protein expression in RRL</i> .....	118
3.3.3	<i>Detection of I-Domain proteins</i> .....	119
3.3.3.1	<i>Detection of I-Domain proteins by S-protein HRP</i> .....	119
3.3.3.2	<i>Detection of I-Domain proteins by anti-RyR2 antibody (ab1093)</i> .....	121
3.3.3.3	<i>Detection of I-Domain proteins by anti-His antibody</i> .....	123
3.3.4	<i>Purification of I-Domain proteins</i> .....	125
3.4	DISCUSSION .....	131
3.4.1	<i>Successful propagation of I-Domain expression cassettes</i> .....	131
3.4.2	<i>Successful expression of I-Domain proteins in vitro</i> .....	131
3.4.3	<i>The C-terminal hexa-His epitope can be used for isolating I-Domain proteins</i> .	132
<b>CHAPTER 4</b>	<b>OPTIMISATION OF MICROINJECTION STRATEGIES .....</b>	<b>134</b>
4.1	INTRODUCTION .....	135
4.1.1	<i>HL-1 cells: an immortalised cardiac cell line</i> .....	135
4.1.2	<i>Phenotypic characteristics of HL-1 cells</i> .....	136
4.1.3	<i>HL-1 cells as a model system</i> .....	138
4.1.4	<i>Microinjection</i> .....	139
4.1.5	<i>Objectives of this chapter</i> .....	140
4.1.6	<i>Specific Hypothesis</i> .....	141
4.2	METHODS.....	142
4.2.1	<i>Preparation of HL-1 cells for MI</i> .....	142

4.2.2	<i>MI apparatus and techniques</i> .....	142
4.2.3	<i>Optimisation of MI parameters</i> .....	144
4.2.4	<i>MI of recombinant protein and cellular Ca<sup>2+</sup> imaging</i> .....	145
4.2.5	<i>Analysis of spatio-temporal Ca<sup>2+</sup> handling in HL-1 myocytes</i> .....	146
4.3	RESULTS.....	150
4.3.1	<i>Optimised parameters for MI</i> .....	150
4.3.2	<i>MI of recombinant proteins and markers into HL-1 myocytes</i> .....	151
4.3.3	<i>MI of RRL affects some aspects of cell Ca<sup>2+</sup>-handling phenotype</i> .....	152
4.3.4	<i>MI of ID<sup>B</sup> into HL-1 myocytes</i> .....	155
4.4	DISCUSSION.....	159
4.4.1	<i>Conditions for successful MI</i> .....	159
4.4.2	<i>MI affects some aspects of Ca<sup>2+</sup> handling in WT HL-1 myocytes</i> .....	159
4.4.3	<i>ID<sup>B</sup> does not affect synchronicity in resting HL-1 myocytes</i> .....	160
<b>CHAPTER 5 INVESTIGATING THE EFFECT OF ID<sup>B</sup> IN DYSSYNCHRONOUS CARDIOMYOCYTES</b> .....		<b>161</b>
5.1	INTRODUCTION.....	162
5.1.1	<i>Cardiac glycosides</i> .....	162
5.1.1.1	<i>Digoxin</i> .....	163
5.1.1.2	<i>Ouabain</i> .....	164
5.1.2	<i>Mechanisms underlying cardiac arrhythmias</i> .....	164
5.1.3	<i>Cardiac glycosides in arrhythmia</i> .....	166
5.1.4	<i>Objectives of this chapter</i> .....	167
5.1.5	<i>Specific Hypothesis</i> .....	167
5.2	METHODS.....	168
5.2.1	<i>MI of cells before and after incubation in ouabain</i> .....	168
5.3	RESULTS.....	170
5.3.1	<i>Effect of ouabain on beating HL-1 myocytes</i> .....	170
5.3.2	<i>MI of HL-1 cells following pre-treatment with ouabain</i> .....	173
5.3.2.1	<i>Control experiments</i> .....	173
5.3.2.2	<i>Effect of ID<sup>B</sup> on ouabain treated cells</i> .....	176
5.3.3	<i>Effect of ouabain on HL-1 myocytes following ID<sup>B</sup> transduction</i> .....	178
5.3.3.1	<i>Controls</i> .....	178
5.3.3.2	<i>Effect of ouabain-treatment on HL-1 myocytes after MI of ID<sup>B</sup></i> .....	180
5.3.4	<i>Bystander effect</i> .....	182
5.3.4.1	<i>Bystander effect in HL-1 cells microinjected following pre-treatment with ouabain</i> .....	183

5.3.4.2	Bystander effect in HL-1 cells microinjected prior to treatment with ouabain .....	185
5.4	DISCUSSION .....	188
5.4.1	<i>Alterations to some Ca<sup>2+</sup> handling parameters do not manifest as altered intercellular synchrony</i> .....	188
5.4.2	<i>Effect of ID<sup>B</sup> on arrhythmic HL-1 myocytes</i> .....	189
5.4.3	<i>Bystander effect</i> .....	192
<b>CHAPTER 6 INVESTIGATING THE EFFECT OF BACTERIALLY SYNTHESISED ID<sup>B</sup> IN HL-1 CARDIOMYOCYTES .....</b>		<b>193</b>
6.1	INTRODUCTION .....	194
6.1.1	<i>E. coli as a system for protein expression</i> .....	194
6.1.2	<i>Factors affecting protein expression in E. coli</i> .....	194
6.1.2.1	The effect of IPTG concentration .....	195
6.1.2.2	The effect of temperature .....	196
6.1.3	<i>Objectives of this chapter</i> .....	197
6.1.4	<i>Specific Hypothesis</i> .....	198
6.2	METHODS.....	199
6.2.1	<i>Bacterial expression of recombinant I-Domain proteins</i> .....	199
6.2.2	<i>Optimisation of culture conditions</i> .....	199
6.2.2.1	IPTG-induction of bacterial protein expression .....	199
6.2.2.2	Protein expression by autoinduction .....	200
6.2.3	<i>Protein extraction</i> .....	201
6.2.3.1	Protein extraction by pressure lysis .....	202
6.2.3.2	Protein extraction by sonication .....	202
6.2.3.3	Protein extraction by B-PER <sup>®</sup> .....	203
6.2.3.4	Protein extraction by BugBuster .....	203
6.2.3.5	Protein extraction by urea.....	204
6.2.4	<i>Microinjection of bacterially produced ID<sup>B</sup> into HL-1 cells</i> .....	204
6.3	RESULTS.....	205
6.3.1	<i>Selection of a suitable protein extraction technique</i> .....	205
6.3.2	<i>Protein Induction by IPTG</i> .....	206
6.3.3	<i>Successful expression and purification of ID<sup>B</sup></i> .....	210
6.3.4	<i>Effect of bacterially-produced ID<sup>B</sup> on resting cells</i> .....	213
6.3.5	<i>Effect of bacterially-produced ID<sup>B</sup> on ouabain-treated HL-1 cells</i> .....	215
6.3.6	<i>Bystander effect</i> .....	217
6.3.6.1	The bystander effect in HL-1 cells .....	218

6.3.6.2	Bystander effect in ouabain-treated HL-1 cells .....	220
6.4	DISCUSSION .....	223
6.4.1	<i>Expression of I-Domain proteins in a bacterial expression system.....</i>	223
6.4.2	<i>Bacterially-produced ID<sup>B</sup> modifies cellular Ca<sup>2+</sup> handling differently to ID<sup>B</sup> produced in vitro without altering synchrony.....</i>	223
6.4.3	<i>Effect of bacterially-produced ID<sup>B</sup> on arrhythmic HL-1 myocytes.....</i>	225
6.4.4	<i>Bystander effect.....</i>	225
<b>CHAPTER 7</b>	<b>DETERMINING THE EFFECTS OF ID<sup>B</sup> ON IP<sub>3</sub>R-DEPENDENT Ca<sup>2+</sup> SIGNALLING IN HEK CELLS .....</b>	<b>226</b>
7.1	INTRODUCTION .....	227
7.1.1	<i>Inositol 1,4,5-trisphosphate receptors.....</i>	227
7.1.2	<i>The role of IP<sub>3</sub>R in cardiac arrhythmias.....</i>	230
7.1.3	<i>HEK293 cells as a model system.....</i>	232
7.1.4	<i>The use of 'noise' analysis to analyse Ca<sup>2+</sup> transients .....</i>	233
7.1.4.1	<i>Relative signal variability (RSV).....</i>	234
7.1.4.2	<i>Indicators of signal variability .....</i>	235
7.1.5	<i>Objectives of this chapter .....</i>	237
7.1.6	<i>Specific Hypothesis .....</i>	237
7.2	METHODS.....	238
7.2.1	<i>Preparation of HEK293 cells for MI.....</i>	238
7.2.2	<i>MI of recombinant protein and cellular Ca<sup>2+</sup> imaging.....</i>	238
7.3	RESULTS.....	241
7.3.1	<i>MI of recombinant proteins and markers in HEK293 cells.....</i>	241
7.3.2	<i>Effect of I-Domain proteins on IP<sub>3</sub>R carbachol-induced Ca<sup>2+</sup> transients .....</i>	242
7.3.2.1	<i>Effect of I-Domain proteins on Ca<sup>2+</sup> transient characteristics .....</i>	243
7.3.2.2	<i>Effect of I-Domain proteins on cell 'noise' in carbachol-responsive cells ...</i>	245
7.3.2.3	<i>Carbachol-induced Ca<sup>2+</sup>-transients are modulated by cellular noise .....</i>	247
7.3.2.4	<i>Effect of I-Domain proteins on cell 'noise' in non-responding cells .....</i>	250
7.3.3	<i>Effect of I-Domain proteins on IP<sub>3</sub>R caffeine-modulated Ca<sup>2+</sup> handling .....</i>	251
7.4	DISCUSSION .....	253
7.4.1	<i>MI of recombinant proteins in HEK293 cells and their effect on Ca<sup>2+</sup> handling.</i>	253
7.4.2	<i>Effect of I-Domain proteins on cell 'noise' .....</i>	254
7.4.3	<i>Bystander effect in HEK cells.....</i>	255

<b>CHAPTER 8</b>	<b>INSIGHTS INTO THE MECHANISTIC BASIS OF THE BYSTANDER EFFECT .....</b>	<b>256</b>
8.1	INTRODUCTION .....	257
8.1.1	<i>The bystander effect</i> .....	257
8.1.2	<i>Objectives of this chapter</i> .....	258
8.1.3	<i>Specific Hypothesis</i> .....	258
8.2	METHODS.....	259
8.2.1	<i>Lucifer Yellow</i> .....	259
8.2.2	<i>Medium transfer</i> .....	259
8.2.2.1	HEK293 cells.....	259
8.2.2.2	HL-1 myocytes.....	260
8.3	RESULTS.....	262
8.3.1	<i>Cell-to-cell coupling in HEK293 cells and HL-1 myocytes</i> .....	262
8.3.2	<i>Medium transfer in HEK cells</i> .....	264
8.3.3	<i>Medium transfer in HL-1 myocytes</i> .....	266
8.4	DISCUSSION .....	269
<b>CHAPTER 9</b>	<b>GENERAL DISCUSSION .....</b>	<b>271</b>
9.1	EXPRESSION OF I-DOMAIN PROTEINS .....	272
9.2	MICROINJECTION TECHNIQUE .....	274
9.3	THE EFFECT OF ID <sup>B</sup> IN HL-1 CARDIOMYOCYTES .....	275
9.4	THE EFFECT OF THE I-DOMAIN ON IP3R-DEPENDENT CA <sup>2+</sup> HANDLING.....	276
9.5	THE BYSTANDER EFFECT .....	277
<b>BIBLIOGRAPHY</b> .....		<b>279</b>
<b>APPENDICES</b> .....		<b>310</b>
	<i>Appendix I – List of Primers</i> .....	311
	<i>Appendix II – Bioinformatic analysis of RyR2 and IP3R I-domains</i> .....	312

## **List of Figures**

Figure 1.1. The Ca <sup>2+</sup> signalling network.....	27
Figure 1.2. Schematic representations of the cardiac action potential (AP) in a ventricular myocyte showing timing and morphology.....	29
Figure 1.3. Cardiac myocyte machinery .....	30
Figure 1.4. Schematic diagram of cardiac cross bridge-formation .....	31
Figure 1.5. Schematic representation of cardiac EC coupling.....	34
Figure 1.6. Schematic representation of the $\beta$ -AR pathway .....	36
Figure 1.7. An electron micrograph of a section through a triad junction of a frog muscle cell.....	41
Figure 1.8. The three-dimensional structure of RyR .....	46
Figure 1.9. Three-dimensional structure of RyR2, indicating various regions that have been located using difference maps.....	49
Figure 1.10. Models for the transmembrane regions of RyR1.....	51
Figure 1.11. The RyR2 macromolecular signalling complex .....	53
Figure 1.12. Physical coupling between skeletal muscle RyRs in the native 'checkerboard' array .....	62
Figure 1.13. CPVT-linked mutations located to the RyR2 I-Domain.....	64
Figure 1.14. The RyR2 I-Domain intrinsically controls RyR2 opening through conformational rearrangement.....	65
Figure 1.15. Schematic of the reported mutation sites RyR1 and RyR2. ....	67
Figure 1.16. Clustering of mutational loci in RyR2 .....	72
Figure 1.17. Schematic diagram summarising the peptide probe approach to the investigation of domain unzipping .....	74
Figure 2.1. pET-29(b) expression vector .....	89
Figure 2.2. Schematic of Ni <sup>2+</sup> affinity purification of histidine-tagged proteins .....	95
Figure 2.3. Schematic of protein purification by S-protein affinity and thrombin cleavage ...	96
Figure 2.4. Phase microscopy images of healthy HEK and HL-1 cells.....	100
Figure 3.1. Schematic representation of the truncated I-Domain constructs .....	105
Figure 3.2. Schematic representation of the I-Domain expression cassettes .....	109
Figure 3.3. Summary of Melon Gel IgG purification strategy.....	112
Figure 3.4. hRyR2 I-Domain cDNA fragments were successfully amplified by PCR. ....	113
Figure 3.5. Verification of pET-29(b)-cloned I-Domain expression cassettes by restriction mapping. ....	114
Figure 3.6. Verification of constructs by sequencing.....	115



Figure 3.7. Comparison of RRL and WG extract protein expression systems.....	117
Figure 3.8. Autoradiography of <sup>35</sup> S-labelled I-Domain proteins .....	118
Figure 3.9. Detection by S-protein HRP conjugate .....	120
Figure 3.10. Immunodetection by anti-RyR2 ab1093.....	122
Figure 3.11. Detection by anti-His antibodies .....	124
Figure 3.12. Unsuccessful purification of ID protein from the RRL expression system using column-based systems.....	126
Figure 3.13. Purification of radiolabelled I-Domain proteins using a zinc-affinity approach.....	128
Figure 3.14. Quantification of the efficacy of the MagZ Zn <sup>2+</sup> -affinity purification system by densitometry .....	129
Figure 3.15. Successful immunodetection of MagZ purified I-Domain proteins in RRL.....	130
Figure 4.1. Phenotypic characteristic features of a typical HL-1 cardiomyocyte.....	136
Figure 4.2. Schematic depicting semi-automated MI into adherent cells.....	144
Figure 4.3. Summary of MI and Ca <sup>2+</sup> imaging protocol .....	146
Figure 4.4. Deciphering intracellular Ca <sup>2+</sup> signalling in HL-1 cardiac cell monolayers .....	147
Figure 4.5. Optimal MI parameters confer efficient injection and cell viability.....	150
Figure 4.6. MI of proteins into HL-1 cells .....	151
Figure 4.7. SALVO analysis of the effects of MI on HL-1 myocyte monolayers.....	153
Figure 4.8. Representative traces of WT and RRL-injected HL-1 myocytes.....	154
Figure 4.9. Synchronicity in WT HL-1 cells compared with RRL injected cells .....	155
Figure 4.10. SALVO analysis of the effects of ID <sup>B</sup> on HL-1 myocyte monolayers.....	156
Figure 4.11. Representative traces of HL-1 myocytes injected with RRL and ID <sup>B</sup> .....	157
Figure 4.12. MI of ID <sup>B</sup> does not alter synchronicity .....	158
Figure 5.1. Structures of endogenous cardiac glycosides belonging to the cardenolide and bufadienolide groups.....	163
Figure 5.2. Schematic representation of early and delayed afterdepolarisations with respect to the normal cardiac action potential. ....	166
Figure 5.3. MI of HL-1 myocytes after incubation in ouabain .....	168
Figure 5.4. MI of HL-1 myocytes prior to incubation in ouabain .....	169
Figure 5.5. Representative traces of WT and ouabain treated HL-1 myocytes .....	171
Figure 5.6. SALVO analysis of the effects of ouabain on HL-1 myocyte monolayers.....	172
Figure 5.7. Synchronicity in WT HL-1 cells compared with RRL injected cells .....	173
Figure 5.8. SALVO analysis of the effects of MI on HL-1 myocyte monolayers pre-treated with 100 nM ouabain.....	175
Figure 5.9. The MI technique does not restore synchrony in ouabain-treated myocytes...	176

Figure 5.10. SALVO analysis of the effects of ID <sup>B</sup> on HL-1 myocyte monolayers pre-treated with 100 nM ouabain .....	177
Figure 5.11. ID <sup>B</sup> partially restores synchrony in dyssynchronous ouabain-treated HL-1 myocytes. ....	178
Figure 5.12. SALVO analysis of the effects of MI on HL-1 myocyte monolayers prior to incubation with 100 nM ouabain.....	179
Figure 5.13. MI before ouabain-treatment does not alter ouabain-induced dyssynchrony.....	180
Figure 5.14. SALVO analysis HL-1 myocytes treated with ouabain after MI with ID <sup>B</sup> .....	181
Figure 5.15. MI of ID <sup>B</sup> prior to ouabain-treatment does not prevent ouabain-induced dyssynchrony.....	182
Figure 5.16. Illustration of non-microinjected bystander cells.....	183
Figure 5.17. SALVO analysis shows a bystander effect in non-injected ouabain-treated HL-1 myocytes.....	184
Figure 5.18. Ouabain-treated HL-1 myocytes not injected with ID <sup>B</sup> showed a comparable level of synchrony as those containing ID <sup>B</sup> .....	185
Figure 5.19. SALVO analysis shows a bystander effect in non-injected ouabain-treated HL-1 myocytes.....	186
Figure 5.20. MI of ID <sup>B</sup> prior to ouabain-treatment does not restore ouabain-induced dyssynchrony in injected or bystander cells. ....	187
Figure 5.21. FRET reporter studies of the effect of ID <sup>B</sup> on ouabain-treated HL-1 myocytes. ....	191
Figure 6.1. Optimisation of protein extraction from bacterial cells .....	206
Figure 6.2. Testing the induction conditions to optimise the production of I-Domain protein in an IPTG-induced bacterial system.....	208
Figure 6.3. Expression of I-Domain and pET29-(b) in Rosetta™ 2(DE3) cells .....	209
Figure 6.4. IPTG induction conditions selected for large-scale culture.....	209
Figure 6.5. Purification of ID <sup>B</sup> from bacterial cells .....	211
Figure 6.6. Successful purification and detection of bacterially produced ID <sup>B</sup> .....	212
Figure 6.7. SALVO analysis of the effects of bacterially produced ID <sup>B</sup> on HL-1 myocyte monolayers. ....	214
Figure 6.8. MI of bacterially-produced ID <sup>B</sup> does not alter synchronicity.....	215
Figure 6.9. SALVO analysis of the effects of bacterially produced ID <sup>B</sup> on HL-1 myocyte monolayers pre-treated with 100 nM ouabain .....	216
Figure 6.10. Bacterially-produced ID <sup>B</sup> restores synchrony in dyssynchronous ouabain-treated HL-1 myocytes.....	217
Figure 6.11. SALVO analysis shows a bystander effect in non-injected HL-1 myocytes ...	219

Figure 6.12. Bystander cells not injected with ID <sup>B</sup> showed a comparable level of synchrony as those containing ID <sup>B</sup> .....	220
Figure 6.13. SALVO analysis shows a bystander effect in non-injected ouabain-treated HL-1 myocytes.....	221
Figure 6.14. Ouabain-treated bystanders not injected with ID <sup>B</sup> showed a comparable level of synchrony as those containing ID <sup>B</sup> .....	222
Figure 7.1. Five-domain structural model IP <sub>3</sub> R .....	228
Figure 7.2. Model for the global structural changes that occur within IP <sub>3</sub> R1.....	229
Figure 7.3. Overview of cardiac IP <sub>3</sub> R signalling and its involvement in EC coupling, excitation–transcription (ET) coupling and arrhythmias.....	231
Figure 7.4. Calculation of SV and RSV .....	234
Figure 7.5. Correlation between common indices of signal variability and gradient.....	235
Figure 7.6. Signal variability (SV) normalised to mean fluorescence (SV <sub>m</sub> ) is independent of fluorescence and gradient.....	236
Figure 7.7. Schematic of MI experiments with HEK293 cells. ....	239
Figure 7.8. Quantifying intracellular Ca <sup>2+</sup> signalling in HEK293 cells .....	240
Figure 7.9. MI of proteins into HEK293 cells.....	241
Figure 7.10. MI of I-Domain proteins reduces the percentage of cells responding to 0.1 mM carbachol. ....	242
Figure 7.11. I-Domain proteins blunt carbachol-evoked Ca <sup>2+</sup> transients .....	243
Figure 7.12. Changes in carbachol-evoked Ca <sup>2+</sup> transients were also seen in non-injected cells .....	244
Figure 7.13. Removal of extracellular Ca <sup>2+</sup> limits cellular response to 0.1mM carbachol ..	245
Figure 7.14. MI of I-Domain fragments reduces cellular ‘noise’ in carbachol-responsive HEK cells .....	246
Figure 7.15. A reduced resting SV <sub>m</sub> is associated with a lack of carbachol-evoked Ca <sup>2+</sup> response in HEK cells.....	247
Figure 7.16. The relationship of SV <sub>m</sub> with amplitude and kinetic properties of carbachol induced Ca <sup>2+</sup> response .....	248
Figure 7.17. MI of I-Domain fragments reduces RSV in carbachol non- responsive HEK cells .....	251
Figure 7.18. MI of I-Domain fragments reduces RSV in response to caffeine addition.....	252
Figure 8.1. Summary of medium transfer experiment protocol with HEK293 cells .....	260
Figure 8.2. Summary of medium transfer experiment protocol with HL-1 cardiomyocytes.....	261
Figure 8.3. Differential extents of cell-to-cell communication in HEK and HL-1 cells.....	263

Figure 8.4. Dilution of transferred medium affects $\text{Ca}^{2+}$ handling in carbachol-stimulated HEK cells. ....	265
Figure 8.5. The relationship between resting $\text{SV}_m$ and carbachol-evoked $\text{Ca}^{2+}$ transients in HEK cells is affected by transferred medium concentration.....	265
Figure 8.7. Synchronicity is not affected by medium transfer .....	268

## **List of Tables**

Table 2.1. Typical PCR reaction mixture .....	87
Table 2.2. Typical thermal cycling conditions.....	87
Table 2.3. Separating acrylamide gel composition .....	92
Table 3.1. Choice of cell-free protein synthesis systems .....	107
Table 3.2. Typical WG extract reaction mixture .....	110
Table 3.3. Typical quick coupled transcription/translation reaction mixture.....	110
Table 4.1. Explanation of SALVO parameters .....	148
Table 5.1. Summary of alterations of spatio-temporal Ca <sup>2+</sup> handling parameters .....	189
Table 6.1. Summary of bacterial induction conditions.....	200
Table 6.2. Summary of protein extraction methods.....	202
Table 6.3. Summary of alterations of spatio-temporal Ca <sup>2+</sup> handling parameters .....	224
Table 7.1. Correlation of SVM with carbachol-evoked Ca <sup>2+</sup> transients.....	260
Table 8.1. Summary of medium dilution strategy.....	260

**List of abbreviations**

Å	Ångström(s)
A	ampere(s)
A <sub>260</sub>	absorbance at 260 nm
aa	amino acid(s)
ab	antibody
AM	acetoxymethyl ester
ANF	atrial natriuretic factor
ANOVA	analysis of variance
AP	action potential
ARVD2	Arrhythmogenic right ventricular dysplasia type 2
ATP	adenosine trisphosphate
BCA	bicinchoninic acid
β-AR	β-adrenergic receptor

β-ARK	β-adrenergic receptor kinase
bp	base pair(s)
°C	degrees Celsius
Ca <sup>2+</sup>	ionised calcium
CaM	calmodulin
CaMKII	calmodulin dependent kinase II
cAMP	cyclic adenosine monophosphate
CCD	central core disease
cDNA	complementary DNA
CFP	cyan fluorescent protein
CICR	Ca <sup>2+</sup> -induced-Ca <sup>2+</sup> -release
COSHH	control of substances hazardous to health
CoV	coefficient of variance

CPVT	Catecholaminergic polymorphic ventricular tachycardia	EDTA	ethylene diamine tetra-acetic acid
CRU	Ca <sup>2+</sup> release unit	eGFP	enhanced green fluorescent protein
CSQ	calsequestrin	EGTA	ethylene glycol-bis (β-minoethylether)-N,N,N',N'-tetra-acetic acid
DAD	delayed afterdepolarisation	EM	electron microscopy
DEAE	diethylaminoethyl	ER	endoplasmic reticulum
dH <sub>2</sub> O	deionised water	ET-1	endothelin 1
DMEM	Dulbecco's modified eagle medium	FCS	foetal calf serum
DMSO	dimethyl sulphoxide	FKBP12	FK506 binding protein 12
DNA	deoxyribonucleic acid	FKBP12.6	FK506 binding protein 12.6
dNTP	2'-deoxyribonucleotide 5'-triphosphate	FRET	fluorescence resonance energy transfer
dpi	dots per inch	g	gram(s)
DP	domain peptide	<i>g</i>	the acceleration due to gravity
DR	divergent region	GFN	gelatin fibronectin
EAD	early afterdepolarisation	GMAG	genetic manipulation advisory group
ECG	electrocardiograph	GST	glutathione-S-transferase
ECL	enhanced chemiluminescence	h	hour(s)

HBS	HEPES-buffered saline	kDa	kiloDalton(s)
HEK	human embryonic kidney cells	KDS	potassium dodecyl sulphate
HRP	horseradish peroxidase	L	litre
HF	heart failure	LB	Luria Bertani medium
hPa	hectopascal	LIZ	Leucine-isoleucine zipper
Hz	Herz	LTCC	L-type Ca <sup>2+</sup> channel
<i>I</i> <sub>Ca</sub>	inward Ca <sup>2+</sup> current	LY	lucifer yellow
ICD	implantable cardioverter defibrillator	M	molar
ID	interacting domain	mA	milliAmperes
IgG	immunoglobulin G	mAKAP	muscle A kinase anchoring protein
IMAC	immobilised metal affinity chromatography	MBq	mega Becquerel
IP <sub>3</sub>	inositol inositol-1,4,5-trisphosphate	MCS	multiple cloning site
IP <sub>3</sub> R	inositol inositol-1,4,5-trisphosphate receptor	MH	malignant hyperthermia
IPTG	isopropyl-3-D-thiogalactoside	MHC	myosin heavy chain
K <sup>+</sup>	ionised potassium	MI	microinjection
kb	kilobase(s)	min	minute(s)



Mg <sup>2+</sup>	ionised magnesium	NMWL	nominal molecular weight limit
mg	milligram(s)	ng	nanogram(s)
ml	millilitre(s)	Ni <sup>2+</sup>	ionised nickel
mM	millimoles/molar	NZY	nutrient Z amine A and yeast extract medium
mm	millimetre	OD	optical density
μg	microgram(s)	ORF	open reading frame
μl	microlitre	pAb	polyclonal antibody
μM	micromoles/molar	PAGE	polyacrylamide gel electrophoresis
μm	micrometer	PBS	phosphate buffered saline
mRNA	messenger RNA	Pc	compensation pressure
ms	milliseconds	PCR	polymerase chain reaction
MW	molecular weight	PDE4D3	phosphodiesterase 4D3
Na <sup>+</sup>	ionised sodium	pg	picogram(s)
NCX	Na <sup>+</sup> /Ca <sup>2+</sup> exchanger	Pi	injection pressure
nM	nanomoles/nanomolar	PKA	protein kinase A
nm	nanometre	PLB	phospholamban

PMCA	plasma membrane $\text{Ca}^{2+}$ ATPase	SALVO	Synchronicity-Amplitude-Length-Variability of Oscillation
pmol	picomoles/molar	SAP	shrimp alkaline phosphatase
PMT	photomultiplier tube	SCD	sudden cardiac death
PP1	protein phosphatase 1	SDS	sodium dodecyl sulphate
PP2A	protein phosphatase 2A	SEM	standard error of the mean
ppm	parts per million	SERCA	sarco(endoplasmic reticulum $\text{Ca}^{2+}$ ATPase
p.s.i.	pound force per square inch	SOCC	store-operated calcium channels
PVDF	polyvinylidene fluoride	sorcini	soluble drug resistance related calcium binding protein
RA	renin-angiotensin	SR	sarcoplasmic reticulum
ROI	region of interest	ssDNA	single strand DNA
RNA	ribonucleic acid	SV	signal variability
rpm	revolutions per minute	TAE	tris-acetate-EDTA buffer
RRL	rabbit reticulocyte lysate	TBS	tris-buffered saline
RSV	relative signal variability	TBS-T	TBS Tween-20
RT	room temperature	TEMED	N,N,N',N'-tetramethylethylenediamine
RyR	ryanodine receptor	Ti	injection time

T <sub>m</sub>	melting temperature
TM	transmembrane
Tn C	the Ca <sup>2+</sup> binding component of troponin
Tris	tris(hydroxymethyl) aminomethane
tRNA	transfer RNA
TT	transverse tubule(s)
U	units
UV	ultraviolet

V	volt(s)
VT	ventricular tachycardia
v/v	volume/volume
WG	wheat germ
w/v	weight/volume
WT	wild type
YFP	yellow fluorescent protein
Zn <sup>2+</sup>	ionised zinc

# ***Chapter 1***

## ***General Introduction***

## 1.1 Calcium signalling in the heart

Calcium ( $\text{Ca}^{2+}$ ) is a universal biological signal responsible for the modulation of a vast range of cellular processes, including neurotransmission, secretion, proliferation, fertilisation and apoptosis (see Berridge *et al.* 2003; Clapham 2007 for reviews). Perhaps one of the most widely studied  $\text{Ca}^{2+}$ -dependent mechanisms is muscle contraction. In cardiac muscle,  $\text{Ca}^{2+}$  is essential in cardiac electrical activity and is the direct activator of the myofilaments, which cause myocyte contraction.

This functional versatility of a simple divalent cation is intriguing, particularly since  $\text{Ca}^{2+}$  cannot be made or metabolised, and despite its importance in cell function sustained or abnormally high concentrations of  $\text{Ca}^{2+}$  are cytotoxic in most cells (Berridge *et al.* 2000). This property makes  $\text{Ca}^{2+}$  unique amongst second messengers, and its functional versatility stems from highly orchestrated release and sequestration (Summarised in Figure 1.1). Cells at rest maintain a low intracellular concentration of  $\text{Ca}^{2+}$  of ~100 nM, but this increases rapidly into the millimolar range upon cell activation. This mobilisation of intracellular  $\text{Ca}^{2+}$  takes place over periods ranging from microseconds to hours, to regulate a wide range of different cellular processes. Some of these transients result in highly localised brief bursts of  $\text{Ca}^{2+}$ , while others produce longer-lasting global increases in  $\text{Ca}^{2+}$  in the form of repetitive waves (Berridge 1997).

The versatility of  $\text{Ca}^{2+}$  signalling is extended by complex spatial and temporal patterns underlying its release and sequestration. Release of  $\text{Ca}^{2+}$  from internal stores in cardiac muscle is modulated by various channels, including the ryanodine receptor (RyR) and the inositol-1,4,5-triphosphate receptor ( $\text{IP}_3\text{R}$ ). Calcium movement through single RyR channels or  $\text{IP}_3\text{R}$  channels produce highly localised elementary signals, termed a quark or blip respectively. These elementary signals can either activate highly localised cellular processes in the immediate vicinity of the  $\text{Ca}^{2+}$  channel, or by activating other channels throughout the cell. Alternatively they may initiate more complex  $\text{Ca}^{2+}$  signalling events resulting from the coordinated opening of clusters of RyRs or  $\text{IP}_3\text{Rs}$ , known as sparks or

puffs, respectively (Berridge 1997; Bootman *et al.* 1997; Lipp & Niggli 1998). Sparks and puffs contribute to  $\text{Ca}^{2+}$  waves and oscillations, which are global  $\text{Ca}^{2+}$  release events.

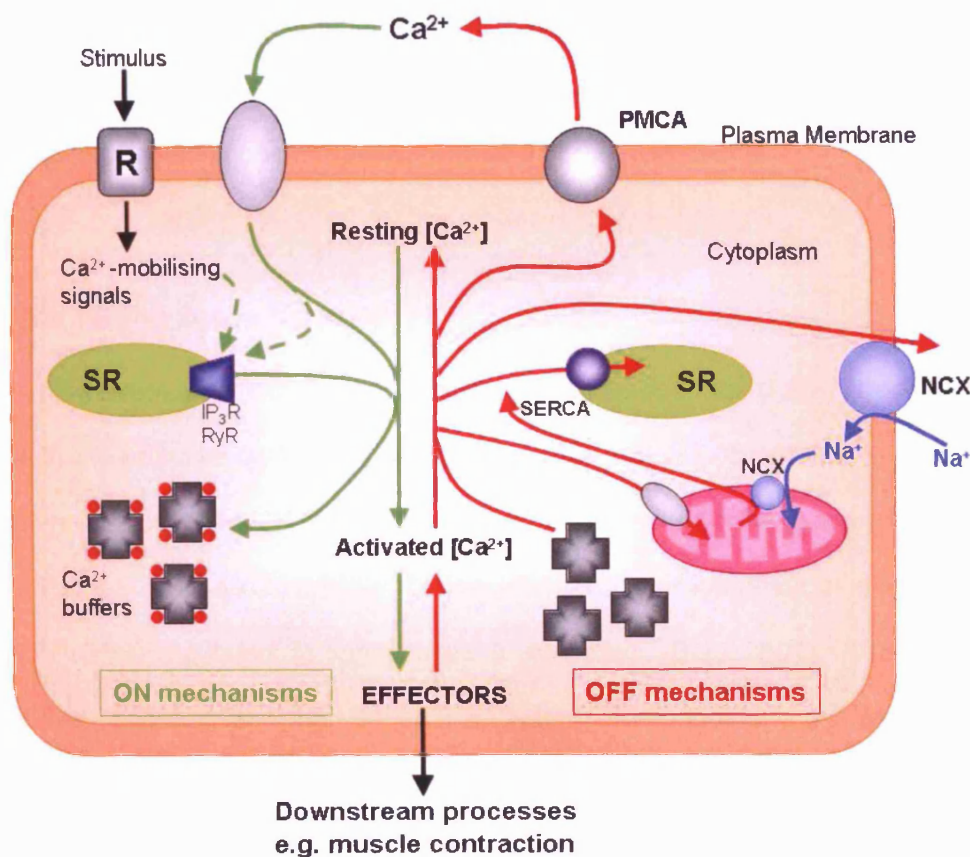


**Figure 1.1. The  $\text{Ca}^{2+}$  signalling network**

Maintaining  $\text{Ca}^{2+}$  homeostasis in the cell depends on highly-regulated interaction between numerous channels, pumps and exchangers, and the  $\text{Ca}^{2+}$  signalling network can be simplified into four functional units (Berridge *et al.* 2000): **1. The generation of  $\text{Ca}^{2+}$ -mobilising signals:** Signalling is triggered by a stimulus (normally acting via a plasma membrane receptor (R)) that generates various  $\text{Ca}^{2+}$ -mobilising signals. **2. ON mechanisms:** During the ON reactions, stimuli induce both the entry of external  $\text{Ca}^{2+}$  and the formation of second messengers that release internal  $\text{Ca}^{2+}$  stored within the SR. Most of this  $\text{Ca}^{2+}$  (shown as red circles) is bound to buffers, whereas a small proportion binds to the effectors that activate various cellular processes operating over a wide temporal spectrum. **3.  $\text{Ca}^{2+}$ -sensitive processes:** The resultant  $\text{Ca}^{2+}$  signal activates various  $\text{Ca}^{2+}$  binding proteins (effectors), which undergo conformational change thereby modulating downstream processes, e.g. troponin C in muscle contraction. **4. OFF mechanisms:** These remove  $\text{Ca}^{2+}$  from the cytoplasm using a combination of different pumping mechanisms. During the OFF reactions,  $\text{Ca}^{2+}$  leaves the effectors and buffers and is removed from the cell by various exchangers and pumps. The  $\text{Na}^+/\text{Ca}^{2+}$  exchanger (NCX) and the plasma-membrane  $\text{Ca}^{2+}$ -ATPase (PMCA) extrude  $\text{Ca}^{2+}$  to the outside, whereas the sarco(endo)plasmic reticulum  $\text{Ca}^{2+}$ -ATPase (SERCA) pumps  $\text{Ca}^{2+}$  back into the ER. Mitochondria also have an active function during the recovery process in that they sequester  $\text{Ca}^{2+}$  rapidly through a uniporter, and this is then released more slowly back into the cytoplasm to be dealt with by the SERCA and the PMCA. When the cells are at rest, the OFF mechanisms maintain a low concentration of  $\text{Ca}^{2+}$ , but are temporarily overwhelmed when external stimuli activate the ON mechanisms (Adapted from Berridge *et al.* 2003).

In the heart, carefully regulated  $\text{Ca}^{2+}$  fluxes achieve a synchronised cellular depolarisation and subsequent activation of the contractile proteins by excitation-contraction (EC) coupling (Bers 2002). To maintain this process, intracellular  $\text{Ca}^{2+}$  homeostasis must be carefully regulated to synchronise depolarisation and contraction during systole (i.e. the time at which ventricular contraction occurs) and that relaxation occurs fully during diastole (i.e. the time at which ventricular relaxation occurs) before the start of the next cycle.

### **1.1.1 The cardiac action potential**

The initiating event in cardiac EC coupling is the action potential (AP). The AP causes a reversal of the membrane potential to a positive value which is controlled by the complex interplay of many ion channels and transporters, and results in the generation of a  $\text{Ca}^{2+}$  transient. The AP is also responsible for the intercellular propagation of excitation in the heart, which allows the heart to function as a syncytium (Bers 2001). The cardiac AP consists of five distinct phases (numbered 0–4), each corresponding to a different pattern of ion flux (Figure 1.2) (Keating & Sanguinetti 2001).

The resting cardiac myocyte membrane is preferentially permeable to  $\text{K}^+$ , and it is this efflux of  $\text{K}^+$  along an electrochemical gradient that dictates the negative membrane potential. Phase 0 represents rapid depolarisation of the myocyte, which is initiated by the rapid opening of voltage-gated  $\text{Na}^+$  channels which causes a rapid influx of  $\text{Na}^+$  ions. Early repolarisation (Phase 1) is then caused by an outward current of  $\text{K}^+$  ions ( $I_{t0}$ ) through transiently opened  $\text{K}^+$  channels due to the inactivation of cardiac  $\text{Na}^+$  channels. This occurs immediately after the peak of depolarisation and is recognised as a partial repolarisation of the membrane. The plateau that follows early repolarisation (Phase 2) is the result of the slowly decreasing inward current of  $\text{Ca}^{2+}$  ions caused by the opening of the L-type  $\text{Ca}^{2+}$  channel (LTCC, also termed dihydropyridine receptors (DHPRs) or  $\text{Ca}_v1.2$ ) and gradually increasing outward current through several types of  $\text{K}^+$  channels. The process of final repolarisation (Phase 3) starts at the end of the plateau phase when the efflux of  $\text{K}^+$  from the

myocyte begins to exceed the influx of  $\text{Ca}^{2+}$ . The excess  $\text{Na}^+$  that had entered the cell during rapid depolarisation (Phase 0) is removed by the  $\text{Na}^+/\text{K}^+$ -ATPase. Similarly, most of the excess  $\text{Ca}^{2+}$  is eliminated by the  $\text{Na}^+/\text{Ca}^{2+}$  exchanger (NCX) and plasma membrane  $\text{Ca}^{2+}$ -ATPase (PMCA) as well as being pumped back into the store to restore the resting potential.

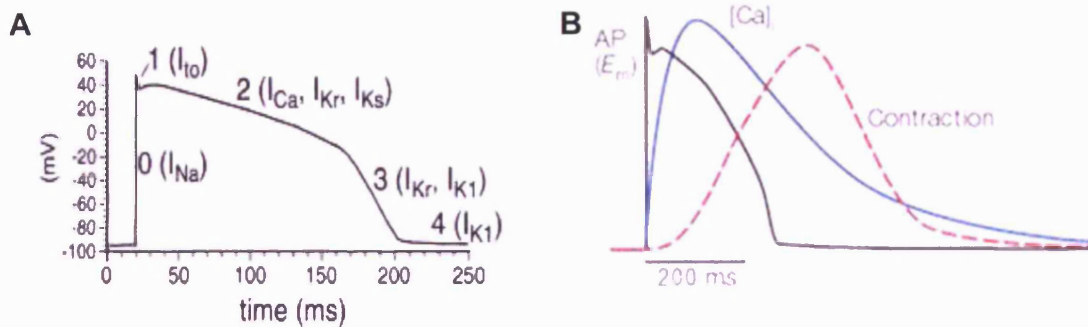


**Figure 1.2. Schematic representations of the cardiac action potential (AP) in a ventricular myocyte showing timing and morphology.**

**Panel A:** The five phases of the AP are mediated by ion fluxes, summarised as follows: **Phase 0** – rapid depolarisation caused by an inward  $\text{Na}^+$  current, signalling the onset of systole; **Phase 1** – early repolarisation, mediated by a transient outward  $\text{K}^+$  current ( $I_{\text{to}}$ ) and closure of the  $\text{Na}^+$  channels; **Phase 2** – the LTCC inward  $\text{Ca}^{2+}$  ( $I_{\text{Ca}}$ ) current contributes to the long plateau duration; **Phase 3** – many outward  $\text{K}^+$  currents and  $\text{Na}^+$  and  $\text{Ca}^{2+}$  efflux contributes late repolarisation and the restoration of the resting membrane potential, seen in Phase 4. Thus, the coordinated opening and closing of cardiac ion channels is responsible for cardiac excitability. **Panel B:** The time course of an AP,  $\text{Ca}^{2+}$  transient and contraction measured in a rabbit ventricular myocyte at  $37^\circ\text{C}$ . (adapted from Keating & Sanguinetti, 2001 and Bers, 2002).

### 1.1.2 The cardiac myocyte

The human myocyte is typically 10-20  $\mu\text{m}$  in diameter and 50-100  $\mu\text{m}$  long with a single central nucleus. Cardiac myocytes form a branched network of cells, known as a functional syncytium, and individual myocytes interconnect via specialised regions of cell membranes known as intercalated discs, which help multiple cardiac muscle cells contract rapidly and synchronously as a unit (Figure 1.3). Each individual cardiomyocyte is composed of bundles of myofibrils. Each myofibril is composed of smaller units called sarcomeres, which are the basic units of contraction and contain two types of interdigitating myofilament: a thick filament made of the protein myosin and a thin filament composed chiefly of actin, which overlap each other (Klabunde 2005).



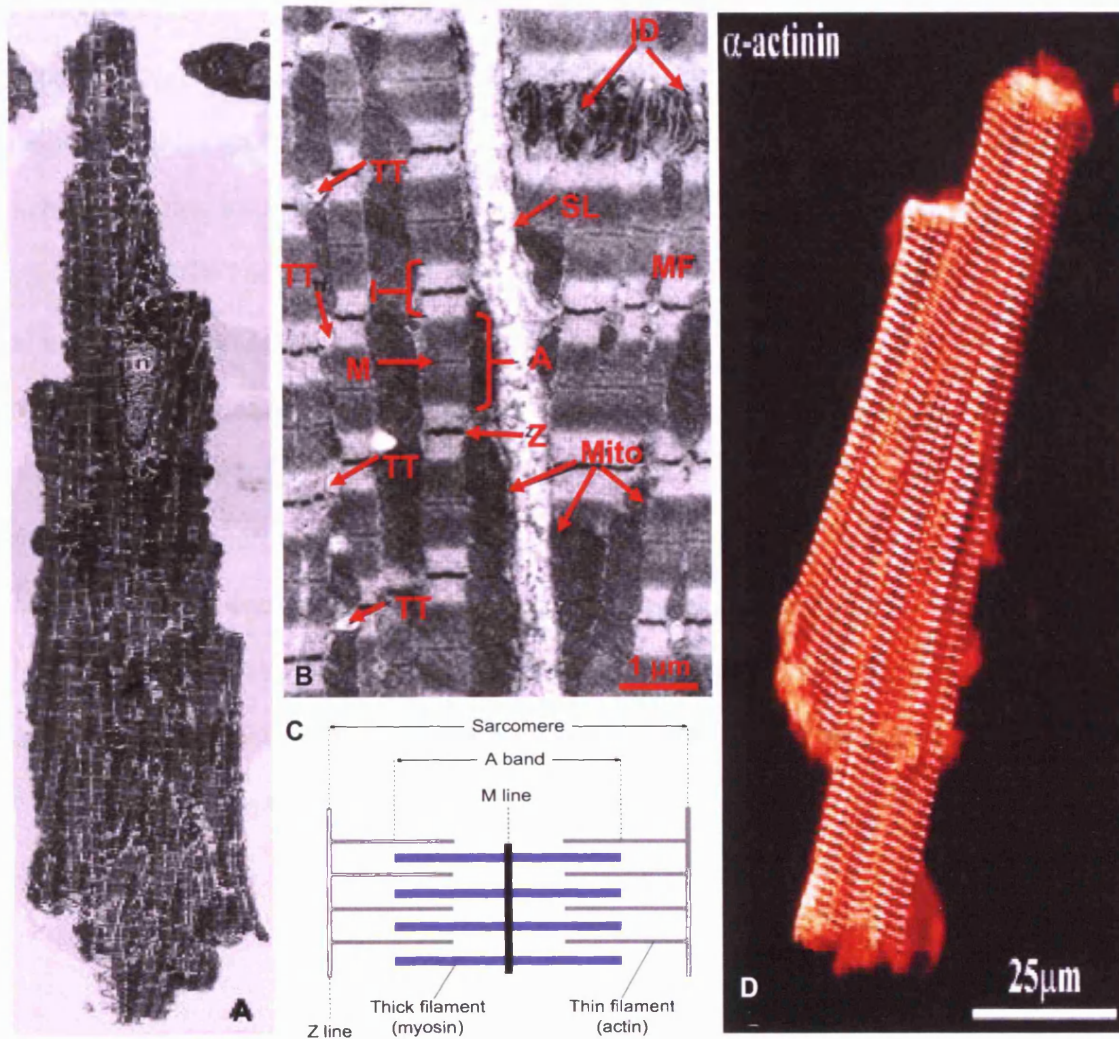


**Figure 1.3. Cardiac myocyte machinery**

**Panel A:** Thin-section electron micrograph of a single ventricular cardiomyocyte, x1,500 magnification. **Panel B:** Electron micrograph of ventricular cells showing details of ultrastructure (adapted from Berne & Levy, 1993). The sarcolemma (SL) is the boundary of the muscle cells and is extensively folded where the cells meet at the intercalated disc (ID) region. The prominent myofibrils (MF) show distinct banding patterns, including the A band (A), dark Z lines (Z), I band regions (I), and M lines (M) at the centre of each sarcomere unit. Mitochondria (Mito) occur either in rows between myofibrils or in masses just underneath the sarcolemma. Regularly spaced t-tubules (TT) appear at the Z line levels of the myofibrils. **Panel C:** Schematic representation of cardiac contractile machinery. **Panel D:** Single ventricular myocyte viewed by confocal microscopy. Image prepared by combining a stack of serial optical sections through the cell. Myofibrils (seen as striations) visualised by immunostaining with an antibody against  $\alpha$ -actinin (a component of the myofibril Z-bands) (Severs 2000).

Chemical interactions between the actin and myosin filaments cause the sarcomeres to shorten as the overlap between the two types of filaments increases via a sliding mechanism. This occurs via cross-bridge formation, whereby the myosin head units bind to

actin (Summarised in Figure 1.4). At rest, the myosin binding sites on the actin filaments are blocked by tropomyosin. During systole, contraction of the myocyte is initiated by a rapid increase in free intracellular  $\text{Ca}^{2+}$  which is released from the SR.  $\text{Ca}^{2+}$  binds to the troponin C subunit of the troponin complex, causing a conformational change and displacing tropomyosin. This frees the binding site and allows the interaction of actin and myosin. Filament sliding then occurs via a change in the angle of the cross bridge, after which the myosin head disengages, and the process is repeated. The energy for contraction is provided by adenosine triphosphate (ATP), which binds to the myosin head units and upon hydrolysis yields energy for cross-bridge movement. Myocyte contraction is an ATP-expensive process, explaining the numerous mitochondria present in myocytes. The onset of relaxation and diastole is subsequently initiated by the removal of free  $\text{Ca}^{2+}$  from the cytosol, by extrusion via the sarcolemmal pumps and exchangers as well as by re-uptake of  $\text{Ca}^{2+}$  into the SR (Klabunde 2005).

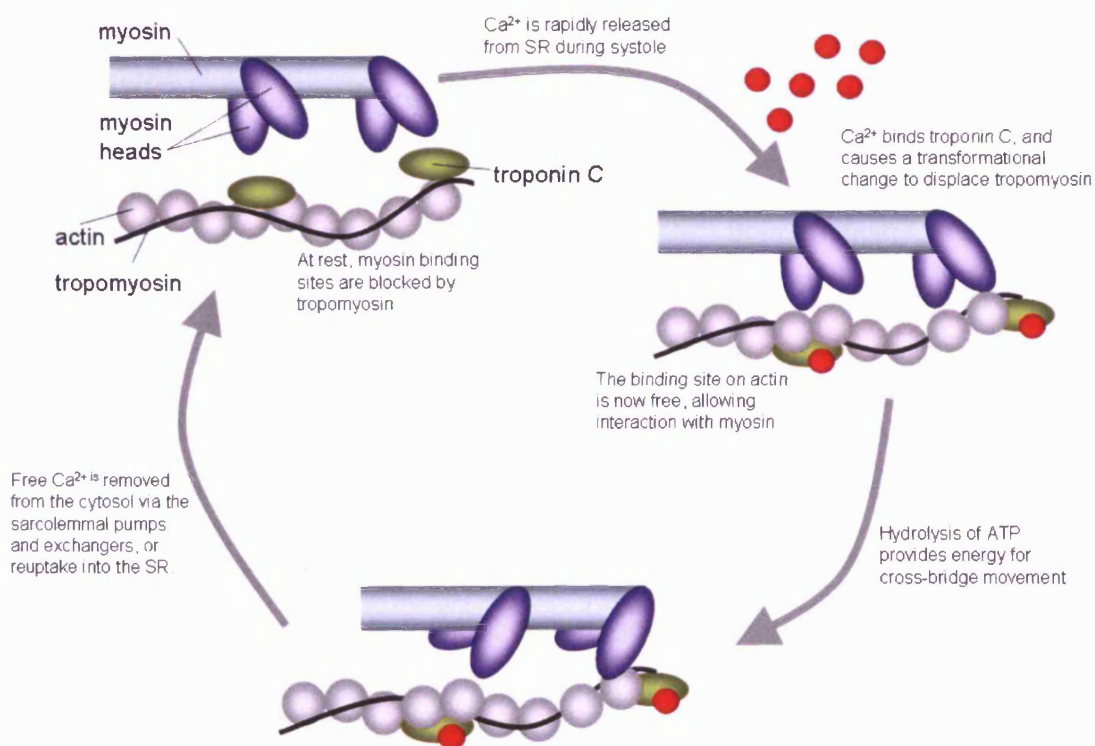


**Figure 1.4. Schematic diagram of cardiac cross bridge-formation**

### 1.1.3 Cardiac excitation-contraction (EC) coupling

Cardiac EC coupling is the key  $\text{Ca}^{2+}$  signalling process within the heart, and refers to the co-ordinated cellular depolarisation and movement of intracellular  $\text{Ca}^{2+}$  around the cardiac cell in order to bring about contraction of the heart. The ubiquitous second messenger  $\text{Ca}^{2+}$  is essential in cardiac electrical activity and is the direct activator of the myofilaments which cause contraction. Myocyte mishandling of  $\text{Ca}^{2+}$  is a central cause of both contractile dysfunction and arrhythmias in pathophysiological conditions.

In the normal heart, intracellular  $\text{Ca}^{2+}$  movements critically regulate subsequent mechanical contractions. In cardiac EC coupling, a small amount of  $\text{Ca}^{2+}$  first enters through the LTCCs during membrane depolarisation. This  $\text{Ca}^{2+}$  influx triggers a large-scale  $\text{Ca}^{2+}$  release - a process termed ' $\text{Ca}^{2+}$  induced  $\text{Ca}^{2+}$  release' (CICR) - through RyR, the  $\text{Ca}^{2+}$  release channel of the sarcoplasmic reticulum (SR). The synchronised release of multiple  $\text{Ca}^{2+}$  sparks throughout the cell increases the concentration of free  $\text{Ca}^{2+}$  within the cytosol from ~100 nM to ~1000 nM during systole (Bers 2001), creating a global intracellular  $\text{Ca}^{2+}$  transient of sufficient magnitude to bring about contraction. Due to the high buffering capacity of the cytosol, which contains numerous  $\text{Ca}^{2+}$  binding proteins (e.g. troponin, calmodulin), the amount of  $\text{Ca}^{2+}$  entering the cytoplasm must be of the order of 100  $\mu\text{M}$  in order for this increase in cytosolic  $\text{Ca}^{2+}$  concentration to be achieved and cause contraction (Bers 2001). Relaxation is initiated by dissociation of  $\text{Ca}^{2+}$  from troponin C, followed by its reuptake into the SR through phospholamban (PLB) regulated  $\text{Ca}^{2+}$ -ATPase (SERCA2a) and subsequent trans-sarcolemmal  $\text{Ca}^{2+}$  removal through the  $\text{Na}^+/\text{Ca}^{2+}$  exchanger (NCX) operating in its forward mode as well as by mitochondrial uptake (Bassani *et al.* 1994; Bers 2002). These two processes balance systolic cellular influx and SR release of  $\text{Ca}^{2+}$  such that there is no net gain or loss of cellular  $\text{Ca}^{2+}$  with each contraction-relaxation cycle. Additionally, it has been shown that RyR2 gating can also be controlled in a concentration-dependent fashion by SR luminal free  $\text{Ca}^{2+}$  (Ching *et al.* 2000), and as SR  $\text{Ca}^{2+}$  content increases a greater proportion of this  $\text{Ca}^{2+}$  pool will be released for any given trigger

(Bassani *et al.* 1995; Janczewski *et al.* 1995; Scoote & Williams 2004). Spontaneous  $\text{Ca}^{2+}$  release from the SR, independent of  $I_{\text{Ca}}$  mediated release, also occurs during normal cellular physiology, although the frequency of  $\text{Ca}^{2+}$  sparks is low and not sufficient to precipitate either a significant change in the cellular membrane potential or the activation of contractile proteins. However, in situations of SR  $\text{Ca}^{2+}$  overload, the frequency of spontaneous  $\text{Ca}^{2+}$  sparks is significantly increased, corresponding to an higher probability of RyR2 activation by an augmented luminal free  $[\text{Ca}^{2+}]$  (Cheng *et al.* 1996). This correlation between SR  $\text{Ca}^{2+}$  load and spontaneous SR  $\text{Ca}^{2+}$  release is a key property in the development of  $\text{Ca}^{2+}$  dependent arrhythmias, and the increased  $\text{Ca}^{2+}$  load or increased sensitivity to normal store load is involved in the generation of cardiac glycoside-linked arrhythmia (such as ouabain, discussed in Chapter 5). Consequently, the inter-reliance of processes involved in EC coupling means that a defect or mutation in any one of its components could lead to abnormal  $\text{Ca}^{2+}$  handling, such as cardiac arrhythmia.

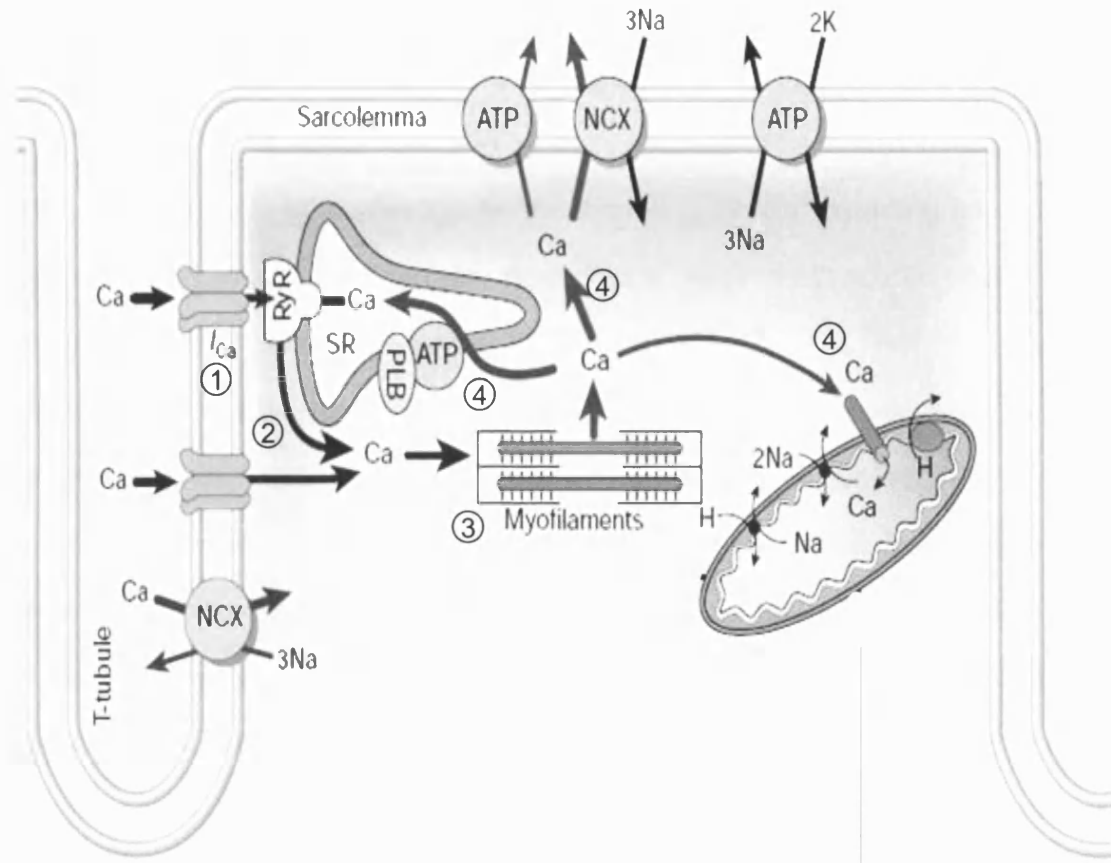


**Figure 1.5. Schematic representation of cardiac EC coupling**

After depolarisation, Ca<sup>2+</sup> enters the cell ( $I_{Ca}$ ) (1), evoking release from the SR via the RyR (2). After initiation of contraction (3), Ca<sup>2+</sup> is extruded from the myofilaments and cytosol by the SR Ca<sup>2+</sup>-ATPase pump modulated by phospholamban (PLB), sarcolemmal Ca<sup>2+</sup>-ATPase pump, Na<sup>+</sup>/Ca<sup>2+</sup> exchanger (NCX), and mitochondrial uniporter (Bers 2002) (4).

### 1.1.3.1 Tuning EC coupling by phosphorylation

An important influence on myocardial Ca<sup>2+</sup> cycling is  $\beta$ -adrenergic receptor ( $\beta$ -AR) stimulation mediated by sympathetic nerves and circulating catecholamines. Activation of these receptors can alter the properties of EC coupling components through signal amplification cascades that results in the phosphorylation of either the ion channels and pumps themselves, or the regulatory proteins attached to them (Scoote & Williams 2004). It has been appreciated for some years that the amplitude of Ca<sup>2+</sup> transients generated by release of SR Ca<sup>2+</sup> into the cytosol determines the contractile force (inotropy) of the heart. Catecholamine mediated phosphorylation will increase (1) the inward Ca<sup>2+</sup> current, (2) SR

$\text{Ca}^{2+}$  loading and (3) its release into the cytosol, thereby enhancing contractile force. The effects of  $\beta$ -AR activation are complex, with the function of most EC coupling proteins being affected by PKA and CaMKII mediated phosphorylation. Phosphorylation is the most important post-translational mechanism for synchronising the  $\text{Ca}^{2+}$  handling machinery and defective phosphorylation has long been viewed as a cause of EC coupling dysfunction in cardiac disease (Bers 2001; George *et al.* 2007a; 2008a).

This signalling cascade begins with  $\beta$ -AR activation, either by sympathetic nerves or circulating catecholamines. As summarised in Figure 1.6, this subsequently allows the activation of adenylate cyclase and the generation of cAMP, which in turn switches on phosphorylation enzymes such as PKA and CaMKII (Scoote & Williams 2004). The functional consequences of phosphorylation can be grouped into inotropic and lusitropic effects. Inotropic effects include: (1) A 2-4 fold greater influx of  $\text{Ca}^{2+}$  through the phosphorylated LTCC channel for any given excitation (Tsien *et al.* 1986; McDonald *et al.* 1994); (2) Phosphorylation of RyR2 increases its sensitivity to activation by  $\text{Ca}^{2+}$  (Valdivia *et al.* 1995; Marx *et al.* 2000a) and this directly increases SR  $\text{Ca}^{2+}$  release. Lusitropic effects include: (1) Greater SR  $\text{Ca}^{2+}$  re-uptake through SERCA as a result of phosphorylation of its regulatory protein PLB, so that a larger SR load is expected; (2) A decrease in myofilament  $\text{Ca}^{2+}$  sensitivity (due to phosphorylation of troponin and the dissociation of  $\text{Ca}^{2+}$ ); (3) Enhanced NCX activity due to its phosphorylation and hence an increase in  $\text{Ca}^{2+}$  efflux, again increasing the rate of relaxation. These lusitropic effects are key to ensuring that there is sufficient SR  $\text{Ca}^{2+}$  available for the next cellular depolarisation, since reduced SR  $\text{Ca}^{2+}$  could result in weakened contractile force (Scoote & Williams 2004).

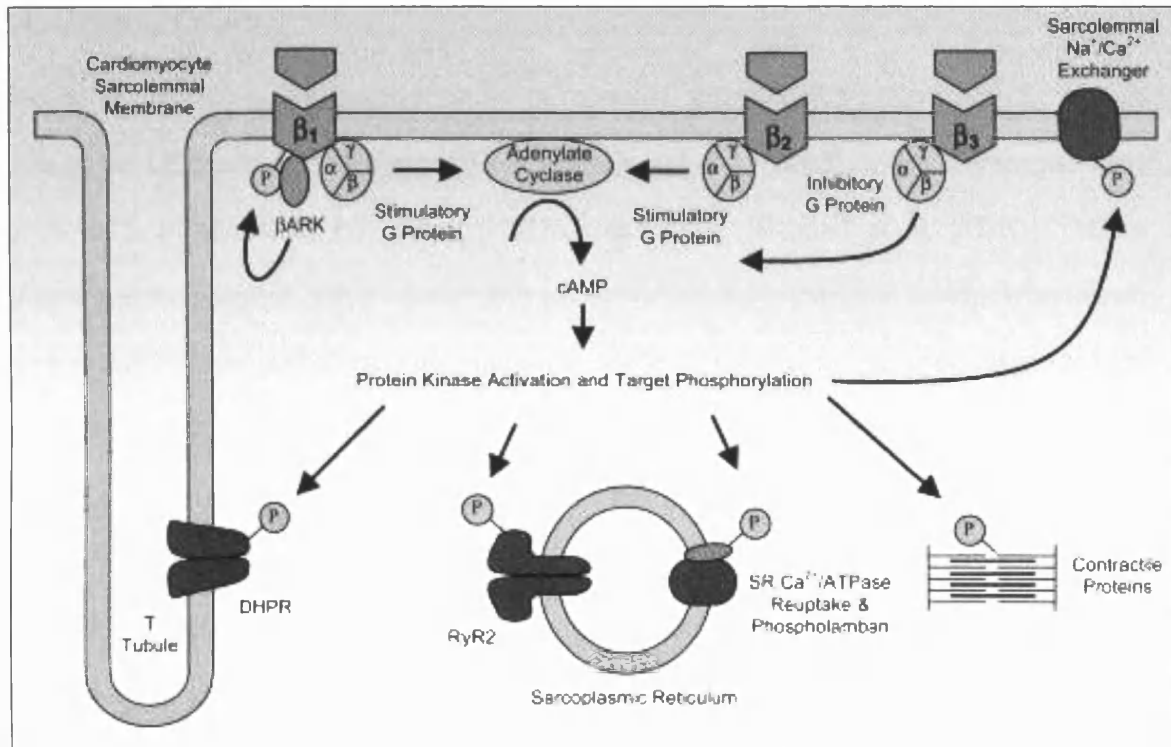


**Figure 1.6. Schematic representation of the  $\beta$ -AR pathway**

$\beta$ -AR dependent EC coupling augmentation in the heart. In the human heart  $\beta_1$  and  $\beta_2$ -adrenergic receptor signal transduction pathways activate protein kinase A (PKA), causing target protein phosphorylation, which enhances both inotropic and lusitropic aspects of EC coupling.  $\beta_3$ -AR activation inhibits protein kinase activation. Phosphorylation of  $\beta$ -AR via  $\beta$ -AR kinase ( $\beta$ ARK) uncouples the receptor from its signal transduction pathways, acting as a negative feedback mechanism in situations of hyper-catecholaminergic drive. Experience with positive inotropic drugs in heart failure demonstrates that maximal functional augmentation via this process is rapidly achieved. Ongoing  $\beta$ -AR activation produces no further functional improvement, rather detrimental functional states are induced which lead to contractile dysfunction and arrhythmogenesis. (Scoote & Williams 2004).

## 1.2 EC coupling in cardiac disease

As discussed above, normal cellular  $\text{Ca}^{2+}$  homeostasis and co-ordinated ion flux is maintained by the balanced activities of EC coupling machinery. Defects in any of the components of the EC machinery would lead to abnormal  $\text{Ca}^{2+}$  handling, and has been implicated in cardiac disease.

### 1.2.1 Heart failure

Heart failure (HF) is the leading cause of mortality, affecting 5.3 million and 3.8 million people in the USA and Europe respectively (Rosamond *et al.* 2008), with a 2-year mortality rate of ~50% in advanced HF cases (NYHA class III-IV) (Lehnart *et al.* 2005a). HF is characterised by contractile dysfunction and activation of neurohormonal factors (Braunwald & Bristow 2000; Yano 2008). In a heart that has suffered myocardial damage, regardless of the initial cause of the damage (such as hypertension, myocardial ischaemia, or cardiomyopathy), HF eventually occurs if such damage persists for a prolonged period (Braunwald & Bristow 2000; Yano *et al.* 2005a, 2008). In the initial stages, compensation for the myocardial damage and maintenance of haemodynamics can occur via activation of both the sympathetic nervous system and the renin-angiotensin (RA) system, resulting in ventricular dilatation and/or hypertrophy. However, if the decreased cardiac function persists, the myocardial damage becomes progressive and irreversible, and the heart can no longer meet the metabolic demand of the body; this is widely regarded as the 'classic' HF phenotype (Braunwald & Bristow 2000; Yano *et al.* 2005a, 2008).

The physiological process that determines contractile performance is EC coupling, and it is appreciated that detrimental alteration of the proteins involved in this process is a potential factor in the pathogenesis of HF. Evidence has accumulated that abnormal intracellular  $\text{Ca}^{2+}$  handling by the SR plays a central role in the pathogenesis of HF, via reduced SR uptake and abnormal SR  $\text{Ca}^{2+}$  release (Hasenfuss & Pieske 2002; Yano *et al.* 2005a, 2008). The reduced SR  $\text{Ca}^{2+}$  uptake leads to a depleted  $\text{Ca}^{2+}$  store, which in turn limits  $\text{Ca}^{2+}$  release. As a result of this, a reduced contractile force is generated (Lindner *et al.* 1998).

A hallmark feature of HF pathogenesis is impaired SR function that predominantly manifests as reduced SR  $\text{Ca}^{2+}$  load via decreased SR  $\text{Ca}^{2+}$ -ATPase (SERCA) activity (Bers 2001; Pogwizd *et al.* 2001; Houser *et al.* 2000). Both an upregulation of NCX and a reduction in SERCA2a activity may be responsible for the reduced SR  $\text{Ca}^{2+}$  content observed in HF (Hasenfuss & Pieske 2002). Both of these alterations could impair the



restoration of SR  $\text{Ca}^{2+}$  stores during diastole, therefore reducing the amount of  $\text{Ca}^{2+}$  available for the next wave of depolarisation. This is believed to be the primary factor in the defective EC coupling seen in HF (Lindner *et al.* 1998).

Since the SR  $\text{Ca}^{2+}$  content is reduced in HF, the threshold SR content for  $\text{Ca}^{2+}$  release may be reduced, leading to a susceptibility to aberrant  $\text{Ca}^{2+}$  release (or spontaneous  $\text{Ca}^{2+}$  leak) at lower cytosolic  $[\text{Ca}^{2+}]$ . RyRs are coupled to proteins at the luminal SR surface (triadin, junctin, and calsequestrin) (Bers 2004). Since these proteins buffer luminal  $\text{Ca}^{2+}$  and modulate the  $\text{Ca}^{2+}$  release process (Bers 2004), structural and functional alterations in these proteins may be causally involved in the development of defective intraluminal  $[\text{Ca}^{2+}]$  regulation seen in HF. A hypersensitivity of RyR2 channel opening to entirely 'normal' cytosolic  $[\text{Ca}^{2+}]$  may contribute to the presence of a spontaneous  $\text{Ca}^{2+}$  leak at much lower levels of cytosolic  $[\text{Ca}^{2+}]$  in HF than in the normal SR (i.e., approximately 100 nM during diastole). This spontaneous  $\text{Ca}^{2+}$  leak may lead to a delayed after-depolarisation (DAD), which can trigger lethal arrhythmias (Brini 2004; Yano *et al.* 2005a).

### **1.2.2 Sudden Cardiac Death (SCD)**

Sudden cardiac death can be defined as natural, nonviolent, unexpected death, occurring within 6 hours of the onset of symptoms from a stable medical condition (Virmani 2001). The rate of cardiac deaths that are sudden is approximately 50%, and decreases with age. The causes of sudden cardiac death are diverse, and are a function of age. In children and adolescents, coronary anomalies, hypertrophic cardiomyopathy and myocarditis are frequent substrates for lethal arrhythmias; in adults, coronary atherosclerosis and acquired forms of cardiomyopathy are the most common findings at autopsies of sudden cardiac death. Congenital coronary artery anomalies, result in sudden death almost exclusively in adults younger than age 35. In the older population (> 35 years old), approximately 60% of sudden coronary death is caused by coronary thrombosis, the rest die with severe coronary disease in the absence of thrombosis. The two major substrates of coronary thrombosis are plaque

rupture and plaque erosion, and are not only different pathologically, but are seen in patients with divergent risk factor profiles. Plaque rupture is the most common cause of fatal coronary thrombus, and is characterized by necrotic core with a thin fibrous cap, infiltrated by macrophages. The factors that result in plaque instability and rupture are largely unknown, and are under intense scrutiny; morphologic studies have identified serum lipid abnormalities as a key risk factor in the development of plaque rupture. Plaque erosion, in contrast to plaque rupture, is seen in younger men and women, is not associated with lipid abnormalities, and does not result from exposure of the lipid core to the lumen (Virmani 2001).

### **1.2.3 Cardiac arrhythmia**

Arrhythmia results from perturbation of the robustly controlled fluxes of  $\text{Na}^+$ ,  $\text{K}^+$ , and  $\text{Ca}^{2+}$  ions both within cardiomyocytes and between the myocardium and the external milieu (Bers 2001) and are responsible for >70% of out-of-hospital cardiac arrests (George *et al.* 2008b). These ionic fluxes are highly interdependent, and therefore localised disruption may exacerbate global ion flux imbalance resulting in complete ablation of synchronous cardiac electrical activity. Over the last two decades, defective mechanisms in arrhythmogenic ion fluxes have been elucidated by functional characterisation of  $\text{Na}^+$  and  $\text{K}^+$  channels containing genetic mutations (termed cardiac channelopathies). One such channelopathy is long QT syndrome, which affects the plateau and repolarisation phases of the human ventricular AP, and has been linked to mutations in both  $\text{Na}^+$  and  $\text{K}^+$  channels (specifically  $\text{K}_{\text{ir}}2.1$ ,  $\text{KCNQ1}$ ,  $\text{KCNH2}$  and  $\text{Na}_v1.5$ ) (Kass 2005; Meisler & Kearney 2005; Moss & Kass 2005). Currently the genetic basis of  $\text{Ca}^{2+}$  handling dysfunction in arrhythmia is the focus of widespread attention.

Intracellular and trans-plasmalemmal  $\text{Ca}^{2+}$  fluxes coordinate multiple facets of cardiac function, and precisely controlled  $\text{Ca}^{2+}$  cycling is a prerequisite for normal cardiac rhythm and contractility. The role of  $\text{Ca}^{2+}$  in arrhythmogenesis falls broadly into two categories – a

direct role by generating afterdepolarisations, and an indirect role by modulating the duration and time course of the cardiac AP (Antoons & Sipido 2008). Afterdepolarisations are carried by a net inward current and can occur within the plateau or repolarisation phase of the AP (early afterdepolarisations, EADs) or after repolarisation has completed (delayed afterdepolarisations, DADs). DADs can directly trigger APs to initiate arrhythmias, and are discussed in greater detail in Chapter 5.

Genetic mutations underlying malignant arrhythmias have recently been identified in cardiac  $\text{Ca}^{2+}$  channels such as LTCCs (Splawski *et al.* 2004) and ryanodine receptors (RyR2), both of which are large multifunctional  $\text{Ca}^{2+}$  release channels that are crucial for cardiac development EC coupling (For reviews see Bers 2004; Chelu *et al.* 2004; Fill & Copello 2002; George *et al.* 2005; Meissner 1994; 2004). However, unlike defects in  $\text{Na}^+$  and  $\text{K}^+$  ion handling, cellular  $\text{Ca}^{2+}$  dysfunction in arrhythmia does not arise exclusively from  $\text{Ca}^{2+}$  channel abnormalities, but also from mutation-linked defects in intra-organellar  $\text{Ca}^{2+}$  storage (Calsequestrin (CSQ) – a major  $\text{Ca}^{2+}$  binding protein in the SR, implicated in catecholaminergic polymorphic ventricular tachycardia (CPVT) (see Section 1.4.1.2)) (Lahat *et al.* 2004; Postma *et al.* 2002; Terentyev *et al.* 2006),  $\text{Ca}^{2+}$  sequestration (phospholamban (PLB) – a regulator of SERCA) (Haghighi *et al.* 2006; Schmitt *et al.* 2003), and altered cytoplasmic  $\text{Ca}^{2+}$  signals by  $\text{Ca}^{2+}$ -binding proteins involved in EC coupling (tropomyosin and troponin) (Hedman *et al.* 2004; Watkins *et al.* 1995). Furthermore, alterations in cytoskeletal architecture that disrupt the spatial organisation of  $\text{Ca}^{2+}$  signalling networks may be highly arrhythmogenic in the absence of any genetic defects in  $\text{Ca}^{2+}$  handling machinery. Consequently, the complex physical and functional interplay between  $\text{Ca}^{2+}$  pumps, channels, stores and exchangers predicts that defects in diverse aspects of cardiomyocyte  $\text{Ca}^{2+}$  cycling directly contribute to an increased arrhythmogenic propensity (George *et al.* 2007a) and RyR is a pivotal component which modulates these interactions.

### 1.3 The ryanodine receptor

The ryanodine receptor (RyR) is an intracellular  $\text{Ca}^{2+}$  release channel located on the SR/ER of muscle and non-muscle cells, which regulates the release of stored  $\text{Ca}^{2+}$  from the SR lumen during  $\text{Ca}^{2+}$  signalling processes such as EC coupling. RyRs were initially observed in skeletal muscle, visualised in electron-micrographs as large electron-dense bridging structures (termed 'feet') situated along the SR (Figure 1.7), between the sarcolemmal t-tubule and the junctional SR (Franzini 1970). Caldwell & Caswell (1982) later provided biochemical evidence for a high molecular weight protein which potentially represented these junctional feet. The RyR later gained its name in the late 1980s after it was found to bind ryanodine (Pessah *et al.* 1985), a plant alkaloid that enabled purification and molecular characterisation of the protein by its selective and specific affinity for the channel.



**Figure 1.7. An electron micrograph of a section through a triad junction of a frog muscle cell**

Shows a central t-tubular element flanked on either side by a terminal cisternae element of the SR. The arrows point to electron dense junctional feet spanning the junctional gap on either side of the t-tubule between the t-tubule and terminal cisternae (Franzini-Armstrong 1973).

Ryanodine is a natural product found in the stems and roots of members of the genus *Ryania*, which grows as a shrub found in Central and South America, and was originally used as an insecticide (Sutko *et al.* 1997). Ryanodine was found to cause irreversible contracture of skeletal muscle and progressive decline in cardiac muscle twitches (Jenden & Fairhurst 1969; Sutko & Willerson 1980). It was later found that ryanodine appeared to bind specifically to the junctional regions of the SR, where the electron-dense “feet” were initially seen (Flucher & Franzini-Armstrong 1996). The RyR is the only cellular target of ryanodine reported to date, which it binds with high affinity and specificity, when in its open conformation, and thus, ryanodine-binding is often used as an index of channel activation *in vitro*.

RyR has been purified from skeletal (Inui *et al.* 1987a; Lai *et al.* 1987) and cardiac muscle (Inui *et al.* 1987a; Lai *et al.* 1988a) using [<sup>3</sup>H]-ryanodine as a selective marker and found to exist in a tetrameric form that sediments as a very large complex by sucrose density gradient centrifugation. The purified protein, incorporated into an artificial planar lipid bilayer, functions as a Ca<sup>2+</sup> channel, with characteristics identical to the Ca<sup>2+</sup> release channel observed upon incorporation of the crude SR fraction (Fill & Copello 2002; Hymel *et al.* 1988; Imagawa *et al.* 1987; Lai *et al.* 1987).

The RyR was found to be a 2.2 MDa homotetramer (Lai & Meissner 1989a) comprising of four 560 kDa subunits (Takeshima *et al.* 1989), and it was later demonstrated that the individual RyRs were organised in a distinct pattern on the SR closely associated with the LTCCs – so-called couplons or Ca<sup>2+</sup> release units (CRUs) (Franzini-Armstrong *et al.* 1999). A typical cardiac couplon may have about 100 RyRs and 10-25 L-type channels (Bers 2001), and the spatial distribution of these two Ca<sup>2+</sup> channels is crucial to the co-ordination of CICR. The importance of this spatial organisation is emphasised by reports that ventricular myocytes from spontaneously hypertensive rats that develop HF, displayed both a reduced ability to trigger SR Ca<sup>2+</sup> release and increased spatial dispersion of the transverse tubules (TTs). The remodelled TTs in these myocytes no longer exhibited regularly organised structures, and moved within the sarcomere away from the Z-line structures and associated

RyRs. These 'orphaned' RyRs were found to be responsible for the dyssynchronous  $\text{Ca}^{2+}$  sparks that have been linked to blunted contractility and, probably  $\text{Ca}^{2+}$ -dependent arrhythmias in diverse models of HF (Song *et al.* 2006).

### 1.3.1 Molecular cloning of RyR isoforms and their tissue distribution

In mammals, three isoforms of RyR each encoded by a separate gene and each with specific tissue distribution, have been cloned and fully sequenced. RyRs were first cloned from mammalian skeletal (RyR1) and cardiac muscle (RyR2) (Marks *et al.* 1989; Otsu *et al.* 1990; Takeshima *et al.* 1989). A third mammalian isoform (RyR3) was cloned from rabbit brain and a mink lung epithelial cell line (Giannini *et al.* 1992; Hakamata *et al.* 1992). According to the most recent GenBank entries for RyR, the gene for RyR1 is located on chromosome 19q13.1 in humans, and spans 106 exons. RyR2 spans 105 exons on chromosome 1q42.1-43, and RyR3 has been mapped to chromosome 15q14-15 and comprises 104 exons.

Similar isoforms have been cloned from non-mammalian vertebrates, including chicken and bullfrog (Ottini *et al.* 1996; Oyamada *et al.* 1994), though they express only two distinct isoforms –  $\alpha$  and  $\beta$ . The non-mammalian vertebrate RyR $\alpha$  isoform is homologous to the mammalian skeletal muscle isoform RyR1, while the RyR $\beta$  is a homologue of the mammalian RyR3. Although RyRs were originally discovered in vertebrates, they have more recently been identified in invertebrates, including *C. elegans* and *D. melanogaster* (Maryon *et al.* 1996; Takeshima *et al.* 1994).

Expression of RyR1 is relatively abundant in skeletal muscle, although it is also expressed at lower levels in cardiac and smooth muscle, cerebellum and adrenal glands (Kuwajima *et al.* 1992; Marks *et al.* 1989; Ottini *et al.* 1996; Takeshima *et al.* 1989). RyR2 is predominantly expressed in cardiac tissue, but is also found in brain, and at lower levels, in the stomach, lungs and thymus (Giannini *et al.* 1995; Nakai *et al.* 1990), while RyR3 is expressed in a variety of tissues including the brain, diaphragm and slow twitch skeletal

muscle (Giannini *et al.* 1992, 1995; Hakamata *et al.* 1992; Ottini *et al.* 1996). Despite the differences in tissue distribution, the three isoforms exhibit significant sequence homology. RyR1 and RyR2 are 66% identical, and RyR3 is 67-70% identical to RyR1 and RyR2 (Franzini-Armstrong & Protasi 1997; Sutko & Airey 1996). The isoform sequences differ in three divergent regions (DR) which are thought to underpin the different physiological roles of the isoforms. The three isoforms of RyR share a common structure, exhibiting an overall mushroom shape with a 4-fold cyclic symmetry around an axis perpendicular to the membrane, consistent with the tetrameric nature of the channel (see Figure 1.8).

### 1.3.2 Structure of the RyR

Three-dimensional structural information is essential to an understanding of the functional properties of RyRs. However, because RyRs are very large integral membrane proteins, the detailed atomic three-dimensional structure of the RyR is not known and awaits crystallisation of the protein though this is proving far more complex than first anticipated due to its large size (George *et al.* 2005). In the absence of atomic resolution of RyR structure, cryo-electron microscopy (cryo-EM) has, to date, been the only feasible technique for obtaining reliable information about the 3D architecture of RyRs. In conjunction with computerised single particle image processing, this method is a powerful approach for determining the 3D structures of macromolecules and macromolecular assemblies. Cryo-EM has eliminated the artefacts associated with chemical fixation, dehydration, and contrast enhancement by heavy metals, which have limited EM in the past, and it permits resolution of the 'true' structure of the specimen. However, to compensate for the low signal-to-noise ratio inherent in micrographs of ice-embedded macromolecules, it is necessary to average thousands of images of individual macromolecules to achieve even a moderate resolution (20 Å) (Franzini-Armstrong *et al.* 1999; George *et al.* 2005).

The RyR is the largest known ion channel, with a total molecular mass of ~2.2 MDa. Based on gel permeation chromatography characteristics (Inui *et al.* 1987b), stoichiometry of

ryanodine binding (Lai *et al.* 1988b, 1989b) and its quatrefoil appearance, it was deduced that the RyR exists as a homotetramer (Lai *et al.* 1988b; Wagenknecht *et al.* 1989), with each subunit consisting of approximately 5000 residues (Franzini-Armstrong & Protasi 1997; Mackrill 1999). The structure consists of two major components; firstly, a large, quatrefoil cytoplasmic assembly (28 nm x 28 nm x 12 nm) widely assigned ten distinct interconnected globular domains, which contain “clamps” located at the corners of the cytoplasmic structure and connecting structures termed “handles” (Radermacher *et al.* 1994), and secondly a differentiated small transmembrane assembly (12 nm x 12 nm x 7 nm) (Figure 1.8).

Recently, computational advances have facilitated the resolution of RyR1 at 9.6 Å (Serysheva *et al.* 2008), using cryo-EM of frozen-hydrated, detergent solubilised individual isolated channels in conjunction with single-particle image processing (Radermacher *et al.* 1994; Samsó *et al.* 2005; Serysheva *et al.* 2005, 2008; Sharma *et al.* 2000; Wagenknecht *et al.* 1989, 1995). The three-dimensional reconstruction revealed that the cytoplasmic domain of RyR is a very open structure with clearly identifiable regions and solvent accessible spaces (Williams *et al.* 2001). The structure of RyR1 has also been determined in both closed and open conformations (Orlova *et al.* 1996; Samsó & Wagenknecht 1998). Although the overall shape of the protein was similar in both conformations, there were some structural differences between the channel states (Serysheva *et al.* 1995; Orlova *et al.* 1996; Sharma *et al.* 2000) which indicate that alterations in the functional state of the RyR involve long-range conformational ordering of both the cytoplasmic and TM domains of the channel:

- Most significantly, the open state showed the presence of a low central density (approximately 2 nm in diameter) in the TM assembly of the open form connecting the luminal and cytoplasmic sides, indicating a single pore within a tetrameric channel.
- In the open state, the channel is slightly taller due to an elongation of the TM assembly and the clamp-shaped domains at the corners of the structure.
- The TM assembly is rotated by approximately 4° with respect to the cytoplasmic region.
- Two subdomains of the clamp region that are adjacent in the closed state are separated



during channel opening.

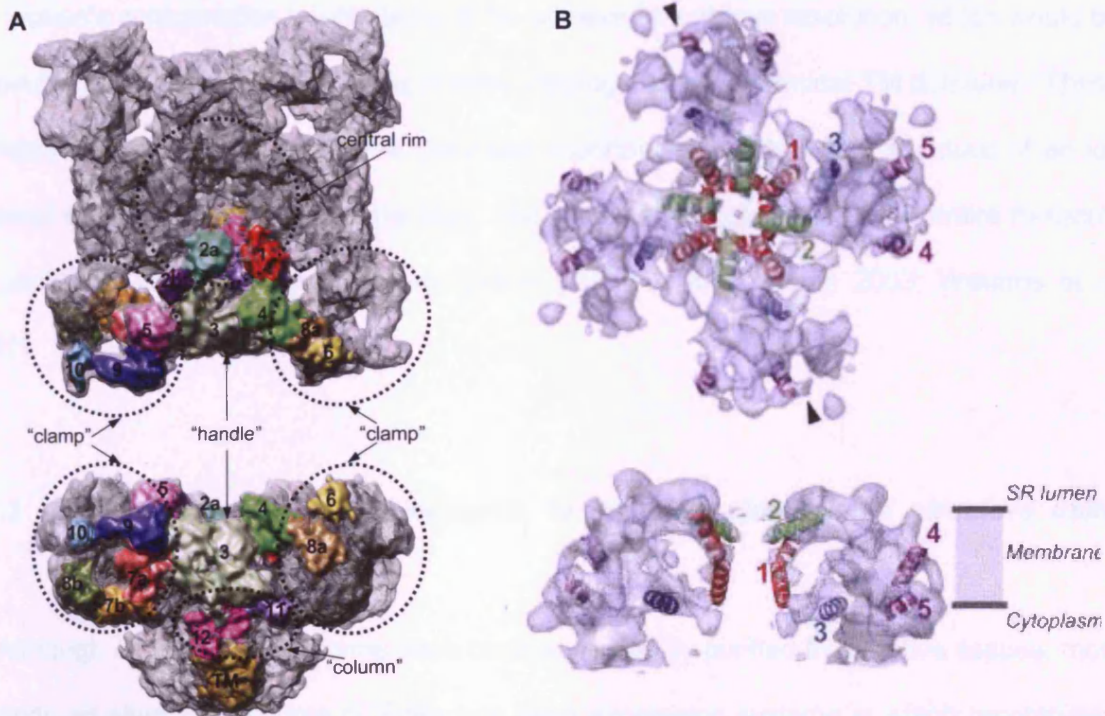


**Figure 1.8. The three-dimensional structure of RyR**

**Panel A:** A 9.6-Å resolution cryo-EM density map of RyR1 in closed state, viewed from cytoplasm (top panel) and in a side view (bottom panel). Domains are shown within one of the RyR1 subunits. A domain is interpreted as compact protein density, and the boundary of a domain tends to be weakly connected with its adjacent densities. Poorly connected densities between subregions 6 and 8a and between 10 and 8b may be hinges between domains with high local structural flexibility. The individual domains are mapped into the distinct morphological units: clamp is formed by subregions 5, 7a, 7b, 8b, 9, and 10 from one monomer and by subregions 6 and 8a from adjacent subunit; handle is formed by subregions 3 and 4; the central rim is formed by subregions 1, 2a, and 2b; and column is formed by subregions 11 and 12 (Serysheva *et al.* 2008). **Panel B:** Putative helices in the RyR1 membrane-spanning region. The top panel shows a stereoview of the membrane-spanning region viewed from the SR luminal side along the 4-fold axis. The densities attributable to  $\alpha$  helices are annotated as colour ribbons: red, the inner helix; green, the pore helix; blue and purple, the other helices. The bottom panel shows a side view (normal to the 4-fold axis) of two of the four subunits of RyR1 with annotated helices showing the relative positions of putative  $\alpha$  helices within the SR membrane. A high contour level is used in to emphasise the strongest densities interpreted as  $\alpha$  helices (Ludtke *et al.* 2005).

Although the resolution of the RyR three-dimensional structure using cryo-EM is constantly improving with the advent of more sophisticated sample preparation techniques and analysis software (Serysheva *et al.* 2005, 2008), the determination of the exact nature of the protein's conformation is only likely to be achieved by atomic resolution, which would be particularly useful in determining the precise topology of the C-terminal TM domains. These membrane-spanning fragments are the most important elements in the structure of an ion channel because they delineate the pore, and constrain the structure of the entire molecule by anchoring the protein into the membrane (Dulhunty & Pouliquin 2003; Williams *et al.* 2001).

### **1.3.3 Correlating the linear sequence to the three-dimensional structure using recombinant RyR**

Although all three RyR isoforms have been successfully purified from native tissues, more recently an alternative source of RyRs has been expression systems in which recombinant wild type or genetically modified RyR proteins can be produced from cDNAs. Gene fusions of RyRs and Glutathione-S-Transferase (GST) or green fluorescent protein (GFP) have been shown to be useful for 'epitope-mapping' within the three-dimensional cryo-EM. In this approach, since the GFP or GST are covalently attached to the RyR, every receptor image contains the label within each of the four RyR subunits, and the positions of various residues can be located on the three-dimensional structure (Liu *et al.* 2004; Zhang *et al.* 2003a). This is an efficient experimental approach for mapping the locations of surface exposed amino acid residues onto the tertiary architecture of the receptor, although is limited by the fact that the presence of the fusion protein may inadvertently cause other, non-directed changes in the three dimensional structure of the RyR.

To date, the amino terminus has been localised on the 3D structure of RyR using a GST fusion protein. Residues Asp-4365, Thr-1366 and Thr-1874 which lie within DR1, DR2 and DR3 respectively, have been located on the three-dimensional structure of RyR2 using

appropriate RyR2-GFP fusion proteins (Liu *et al.* 2002, 2004; Zhang *et al.* 2003a). DR1-3 refer to 3 divergent regions where the amino acid sequences of the three isoforms are highly variable relative to the average sequence identity among the isoforms, which is nearly 70% (Sorrentino & Volpe 1993). These DRs have been the focus of a number of structural and functional studies, as they are thought to be largely responsible for the differing properties of the RyR isoforms. For example, sequence variations in DR2 between RyR1 and RyR2 have been shown to account for these isoforms' differing sensitivities to  $\text{Ca}^{2+}$  inactivation (Du *et al.* 2000).

A similar approach was used to localise the binding sites of various ligands, and the binding sites for two accessory proteins calmodulin (CaM) and FKBP12 have been localised by determining differences in shape between free RyR and RyR protein-bound complexes (Wagenknecht *et al.* 1997). Both CaM and FKBP12 are situated > 10 nm away from the TM pore, suggesting that conformational changes can be transmitted over long distances within the protein structure.

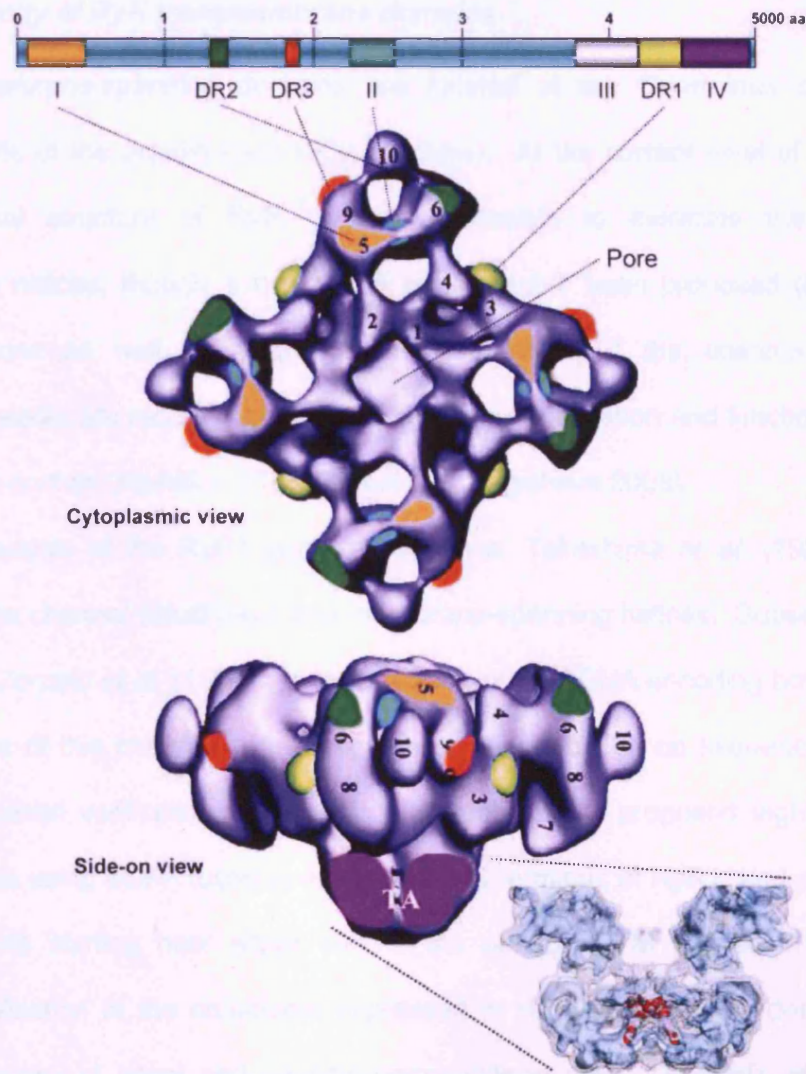


**Figure 1.9. Three-dimensional structure of RyR2, indicating various regions that have been located using difference maps.**

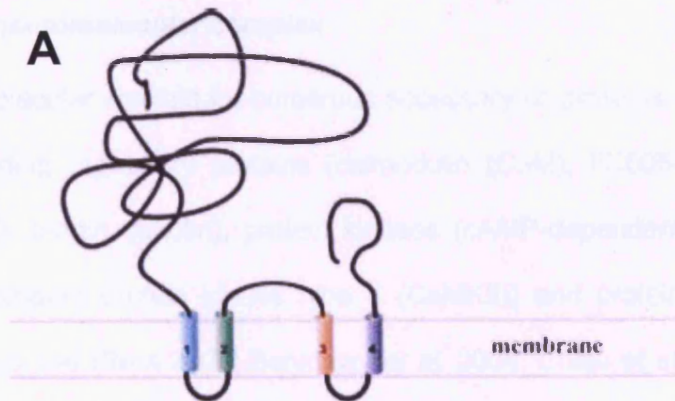
Correlation of RyRs amino acid sequence to its three-dimensional structure; showing the three-dimensional mapping of several domains as depicted on the schematic in the top panel. Three-dimensional structure of RyR2, indicating various regions that have been located using difference maps. DR1-3 refers to divergent regions of RyR (DR1–D4365, DR2–T1366, and DR3–T1874) (Liu *et al.* 2004). CPVT I-IV refers to domains of identified as CPVT-linked mutational hotspots in RyR2 (George *et al.* 2008b).

### 1.3.4 Topology of RyR transmembrane domains

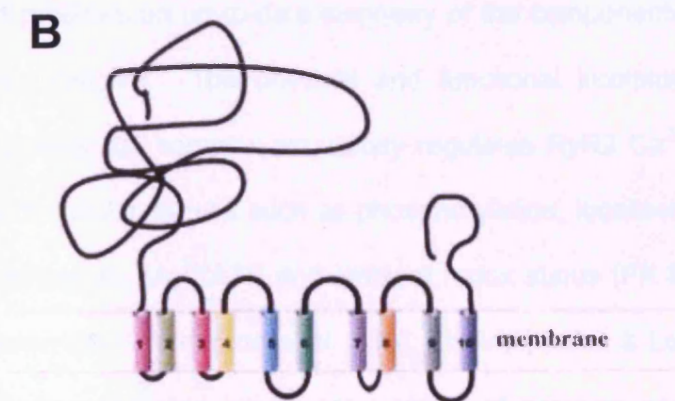
Putative membrane-spanning domains are located at the C-terminus of RyR, and comprise 10-20% of the protein (500-1000 residues). At the current level of resolution in three-dimensional structure of RyR, it is not possible to elucidate the number of transmembrane helices, though a number of models have been proposed (Figure 1.10). Higher resolutions as well as additional reconstructions of the channel in different conformational states are required to further define the organisation and function of the RyR transmembrane domain (Hamilton 2005; Hamilton & Serysheva 2008).

From the analysis of the RyR1 primary sequence, Takeshima *et al.* (1989) originally predicted that the channel would have four membrane-spanning helices. Subsequent to this seminal paper, Zorzato *et al.* (1990) reported cloning of the cDNA encoding both the human and rabbit forms of this channel. However, these models based on sequence predictions require experimental verification. Recently, Du *et al.* (2002) proposed eight TM helices based on studies using eGFP fused in-frame to the C-terminus of RyR1, and a series of C-terminal deletions starting near either end of the predicted TM helices M1-M10. The subcellular localisation of the constructs expressed in HEK293 cells was determined with confocal microscopy of intact and saponin-permeabilised cells. The role of the M4a/4b hairpin loop in channel is thought to act as a negative regulatory module to stabilise the channel in its closed state (Du *et al.* 2004). This theory was supported by the observation that removal of this region increased the magnitude of voltage-gated SR release, and also resulted in increased channel sensitivity to activation by caffeine and  $\text{Ca}^{2+}$ , and reduced sensitivity to  $\text{Ca}^{2+}$  dependent inactivation (Du *et al.* 2004). In Du's proposed model, TM9 appears as a 'P-loop', containing a selectivity filter, based on mutational analyses and analogies with better characterised ion channels, such as the inositol 1,4,5-trisphosphate receptor ( $\text{IP}_3\text{R}$ ) and the bacterial KcsA channel (MacKinnon 2003), which are all tetrameric and structurally homologous.

Takeshima *et al.* (1989)



Zorzato *et al.* (1990)



Du *et al.* (2002)

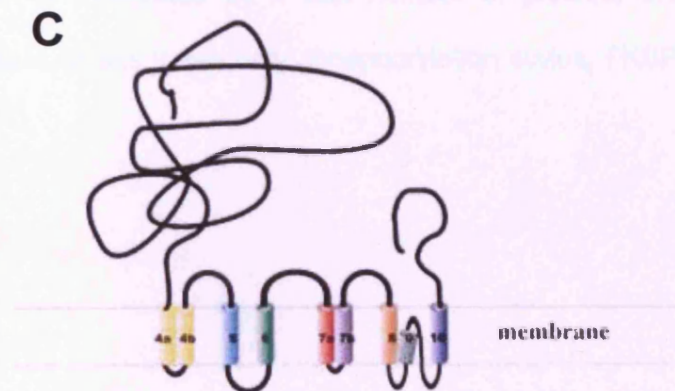


**Figure 1.10. Models for the transmembrane regions of RyR1.**

Schematic representations of the proposed models of TM topology. The validation of these putative TM models requires unequivocal structural data, and recent structural data shows that some of that TM8 may lie in the plane of the membrane (Hamilton & Serysheva 2008).

### 1.3.5 Regulation of RyR by the macromolecular complex

*In vivo*, RyR channels exist as a molecular scaffold for numerous accessory co-proteins - the macromolecular complex – including regulatory proteins (calmodulin (CaM), FK506-binding proteins (FKBP), sorcin, CSQ, triadin, junctin), protein kinases (cAMP-dependent protein kinase (PKA), Ca<sup>2+</sup>/CaM dependent protein kinase type II (CaMKII)) and protein phosphatases (PP1, PP2A) (for reviews see (Bers 2004; Benkusky *et al.* 2004; Chelu *et al.* 2004; Marks 2001, 2002). Figure 1.11 provides an up-to-date summary of the components of the RyR macromolecular signalling complex. The physical and functional interplay between the components of the macromolecular complex exquisitely regulates RyR2 Ca<sup>2+</sup> release in response to a diverse array of cellular signals such as phosphorylation, localised cytoplasmic and SR luminal Ca<sup>2+</sup> environments, Mg<sup>2+</sup>/ATP and ambient redox status (Fill & Copello 2002; Marks *et al.* 2002; Meissner 2004; Wehrens *et al.* 2006; Zissimopoulos & Lai 2006). The macromolecular complex is modulated by a vast number of proteins and endogenous factors, but for the purposes of this thesis only phosphorylation status, FKBP, CSQ and Ca<sup>2+</sup> will be discussed.

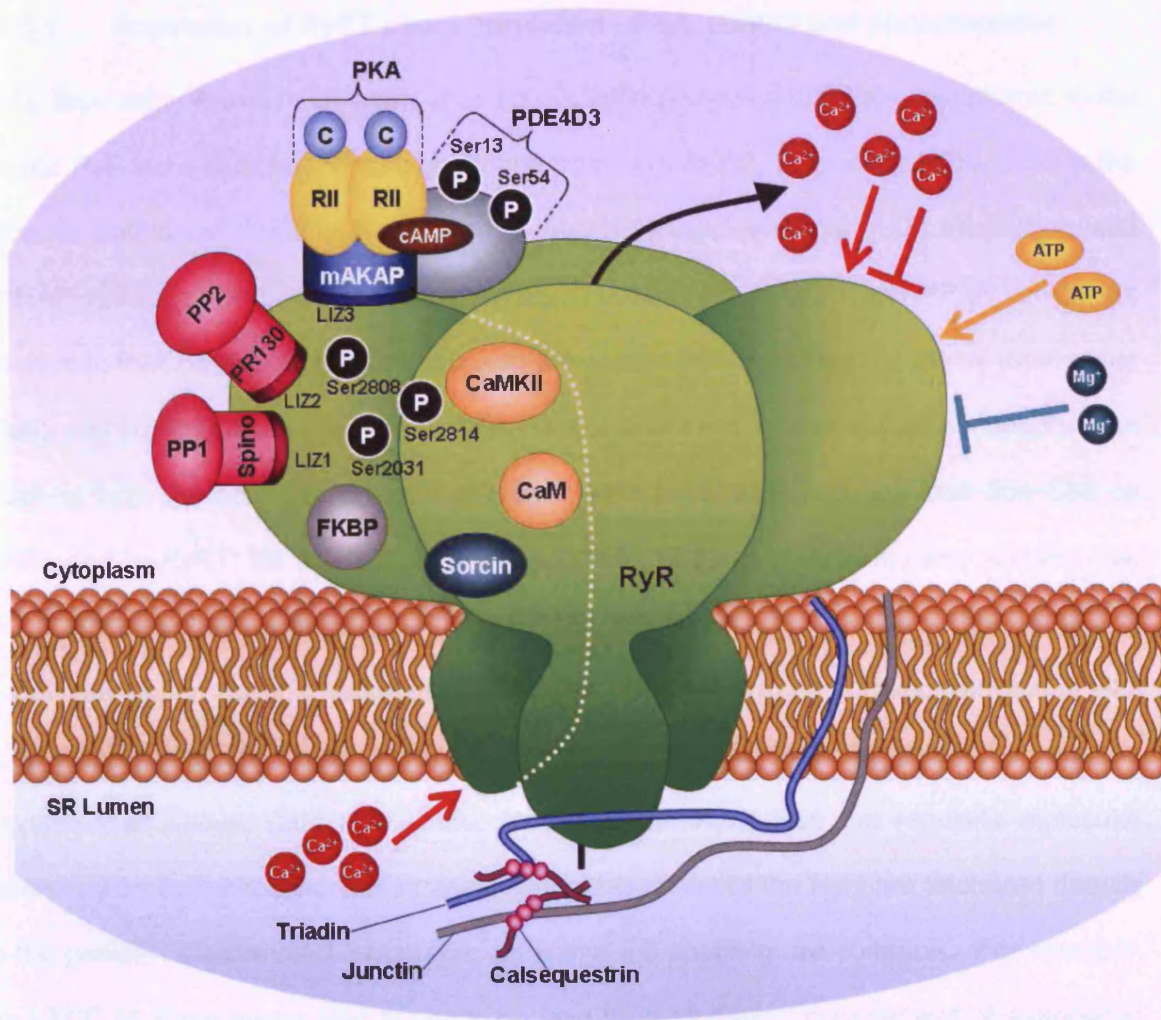


**Figure 1.11. The RyR2 macromolecular signalling complex**

Four RyR2 monomers contribute to the tetrameric  $\text{Ca}^{2+}$  release channel macromolecular complex. Regulatory proteins and enzymes associate with the large cytoplasmic RyR2 domain. CaM, FKBP12.6, and sorcin are thought to bind directly to the RyR2 monomers, whereas binding of other subunits is mediated by specific targeting proteins. Leucine-isoleucine zipper (LIZ) motifs on RyR2 bind to corresponding LIZ peptides in anchoring proteins spinophilin (targeting PP1), PR130 (targeting PP2A), and mAKAP (targeting PKA and PDE4D3). The mechanism for CaMKII binding to RyR2 is currently unknown. **Triadin**, **junctin** and **CSQ** interact with RyR2 on the luminal side of the channel complex. **CaM** acts as an intracellular  $\text{Ca}^{2+}$  sensor (Levitan 1999) and also influences SR  $\text{Ca}^{2+}$  release through a direct interaction with RyRs. At stimulatory  $\text{Ca}^{2+}$  levels,  $\text{Ca}^{2+}$  cooperatively binds CaM such that CaM can bind to and activate target proteins with high affinity. When CaM binds to target proteins the  $\text{Ca}^{2+}$  affinity is typically altered significantly. **Sorcin** is a soluble protein, which binds to RyR2 only when  $[\text{Ca}^{2+}]$  is elevated, and rapidly reduces RyR open probability and inhibits the channel, though this is reversed by PKA-dependent phosphorylation of sorcin. This suggests that  $\beta$ -adrenergic stimulation decreases sorcin-mediated inhibition of RyR2, allowing for increased  $\text{Ca}^{2+}$  release during EC coupling. **Mg<sup>2+</sup>** is a potent inhibitor of RyR, and exerts its inhibitory effects by competing with  $\text{Ca}^{2+}$  for the high-affinity  $\text{Ca}^{2+}$ -binding site, and by binding the low affinity inactivation sites with an affinity comparable to that of  $\text{Ca}^{2+}$  (Copello *et al.* 2002; Laver *et al.* 1997). **ATP** increases the sensitivity of the channel to  $\text{Ca}^{2+}$  activation and decreases its sensitivity to  $\text{Ca}^{2+}$  inactivation (Meissner *et al.* 1997).



### 1.3.5.1 Regulators of RyR2 phosphorylation - PKA, CaMKII and phosphatases

As depicted in Figure 1.11, Marx *et al.* (2000, 2001b) showed that PKA is anchored to the cardiac RyR via a muscle A kinase anchoring protein (mAKAP). Residues 3003–3039 in the cytosolic domain of RyR2 participate in a leucine-isoleucine zipper (LIZ) interaction with mAKAP which in turn binds to the regulatory subunit of PKA. PP1 and PP2A, which are involved in RyR dephosphorylation, are also associated with RyR2 via LIZ motifs (Marx *et al.* 2000), and possibly function to dephosphorylate distinct sites or to modulate phosphorylation resulting from the action of different kinases. PP1 associates with residues 554–588 on RyR2 (and to RyR1) via a LIZ motif on spinophilin. Marx *et al.* (2001b) also showed that PP2A associates with a targeting protein PR130 which interacts with RyR2 (but not RyR1) via leucine zipper motifs at residues 1603–1631. CaMKII also co-immunoprecipitates with RyR2 (Zhang *et al.* 2003b), but the molecular site of interaction has not yet been elucidated. As discussed above, CaM also binds directly to the RyR, thus the requisite molecular machinery for both phosphorylation and dephosphorylation of the RyR are anchored directly to the protein. Macromolecular complexes within EC coupling are common. For example, the LTCC ( $\leq 10\text{nm}$  away) also appears to have its own distinct complement of associated PKA, CaM and CaMKII (Ruehr *et al.* 2004), and may directly associate with  $\beta$ -AR, G-protein or adenylyl cyclase, thus localising cAMP signals to activate RyR-associated PKA. This emphasises the likely functional importance of these local signalling complexes, in the direct vicinity of target proteins (Bers 2004).

Initially, RyR2 was proposed to have a single phosphorylation site (Ser2808) and it was originally described as the site for CaMKII phosphorylation (Witcher *et al.* 1991). Although several recent studies have suggested that Ser2808 is the major PKA substrate in HF pathogenesis (Marx *et al.* 2000), Ser2808 is a target for multiple kinases (Huke & Bers 2008; Xiao *et al.* 2006) and its constitutive high-level phosphorylation in both normal and failing hearts (Carter *et al.* 2006) suggests that the phosphorylation status of Ser2808 is not a reliable index of abnormal PKA-mediated phosphorylation of RyR2 in HF.

Many studies aiming to identify the PKA-mediated phosphorylation sites have provided conflicting results with respect to the number of PKA sites, and which of them is PKA specific. Although RyR2 S2808 was initially reported to be CaMKII specific (Witcher *et al.* 1991), it was later proposed that this residue is the sole PKA site and is phosphorylated exclusively by PKA (Marx *et al.* 2000b; Reiken *et al.* 2003; Wehrens *et al.* 2004a). However, many studies have shown that S2808 is already phosphorylated to up to 75% even in normal hearts (Carter *et al.* 2006), and can be efficiently phosphorylated by several protein kinases including PKA, PKG and CaMKII (Stange *et al.* 2003; Witcher *et al.* 1991; Xiao *et al.* 2005, 2006). Furthermore, recent studies have identified a second PKA site at RyR2 residue S2031, and both appeared to be phosphorylated *in vivo*, whereby S2808 is constitutively phosphorylated and S2031 was phosphorylated by PKA under conditions of cellular activation (Xiao *et al.* 2005, 2006). Expression of constitutively dephosphorylated mutant channels containing a Ser→Ala substitution at the putative phosphorylation sites (S2808A, S2031A) either individually or as a double mutant, did not resolve this discrepancy. Marks' group observed that a single S2808A substitution abolished PKA dependent phosphorylation, whereas S2031A did not (Lehnart *et al.* 2005a; Wehrens *et al.* 2006). Contrastingly, another group demonstrated that PKA-dependent phosphorylation occurred with either individual mutant and was abolished only in the double mutant (Xiao *et al.* 2005, 2006).

Dephosphorylation of RyR2 is carried out primarily by PP1 and PP2A (Marx *et al.* 2000; 2001b). The phosphorylation status of RyR2 is a result of the regulated balance between protein kinases and phosphatases. Therefore disease-linked RyR2 'hyperphosphorylation' may arise from decreased activity of channel-associated phosphatases (PP1 and 2A), and this will be discussed further in Section 1.4.1.1.

The functional effects of RyR phosphorylation/dephosphorylation have been examined by SR Ca<sup>2+</sup> flux measurements, single channel recordings, and by ryanodine-binding assays. Addition of exogenous PKA results in increased RyR activity because of enhanced sensitivity to Ca<sup>2+</sup> activation, and substantially reduced Mg<sup>2+</sup> inhibition, and these effects

were reversed by PP (Marx *et al.* 2000; Reiken *et al.* 2003; Takasago *et al.* 1991; Valdivia *et al.* 1995). One study reported that PKA activated RyR but only during rapid rises in local  $\text{Ca}^{2+}$  concentration, whereas under fixed  $\text{Ca}^{2+}$  levels, it promoted channel closure (Valdivia *et al.* 1995). Exogenous CaMKII displayed enhanced RyR channel activity (Currie *et al.* 2004; Wehrens & Marks 2004b; Witcher *et al.* 1991), and interestingly, PKA- and CaMKII-dependent phosphorylation produced different functional effects in parallel investigations, suggesting that they target different residues, or a different number of residues (Takasago *et al.* 1991). Furthermore, Rodriguez *et al.* (2003) showed that CaMKII phosphorylates RyR2 to a four-fold higher stoichiometry than PKA, suggesting that sites in addition to Ser-2808 are CaMKII targets, and could be critical mediators of RyR2 function.

#### 1.3.5.2 *FK-binding proteins (FKBP)*

FKBPs bind to and co-purify with RyRs (Jayaraman *et al.* 1992; Marks *et al.* 1989; Timerman *et al.* 1993, 1994, 1996). FKBP12 binds tightly to RyR1, and while the heart expresses both FKBP12 and 12.6, the latter preferentially associates with RyR2, due to a much higher affinity (Timerman *et al.* 1996). FKBPs also catalyse peptidylprolyl-*cis-trans*-isomerisation, a function believed to be involved in protein folding, but their isomerase activity is not essential for RyR effects (Bers 2004; Kay 1996; Mackrill 1999; Marks 2000).

The molar ratio of FKBP to RyR is one-to-one i.e., one FKBP protein is bound to each of the four subunits of the RyR channel complex (Timerman *et al.* 1993; 1996). The binding site for FKBP12.6 on RyR2 was initially proposed to be in the central domain of the protein (aa 2361-2496), which was identified using yeast two-hybrid analysis (Marx *et al.* 2000). This region corresponded to that in RyR1 which interacts with FKBP12 (Bultynck *et al.* 2001; Cameron *et al.* 1997; Gaburjakova *et al.* 2001). However, other loci for FKBP12.6 binding have recently been mapped to the N- and C-termini (Masumiya *et al.* 2003; Zissimopoulos & Lai 2005). Nonetheless, due to the complexity of the tetrameric RyR2 structure and the fact that this domain was assigned functionality on the basis of the study of fragments of the

RyR2 rather than the full length protein, it is entirely feasible that all of these loci contribute to a single FKBP12.6 binding site in the intact molecule (George *et al.* 2005).

Removal of FKBP12.6 from the RyR2 (using FK506 or rapamycin) activates the RyR (Kaftan *et al.* 1996; Xiao *et al.* 1997), and studies in intact myocytes showed that removal of FKBP12.6 by FK506 increased the resting spark frequency and enhanced  $\text{Ca}^{2+}$  transients (McCall *et al.* 1996). Contrastingly, other groups have reported that FKBP12.6 removal has very little impact on RyR2 channel function (Barg *et al.* 1997; Timerman *et al.* 1996; Xin *et al.* 2002). Several studies have shown that FKBP12/12.6 removal promotes the appearance of subconductance states in single channel experiments (Ahern *et al.* 1994; 1997; Brillantes *et al.* 1994; Kaftan *et al.* 1996; Marx *et al.* 2000). This observation led to the proposal of a controversial model where FKBP physically stabilises the coordinated gating of the four RyRs in one RyR homotetramer so that openings go from the fully closed to the fully open state, and the proposal that FKBP could be involved in coupled gating mediating the simultaneous opening and coordinated closure of channels *in vivo* (Marx *et al.* 2000). However, recent evidence shows that although synchronous RyR opening does occur (Wang *et al.* 2004), it is unlikely to be directly mediated by FKBP since the region which mediates inter-tetrameric interaction (encompassing domains 6 and 10) is spatially distinct from the FKBP binding site (Yin *et al.* 2005a) (see Section 1.3.3).

There are reports that suggest that FKBP12.6 is critical to normal RyR2 function in the heart (Kaftan *et al.* 1996; McCall *et al.* 1996), and that abnormal FKBP12.6-RyR2 interactions, occurring as a result of channel hyperphosphorylation may be implicated in HF (Marks 2000; Marx *et al.* 2000; Ono *et al.* 2000; Yano *et al.* 2000). This hyperphosphorylation was proposed to cause a persistent diastolic SR  $\text{Ca}^{2+}$  leak, thought to limit the SR load and contraction in the failing heart. This model is the focus of much controversy, and will be discussed in more detail in Section 1.4.1.1.

### 1.3.5.3 *Calsequestrin*

Calsequestrin (CSQ) is a high-capacity  $\text{Ca}^{2+}$  binding protein, localised to the junctional SR membrane and whose primary function appears to be buffering of intra-luminal  $\text{Ca}^{2+}$  (Yano & Zarain-Herzberg 1994). Cardiac CSQ is a highly acidic 45kDa protein with 119 Glu and Asp residues that permit it to bind 20-40  $\text{Ca}^{2+}$  ions per molecule (Yano & Zarain-Herzberg 1994). Triadin (~35kDa) and junctin (~26kDa) are integral SR proteins which physically couple CSQ to the RyR2 via 'polar zippers' formed between 'KEKE' motifs present in their primary structures and acidic moieties near the inner mouth of the RyR channel domain (Lee *et al.* 2004; Zhang *et al.* 1997), forming a quaternary complex (Mackrill 1999; Zhang *et al.* 1997).

Transgenic mice in which CSQ had been overexpressed >10-fold developed cardiac hypertrophy (Sato *et al.* 1998). Cardiomyocytes from these mice display a 10-fold increase in the amplitude of caffeine induced  $\text{Ca}^{2+}$  release compared to controls, as would be expected for cells possessing a greater level of intra-SR  $\text{Ca}^{2+}$  buffer. Conversely, these cells exhibited a decreased spontaneous RyR2 activity, which was explained by a decrease in free SR  $\text{Ca}^{2+}$ . More moderate levels of adenoviral CSQ expression (2-4 fold) in adult ventricular myocytes resulted in enhanced  $\text{Ca}^{2+}$  transient and spark amplitude (Terentyev *et al.* 2003a). These results, along with the implication of CSQ in heart disease (see Section 1.4.1.2), indicate that cardiac CSQ plays pivotal roles both in  $\text{Ca}^{2+}$  storage and in regulation of  $\text{Ca}^{2+}$  release via RyR2.

### 1.3.6 *Regulation of the RyR macromolecular complex by endogenous factors*

RyR channel activity is regulated by a wide variety of endogenous molecules, with  $\text{Ca}^{2+}$ ,  $\text{Mg}^{2+}$  and ATP being the key regulators, but for the purposes of this thesis only  $\text{Ca}^{2+}$  will be discussed.

### 1.3.6.1 Cytosolic $\text{Ca}^{2+}$

$\text{Ca}^{2+}$  is an important physiological regulator of the channel and other ligands either cannot activate the channel in its absence (e.g. CaM) or they require  $\text{Ca}^{2+}$  for maximum effect (e.g. ATP). Cytosolic  $\text{Ca}^{2+}$  has a biphasic effect on RyR1 channel activity; the threshold for channel activation is approximately 100 nM with a maximum range of 10-100  $\mu\text{M}$ , whereas millimolar  $\text{Ca}^{2+}$  inhibits the channel. This bell-shaped dependence suggests that RyR contains high-affinity  $\text{Ca}^{2+}$  binding sites that stimulate the channel and low-affinity sites that inhibit it (Chu *et al.* 1993; Copello *et al.* 2002; Laver *et al.* 1995). RyR2 and RyR3 are less sensitive to inhibition by high  $\text{Ca}^{2+}$  concentrations and almost maximal activation can be achieved by  $\text{Ca}^{2+}$  alone at approximately 100  $\mu\text{M}$ , unlike RyR1 which can not be fully activated by  $\text{Ca}^{2+}$  alone (Jeyakumar *et al.* 1998; Murayama & Ogawa 2002; Rousseau & Meissner 1989).

### 1.3.6.2 Luminal $\text{Ca}^{2+}$

The rate of  $\text{Ca}^{2+}$  release from the SR is sensitive to the store  $\text{Ca}^{2+}$  content and single channel recordings have demonstrated RyR regulation by luminal  $\text{Ca}^{2+}$  (Györke & Györke 1998; Sitsapesan & Williams 1994, 1995). Although differences exist between RyR1 and RyR2, increasing luminal  $\text{Ca}^{2+}$  concentration augments channel activity by increasing the channel sensitivity to agonists such as cytoplasmic  $\text{Ca}^{2+}$ , ATP and caffeine and by alleviating  $\text{Mg}^{2+}$  inhibition. However, increasing luminal  $\text{Ca}^{2+}$  levels above a threshold causes a decrease in channel activity. The mechanism of RyR activation by luminal  $\text{Ca}^{2+}$  is thought to involve either  $\text{Ca}^{2+}$  regulatory sites through an allosteric effect in single isolated channels, whereas in close-packed RyR1 arrays, luminal  $\text{Ca}^{2+}$  flowing through one channel directly interacts with cytosolic regulatory sites of neighbouring channels (Laver *et al.* 2004). The luminal  $\text{Ca}^{2+}$  sensor can either be an intrinsic property of RyR or is imparted by accessory proteins. Evidence for the former is provided by proteolysis studies suggesting the presence of both activating and inactivating  $\text{Ca}^{2+}$  sites on the RyR luminal side (Ching *et al.* 2000).

Contrastingly dissociation of CSQ, triadin and junction abolished RyR2 regulation by luminal  $\text{Ca}^{2+}$  (Györke *et al.* 2004), whereas CSQ association amplified channel responses to luminal  $\text{Ca}^{2+}$  (Beard *et al.* 2005).

### 1.3.7 Functional interactions within the RyR

#### 1.3.7.1 Inter-channel interaction

A characteristic feature of RyRs is their organisation into ordered two-dimensional arrays within the membrane, observed in both skeletal and cardiac muscle by EM (Protasi *et al.* 1996; Saito *et al.* 1988; Yin *et al.* 2008). This regular organisation is an intrinsic property of the RyR, as recombinant RyR1 forms extensive arrays *in vivo* (Takekura *et al.* 1995) and purified RyR1 self-assembles into large two-dimensional crystalline arrays *in vitro* (Yin & Lai 2000; Yin *et al.* 2005a). In these checkerboard-like lattices, each RyR is interlocked with four adjacent channels through a specific intermolecular domain-domain interaction that appears to involve sequences in the proximity to the region identified as DR2 (Liu *et al.* 2004; Yin *et al.* 2005b). In arrays, the cytoplasmic assembly of each RyR interacts along the edges of the clamp domain with the corresponding regions of its nearest neighbours such that the edges of adjoining RyRs overlap by ~12 nm (Saito *et al.* 1988). Biochemical evidence has suggested residues 2540-3207 in the central region of RyR2 are responsible for the tetramer-tetramer interactions in array formation (Blayney *et al.* 2004). It has been proposed that inter-tetramer contact in this array formation is mediated by an accessory protein (FKBP) and that these interactions could be responsible for the concerted opening and closing of channels seen *in vivo* (Marx *et al.* 1998). However, as discussed above, this notion has been disputed by three-dimensional modelling which suggests that domains most likely to undergo protein-protein interactions are spatially distinct from the FKBP binding site (Wagenknecht *et al.* 1997), suggesting that the intrinsic structure of the RyR is responsible for the formation of these ordered arrays (Liu *et al.* 2004; Yin *et al.* 2005b, 2008).

Theoretical modelling (Stern *et al.* 1997, 1999) and experimental observations (Marx *et al.*

1998b, 2001a; Wang *et al.* 2004) of E–C coupling in muscle cells have suggested that RyR behaves in an intermolecular allosteric manner in native SR membranes. The contact between RyRs in the array provides potential mechanistic insight. In the native checkerboard array, RyRs are interlocked through intermolecular domain–domain interaction (i.e. they are ‘physically coupled’), whereby a conformational change of one activated RyR can likewise be communicated to four adjacent RyRs through intermolecular domain–domain interaction. Thus, allosterically mediated conformational changes induced in these neighbouring RyRs trigger their activation and consequent  $\text{Ca}^{2+}$  release and may explain how a number of RyRs within a cluster open and close simultaneously during a  $\text{Ca}^{2+}$  spark. The existence of an allosteric coupling mechanism for RyR activation would help to address a variety of fundamental issues that are crucial to  $\text{Ca}^{2+}$  signalling and E–C coupling in muscle cells (Yin *et al.* 2008).



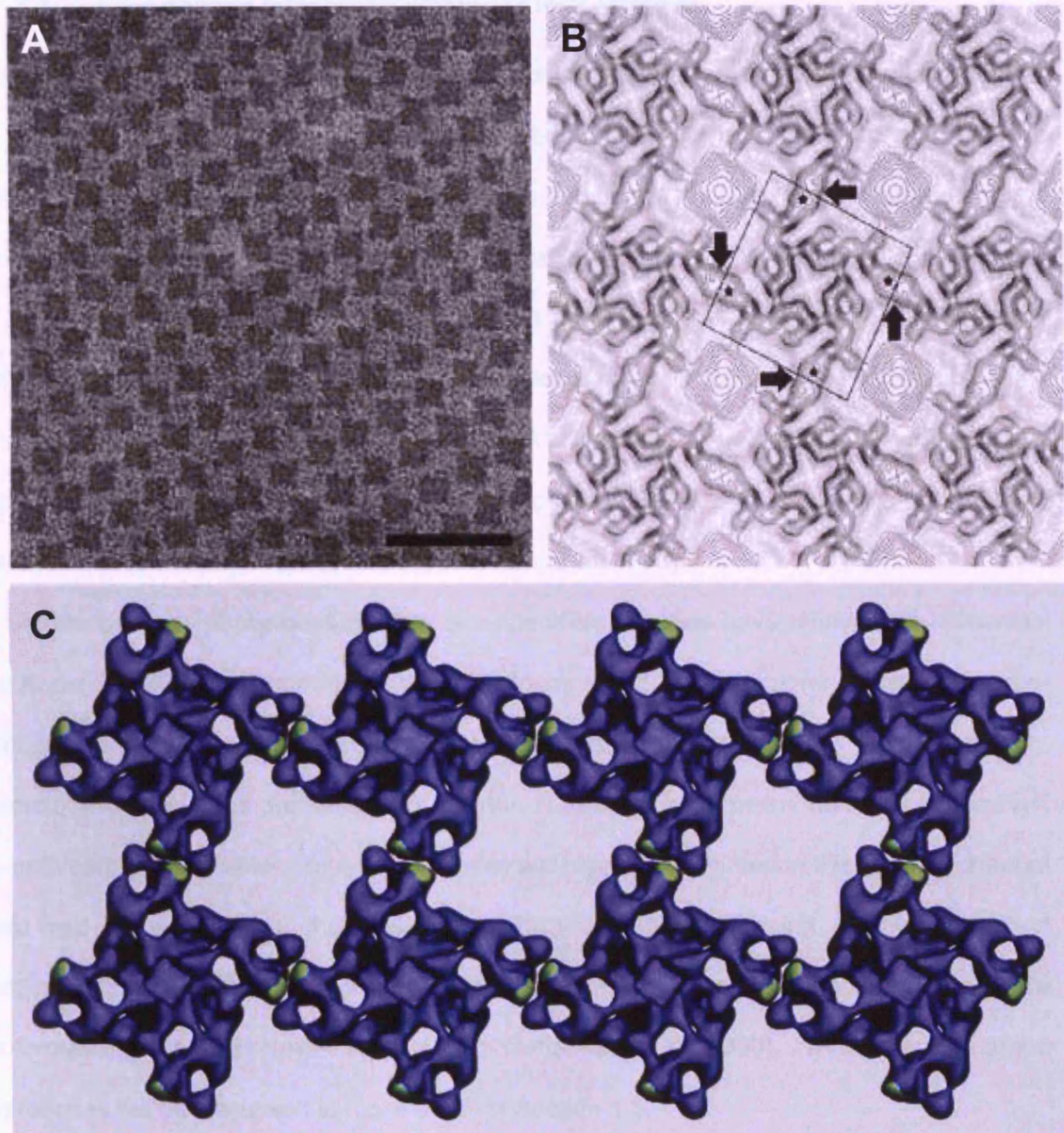


**Figure 1.12. Physical coupling between skeletal muscle RyRs in the native 'checkerboard' array**

**Panel A:** Electron micrographs showing RyRs in the native checkerboard-like array. Scale bar: 100nm; **Panel B:** Calculated projection maps showing RyRs in the lattice formation. The square box outlines one RyR molecule; the arrows indicate the physical coupling occurring between adjacent RyRs in the native checkerboard-like array; **Panel C:** RyR molecules are linked to form a two-row array as is found in skeletal muscle. Domain 6, which lies in the clamp structure, where DR2 has been located by GFP insertion (in green), is one of the domains that is likely, based upon its location, to be involved in RyR–RyR interactions (Liu *et al.* 2004).

### 1.3.7.2 Inter-domain interaction within the RyR tetramer

As well as being involved in inter-tetramer interactions, regions of the cytoplasmic domain of RyR1 and RyR2 have also been implicated in inter-domain interactions within the tetrameric channel, and it is these interactions which are thought to mediate the global conformational change associated with Ca<sup>2+</sup> release.

The extreme RyR C-terminus is known to be capable of self-association (Stewart *et al.* 2003). This region has been identified as a molecular determinant of oligomerisation since deletion of the final 15 amino acids from RyR1 resulted in an inactive channel, due to impaired assembly of a tetrameric complex (Gao *et al.* 1997), while the extreme C-terminal 100 residues form dimers and tetramers (Stewart *et al.* 2003).

Studies using synthetic peptides and site-specific antibodies have shown that N-terminal (residues 590-609) and central domain (residues 2442-2477) regions undergo domain-domain interaction (Kobayashi *et al.* 2004). Additionally, using a peptide probe approach, Ikemoto and colleagues demonstrated that the N-terminal and central domains of the RyR (in both cardiac and skeletal muscle isoforms) are closely associated in the inactive channel state and in fact stabilise the closed conformation, while loosening of this interaction ('unzipping') by mutation and/or competitive binding of a peptide produced the active conformational state (El-Hayek *et al.* 1999; Yamamoto *et al.* 2000). These peptide probe approaches will be discussed in more detail in Section 1.5.

### 1.3.8 The RyR2 I-Domain

We recently identified a region involved in the critical regulation inter-domain interactions - the RyR2 I-Domain (interacting domain, aa 3722-4610). This is a surface-accessible, hinge-like region of RyR2 that is the location for 32% of all reported CPVT-linked mutations (Figure 1.13), and is critically involved in the intrinsic regulation of the channel by transducing regulatory cytoplasmic events to the Ca<sup>2+</sup> pore-forming domain (George *et al.* 2004, 2006).

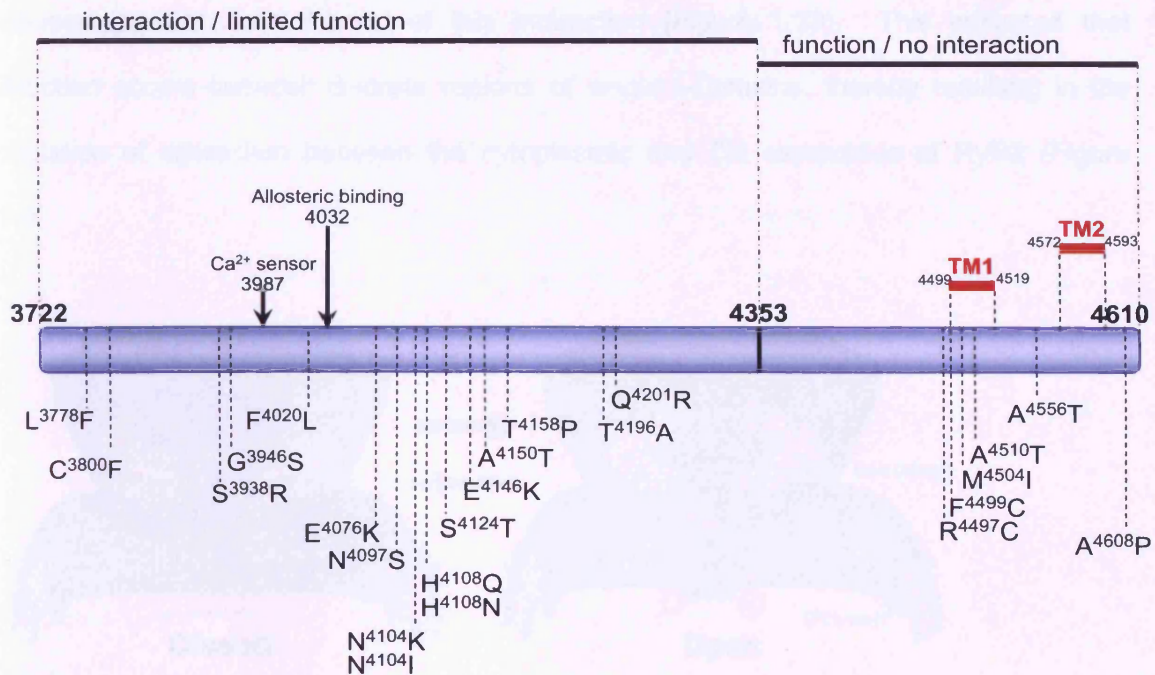


**Figure 1.13. CPVT-linked mutations located to the RyR2 I-Domain**

The I-Domain contains 23 of the 71 CPVT-linked mutations so far identified in RyR2. Residues 3722-4353 has been found to be sufficient for interdomain interaction to occur, while residues 4353-4610 markedly enhanced the functional impact of this interaction, indicating that interaction between discrete regions of single I-Domains result in the mediation of interaction between the cytoplasmic and TM regions of RyR2. Interestingly, no mutations have been identified in the region 4353-4499 (termed ID<sup>B</sup>, see Chapter 3) implying that this region may be vital for viable channel function.

The I-Domain was initially identified using Fluorescence Resonance Energy Transfer (FRET) analysis, by demonstrating a specific association between RyR2 cytoplasmic domains and the membrane-localised TM region, which resulted in inhibitory (suppressed resting intracellular [Ca<sup>2+</sup>]) and excitatory (restored caffeine sensitivity) modulation of RyR Ca<sup>2+</sup> channel functionality. By successive amino-terminal extension, the region mediating interaction between RyR2 TM and cytoplasmic domains was mapped to amino-acid residues 3722-4610, which we termed the I-Domain. Because the determinants of inter-subunit interaction involved in RyR tetramerisation are located in regions distinct from the I-Domain (Stewart *et al.* 2003), it was suggested that the I-Domain mediated interaction within, and not between, RyR2 subunits in the intact tetramer. It was found that amino acid residues 3722-4353 were sufficient for interdomain interaction to occur, while residues 4353-4610 markedly

enhanced the functional impact of this interaction (Figure 1.13). This indicated that interaction occurs between discrete regions of single I-Domains, thereby resulting in the modulation of interaction between the cytoplasmic and TM assemblies of RyR2 (Figure 1.14).

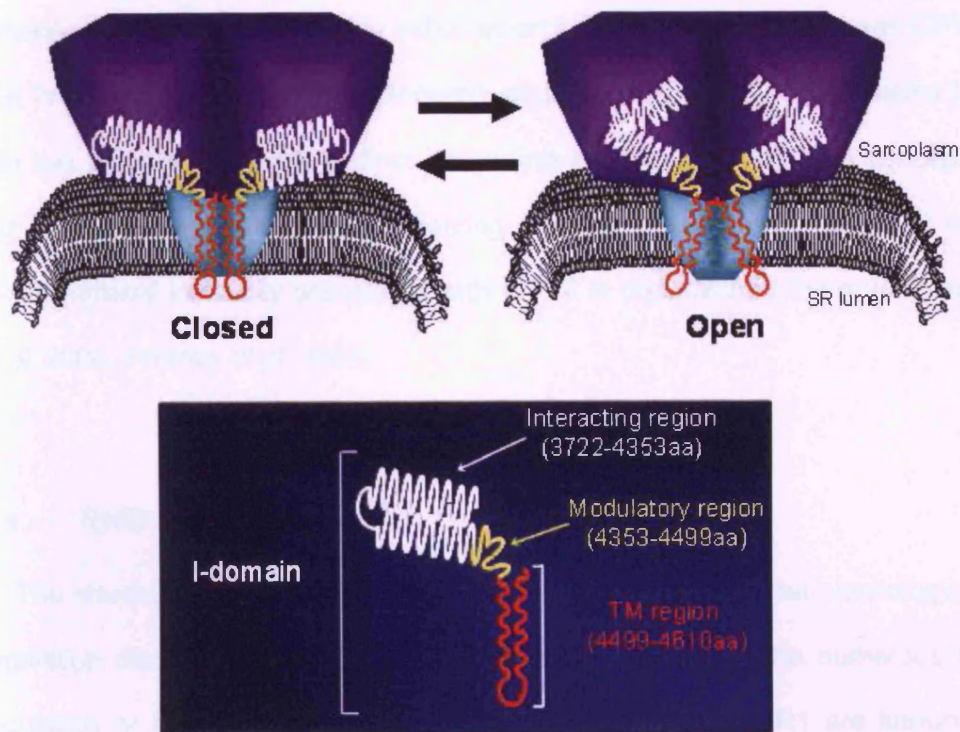


**Figure 1.14. The RyR2 I-Domain intrinsically controls RyR2 opening through conformational rearrangement**

Schematic diagram, showing that conformational re-ordering within the I-domain is associated with RyR2 channel opening and closing, based on data obtained from fluorescence resonance energy transfer (FRET) studies of cytoplasmic (light grey) and transmembrane domain (dark grey) interactions (George *et al.* 2004, 2006). Functionally distinct sub-regions within the I-Domain are predicted from experimental data and computational analysis (George *et al.* 2004; 2007b).

The I-Domain of RyR2 comprises two distinct domains, the interaction domain located at residues 3722-4353 and the modulatory domain, containing two putative TM domains located at residues 4353-4610 (George *et al.* 2004, 2006). Our data suggests that conformational rearrangements within the I-Domain can physically transduce the 'sensing' of cellular signals by cytoplasmic domains to regulate the TM Ca<sup>2+</sup> pore-forming region, and

that these events are perturbed following RyR2 mutation (George *et al.* 2004, 2006). Experimental and computational analysis have revealed that the I-Domain comprises sub-regions of distinct functionality, including the region responsible for interaction, a region that confers agonist sensitivity (modulatory region) and two predicted TM domains. This is supported by analysis of the putative locations of the CPVT domains on the three-dimensional RyR2 reconstruction indicates probable interactions between CPVT domains III and IV (which encompass the I-Domain), and it is likely that CPVT domains may assemble into two pairs of physically distinct interacting loci within RyR2. This concept is consistent with data from our laboratory suggesting that the precise mode of RyR2 mutation-linked conformational instability associated with CPVT is predicted by the mutational loci (George *et al.* 2006; Thomas *et al.* 2004)

#### **1.4 RyR2 and pathology**

The structural and functional complexity of RyR and its critical physiological role in Ca<sup>2+</sup> regulation discussed above, predicts that defects in any of the numerous facets of RyR regulation or function would be pathogenic. Mutations in RyR1 are known to cause the skeletal muscle pathologies malignant hyperthermia (MH) and central core disease (CCD). Mutations in corresponding regions of RyR2 are associated with catecholaminergic polymorphic ventricular tachycardia (CPVT) and arrhythmogenic right ventricular cardiomyopathy type 2 (ARVC2) (Figure 1.15), and acquired or genetic defects in RyR2 that result in defective Ca<sup>2+</sup> release have been shown to underlie an increased propensity for ventricular arrhythmias. The discovery of these RyR2 mutation-related arrhythmia syndromes has triggered a large upsurge of interest in elucidating the molecular mechanisms underlying mutant channel dysfunction, since this represents a pre-requisite for the design of new therapeutic strategies based on detailed structure–function analysis, but may also provide fundamental insights into the mechanisms of arrhythmogenic RyR2 dysfunction commonly occurring in HF.

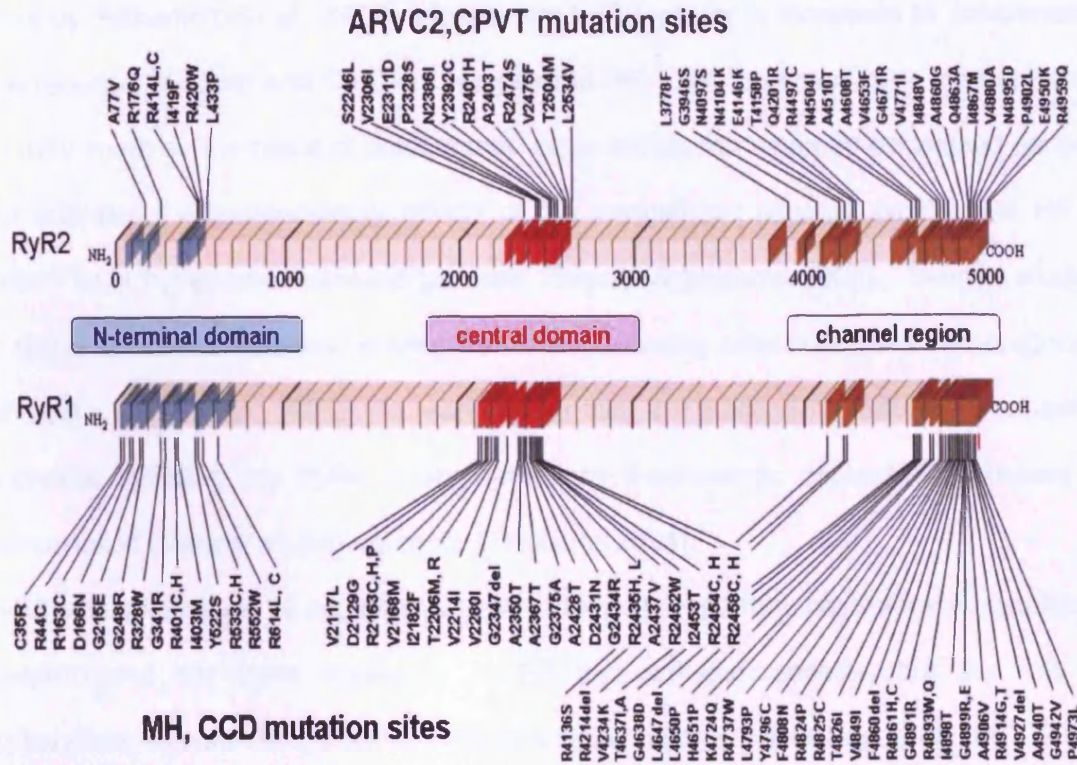


Figure 1.15. Schematic of the reported mutation sites RyR1 and RyR2.

The three hotspot regions and the RyR mutations found in these regions are indicated. The regions encompass the amino acid residues as indicated: N-terminal domain, amino-acids 0–600; central domain, amino-acids 2,100–2,500; channel region, amino-acids 4,100–5,000 (Yano 2008).

#### 1.4.1.1 RyR2 in Heart Failure

Traditionally, RyR2 has not been considered to have a direct role in the pathogenesis of HF which has been attributed more to defects in SR  $\text{Ca}^{2+}$  loading. However there is now substantial evidence that RyR2 dysfunction is pivotal in cardiac deterioration and HF. Expression levels of functional RyR2 channels in HF, as measured by ryanodine binding have shown conflicting results. These measurements have shown the levels of RyR2 to be unchanged (Nimer *et al.* 1995), increased (Sainte Beuve *et al.* 1997) and decreased (Vatner *et al.* 1994) in a variety of animal HF models. Other studies suggest that the number of RyR2s relative to LTCCs is reduced, causing a functional uncoupling of the two channels, resulting in reduced SR  $\text{Ca}^{2+}$  release (Milnes & MacLeod 2001).

Work by Yamamoto *et al.* (1999) implied that RyR2 activity is increased to compensate for the reduced SR load and  $\text{Ca}^{2+}$  release seen in HF. This compensatory modulation of RyR2 may come as the result of catecholaminergic stimulation whereby decreased cardiac output activates the compensatory effects of the sympathetic nervous system and HF is described as a hyper-catecholaminergic state (Scoote & Williams 2002). Several studies have shown a close correlation between levels of circulating catecholamines and prognosis of HF (Cohn *et al.* 1984, 1995). In response to this, the function of various EC coupling components, including the RyR2 is augmented by  $\beta$ -adrenergic dependent increases in phosphorylation (Marx *et al.* 2000; Scoote & Williams 2004).

RyR2 phosphorylation is regarded as an extremely important physiological regulatory mechanism and has been implicated in HF and arrhythmogenesis, but the role of phosphorylation in channel dysfunction remains highly controversial (Bers *et al.* 2003, 2006; Lehnart *et al.* 2004; Marks 2003; Wehrens *et al.* 2005). A model in which abnormal cAMP-dependent protein kinase (PKA)-mediated 'hyper-phosphorylation' of RyR2 at Ser2808 abolished the interaction between RyR2 and FKBP12.6, an accessory co-protein, and resulted in arrhythmogenic diastolic  $\text{Ca}^{2+}$  leak, was proposed by Marx *et al.* as the primary causative basis of RyR2 dysfunction in HF (Marx *et al.* 2000). Additionally, decreased PP1 and PP2A levels have been implicated in HF as a potential explanation for the PKA hyperphosphorylation of the RyR2 channel (Marx *et al.* 2000).

In a series of confirmatory experiments, this mechanism was extrapolated to other cardiac and skeletal muscle pathologies including CPVT (Marks 2003; Reiken *et al.* 2003; Wehrens *et al.* 2003), and in further support, the substitution of Ser2808 with alanine, thereby preventing PKA-mediated phosphorylation at this residue, protected RyR2 channels from PKA-induced defects (Lehnart *et al.* 2005a; Wehrens *et al.* 2003). This mechanism has attracted huge interest as it provides a feasible and attractive 'unifying' mechanism of RyR2 dysfunction in cardiopathology. However, despite being extensively tested in numerous experimental models, this mechanism has been corroborated in only one other laboratory (Yano *et al.* 2003, 2005b), and many recent studies have highlighted fundamental

inconsistencies relating to key tenets of this model.

Li *et al.* (2002) showed that a maintained increase in global and local SR  $\text{Ca}^{2+}$  release in response to enhanced phosphorylation was due to phosphorylation of PLB, and this was consistent with the finding that changes in RyR2 phosphorylation associated with HF had no effect on cardiac function (Jiang *et al.* 2002a). Furthermore, the improved synchronisation of  $\text{Ca}^{2+}$  sparks in failing myocytes following  $\beta$ -AR stimulation is contrary to what may have been expected if PKA-mediated phosphorylation was the major cause of the impaired  $\text{Ca}^{2+}$  handling dynamics (Litwin 2006). In contrast to studies in which enhanced RyR2 phosphorylation promoted sudden death (Antos *et al.* 2001), and the demonstration that persistent channel phosphorylation in PDE4D3-deficient mice (a cAMP-specific phosphodiesterase) was linked to age-related cardiomyopathy (Lehnart *et al.* 2005b), prolonged RyR2 phosphorylation via inhibition of PP1 was cardioprotective (Yamada *et al.* 2006). This finding supported previous reports that PKA-mediated RyR2 phosphorylation reduced channel functionality (Valdivia *et al.* 1995), and also that dephosphorylation stimulated channel activity in cardiac myocytes (Terentyev *et al.* 2003b). Additionally, Carter *et al.* (2006) showed that Ser2808 exhibited basal phosphorylation levels of ~75% and proposed that this represented the lowest activation state of RyR2, whereby increased or decreased phosphorylation (by PKA or PP1, respectively) activated the channel via distinct mechanisms.

Although the importance of RyR2 phosphorylation under normal physiological conditions remains controversial, it may still play a role in generating triggered arrhythmias, which are thought to occur during SR  $\text{Ca}^{2+}$  overload. Pogwizd *et al.* (2001) showed that the residual  $\beta$ -adrenergic receptor responsiveness was sufficient to load the SR with enough  $\text{Ca}^{2+}$  to reach the threshold needed to initiate spontaneous  $\text{Ca}^{2+}$  release. Since NCX is upregulated in HF, for every given SR  $\text{Ca}^{2+}$  release there is a greater efflux of  $\text{Ca}^{2+}$  via NCX and an inward arrhythmogenic  $\text{Na}^+$  current, which could cause DADs.



### 1.4.1.2 ARVC2 / CPVT

CPVT is a highly malignant form of arrhythmogenic disorder characterised by exercise- or emotionally-induced polymorphic tachycardia in the absence of any detectable structural heart disease (Liu *et al.* 2008). CPVT was first reported as a bidirectional VT precipitated by effort and emotional stress testing of a 6-year old girl with no evidence of any structural abnormality in the heart (Reid *et al.* 1975). Later a series of cases in familial as well as in sporadic forms were reported, and the term CPVT to refer to a disease characterised by adrenergically mediated bidirectional and/or polymorphic ventricular tachycardia (VT) in the absence of cardiac pathology (Leenhardt *et al.* 1995a). In 2001 independent groups led by Priori and Lahat identified mutations in RyR2 and cardiac calsequestrin (CASQ2) underlying autosomal dominant and autosomal recessive forms of CPVT (Lahat *et al.* 2001; Priori *et al.* 2001). The prevalence of CPVT in the population is not known, but has been estimated around 1:10,000. CPVT is now acknowledged as one of the most severe of the inherited arrhythmogenic disorder because in some cases the first event is lethal and it is a significant cause of sudden death at young age. The severity of the phenotype underscores the importance of its early diagnosis and prophylactic treatment.

In 1999, Swan *et al.* studied two CPVT families and assigned the CPVT locus to chromosome 1q42-q43 (Swan *et al.* 1999). Subsequently, Priori *et al.* demonstrated that the gene for CPVT encodes RyR2, and identified RyR2 mutations in four families with the typical pattern of CPVT and autosomal dominant pattern of inheritance (Priori *et al.* 2001). Shortly after, Lahat *et al.* mapped a recessively inherited CPVT locus to chromosome 1p13-21 and identified a missense mutation in a highly conserved region of CASQ2, the major Ca<sup>2+</sup> reservoir within the SR of cardiac myocytes, suggesting that CASQ2 mutations cause the autosomal recessive form of CPVT (Lahat *et al.* 2001).

ARVC2 was first described by Nava *et al.* (1988) and is distinct from the other forms of ventricular dysplasia because it is associated with exercise/stress-induced VT and SCD. Unlike CPVT, ARVC2 is characterised by fibro-fatty infiltrates in the myocardium and

dysplasia of the right ventricle. Despite the morphological differences, CPVT and ARVC2 are allelic – they are caused by mutation of the same gene and share a common pre-disposition to effort induced VT, suggesting that they could belong to a single clinical entity with a broad range of phenotypic variability influenced by other genetic or epigenetic factors.

#### **1.4.1.3 The 'hot-spot' nature of RyR2 mutational loci**

As discussed in Section 1.3.7.2, RyR2 is organised as a complex series of discrete domains, which interact to modulate channel function. Almost every region of the RyR2 protein contributes to channel modulation (George *et al.* 2005), but arrhythmogenic mutations cluster in four discrete regions, presently termed domains I, II, III and IV (Figure 1.16). These 'hot-spots' are well conserved across species and RyR isoforms, and there are no reported mutations in three regions of sequence divergence (DR1-3) that are proposed to underscore the functional differences between RyR isoforms. The finding that 'total exon' screening has only detected mutations occurring within these hot-spots emphasises that mutational clustering is not an artefact of genetic screening but is likely to be a pathophysiological feature of CPVT. The functional significance of mutation clustering remains unclear, but structure-function analysis suggests that CPVT domains I–IV are predominantly associated with intra-RyR2 domain interactions and cytoplasmic Ca<sup>2+</sup>-dependent channel modulation (George *et al.* 2007a), and accordingly the I-Domain coincides with CPVT domain IIII.

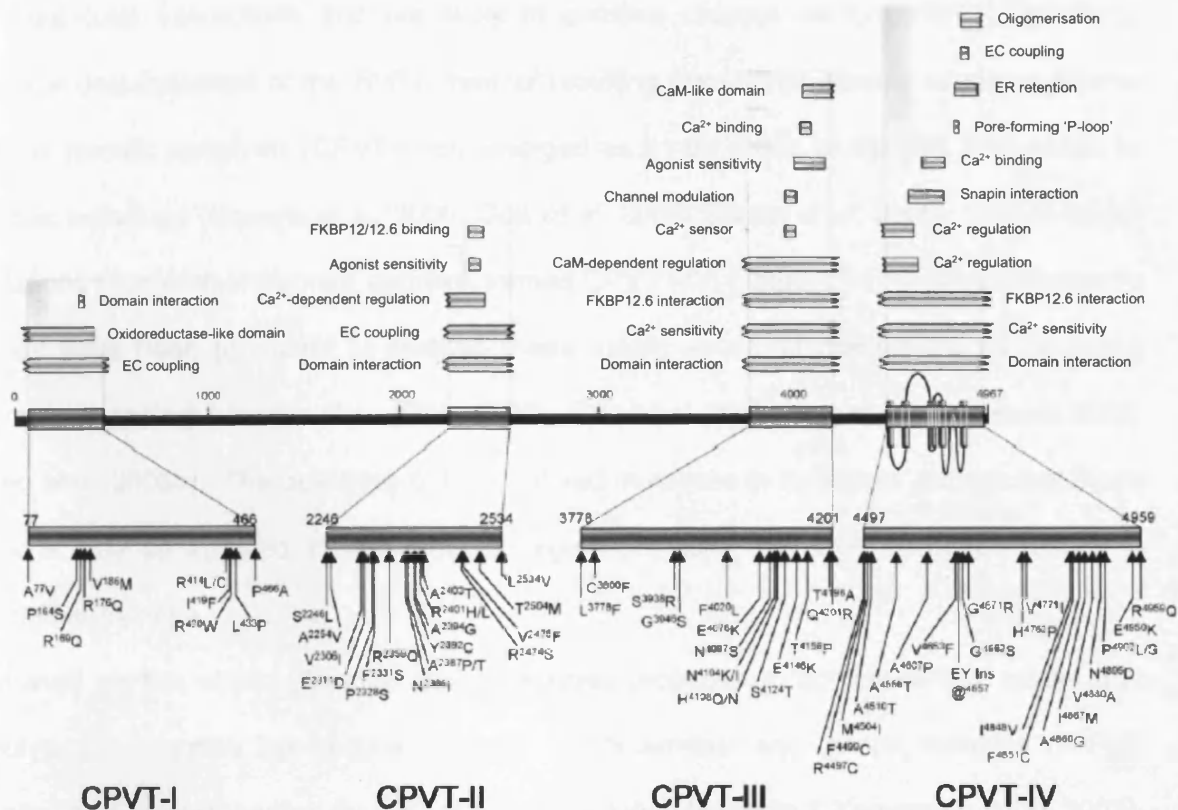


**Figure 1.16. Clustering of mutational loci in RyR2**

The 71 CPVT-linked mutations cluster into four discrete regions of RyR2 (CPVT-I, 77–466; CPVT-II, 2246–2534; CPVT-III, 3778–4201; CPVT-IV, 4497–4959). The assignment of four discrete clusters considers the non- $\text{Ca}^{2+}$  pore-forming channel part of the carboxyl-terminal (domain III) distinct from those occurring in the vicinity of the  $\text{Ca}^{2+}$  pore-forming region (domain IV), a delineation that has not been considered in previous domain nomenclature. The predominant functional characteristics of these domains are  $\text{Ca}^{2+}$ -dependent channel modulation and involvement in interdomain interactions (George *et al.* 2007a).

### 1.5 Defective inter-domain interactions and channel destabilisation in mutation-linked RyR2 dysfunction

Analysis of mutational loci in the context of RyR2 structure and function, reveals that mutations alter the ability of RyR2 to sense intracellular environment. Furthermore, the structural and functional complexity of RyR2 predicts that arrhythmogenic mutation-linked defects occur in diverse aspects of channel functionality.

RyR open-to-closed transitions are associated with long-range conformational reordering (Orlova *et al.* 1996; Sharma *et al.* 2000) and many regions of RyR participate in

intramolecular interactions that are likely to stabilise channel conformation. Therefore, physical destabilisation of the RyR2 channel resulting from either chronic acquired defects (HF) or genetic mutations (CPVT), has emerged as a new mode of channel dysfunction in cardiac pathology (George *et al.* 2006; Oda *et al.* 2005; Okuda *et al.* 2005). CPVT-linked mutations (clustered in discrete domains termed CPVT I-IV, Figure 1.16) or other pathogenic stimuli have been proposed to weaken these innate structural interactions by so-called 'domain unzipping' (George *et al.* 2005, 2007a; Oda *et al.* 2005; Yamamoto & Ikemoto 2002; Yano *et al.* 2005b). The clustering of CPVT-linked mutations in 'hot-spots' implies that these regions may be involved in vital channel regulation, such that their disruption results in cardiac arrhythmia.

Based on this notion, Ikemoto and colleagues proposed a 'domain-switch' model that involves inter-domain interactions between the N-terminal and central domains of RyR serving as a key mechanism for  $\text{Ca}^{2+}$  channel regulation (Ikemoto & Yamamoto 2000, 2002). The model assumes that in the resting or non-activated state, the N-terminal and central domains make close contact at several sub-domains, which have yet to be determined. The conformational constraints imparted by the 'zipped' configuration of these two domains stabilise the closed state of the  $\text{Ca}^{2+}$  channel. Under normal stimulating conditions, such as during EC coupling, the inter-domain contacts are weakened, resulting in an 'unzipped' configuration which leads to channel opening. According to this model, a mutation occurring within one of the sub-domains involved in maintaining the 'zipped' configuration would lead to weakened inter-domain contacts at that point. This results in a 'partially unzipped' configuration, which is more readily activated by stimuli than the correct fully 'zipped' channel, and manifests as the hyper-sensitisation and/or hyper-activation effects seen in channels containing disease-linked mutations, in both skeletal and cardiac RyR channels, implicating a structural basis for mutation-linked  $\text{Ca}^{2+}$  release dysfunction (George *et al.* 2006).

This proposed model has been tested by examining the effects of a family of synthetic peptides corresponding to the putative critical domains of RyR (designated domain peptides,

DP) on several aspects of channel function (Hamada *et al.* 2007a; Kobayashi *et al.* 2004; Oda *et al.* 2005; Yamamoto *et al.* 2000; Yang *et al.* 2006). The underlying assumption in rationalising the use of synthetic DPs as functional probes, is that these short peptides can mimic the native conformation of these epitopes in the folded channel architecture. The peptide probe strategy is summarised in Figure 1.17, and has been successful in identifying a number of interacting sub-domains in the N-terminal and central domains of RyR.

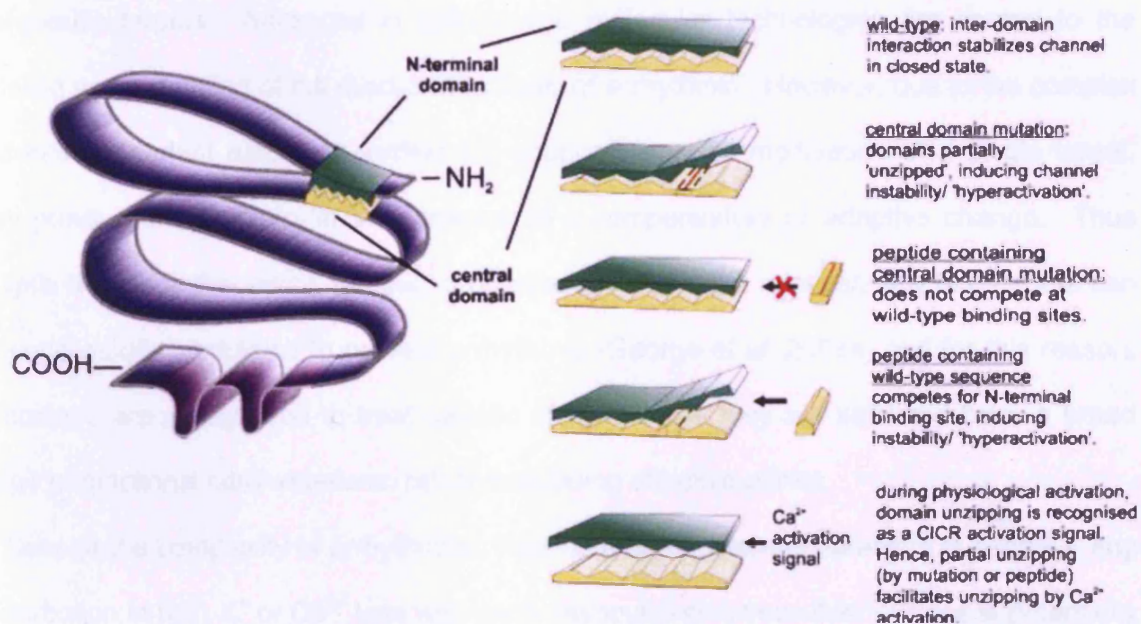


**Figure 1.17.** Schematic diagram summarising the peptide probe approach to the investigation of domain unzipping

The proposed interaction between the N-terminal and central domains, showing the postulated domain unzipping caused either by a mutation or a competitive interaction with the peptide probe (Yang *et al.* 2006).

## 1.6 Treating cardiac arrhythmias

Despite the global prevalence and mortality associated with cardiac arrhythmias, effective anti-arrhythmic strategies are lacking, with the majority of therapies sub-optimal and in some cases actually pro-arrhythmic. Although device-based therapies, such as implantable cardioverter devices (ICD), have revolutionised the treatment of highly symptomatic

arrhythmias, their widespread use is limited by the high costs associated with this treatment strategy, and therefore, for the majority of individuals with increased arrhythmia susceptibility, the primary treatment option is drug-based therapy (George *et al.* 2008a). However, existing pharmacological strategies do not address the causal mechanisms of arrhythmia and have varying degrees of efficacy.

As discussed above, a vast number of ions, receptors and pathways are involved in maintaining normal cardiac rhythm, and consequently provide numerous potential therapeutic targets. Advances in cellular and molecular technologies are central to the detailed understanding of the mechanistic basis of arrhythmia. However, due to the complex and interdependent nature of cardiac EC coupling, specific modulation of a single target, may prove pro-arrhythmic, in the absence of a compensatory or adaptive change. Thus despite the many theoretical targets, in practice there may be relatively few targets that can be successfully modulated to prevent arrhythmia (George *et al.* 2008a) and for this reason,  $\beta$ -blockers are widely used to treat cardiac arrhythmias – they are safe and have a broad range of functional consequences, rather than being effective *per se*.

Despite the complexity of arrhythmias, their central mechanistic paradigm is simple – any perturbation in  $\text{Na}^+$ ,  $\text{K}^+$  or  $\text{Ca}^{2+}$  ions with cardiomyocytes or across their surface is potentially arrhythmogenic. Therefore, it is possible that phenotypically similar arrhythmias can occur due to distinct acquired or genetically-linked cardiac disorders, and that the underlying mechanisms of ion dysfunction at the molecular level will impact the efficacy and tolerability of specific therapeutic strategies. Consequently, a key consideration in new anti-arrhythmic development is that the potential efficacy and/or pro-arrhythmic risk of a particular drug is largely dictated by the precise cardiac status of the individual.

### **1.6.1 Intracellular targets for anti-arrhythmics**

Altered ionic fluxes through surface membrane ion channels, pumps and exchangers ultimately mediate cardiac electrical dysfunction, and therefore are targets of most anti-

arrhythmic approaches. However, as the role of the SR is now emerging as an intracellular substrate for arrhythmogenesis, intracellular regulators are becoming attractive therapeutic targets. In particular, RyR2 and CaMKII, are the focus of current anti-arrhythmic strategies.

K201 (also termed JTV-519 or ICP-Calstan 100) (Kaneko 1994) is a mixed-action ion-channel modulator (Hachida *et al.* 1999; Kimura *et al.* 1999; Nakaya *et al.* 2000), and is a novel anti-arrhythmic aimed at normalising RyR2 Ca<sup>2+</sup> handling dysfunction *via* restoration of the macromolecular signalling complex (Bers 2004; Marks *et al.* 2002). K201 appears to have profoundly beneficial effects in the context of HF, which although primarily attributable to its stabilising effects on RyR2, it is acknowledged that K201 interacts with many components of the cardiac EC coupling machinery, including LTCC, NCX and SERCA (Bers 2004; Marks *et al.* 2002). Therefore, it may be that the beneficial effects of K201 may be a consequence of its lack of target specificity (George *et al.* 2008a). Despite its success in the normalisation of Ca<sup>2+</sup> handling in HF (Hunt *et al.* 2007), K201 has recently proved completely ineffective in preventing malignant arrhythmias in a mouse model of RyR mutation-linked CPVT (Liu *et al.* 2006), which supports the theory that no unifying mechanism underlying RyR2 dysfunction in HF and CPVT exists (George & Lai 2007b). Clearly, the molecular pharmacology of K201 needs to be unequivocally resolved and its clinical utility in rescuing cardiac function needs to be demonstrated in clinical trials, which are currently taking place and the results of which are keenly anticipated.

### **1.6.1.1 Targeting the RyR2 I-Domain**

An attractive and feasible route for the pharmacological modulation of RyR2 may include the use of recombinant proteins or small synthetic peptides that target specific functional epitopes within RyR2 to stabilise the channel (Ikemoto & Yamamoto 2002; Yamamoto & Ikemoto 2002). Since this approach confers sequence-specific interaction, and thus can be tailored to numerous intra-RyR2 targets, it offers the potential ability to modulate discrete aspects of RyR2 function. However, it is vital in this approach that the targeted RyR2

epitopes must be spatially accessible to permit their modification by exogenous peptides. A potential target for this type of approach is the I-Domain (3722-4610) (Figure 1.14), which, according to cryo-EM studies is a surface-accessible region and is therefore amenable to stabilisation. Furthermore, this hinge-like region of RyR2 is the location for 32% of all reported CPVT-linked mutations (Figure 1.13) and is critically involved in the intrinsic regulation of the channel (George *et al.* 2004, 2006), making it an attractive target for future peptide-based therapeutic approaches.

### **1.7 Aims of this thesis**

Interdomain interactions within the complex three-dimensional architecture of the cardiac RyR (RyR2) are pivotal in channel regulation. Acquired or genetic abnormalities that perturb these stabilising intra-molecular interactions are pathogenic. The interacting- or I-Domain of human RyR2 has been found to mediate the interaction between the cytoplasmic and transmembrane (TM) assemblies, and the general aim of this thesis is to further elucidate the precise roles of functional motifs within the I-Domain, and their effect on cellular  $\text{Ca}^{2+}$  cycling using a peptide probe-based approach. The intention of this approach was to gain an insight into the mechanism by which disruption of interdomain interactions via the I-Domain could result in abnormal  $\text{Ca}^{2+}$  handling, and whether targeting this region could normalise this interaction. It is anticipated that this investigation could provide clues to developing future epitope-targeting strategies for the therapeutic normalisation of  $\text{Ca}^{2+}$  cycling in cardiac disease.

### **1.8 General Hypothesis**

This thesis will investigate the hypothesis that the I-Domain region of RyR2 modulates  $\text{Ca}^{2+}$  handling in living mammalian cells. Specifically, work will be presented that will evaluate the phenotypic consequences of recombinant I-Domain sequences on RyR2-



dependent  $\text{Ca}^{2+}$  events in mouse cardiac cells (HL-1 cells) and human embryonic kidney (HEK) cells.

## ***Chapter 2***

### ***Materials and Methods***

## 2.1 General Materials and Methods

All reagents and chemicals were of analytical grade and were obtained from Sigma or Calbiochem, unless otherwise stated. All reagents and equipment for polyacrylamide gel electrophoresis were obtained from Biorad and Hoefer respectively, unless otherwise stated. All reagents were dissolved in deionised water (dH<sub>2</sub>O) and stored at room temperature unless otherwise stated. All filter sterilisation was through 0.2 µM filters (Sartorius).

General molecular biology, biochemical and cell culture techniques were based on procedures outlined in *Short Protocols in Molecular Biology* (Ausubel *et al.* 2002) and *Molecular Cloning: a Laboratory Manual* (Sambrook & Russell 2001) as described below, and on published methods optimised in this laboratory.

## 2.2 Molecular Biology

All growth media and antibiotics were obtained from Sigma. Sterile plasticware and glassware were obtained from Greiner and Fisher. All non-sterile glassware was washed in detergent-free water and autoclaved (135°C, 4 bars, 90 minutes). Growth media were autoclaved under the same conditions prior to the addition of antibiotics. Aseptic technique was employed throughout all protocols, and surfaces were swabbed with 70% (v/v) ethanol before and after use.

### 2.2.1 Molecular biology reagents

- *NZY medium*: 16 g/L NZ, 5 g/L yeast extract. Autoclaved.
- *LB medium*: 10 g/L tryptone, 5 g/L yeast extract, 5 g/L NaCl, 15 g/L agar (for plates only). Autoclaved, and allowed to cool to ~ 50°C before adding the appropriate antibiotic.
- *Kanamycin, 30 mg/ml stock*: filter sterilised and stored at -20°C. Used at a working concentration of 30 µg/ml. Kanamycin works as a bactericidal agent that binds to 70S ribosomes and causes misreading of mRNA, and thereby terminates protein synthesis.

Transformed bacteria will contain the kanamycin resistance gene, which encodes aminoglycoside phosphotransferase that modifies the antibiotic and prevents its interaction with the ribosomes.

- *Freezing down medium*: 50% (v/v) LB medium, 50% (v/v) glycerol. Autoclaved.
- *Resuspension solution*: 50 mM Tris, 10mM EDTA, 100µg/ml RNase A; pH adjusted to 7.5 with HCl. Filter sterilised.
- *Lysis solution*: 0.2 M NaOH, 1% (w/v) SDS. Filter sterilised.
- *Neutralisation solution*: 4.09 M guanidine-HCl, 0.759 M CH<sub>3</sub>COOK; pH adjusted to 4.2 with glacial CH<sub>3</sub>COOH. Filter sterilised.
- *Ethanol, 80% (v/v)*: a stock solution was prepared and filter sterilised.
- *Tris, 2 M*: a stock solution was prepared and the pH was adjusted to 8.0 with HCl.
- *DNA modifying and restriction enzymes*: all enzymes and appropriate buffers were obtained from New England Biolabs, Roche and Promega.
- *TAE, 50x stock*: 2 M Tris, 2 M acetic acid, 50 mM EDTA.
- *DNA Loading buffer, 2x stock*: 2x TAE, 50% (v/v) glycerol, 0.25% (w/v) orange G.
- *Molecular weight DNA markers*: 1kb Plus ladder obtained from Invitrogen.
- *Column equilibration buffer (QBT)*: 750 mM NaCl; 50 mM MOPS, pH7.0; 15% (v/v) isopropanol, 0.15% (v/v) Triton<sup>®</sup> X-100.
- *Medium salt column buffer (QC)*: 1 M NaCl; 50 mM MOPS, pH 7.0; 15% (v/v) isopropanol.
- *Column elution buffer (QF)*: 1.25 M NaCl; 50 mM Tris, pH 8.5; 15% (v/v) isopropanol.
- *Sequencing kit*: BigDye terminator v5, obtained from Applied Biosystems.

### 2.2.2 Oligonucleotides

Custom oligonucleotide primers were ordered from Sigma-Genosys, and were obtained as lyophilised pellets. Pellets were resuspended in an appropriate volume of sterile dH<sub>2</sub>O to give a stock concentration of ~ 250 µM, according to the manufacturer's instructions. Primer concentration was confirmed by spectrophotometric quantification of a 1:100 dilution (in

duplicate), by measuring the absorbance at 260 nm ( $A_{260}$ ) in a quartz cuvette using a spectrophotometer (MBA2000, Perkin-Elmer). Using the nucleotide sequence, the molecular weight and the melting temperature of the oligonucleotides, the concentration was calculated (given that  $A_{260} = 1$  corresponds to ~20-39  $\mu\text{g/ml}$  of ssDNA depending on the base composition, with ~ 33  $\mu\text{g/ml}$  taken on assumption of an equal mixture of the four bases). Working concentrations (20 $\mu\text{M}$  for PCR amplification; 3.2 $\mu\text{M}$  for DNA sequencing) were prepared and primers were stored at -20°C. A list of the primers used in this study is given in Appendix I.

### 2.2.3 Propagation of recombinant DNA constructs

*Epicurian coli* ultracompetent XL-10 Gold cells (Stratagene) have been shown to consistently propagate *bona fide* RyR2 plasmid (George *et al.* 2003a, 2003b) and were consequently used for the propagation of recombinant DNA constructs. This strain of *E. coli* contains the *recA1* gene locus which minimises host rearrangement of recombinant DNA, and has been specifically optimised for increased transformation efficiency and stability of larger fragile templates such as hRyR2. Bacteria were cultured at 37°C under aseptic conditions in LB medium, either on solid medium on LB-agar plates (Hereaus) or in suspension with shaking at 225 rpm (Innova 4300 shaker, New Brunswick). The LB medium contained kanamycin at 30  $\mu\text{g/ml}$  for selective growth of bacteria containing the plasmid.

XL-10 Gold cells were transformed as follows: The ultracompetent cells (25 $\mu\text{l}$ ) were thawed on ice and treated with 1 $\mu\text{l}$  0.5 M  $\beta$ -mercaptoethanol for 10 minutes, before the addition of DNA (50 ng for transformation of a ligation mix, or 10 ng for re-transformation of a plasmid). Cells were incubated for a further 30 minutes on ice, before heat-shock treatment at 42°C for exactly 30 seconds then immediate transfer to ice for 3 minutes. NZY medium (900 $\mu\text{l}$ ) pre-warmed to RT was added and the suspension was incubated at 37°C for 1 hour with continuous shaking (225 rpm). Following this incubation time, the suspension was plated on LB-Agar medium containing kanamycin (30  $\mu\text{g/ml}$ ), which was incubated at 30°C

until the appearance of discrete colonies (typically after 16-18 hours incubation). From these colonies, any larger colonies (diameter >1mm) were disregarded, and only the smallest colonies were selected for screening.

#### **2.2.4 Generating frozen stocks of bacterial cells**

For long-term storage of transformed bacteria, frozen glycerol stocks were made from 750µl of liquid culture grown in the presence of antibiotic for 16 h mixed with sterile glycerol in a 1:1 ratio. The glycerol stocks were snap-frozen on dry ice and stored at -80°C in cryovials. Bacteria from this frozen stock were cultured by streaking 10µl of the stock onto LB-agar plates containing antibiotic.

#### **2.2.5 Small-scale plasmid DNA isolation ('mini-prep')**

Colonies were screened for the presence of recombinant plasmid using the Wizard SV mini-prep plasmid purification kit (Promega), which employs the SDS-alkaline denaturation method for plasmid DNA isolation. Single colonies were inoculated into 5ml LB medium containing kanamycin (30 µg/ml) and incubated overnight at 37°C with continuous shaking (225rpm). A proportion (3ml) of each culture was subsequently pelleted at 13,000 xg for 2 minutes (Microfuge R, Beckman). The pellets were resuspended in 250µl resuspension solution containing RNase A to ensure that any contaminating RNA which could affect downstream applications is digested, and subsequently lysed in 250µl lysis solution containing SDS and NaOH. The SDS solubilises phospholipid and protein components of the cell membrane leading to the release of the cell contents, while the NaOH denatures the chromosomal DNA and plasmid DNA as well as proteins. The lysate was then neutralised by addition of 350µl neutralisation solution containing acidic potassium acetate. The rapid neutralisation with high salt concentration results in precipitation of potassium dodecyl sulphate (KDS) and causes chromosomal DNA to base-pair in an intra-strand manner,

forming an insoluble aggregate that precipitates out of solution. Denatured proteins, chromosomal DNA, and cellular debris are co-precipitated in insoluble salt-detergent complexes, and were removed by centrifugation at 13,000  $xg$  for 10 minutes. The circular covalently closed plasmid DNA renatures correctly by inter-strand hybridisation and remains in solution. The cleared lysate containing the plasmid DNA was then applied to a spin column containing a silica-gel DNA binding membrane, and centrifuged for a further 1 minute at 13,000  $xg$ . The membrane was washed twice with an 80% ethanol buffer, and the DNA was eluted off the membrane in 50 $\mu$ l 10 mM Tris pH 8.

After purification, recombinant plasmids were verified by restriction endonuclease mapping; typically with two separate enzyme digest reactions, each producing a distinct band pattern. DNA fragments were then analysed by agarose gel electrophoresis (Section 2.2.6) before being prepared on a larger scale (Section 2.2.7).

### **2.2.6 Agarose gel electrophoresis**

DNA fragments were separated on an agarose gel and using a 1 kb DNA molecular weight marker (Invitrogen) for size calibration. All gels contained 1% agarose (ultra-pure, Eurogentec), and were prepared by dissolving the agarose (1% w/v) in 1x TAE buffer. The solution was heated in a microwave until boiling, then left to cool to below 50°C before addition of ethidium bromide (0.1  $\mu$ g/ml), and poured into a gel casting tray which was assembled according to the manufacturer's instructions (BioRad). Once the gel was set, DNA samples in 1x DNA loading buffer were loaded onto the gel alongside the 1 kb molecular weight marker. The DNA loading buffer contains Orange G for visualisation, which co-migrates with DNA fragments at ~200 bp. Electrophoresis was carried out by submerging the gel in 1x TAE and subjecting it to a constant voltage of 5 V per cm, until the dye front had travelled approximately two thirds the length of the gel. Gels were visualised with UV transillumination and imaged using a gel documentation system (BioRad) with a Hamamatsu camera and Quantity One Software (BioRad).

### 2.2.7 Large-scale plasmid isolation ('maxi-prep')

Cultures which produced plasmid DNA giving the correct endonuclease digest pattern, with negligible evidence of degradation were selected for large-scale maxi-prep culture. Restriction-digest verified mini-prep culture (1ml) was inoculated in 5ml LB broth for 1-2 hours, before being transferred to 250ml LB broth containing kanamycin (30µl/ml) and incubated for 16-18 hours at 37°C with continuous shaking (225rpm).

The bacterial suspension was pelleted by centrifugation (8000 *xg*, 20 minutes, 4°C; Avanti J-25, Beckman) and plasmid extraction was performed using the QIAGEN PlasmidMaxi Kit, following the manufacturer's instructions. This protocol is based on a modified alkaline lysis procedure, followed by binding of plasmid DNA to QIAGEN Anion-Exchange Resin, which is positively charged with diethylaminoethyl (DEAE) groups, under optimised low-salt and pH conditions. The pellets underwent bacterial lysis using the same reagents as previously described (Section 2.2.5). Samples were then incubated on ice for 20 minutes, before insoluble cell matter was removed by centrifugation (20 000 *xg*, 30 minutes, 4°C). The supernatant was applied to a QIAGEN-tip 500 pre-equilibrated with column equilibration buffer (QBT). The plasmid DNA was then washed twice with a medium-salt column wash buffer (QC) to remove impurities such as RNA and proteins. The plasmid DNA was then eluted off the column with a high-salt elution buffer QF. Plasmid DNA was precipitated using isopropanol (0.7 volumes) overnight at -20°C. Following centrifugation, (15 000 *xg*, 30 minutes, 4°C) the DNA pellet was washed in 5ml 70% ethanol and further centrifuged (15,000 *xg*, 10 minutes, 4°C). The pellet was then incubated with 500µl Tris (pH 8, 10 mM) at 37°C for 5 minutes to resuspend the plasmid DNA. Tris (10 mM, pH 8) was used instead of dH<sub>2</sub>O, as DNA is more readily soluble under alkaline conditions and does not interfere in downstream applications.



### 2.2.8 Spectrophotometric DNA quantification

DNA exhibits peak light absorption at 260 nm, and DNA concentration was determined by spectrophotometric quantification of a 1:50 dilution sample (in duplicate) at this wavelength. The concentration was calculated taking into account that an  $A_{260}$  of 1 corresponds to 50 µg/ml of double stranded DNA. Any contaminating proteins present will have a peak light absorbance at 280 nm, therefore plasmid purity can be quantified by using the ratio of  $A_{260}/A_{280}$ . Values  $\geq 1.8$  indicate plasmid preparations of high purity.

### 2.2.9 DNA Sequencing

All recombinant plasmids were confirmed by automated DNA sequencing using the BigDye Terminator cycle sequencing kit (ABI Prism) and ABI Prism 377 sequencer (Applied Biosystems) according to the manufacturer's protocol using 3.2 pmol sense sequencing primer and 500 ng plasmid DNA. Automated sequencing is based on the incorporation of fluorescent dyes into fragments of DNA, which are optimised for detection with an argon laser. The fluorescent terminator dyes contain a fluorescein donor dye (6-FAM), conjugated to one of four dichlororhodamin (dRhodamine) acceptor dyes. The fluorescein donor determines the excitation maximum of each dye, while the emission spectrum is dependent on the dRhodamine acceptor. The fluorescently labelled DNA fragments are then separated by capillary array electrophoresis, and are passed through a laser beam as they enter the detection cell. The laser excites the fluorescent dyes, and the resulting fluorescence is converted into electronic form which is analysed by the sequencing software and visualised as a sequence electropherogram.

### 2.2.10 PCR amplification of DNA

PCR reactions were carried out using a Perkin-Elmer GeneAmp system 2400 thermal cycler. Phusion™ High-Fidelity DNA Polymerase (Finnzymes) was used for the generation of high fidelity products suitable for cloning. This enzyme, possessing 3'→5' exonuclease “proofreading” activity, exhibits low error rate and high efficiency. The reaction mixture components and thermal cycling conditions are shown in Table 2.1 and Table 2.2. PCR products were verified by agarose gel electrophoresis (Section 2.2.6) and purified using the QIAquick PCR purification kit (Qiagen) as described in Section 2.2.11.

**Table 2.1. Typical PCR reaction mixture**

Reagent	Final Concentration	Volume
DNA Template	50 ng	0.5µl of 200 ng/µl stock
Forward Primer	20 pmol	1µl of 20 µM stock
Reverse primer	20 pmol	1µl of 20 µM stock
HF buffer (with 1.5 mM MgCl <sub>2</sub> )	1x	5µl of 10x stock
dNTP mix	0.2 mM	0.5µl of 20 mM stock
DNA polymerase	1 U	0.5µl of 2 U/µl stock
Nuclease-free dH <sub>2</sub> O	Up to 50µl	41.5µl

**Table 2.2. Typical thermal cycling conditions**

Step	Temperature	Time	Number of cycles
Initial denaturation	98°C	2 minutes	1
Denaturation	98°C	10 seconds	
Annealing*	60°C	30 seconds	28
Extension	72°C	60 seconds	
Final Extension	72°C	5 minutes	1
Storage	4°C	Indefinite	1

\*Annealing temperature is dictated by the  $T_m$  of the primer, but is typically 58-60°C

### 2.2.11 Cloning of DNA fragments

Plasmid DNA (1 µg) was digested with suitable restriction enzymes (5-10 U per 20µl reaction) for 2 hours at 37°C, before separation on an agarose gel to confirm correct fragment size. The required band was excised from the gel using a sterile scalpel under ultra-violet light ( $\lambda$ ) and purified using QIAEX II gel extraction kit (Qiagen). Briefly, this agarose gel slice was dissolved in a high-salt buffer containing DNA-binding beads for 5 minutes at 50°C. The high-salt buffer containing 4 M chaotropic guanidium salt disrupts the hydrogen bonds present in the agarose gel and allows the DNA to bind to the silica beads. The beads were then sedimented by centrifugation at 14,000  $xg$  for 30 seconds, and then washed once with high salt buffer, followed by a further two times with a 70% ethanol buffer. DNA was eluted from the beads in 30µl 10 mM Tris pH 8.5.

PCR products were digested in the same way, and 10% of the reaction was analysed by gel electrophoresis. The remainder of the reaction was purified with the QIAquick PCR Purification Kit (QIAGEN), which employs a DNA-binding 'spin' column. The PCR products were added to the column and centrifuged at 14,000  $xg$  for 1 minute before washing twice with an 80% ethanol buffer. The DNA was then eluted in 30µl nuclease-free water.

The DNA fragments were ligated into pET-29(b) plasmid vector (Novagen), a kanamycin resistant translation vector, with protein expression driven by a T7 phage ribosome binding site. pET-29(b) carries two fusion tags; an N-terminal S-Tag/thrombin configuration plus a C-terminal polyHis sequence (Figure 2.1). This combination of fusion tags was chosen due to their small size, and they also facilitate detection by immunoblot analysis (Section 2.3.6) as well as affinity purification with the corresponding resin and buffers (Sections 2.3.7 and 2.3.8).

Prior to ligation, the linearised pET-29(b) vector was treated with 1µl Shrimp Alkaline Phosphatase (SAP, Promega) for 30 minutes at 37°C. SAP treatment removes the 5'-phosphate group from the linearised vector, and reduces the possibility of self-ligation. The SAP was then inactivated by heat denaturation at 65°C for 15 minute.

Ligation was carried out using the Rapid DNA Ligation Kit (Roche), according to the manufacturer's guidelines. The insert to be ligated was mixed with the appropriately digested plasmid vector (50 ng) in a 3:1 molar ratio, along with a ligase buffer and T4 DNA ligase. To calculate the appropriate amount of insert to include in the ligation reaction, the following equation was used:

$$\frac{\text{ng of vector} \times \text{kb size of insert}}{\text{kb size of vector}} \times \text{insert : vector molar ratio} = \text{ng of insert DNA}$$

The ligation mixture was then incubated at 4°C for 16 hours before being used to transform competent bacteria.

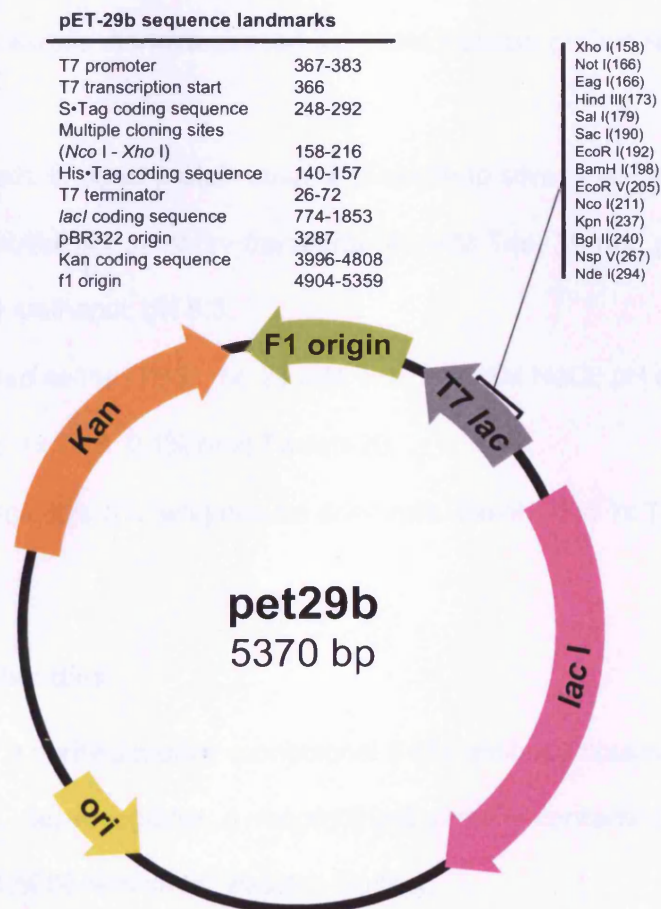


Figure 2.1. pET-29(b) expression vector

## 2.3 Protein Biochemistry

### 2.3.1 Protein biochemistry reagents

- *Ammonium persulphate*: 10% (w/v); always freshly prepared and kept on ice.
- *Tris, 0.5 M*: a 0.5 M solution was prepared, and pH adjusted to 6.8 with HCl. Stored at 4°C.
- *Tris, 1.5 M*: a 1.5 M solution was prepared, and pH adjusted to 8.8 with HCl. Stored at 4°C.
- *Running buffer, 1x*: 25 mM Tris, 250 mM glycine, 0.1% (w/v) SDS.
- *SDS-gel loading buffer, 2x*: 100 mM Tris pH 6.8, 20% (v/v) glycerol, 4% (w/v) SDS, 10% (v/v)  $\beta$ -mercaptoethanol, 0.2% (w/v) bromophenol blue. Filter sterilised and always freshly prepared
- *Molecular weight markers*: prestained Kaleidoscope protein markers, obtained from Bio-Rad.
- *Protein stain*: Imperial protein stain or SilverSnap silver staining kit, both from Pierce.
- *Transfer buffer (for semi-dry transfers)*: 48 mM Tris, 39 mM glycine, 0.037% (w/v) SDS, 20% (v/v) methanol, pH 8.3.
- *Tris-buffered saline (TBS), 1x*: 20 mM Tris, 137 mM NaCl; pH adjusted to 7.6 with HCl.
- *TBS-T, 1x*: 1x TBS, 0.1% (v/v) Tween-20.
- *Blocking solution*: 5% (w/v) non-fat dried milk dissolved in 1x TBS-T

### 2.3.2 Antibodies

- *Ab-6xHis*: a purified murine monoclonal 6-His antibody obtained from Covance Research Products, raised against a recombinant protein containing the sequence HHHHHH. Used at 1:5000 dilution for western blotting.
- *pAb-1093*: rabbit anticonal antiserum, raised against residues 4515-4564 of the cardiac ryanodine receptor (EDKGGKQKLRQLHTRYGEPEC). The antibody was purified using

MelonGel IgG Purification kit (Pierce) and subsequently used at 1:500 dilution for Western blotting.

- *S-protein HRP Conjugate*: a 104 aa S-protein, which binds with high affinity and specificity to the 15 aa S-Tag fusion tag expressed from the pET-29(b) protein expression vector. Obtained from Novagen, and used at 1:7500 dilution for Western blotting.

### 2.3.3 SDS-Polyacrylamide gel electrophoresis (SDS-PAGE)

Protein profiles were visualised by SDS-PAGE on 140 x 160 x 1.5 mm gels (SE600, Hoefer). A separating gel of appropriate acrylamide concentration was prepared as described in Table 2.3. The acrylamide/bisacrylamide forms a cross-linked polymer network in the presence of ammonium persulphate, and the size of pores created in the gel is inversely related to the amount of acrylamide used. Large proteins were resolved on gels with a low concentration of acrylamide, and vice versa. The separating gel was poured into the gel casting system, which was assembled according to the manufacturer's instructions, and covered with a thin layer of water. The gel was left to set for ~ 2 hours, before carefully removing the water layer with filter paper. The stacking gel (4% (w/v) acrylamide) was then prepared as the separating gel, but using 0.5 M Tris pH 8 buffer. This was then poured on top of the separating gel, and a 15-lane comb was inserted to form the wells. The stacking gel has a larger pore size and a lower pH than the separating gel, making the proteins in each sample condense into a tight band before entering the separating gel. Once the stacking gel was set, protein samples were incubated at 50°C for 10 minutes in 2x or 5x Laemmli buffer containing SDS, a strong anionic detergent which denatures non-covalent bonds in the secondary and tertiary structures and applies a uniform negative charge density to each protein to allow the proteins to separate according to mass. The samples were then loaded onto the gel alongside Kaleidoscope prestained protein molecular weight markers (BioRad) which consist of seven uniquely coloured proteins with molecular weight range of

approximately 200 – 6.5 kDa. Electrophoresis was carried out at a constant current (typically 10-15 mA overnight at 4°C) until the bromophenol blue dye-front had nearly run off the gel. Protein separation was visualised by protein staining of the gel (Section 2.3.4), or gels were then transferred to membrane and analysed by immunoblotting (Sections 2.3.5 and 2.3.6).

**Table 2.3. Separating acrylamide gel composition**

Reagent	Final
Acrylamide/bis-acrylamide (37.5:1), 40%	X*
Tris, 1.5 M, pH 8.8	25% (v/v)
SDS, 20% (w/v)	0.5% (v/v)
Ammonium persulphate, 10% (w/v)	0.5% (v/v)
TEMED	0.05% (v/v)
dH <sub>2</sub> O	Up to 30ml

\* Where X is dependent on the % of acrylamide required, according to the sizes of the proteins separated

### 2.3.4 Staining proteins on an SDS-PAGE gel

Proteins were visualised on an SDS-PAGE gel by staining with Imperial Protein Stain (Pierce) or SilverSnap Stain (Pierce), before being scanned and dried onto filter paper in a vacuum gel dryer.

Imperial Protein Stain is a Coomassie R-250 dye-based reagent, claimed by the manufacturer to be sensitive to as little as 3 ng protein. After electrophoresis, gels were washed with dH<sub>2</sub>O three times for 5 minutes, then left overnight at RT in Imperial Protein Stain on a rocking platform. After this time, the stain was discarded and the gel was destained in dH<sub>2</sub>O on a rocking platform at RT overnight.

SilverSnap Stain is an ultrasensitive silver stain system, and can detect  $\geq 0.25$  ng protein. After electrophoresis, gels were washed twice with dH<sub>2</sub>O for 5 minutes, then fixed in 30% ethanol:10% acetic acid for 2 x 15 minutes on a rocking platform. The fixing solution was

discarded, and the gel washed in 10% ethanol for 2 x 5 minutes, then in dH<sub>2</sub>O for 2 x 5 minutes. The gel was subsequently sensitised for exactly 1 minute in Sensitizer Working Solution (1:500 SilverSnap Sensitizer : dH<sub>2</sub>O) before being washed for 2 x 1 minute in dH<sub>2</sub>O. The gel was then incubated in Stain Working Solution (1:50 SilverSnap Enhancer : SilverSnap Stain) for 30 minutes at RT on a rocking platform. After this time the gel was washed briefly in dH<sub>2</sub>O for 2 x 20 seconds, then incubated in Developer Working Solution (1:50 SilverSnap Enhancer : SilverSnap Developer) for 2-3 minutes at RT on a rocking platform, until protein bands began to appear. The reaction was stopped by transferring the gel to 5% (v/v) acetic acid.

### **2.3.5 *Electro-transfer of proteins onto a membrane***

Proteins from SDS-PAGE gels were transferred onto polyvinylidene difluoride (PVDF) membrane with a pore size of 0.45 µm (Immobilon-P, Millipore) using a semi-dry transfer system (Hoefer). The PVDF membrane was prepared, according to the manufacturer's guidelines, by soaking in methanol for 10-30 seconds then in semi-dry transfer buffer for 30 minutes. Protein transfer was carried out at RT for 3 hours at 250 mA, with voltage limited to 25 V.

### **2.3.6 *Immunoblot analysis***

Following protein transfer, non-specific binding sites were blocked by incubating the PVDF in membrane blocking buffer for 90 minutes at RT or overnight at 4°C. Primary antibody was added in the appropriate dilution (Section 2.3.2) in membrane blocking buffer for 90 minutes at RT or overnight at 4°C. The membrane was then washed with TBS-T (5x 10 minutes, 2x 5 minutes) to remove surplus non-bound primary antibody. A suitable HRP-conjugated secondary antibody was then added in membrane blocking buffer (1:10,000 dilution) for 90 minutes at RT. The membrane was washed as before in TBS-T. The



immunoreactive protein bands were visualised using enhanced chemiluminescence (ECL) reagent (GE Healthcare), a highly sensitive detection method which can detect as little as 1 pg of antigen, dependent on the quantities of labelled secondary antibody present. Chemiluminescence systems generate light by oxidation of luminol in the presence of hydrogen peroxide (H<sub>2</sub>O<sub>2</sub>) and HRP under alkaline conditions. Immediately following oxidation, the luminol is in an excited state which then decays to ground state via a light emitting pathway. The ECL system enhances the emitted light signal by the oxidation of luminol by the HRP in the presence of phenol, which has the effect of increasing the light output approximately 1000-fold and extending the time of light emission. The light produced by this enhanced chemiluminescent reaction peaks after 5–20 minutes and decays slowly thereafter with a half life of approximately 60 minutes. The maximum light emission is at a wavelength of 428 nm which can be detected after a short exposure to high performance chemiluminescence film (Hyperfilm, GE Healthcare) and developed using an automated image developer.

### **2.3.7 Purification of histidine-tagged proteins using a Ni<sup>2+</sup> affinity technique**

There are many commercially available systems for the nickel-affinity purification of His-tagged proteins. For the purposes of this study, His GraviTrap™ (GE Healthcare) was used due to the speed and ease of the purification of large volumes of bacterial culture. His GraviTrap™ is a prepacked, single-use gravity-flow Ni Sepharose™ 6 Fast Flow column for purification of histidine-tagged proteins by immobilised metal-affinity chromatography (IMAC). This system allows the purification of large sample volumes, and the histidine-tagged protein is effectively eluted in a small volume.

Purification of histidine-tagged proteins on His GraviTrap can be divided into four stages: equilibration, sample application, washing, and elution (Figure 2.2). The column was first equilibrated with 20 mM imidazole washing/binding buffer (10ml). The sample is then loaded and allowed to flow through the column, before washing with 20 mM imidazole buffer (10ml).

His-tagged protein was then eluted in 10ml 500 mM imidazole elution buffer (2 x 3ml).

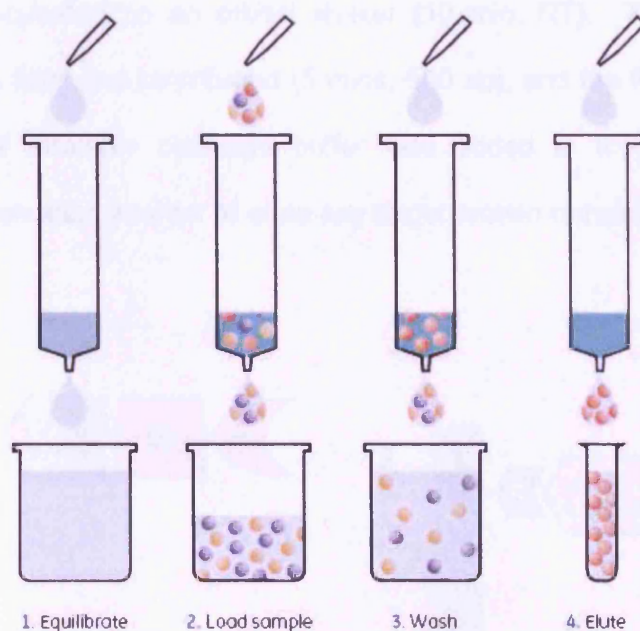


**Figure 2.2. Schematic of Ni<sup>2+</sup> affinity purification of histidine-tagged proteins**

Four-stage purification of HexaHis-tagged proteins. First, the column is equilibrated. The sample is then loaded and washed to remove contaminants. Purified protein is then eluted with 500 mM imidazole.

### 2.3.8 Purification of S-tagged proteins by S-protein affinity

The S-tag Thrombin Purification Kit (Novagen) was used for affinity purification of S-tag using S-protein agarose which specifically retains S-tag fusion proteins. In this strategy, the protein was released from the S-protein agarose by thrombin digestion which occurs at the thrombin cleavage site located between the S-tag sequence and the cloning region.

The protein was first incubated with the S-protein Agarose (2ml) and incubated on an orbital shaker (30 mins, RT). This was then centrifuged (10 mins, 500 xg) and the supernatant decanted, the resultant agarose pellet containing the target protein was resuspended in 1x bind/wash buffer (5ml). The centrifugation and washing steps were repeated twice more. After the washing steps, the pellet was resuspended in 1x thrombin

cleavage buffer (5ml) supplemented with biotinylated thrombin (25 U), and incubated on an orbital shaker (3 hr, RT). After this incubation time, streptavidin agarose (800 $\mu$ l) was added to the slurry and incubated on an orbital shaker (10 min, RT). The mixture was then transferred to a spin filter and centrifuged (5 mins, 500  $xg$ ), and the flow-through collected. A further 1.25ml of thrombin cleavage buffer was added to the spin filter and then centrifugation was repeated, in order to elute any target protein remaining on the filter.

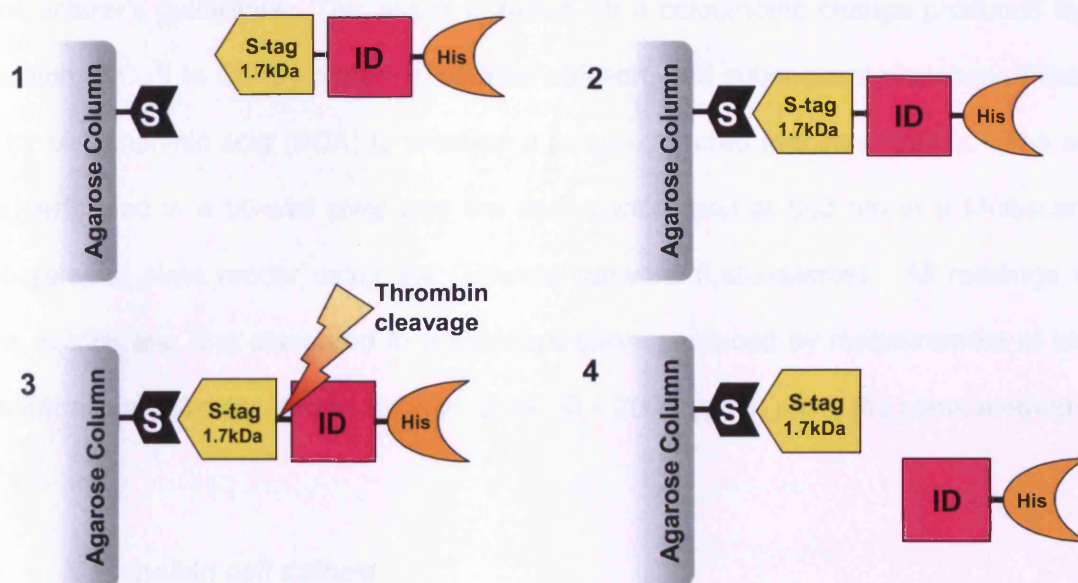


**Figure 2.3. Schematic of protein purification by S-protein affinity and thrombin cleavage**

The S-tagged protein is captured by S-protein agarose and washed to remove contaminants, before being S-tag is cleaved off by thrombin digestion.

### 2.3.9 Densitometric analysis

Densitometric quantification of the density of stained protein bands is a technique widely used to compare the amounts of different MW proteins present in one or more samples, and was carried out using QuantityOne imaging software (BioRad).

Images were obtained by scanning the SDS-PAGE gel or exposed chemiluminescence film. Densitometry was subsequently carried out by defining an equal area around the

bands of interest and quantifying its optical density (OD/mm<sup>2</sup>). Densitometry is only valid at sub-saturating levels of signal development. QuantityOne has an in-built feature that determines whether the signal is within 256 shades of gray (i.e. sub-saturation) of background signal levels.

### **2.3.10 Determination of protein concentration**

Protein concentration was determined using BCA assay kit (Pierce) per the manufacturer's guidelines. This assay is based on a colorimetric change produced by the reduction of Cu<sup>2+</sup> to Cu<sup>+</sup> by protein in alkaline solution, and subsequent chelation of the Cu<sup>+</sup> ion by bicinchoninic acid (BCA) to produce a purple coloured reaction product. The assay was performed in a 96-well plate and the absorbance read at 560 nm in a Multiscan EX (Labsystems) plate reader using the Genesis software (Labsystems). All readings were done in triplicate, and compared to a standard curve produced by measurement of known concentrations of bovine serum albumin (BSA) (0 – 2000 µg/ml) using the same method.

## **2.4 Mammalian cell culture**

All growth media and reagents were supplied by Invitrogen and all chemicals were obtained from Sigma unless otherwise stated. Sterile culture flasks and bottles were supplied by Nunc (Fisher) or Greiner. Class II cell culture containment hoods (Microflow biological safety cabinets) were employed for all procedures.

### **2.4.1 Mammalian cell culture reagents**

- *Dulbecco's Modified Eagle Medium (DMEM)*: supplemented with 10% (v/v) foetal calf serum, 2 mM glutamine and 100 µg/ml penicillin/streptomycin (all filter sterilised). Stored at 4°C.
- *Cell fixing solution*: 4% (w/v) paraformaldehyde in PBS, always freshly prepared.

- *Poly-L-lysine, 0.1% solution*: used to coat coverslips (150µl/coverslip). Stored at 4°C.
- *Saline solution*: 0.9% (w/v) supplied by Baxter Medical Supplies.
- *Trypsin-EDTA*: 1x in HBS without Ca<sup>2+</sup> or Mg<sup>2+</sup>, stored at – 20°C.
- *Freeze-down medium*: 10% (v/v) dimethyl sulphoxide (DMSO) in foetal calf serum, filter sterilised and stored at 4°C.
- *Phosphate buffered saline (PBS)*: 137 mM NaCl, 2.7 mM KCl, 4.3 mM Na<sub>2</sub>HPO<sub>4</sub>, 1.4 mM KH<sub>2</sub>PO<sub>4</sub>, pH adjusted to 7.4 using HCl, filter sterilised.
- *Gelatin fibronectin (GFN)*: 1.25% (v/v) fibronectin, 0.002% (w/v) gelatin in dH<sub>2</sub>O, filter sterilised.
- *Norepinephrine, 10 mM*: made up in 30 mM ascorbic acid solution.
- *Claycomb medium*: supplemented with 10% (v/v) foetal calf serum, 2 mM glutamine, 100 µg/ml penicillin/streptomycin and 100 µM norepinephrine (all filter sterilised).

#### 2.4.2 Mammalian cell lines

- *HL-1 cells*: cardiac cell line derived from the AT-1 mouse atrial cardiomyocyte tumour lineage (Claycomb *et al.* 1998). This cell line is described in detail in Chapter 4.
- *HEK293*: cells derived from human embryonic kidney cells immortalised by adenovirus 5 DNA infection (Graham *et al.* 1977).

#### 2.4.3 Culture of Human Embryonic Kidney (HEK) 293 cells

HEK293 cells were cultured in DMEM containing 4.5 g/L glucose (Invitrogen) supplemented with foetal calf serum (10% v/v), and penicillin/streptomycin/glutamine (1% v/v) (Invitrogen) in an incubator at 37°C, 5% CO<sub>2</sub> and ~80% humidity (Heraeus) using 150ml flasks (Nunc). Cells were maintained in 75 cm<sup>2</sup> flasks containing 20ml medium, and these were harvested, and passaged when 70% confluency was reached, as shown in Figure 2.4. They were harvested by brief trypsinisation (2ml) at 37°C before being pelleted (1100 rpm, 3

min). The resulting pellet was resuspended in 5ml of medium, and 1ml was used to seed a new culture flask. The remainder was discarded or preserved in liquid nitrogen (see Section 2.4.5).

#### **2.4.4 Culture of HL-1 cardiomyocytes**

HL-1 cells were cultured in Claycomb medium (SAFC) supplemented with foetal calf serum (10% v/v), and penicillin/streptomycin/glutamine (1% v/v) (Invitrogen) in an incubator at 37°C, 5% CO<sub>2</sub> and ~80% humidity (Heraeus) using 150ml flasks (Invitrogen). Cells were maintained in GFN-coated 25 cm<sup>2</sup> flasks containing 7ml medium, and these were harvested, split and re-seeded at a ratio of 1 in 3 when superconfluency was reached (Figure 2.4). Cells were harvested by trypsinisation for 2 mins at 37°C and washed with dH<sub>2</sub>O to remove any cells that were not strongly adhered to the GFN matrix. Non-adherence directly to the GFN matrix is the primary cause of dedifferentiation from the cardiac cell phenotype in this cell population. This was followed by a second trypsinisation step at 37°C until all of the cells were released from the matrix, before being pelleted (1100 rpm, 3 min). The resulting pellet was resuspended in 6ml of medium, and 2ml was used to seed a new culture flask. The remainder was discarded or preserved in liquid nitrogen (see Section 2.4.5).

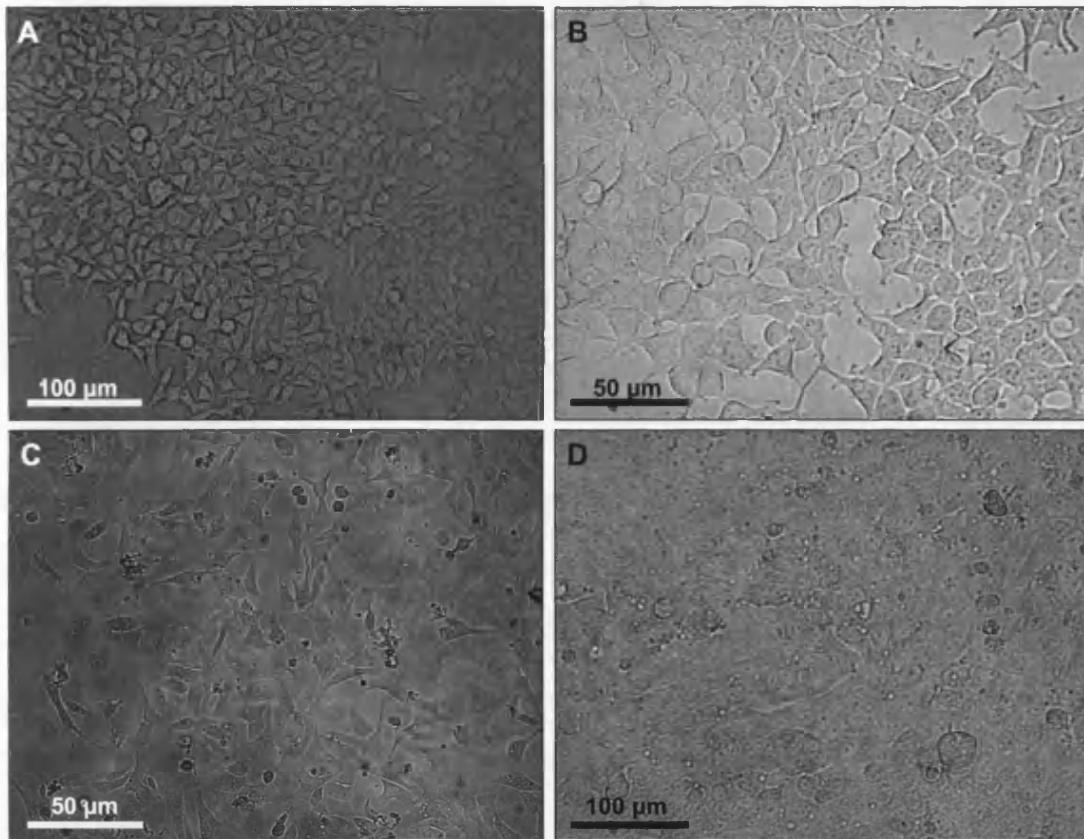


**Figure 2.4. Phase microscopy images of healthy HEK and HL-1 cells**

**Panels A** and **B** show a phase image of healthy HEK cells at ~70% confluency; 20x and 40x magnification respectively. **Panel C** shows a phase image of healthy non-confluent HL-1 cells with 20x magnification. **Panel D** shows healthy HL-1 cells at 'superconfluency', which are ready to be harvested and split. At 'superconfluency' HL-1 cell boundaries in the myocyte monolayer are difficult to determine. All images taken on a Zeiss Axiovert 200 microscope

#### 2.4.5 Generating frozen stocks of mammalian cell lines

Cells were harvested and pelleted as above and the cell pellet was resuspended in 1ml of freeze-down medium using a wide-bore syringe and transferred to labelled cryo-vials (NUNC). Vials were wrapped in several layers of tissue paper to prevent rapid freezing and stored for 24h at  $-80^{\circ}\text{C}$ . Once fully frozen, the insulating tissue was removed and vials were transferred into liquid nitrogen storage.

To establish cultures from stocks, cells were rapidly thawed by hand warming and the DMSO was removed by pelleting the cells at 500 g for 2 min. Cells were resuspended in the appropriate supplemented media and re-seeded as above.

## **2.5 Computer software and data analysis**

Numerical data were stored in spreadsheets and plotted in graphical form using Excel (Microsoft) or GraphPad Prism. Western blots were scanned at 300dpi using a densitometer (GS-700, Bio-Rad), and image processing was undertaken using Photoshop (Adobe) and PowerPoint (Microsoft). Densitometric analysis was performed on 'raw data' images using Quantity One software (Bio-Rad). All measurements were calibrated against an area of the blot that did not contain protein.

DNA and protein sequence analysis was done using software contained within the Genetic Computing Group package (GCG, University of Wisconsin, USA) or JEMBOSS, both of which can be accessed via the MRC website (<http://www.hgmp.mrc.ac.uk>) or using software available at the NCBI website (<http://www.ncbi.nlm.nih.gov>).

Calcium imaging data were analysed by SALVO for HL-1 myocytes (see Chapter 4) or in Microsoft Excel for HEK 293 cells, and all statistical analysis was performed using an unpaired Student's t-test after testing the data sets for normality and equality of variance (GraphPad Prism). In all cases, datasets containing equal number of experimental measurements were compared. It is important to note that in Figures 4.8 and 4.9, a paired t-test would have been an appropriate method to compare HL-1 WT and experimental data sets as the measurements are taken from the same populations, before and after microinjection. However, in order to allow all statistical observations to be compared fairly, an unpaired t-test was used in all cases. All statistical outputs were validated using different software packages (Microsoft Excel, Minitab, and Graphpad Prism), all of which returned the same conclusions. Unless otherwise stated, all data are presented as the mean  $\pm$  standard error of the mean (SEM), and a p value of  $<0.05$  was considered to be significant.

## **2.6 Health and Safety**

All reagents were handled and stored as recommended by manufacturer's safety sheets. All experiments were carried out in accordance with COSHH regulations and local college



regulations. All genetic manipulation was registered and carried out in accordance with local GMAG guidelines. All bacteria, yeast and mammalian cell culture waste were disinfected with Actichlor (Adams) at 1000ppm available chlorine (1 tablet per litre of waste) prior to disposal.

## ***Chapter 3***

***In vitro expression and purification***

***of I-Domain proteins***

## 3.1 Introduction

### 3.1.1 The RyR2 I-Domain

The I-Domain of RyR2 comprises two distinct domains, the interaction domain located at residues 3722-4353 and the modulatory domain located at residues 4353-4610 (George *et al.* 2004, 2006). As discussed in Chapter 1, the I-Domain contains approximately 30% of all known VT-linked RyR2 mutations, and functions to critically regulate the interaction between the regulatory cytoplasmic region and the transmembrane (TM) Ca<sup>2+</sup>-pore-forming domain (George *et al.* 2004).

Since the functionality of the I-Domain may be predominantly conferred by the precise primary amino-acid sequence of this region, a bioinformatic approach was used to yield greater insight into the mechanistic basis of RyR2 regulation by the I-Domain. A comparatively simple bioinformatic strategy revealed striking structural homology between sub-fragments of the RyR2 I-Domain and I-Domain-like regions of inositol 1,4,5-trisphosphate receptors (IP<sub>3</sub>R), despite the absence of any notable primary sequence homology between these two Ca<sup>2+</sup> release channels (Appendix II) and the lack of homology between the entire RyR2 I-Domain and corresponding regions of IP<sub>3</sub>R. Based on this structural homology modelling, the I-Domain was divided into the three sub-fragments used throughout this study (Figure 3.1). This chapter will describe the generation of expression cassettes encoding recombinant I-Domain fragments, and the optimisation of expression and purification strategies linked to an *in vitro* cell-free expression system.

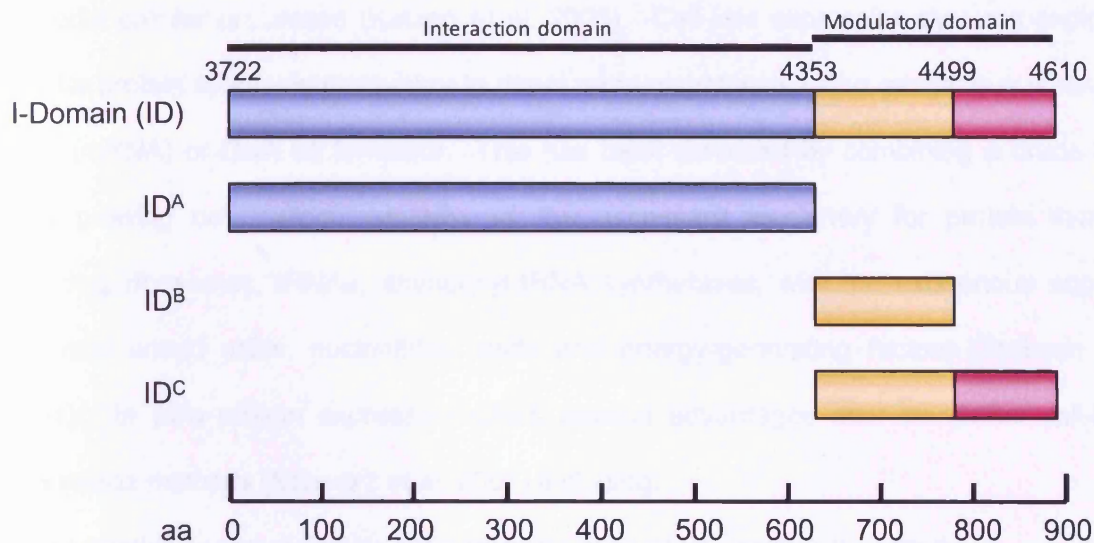


**Figure 3.1. Schematic representation of the truncated I-Domain constructs**

Residues 3722-4353 are important for intramolecular interaction while having limited functional importance, whereas residues 4353-4610 are functionally important, yet had little effect on interaction. Two TM domains (4499-4519 and 4572-4593) are predicted in the region 4499-4610, which may also contribute to the functionality of this region of the molecule (George 2004).

### 3.1.2 Cell-free protein expression

Integral membrane proteins and receptors play key roles in numerous human diseases and they currently represent important drug targets (Klammt *et al.* 2006). However, they can be problematic to synthesise in mammalian or bacterial cell systems as their production can be toxic to the cells, and typically *in vivo* expression in eukaryotic or prokaryotic cells does not successfully generate sufficient membrane proteins for subsequent study. As a result of this, *in vitro* cell-free expression systems are emerging as important tools in the synthesis of membrane proteins, toxins, and other proteins whose expression is detrimental to cell physiology (Schwarz *et al.* 2007).

*In vitro* translation systems are largely based on the pioneering studies of Nirenberg and Matthaei (1961) who first showed that cell integrity was not required for protein synthesis to occur. Now commonly used, cell-free protein synthesis is a valuable tool for studying the mechanisms of protein synthesis separate from the complexities of other mammalian or

bacterial cellular processes (Katzen *et al.* 2005). Cell-free expression systems exploit the cellular protein synthesis machinery to direct protein synthesis using exogenous messenger RNA (mRNA) or DNA as template. This has been achieved by combining a crude lysate from growing cells, which contains all the necessary machinery for protein synthesis including ribosomes, tRNAs, aminoacyl-tRNA synthetases, with the exogenous supply of essential amino acids, nucleotides, salts and energy-generating factors (Jackson *et al.* 2004). *In vitro* protein expression offers several advantages over traditional cell-based expression methods (Schwarz *et al.* 2007) including:

- the relative speed of protein synthesis and ease of interpreting the results
- the ease of synthesising radiolabelled proteins for detection by autoradiography
- the specific labelling of recombinant proteins for monitoring and isolation.
- the capacity to synthesise toxic, proteolytically sensitive or unstable gene products

Cell-free protein synthesis systems have been developed from several organisms, but the most widely used systems are derived from *E. coli*, and wheat germ (WG) extracts and rabbit reticulocyte lysates (RRL). Cell-free systems can be utilised either in a 'coupled' mode, where DNA is used as template, or as an 'uncoupled' system, which requires mRNA template produced from native sources or by *in vitro* transcription. The DNA template may be a circular or linear fragment, but must contain a promoter (e.g. T7) and a translation initiation signal such as the Kozak sequence (CCCGCCGCCCACCATGG) (Kozak 1987). To increase the expression level, a transcription and translation termination signal (TGA) is also required.

The choice of a cell-free system for protein synthesis is generally determined by the origin of the proteins to be expressed and their downstream applications (Summarised in Table 3.1). The commonly used *E. coli* S30 extract, WG extract and RRL systems are commercially available in both coupled and uncoupled formats. Coupled systems are generally simpler and more efficient; they also avoid problems associated with mRNA

degradation and mRNA secondary structure (Alimov *et al.* 2000). *E. coli* based systems provide higher yields and more homogenous samples suitable for structural studies, however their applicability is generally limited to expressing only those proteins which can successfully be expressed by intact *E. coli* (Torizawa *et al.* 2004; Vinarov *et al.* 2006). Eukaryotic-based systems, although typically yielding less product, synthesise proteins that are better suited for use in functional studies. In light of this, only coupled eukaryotic systems have been considered for the purposes of this study.

**Table 3.1. Choice of cell-free protein synthesis systems**

	E. coli extract	RRL	WG extract
Productivity per ml	6 mg	6 µg	4 mg
Synthesised protein	Many incomplete polypeptides	Mainly full length	Mainly full length
Post-translational modifications	No	Yes	Yes
Recommended template source	Bacteria	Animal, plant, bacteria, mammalian virus and plant virus	Animal, plant, bacteria, and plant virus

### 3.1.3 Objectives of this chapter

This chapter describes the optimisation of a reliable *in vitro* protein expression and purification strategy for the production of the I-Domain and truncated I-Domain proteins. The purified proteins will be used for microinjection into mammalian cells to investigate their effect on cellular Ca<sup>2+</sup> handling and phenotype.

## 3.2 Methods

### 3.2.1 Preparation of hRyR2 I-Domain expression plasmids

The vector containing the I-Domain of human RyR2 (hRyR2), obtained from Dr. Chris George, was generated as follows: a cDNA fragment encoding the I-Domain of hRyR2 (11288-13950 bp; aa 3722-4610) was generated by PCR amplification using Phusion polymerase (Finnzymes) (see Chapter 2) and oligonucleotides designed to incorporate 5' EcoRI and 3' XhoI restriction sites (Appendix I). Following restriction enzyme ligation, the amplified fragment was ligated into EcoRI/XhoI-digested pET-29(b) vector (Novagen), generating the I-Domain expression cassette fused in-frame with the S-tag (C-terminus) and His-tag (N-terminus) (Figure 3.2, A). Additional truncated I-Domain expression cassettes were produced by the same strategy using the oligonucleotide primers shown in Appendix I (Figure 3.2, B).

Recombinant vectors were transformed into *Epicurian coli* XL-10<sup>®</sup> ultracompetent cells (Stratagene), before selected colonies underwent small-scale alkaline lysis plasmid purification and restriction enzyme mapping using agarose gel electrophoresis (see Chapter 2). The restriction fragments were visualised using ethidium bromide fluorescence and UV transillumination before colonies displaying the correct restriction profile were selected for large-scale plasmid isolation and verification by DNA sequencing.

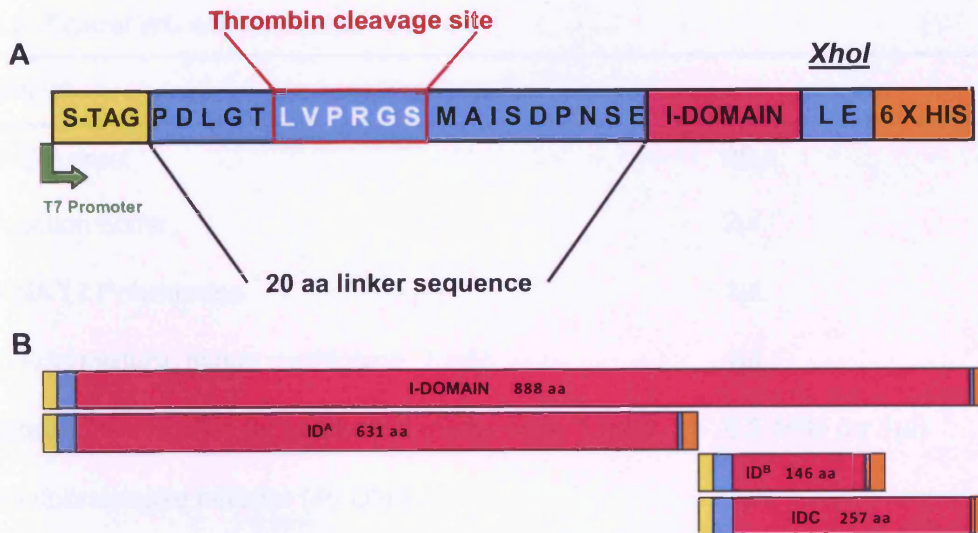


**Figure 3.2. Schematic representation of the I-Domain expression cassettes**

**Panel A:** Each recombinant protein consists of I-Domain fragments fused to a 15 aa (KETAAAKFERQHMD S) N-terminal S-tag fusion, a 20 aa linker containing a thrombin cleavage site for S-tag removal following purification, and a dipeptide linker encoding the XhoI restriction site and six histidine residues as described above. This expression cassette will permit bimodal detection/purification of the recombinant proteins. **Panel B:** The expression cassettes represented with relative size-based scaling of the tags and linker sequences.

### 3.2.2 Cell-free protein expression

As discussed above, both WG (TNT Coupled Wheat Germ Extract System, Promega) and RRL (TNT Quick Coupled Transcription/Translation System, Promega) cell-free systems were employed in this study.

The TNT coupled WG extract is advantageous because it has low background incorporation due to its low level of endogenous mRNA, and typically produces a protein yield which can be up to two orders of magnitude higher than the RRL system (Anderson *et al.* 1976; Endo & Sawasaki 2006; Jackson *et al.* 2004; Katzen *et al.* 2005). In this system, protein expression can only take place if the DNA template is linear, hence the plasmid DNA was linearised by *Sma*I digestion (37°C, 2 hours). Reactions were carried out in 50µl volumes as outlined in Table 3.2. Reaction samples were incubated in a 30°C water bath for 90 minutes, and terminated by placing on ice.



**Table 3.2. Typical WG extract reaction mixture**

Component	
TNT WG extract	25µl
TNT reaction buffer	2µl
TNT RNA T7 Polymerase	1µl
Amino Acid mixture, minus methionine, 1 mM	1µl
[ <sup>35</sup> S]-labelled methionine (or unlabelled methionine, 1 mM)	0.5 MBq (or 1µl)
RNasin ribonuclease inhibitor (40 U/µl)	1µl
Linearised plasmid DNA template	1 µg
Nuclease-free dH <sub>2</sub> O	Up to 50µl

The TNT Quick Coupled Transcription/Translation System is based on RRL in which recombinant proteins are synthesised from either linear or circular DNA templates using a T7 promoter. Reactions were carried out in 50µl volumes, as summarised in Table 3.3, by adding plasmid DNA and [<sup>35</sup>S]-labelled methionine (obtained as Pro-mix (92.5 MBq), GE Healthcare) or unlabelled methionine to the provided TNT Master Mix (containing T7 RNA polymerase, nucleotides, amino acids (minus Methionine), salts and ribonuclease inhibitor). Reaction samples were incubated in a 30°C water bath for 90 minutes, and terminated by placing on ice.

**Table 3.3. Typical quick coupled transcription/translation reaction mixture**

Component	
TNT T7 Quick MasterMix	40µl
[ <sup>35</sup> S]-labelled methionine (or unlabelled methionine, 1mM)	0.5 MBq (or 1µl)
Linearised plasmid DNA template	1 µg
Nuclease-free dH <sub>2</sub> O	Up to 50µl

Proteins synthesised by both systems were purified by magnetic bead affinity purification (Section 3.2.5). The radiolabelled proteins were subsequently visualised by autoradiography (Section 3.2.3) following SDS-PAGE, while the non-labelled proteins intended for microinjection into cells were visualised by Western blotting (Section 2.3.6).

### **3.2.3 *Autoradiography***

SDS-PAGE gels (Section 2.3.3) containing radiolabelled proteins were washed in fixing buffer for 1 hour, then soaked in dH<sub>2</sub>O for 1 hour to rehydrate them. To enhance radiographic detection, the gel was washed with ~ 50ml Amplify™ Fluorographic Reagent (GE Healthcare) for a further hour, before being dried onto filter paper (Whatman) using a vacuum gel dryer. The dried gel was then exposed to high performance chemiluminescence film (Hyperfilm, GE Healthcare) and developed using an automated image developer in order to visualise the protein bands.

### **3.2.4 *Antibody purification using affinity strategies***

The Melon Gel IgG purification system (Pierce) purifies antibodies from serum by removing contaminating proteins often present in high abundance, and was used according to the manufacturer's guidelines which are summarised in Figure 3.3. Briefly, 500µl of the supplied binding gel is placed in a spin tube and centrifuged (2000 xg, 1 min, RT) to prepare the support matrix. This is then equilibrated by washing twice with the supplied purification buffer followed by centrifugation (2000 xg, 10 secs, RT). The serum antibody is diluted with the purification buffer (1:10) and applied to purification support matrix which binds non-antibody serum proteins, such as albumin and transferrin. The serum is incubated with the purification support matrix for 5 mins at RT with continuous end-over-end mixing. Subsequently, the purified antibody is eluted off the matrix by centrifugation (2000 xg, 1 min, RT).

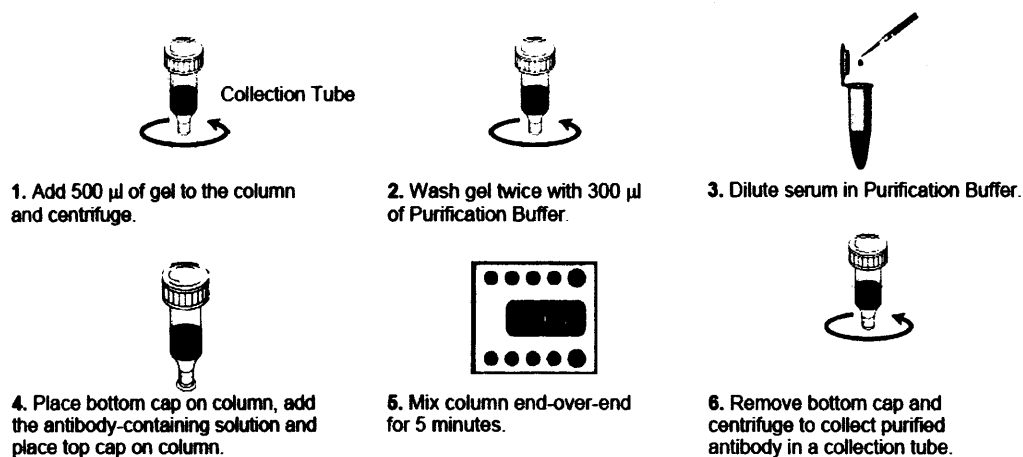


**Figure 3.3. Summary of Melon Gel IgG purification strategy**

Taken from <http://www.piercenet.com>

### 3.2.5 $Zn^{2+}$ -affinity purification of recombinant proteins

The MagZ protein purification system (Promega) was used for the isolation of the I-Domain proteins, and was carried out according to the manufacturer's guidelines. Briefly, the entire protein synthesis reaction (50 $\mu$ l) was diluted in the supplied binding/wash buffer (containing 20 mM sodium phosphate and 500 mM NaCl). This was then incubated with MagZ particle slurry (60 $\mu$ l) for 15 mins at RT on an orbital rotator. The MagZ particles were then washed four times with the binding/wash buffer and the purified proteins were subsequently eluted using 0.6 M imidazole (pH 7.5).

### 3.3 Results

#### 3.3.1 Generation of truncated I-Domain constructs

Fragments of hRyR2 I-Domain were successfully amplified by PCR using the conditions and oligonucleotide primers described in Chapter 2 and Appendix I (Figure 3.4). Plasmid pET-29(b) encoding the truncated I-Domain fragments were generated and restriction enzyme mapping was used to confirm the correct ligation of the fragments into the vector (Figure 3.5). DNA sequencing was used to verify the integrity of the I-Domain fragments and the restriction boundaries (Figure 3.6).

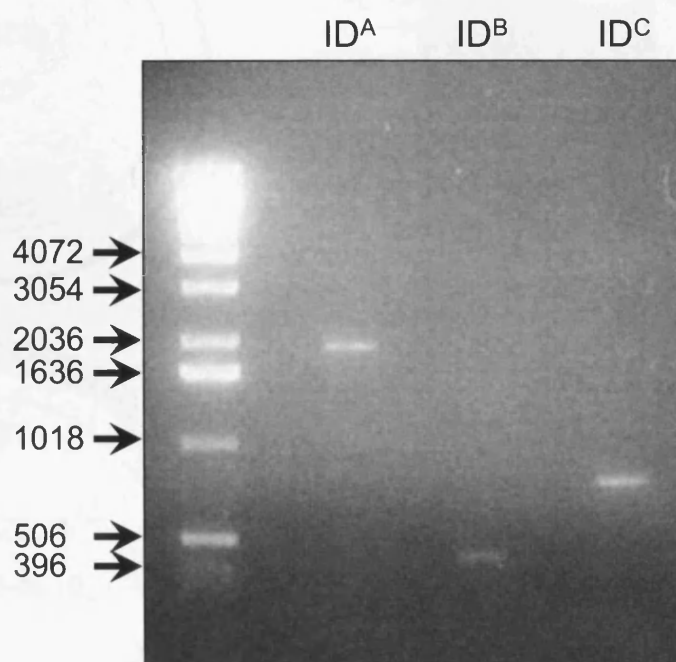


**Figure 3.4. hRyR2 I-Domain cDNA fragments were successfully amplified by PCR.**

Agarose gel electrophoresis (1 % (w/v)) showing amplification of discrete I-Domain cDNA fragments of the correct size (ID<sup>A</sup>, 1892 bp; ID<sup>B</sup>, 436 bp; ID<sup>C</sup>, 770 bp) from the full-length I-Domain template. Numbers indicate DNA marker sizes in base pairs (bp).

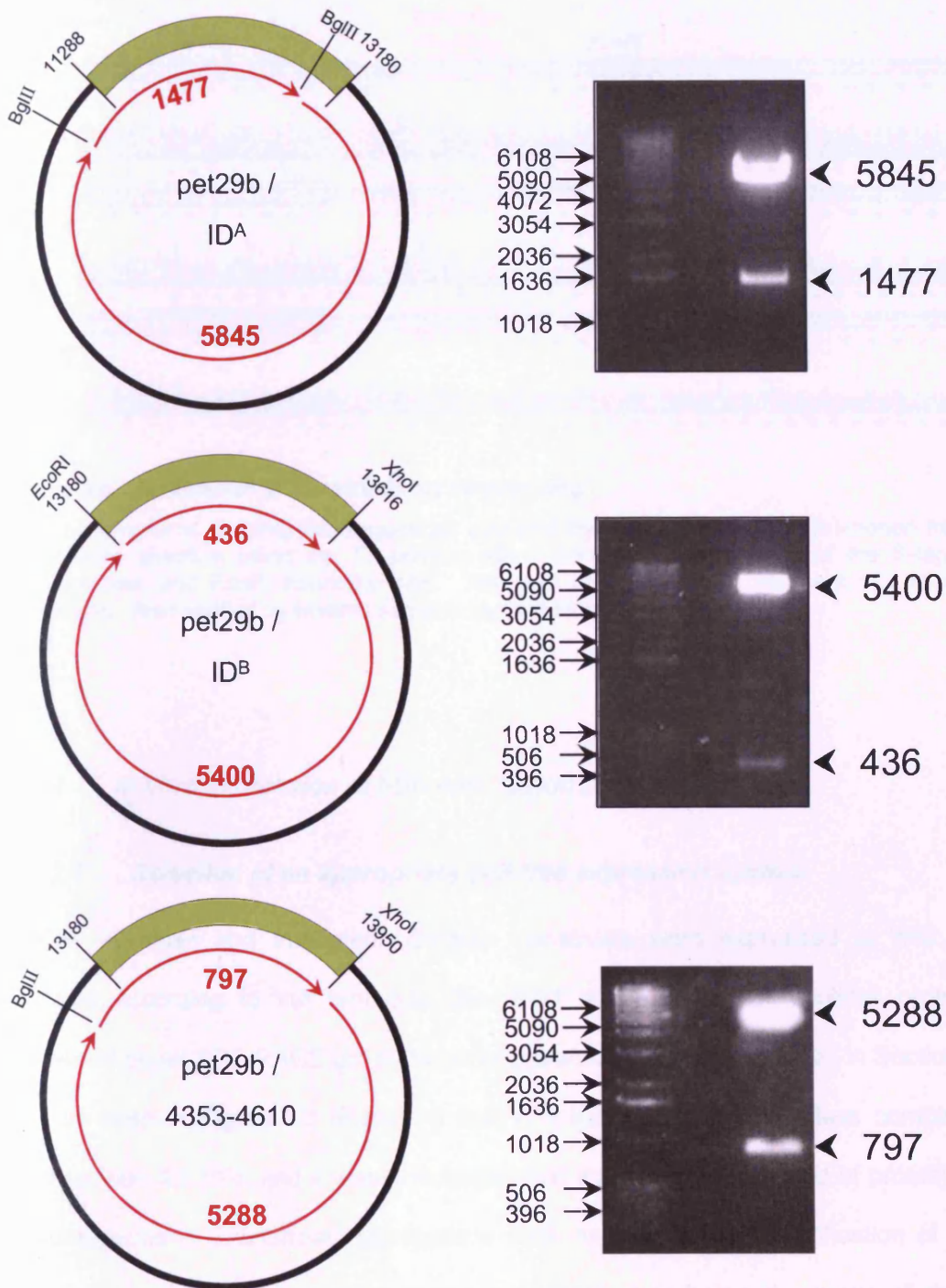


**Figure 3.5. Verification of pET-29(b)-cloned I-Domain expression cassettes by restriction mapping.**

Restriction maps of pET-29(b) containing I-Domain or truncated I-Domain digested with the enzymes shown, and verified by agarose gel electrophoresis. Numbers indicate fragment sizes in base pairs (bp).

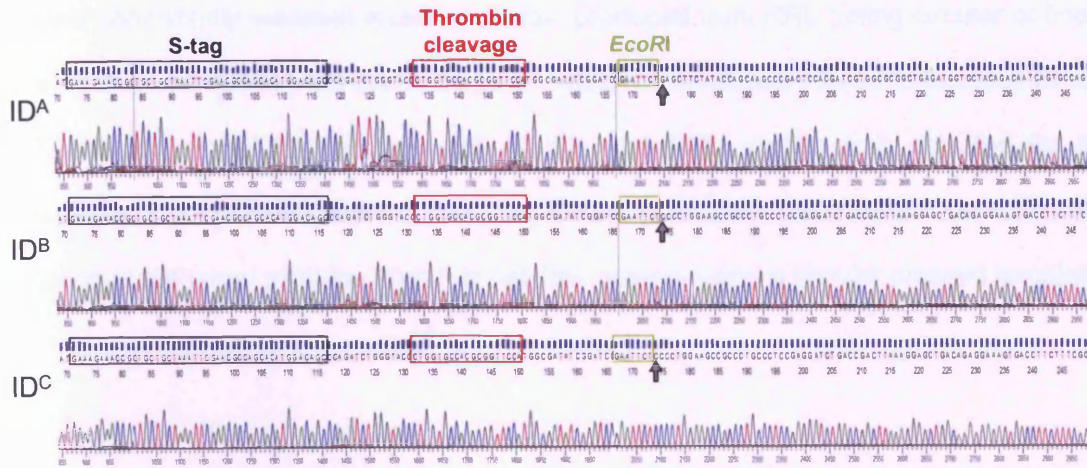


**Figure 3.6. Verification of constructs by sequencing**

Electropherograms showing the sequences obtained by sequencing pET-29(b)-cloned fragments in the forward direction using the T7 priming site. Confirms the presence of the S-tag, thrombin cleavage site, and EcoRI restriction site. The start of the I-Domain fragment is indicated by the arrowhead. Also verified by reverse sequencing (not shown).

### 3.3.2 *In vitro* expression of I-Domain fusion proteins

#### 3.3.2.1 Selection of an appropriate cell-free expression system

The I-Domain and truncated I-Domain constructs were expressed in WG and RRL systems according to the protocols described above, and the resultant proteins were visualised on an SDS-PAGE gel by Imperial protein staining as described in Section 2.3.4. It can be seen in Figure 3.7 (Panel A) that WG extract comprises a less complex protein mixture than the RRL and it was anticipated that this lower background of protein would be advantageous in downstream applications such as detection and purification of the target proteins. In both systems, the proteins expressed were below the levels of detection of Imperial protein stain, indicating that the high protein yields reported in some studies (Table 3.1) could be achieved for I-Domain proteins.

Next, the I-Domain and truncated I-Domain constructs were expressed and radiolabelled with  $^{35}\text{S}$ -methionine using WG and RRL as previously described. Autoradiography showed that both WG and RRL expressed proteins of the anticipated molecular weight. However,

there was consistently elevated levels of protein produced from RRL (using circular or linear template) when compared with the WG system which conspicuously failed to produce ID and ID<sup>B</sup> (Figure 3.7, Panel B). As a result of this, the RRL system was selected for the expression of the I-Domain proteins, and the following sections describe the detection and purification of the target proteins from this cell-free system using a circular plasmid template.

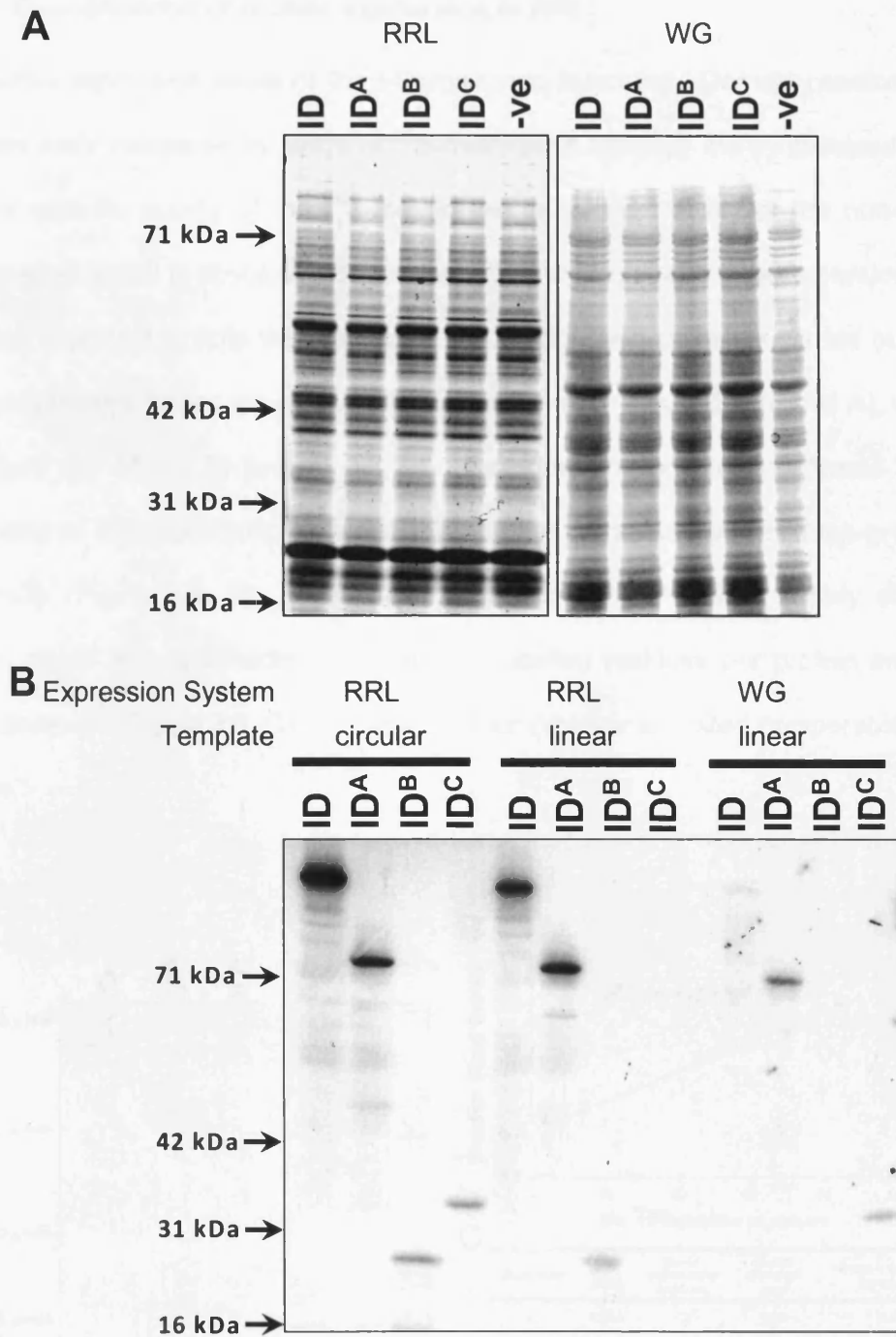


**Figure 3.7. Comparison of RRL and WG extract protein expression systems**

**Panel A:** Imperial protein stain of 25 $\mu$ l RRL and WG expressing full-length and truncated I-Domain proteins. The right-hand lane of each gel shows 25 $\mu$ l of the RRL or WG containing no DNA template, and shows no noticeable difference in protein profile to those containing the target proteins. **Panel B:** Expression of radiolabelled I-Domain proteins from 25 $\mu$ l of RRL or WG, using circular and linear DNA templates. MW of the fragments are ID – 106.3 kDa, ID<sup>A</sup> – 76.7 kDa, ID<sup>B</sup> – 21.8 kDa, ID<sup>C</sup> – 34.4 kDa. The differences in band intensity between the constructs is dependent on the number of radiolabelled residues present in each construct, and will be discussed in the next section.



### 3.3.2.2 Quantification of protein expression in RRL

The relative expression levels of the I-Domain and truncated I-Domain constructs in the RRL system were compared by virtue of  $^{35}\text{S}$ -methionine labelling the synthesised proteins. For a given specific activity of the  $^{35}\text{S}$ -methionine label, the density of the non-saturated autoradiographic signal is absolutely dependent upon the number of labelled residues in the protein. It is important to note that densitometry can only be accurately carried out on non-saturating exposures, hence the weaker signals observed in Figure 3.8 (Panel A), compared with in Figure 3.7 (Panel B) section 3.3.2.1. Densitometric analysis confirmed the direct proportionality of the relationship between the number of radioactive residues present and signal density (Figure 3.8, B). This linear relationship ( $r^2 = 0.9951$ ) clearly shows that variation in signal density reflects the number of labelled residues per protein and not the level of expression (Figure 3.8, C), and that the four proteins exhibited comparable levels of expression.

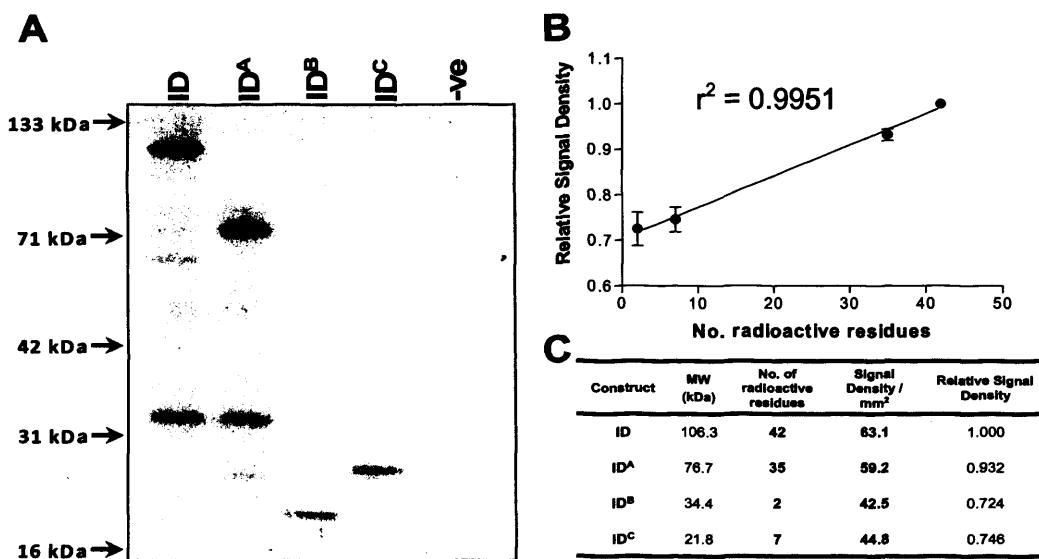


**Figure 3.8. Autoradiography of  $^{35}\text{S}$ -labelled I-Domain proteins**

**Panel A:** SDS-PAGE (10% (v/v)) analysis of 25 $\mu\text{l}$  RRL protein expressing radiolabelled I-Domain proteins. All proteins were expressed successfully and consistent with the predicted MW, summarised in **panel C**. The final lane showed no non-specific incorporation of radiolabelled methionine in RRL (25 $\mu\text{l}$ ) not supplemented with DNA template. **Panel B:** Densitometric analysis of  $^{35}\text{S}$ -labelled I-Domain proteins shows a linear correlation between the number of labelled methionine residues and signal density ( $n=5$ ), indicating that all constructs were expressed at comparable levels.

### **3.3.3 Detection of I-Domain proteins**

I-Domain proteins expressed using the RRL were successfully detected by S-protein HRP conjugate, anti-RyR ab1093 and anti-His tag antibodies as described in Chapter 2.

#### **3.3.3.1 Detection of I-Domain proteins by S-protein HRP**

The S-tag / S-protein HRP protein detection system is based on the strong interaction between the 15aa S-tag and 103aa S-protein, both of which are derived from RNase A. The 15aa S-tag protein fused to the N-terminus of the I-Domain proteins displays a very strong and highly specific affinity to S-protein and thus proteins fused to the S-tag can be directly detected with S-protein conjugated with HRP.

Detection by S-protein HRP does not require a secondary antibody, and as a result the signal density is directly proportional to the level of protein expression (Figure 3.9). The four ID proteins were successfully detected by S-protein HRP, exhibiting protein bands at the correct molecular weight. Densitometric analysis of the S-protein HRP signal showed that all I-Domain proteins were expressed at equivalent levels in RRL, which corroborated the observations from the radiolabelled proteins (Figure 3.8).

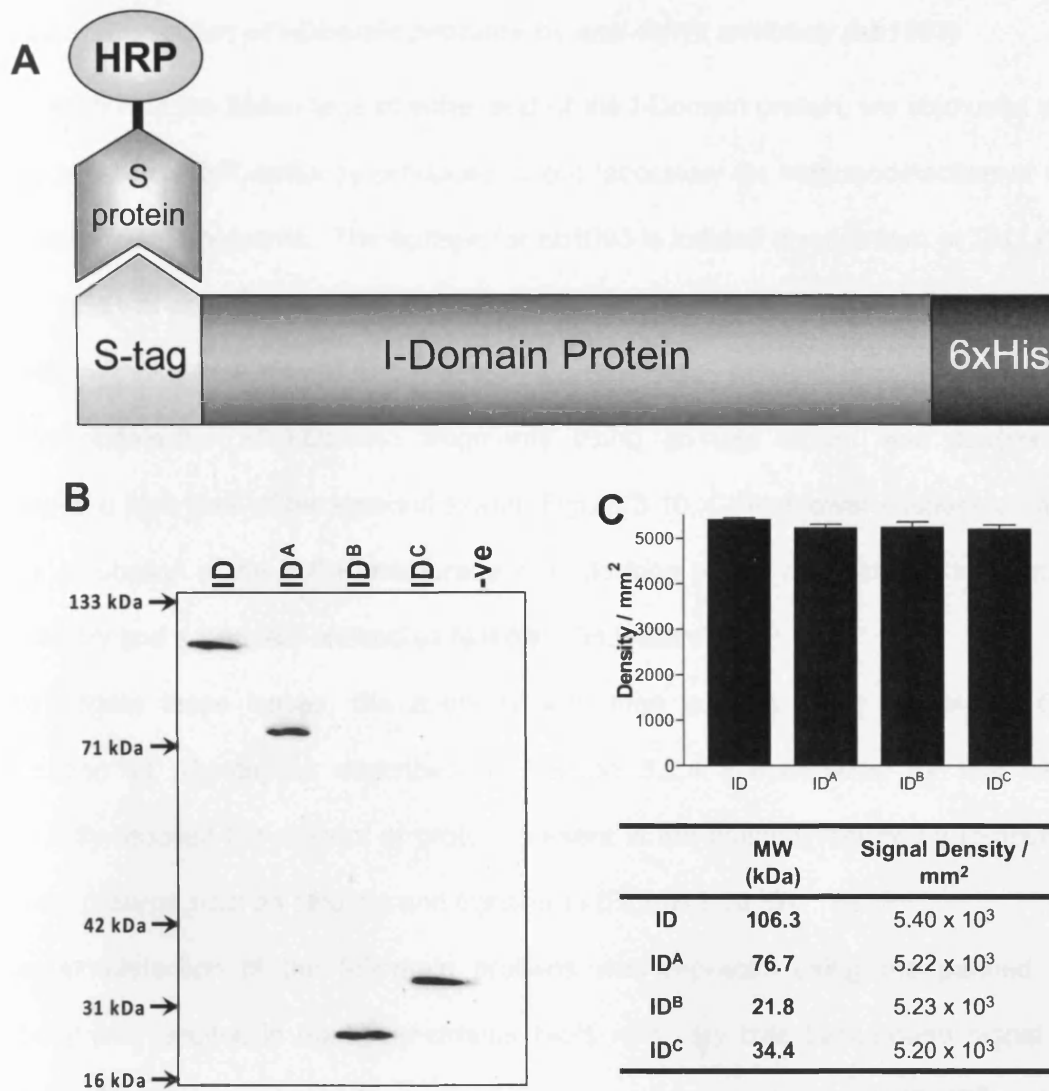


**Figure 3.9. Detection by S-protein HRP conjugate**

**Panel A:** Schematic representing the detection strategy using the S-protein affinity to the N-terminal S-tag. **Panel B:** A representative SDS-PAGE (10% (v/v)) with 25 $\mu$ l RRL expressing correctly sized full-length and truncated I-Domain proteins. The final lane contains 25 $\mu$ l RRL without exogenous DNA template, and shows negligible background S-protein detection. **Panel C:** Densitometric analysis of the S-protein HRP signals (n=5) for each I-Domain protein clearly shows that all constructs are expressed at the comparable levels in RRL.

### 3.3.3.2 Detection of I-Domain proteins by anti-RyR2 antibody (ab1093)

In addition to the fusion tags at either end of the I-Domain protein, we also used ab1093, a polyclonal anti-RyR antibody produced in our laboratory for immunodetection of most of the recombinant fragments. The epitope for ab1093 is located downstream of TM1 (Tunwell *et al.* 1996) at residues 4454-4474 of hRyR2, and is present in the truncated I-Domain proteins, with the exception of ID<sup>A</sup>.

Immunodetection of I-Domain fragments using ab1093 serum was successful but displayed a high level of background signal (Figure 3.10, C) that lower dilutions of antibody, longer incubation of the PVDF membrane with blocking buffer, and reduced incubation with the primary and secondary antibodies failed to eliminate.

To negate these issues, the antibody was then purified using the Melon Gel IgG purification kit (Pierce) as described in Section 3.2.4. Purification by this technique profoundly reduced the amount of protein present in the antibody serum by removing non-relevant proteins such as albumin and transferrin (Figure 3.10, B).

Immunodetection of the I-Domain proteins was repeated using the purified ab1093 antibody and resulted in markedly cleaner blots with very little background signal (Figure 3.10, C). The improved blots clearly show that, as anticipated, full length ID, ID<sup>B</sup> and ID<sup>C</sup> are detected by ab1093 and show the correct molecular weights. Unlike <sup>35</sup>S labelling and S-tag detection, the signals obtained by ab1093 immunodetection are not linear due to the use of a secondary antibody. As predicted, ID<sup>A</sup> is not detected by this antibody, as the epitope is not present in this protein.

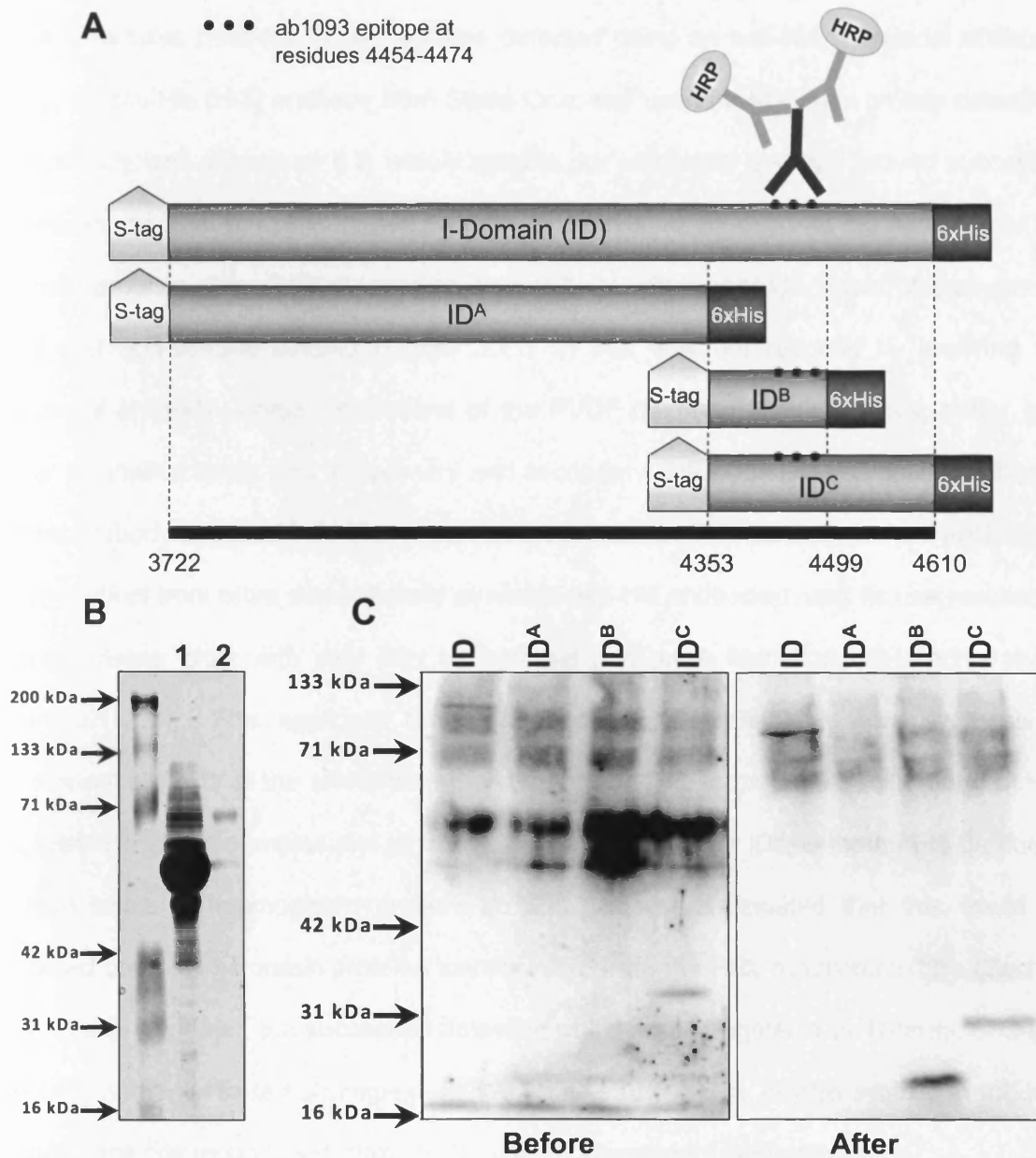


**Figure 3.10. Immunodetection by anti-RyR2 ab1093**

**Panel A:** Schematic illustrating the location of ab1093 epitope at residues 4454-4474, and the detection strategy using ab1093. **Panel B:** SDS-PAGE analysis of ab1093 (5 $\mu$ l) before (Lane 1) and after (Lane 2) IgG purification. **Panel C:** Immunoblot analysis of RRL (25 $\mu$ l) synthesised full-length and truncated I-Domain proteins using ab1093 before (left) and after (right) IgG purification.

### 3.3.3.3 Detection of I-Domain proteins by anti-His antibody

The C-terminal hexa-his fusion tag was detected using an anti-His polyclonal antibody. Initially, an anti-His (H-3) antibody from Santa Cruz was used for I-Domain protein detection. This antibody was chosen as it is widely used in our laboratory and has proven successful for detection of other hexa-his tagged proteins. However, when used for the detection of the I-Domain proteins, this antibody produced poor blots with very high levels of background signal and non-specific binding (Figure 3.11, B) that was not reduced by lowering the dilutions of antibody, longer incubations of the PVDF membrane with blocking buffer, and shorter incubation times with the primary and secondary antibodies. As a result, a different anti-His antibody obtained from Covance was investigated. This clonally-derived antibody is entirely distinct from other commercially available anti-His antibodies, and its use resulted in strikingly clearer blots with very little background and much higher signal-to-noise levels (Figure 3.11, B). This approach further corroborates the reliable *in vitro* synthesis of recombinant proteins of the anticipated molecular size. The large non-specific band at ~20 kDa, visible in all the samples and which obscures the signal for ID<sup>B</sup>, is thought to be due to the high levels of haemoglobin present in RRL. It was anticipated that this would be eliminated once the I-Domain proteins were purified from the RRL reaction mixture (Section 3.3.4). Taken together, the successful detection of I-Domain fragments by N-terminal S-tag, anti-RyR2 and anti-His-tag strategies verifies the use of the RRL *in vitro* system to robustly produce *bona fide* recombinant proteins for use in downstream applications.

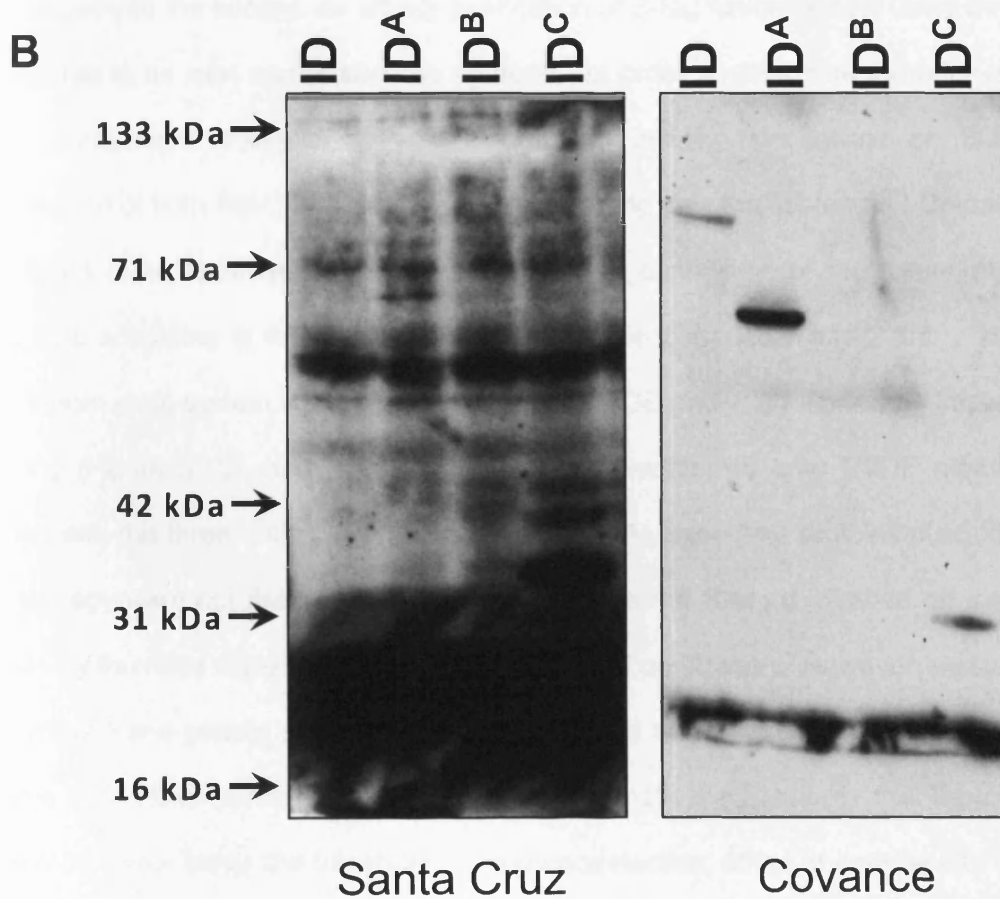
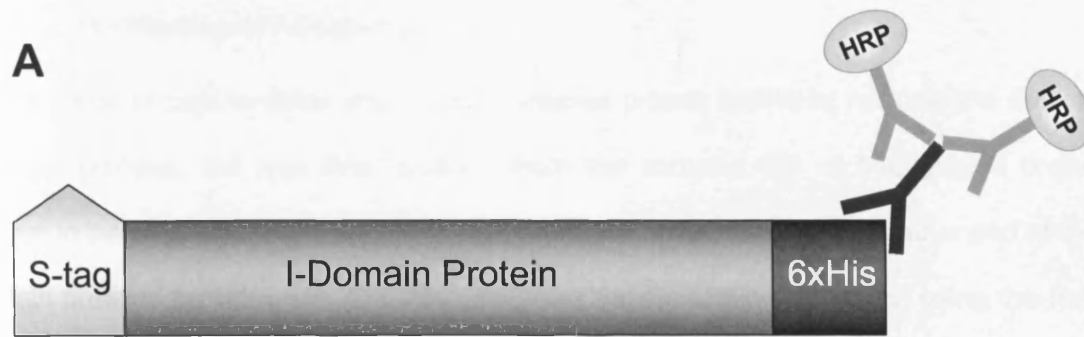


**Figure 3.11. Detection by anti-His antibodies**

**Panel A:** Schematic representing the detection strategy using the C-terminal hexa-His epitope. **Panel B:** Immunoblot analysis of RRL (25µl) expressing the I-Domain and truncated I-Domain proteins using anti-His antibody from Santa Cruz (Left) and Covance (Right).

### 3.3.4 Purification of I-Domain proteins

The fusion of tags to either end of an expressed protein facilitates not only the detection of target proteins, but also their isolation from the complex mix of background proteins present in the RRL expression system. The presence of two tags, one on either end of the I-Domain proteins provides two possible strategies for purification – the first using the Hexa-His tag and an immobilised metal affinity chromatography (IMAC) approach using Ni<sup>2+</sup> sepharose, and the second via affinity purification of S-tag fusion protein using the S-protein conjugated to an inert carrier such as agarose. In order to determine the relative merits of these purification strategies, it was decided to initially concentrate on pursuing the optimisation of both IMAC and S-tag approaches using only the full-length I-Domain. Both of IMAC and S-tag techniques were employed in the purification of the full-length I-Domain from RRL according to the protocols described in Sections 2.3.7 and 2.3.8. The resultant eluate from each system was visualised by SDS-PAGE analysis followed by Imperial protein staining (Figure 3.12), and equivalent gels were transferred onto PVDF membrane and blotted with the three antibodies described above. As expected, proteins purified by the S-tag strategy were not detected by S-protein HRP as the S-tag is cleaved off the I-Domain protein by thrombin digestion during the last stage of purification. However, western blotting (not shown) and protein staining (Figure 3.12) failed to detect any I-Domain protein in the eluates from either purification strategies. To eliminate the possibility that the protein was present in levels below the threshold for immunodetection, 500µl of each eluate (equivalent to 25µl of original RRL reaction mixture) was concentrated using a Microcon centrifugal filter device (Millipore, 50,000 NMWL) and analysed in the same way (Figure 3.12). Once again, no I-Domain protein was detected by protein staining (Figure 3.12) or western blot (not shown) and it was concluded neither of these strategies were suitable for the isolation of I-Domain protein from RRL.



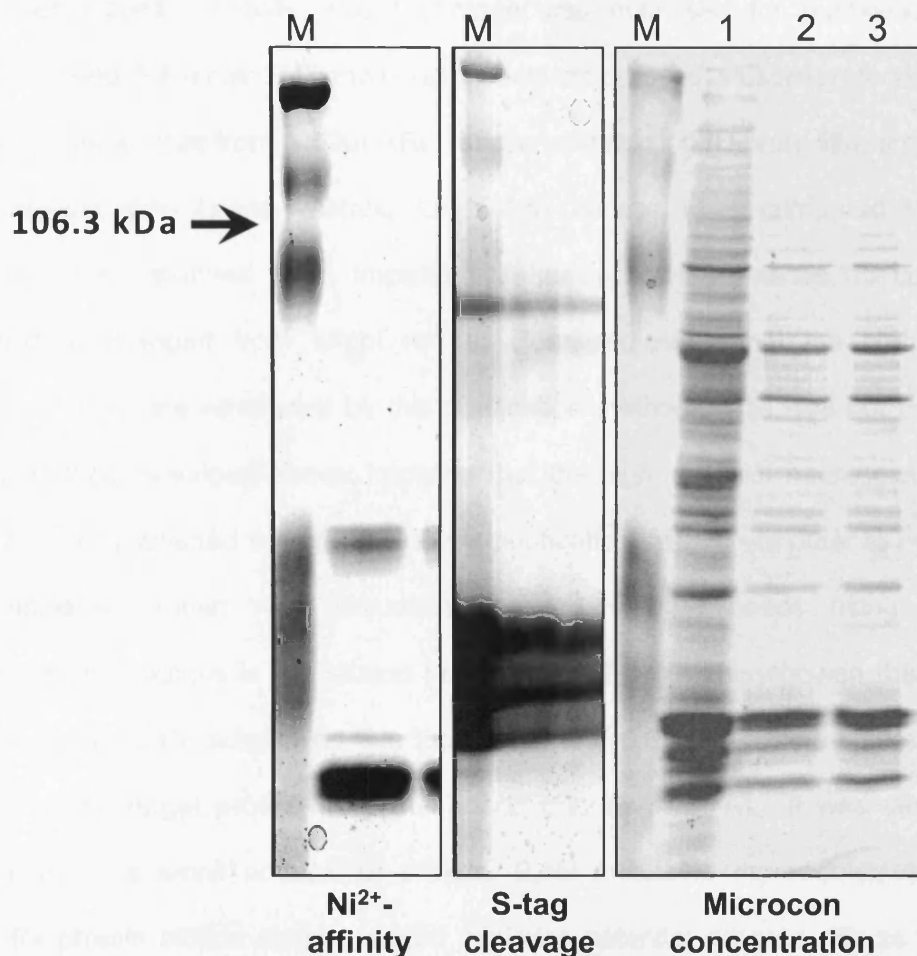


**Figure 3.12. Unsuccessful purification of ID protein from the RRL expression system using column-based systems**

Eluates (100 $\mu$ l) from the Ni<sup>2+</sup> affinity and S-protein affinity systems before microcon concentration (left and middle panels, respectively) were separated by SDS-PAGE (10% (v/v)), and visualised with Imperial protein stain. Eluates resulting from these strategies (500 $\mu$ l) were concentrated in a centrifugal filter device and were compared with 20 $\mu$ l RRL expressing ID (right panel). All of these systems failed to produce any detectable ID protein staining (shown above), and immunoblot analysis also failed to detect the ID protein (not shown).

Given the failures of a Ni<sup>2+</sup>-based IMAC approach and S-tag affinity purification systems to purify recombinant I-Domain protein from RRL, an alternative purification strategy was necessary. A new development in IMAC technology has been the MagZ protein purification system (Promega) which uses zinc paramagnetic beads (Section 3.2.5) rather than the Ni<sup>2+</sup>-based chemistries to selectively bind the C-terminal hexa-His tag, which was developed to overcome the problems associated with the co-purification of haemoglobin using traditional

$\text{Ni}^{2+}$ -affinity techniques. Initially, this technique was optimised for purification of  $^{35}\text{S}$ -methionine labelled full-length I-Domain using imidazole-based elution protocols. Figure 3.13 (Panel A) shows that from a 50 $\mu\text{l}$  RRL reaction expressing ID, very little protein is lost during the binding (lane 2) and washing (lanes 3-6) process, when compared with Lane 1 that contains 2 $\mu\text{l}$  of 'unpurified' RRL. Importantly, after the first two washes, the colour of the reaction mixture changed from bright red to clear, indicating that the high levels of haemoglobin in RRL are eliminated by this purification method. This was not seen by the  $\text{Ni}^{2+}$  affinity method described above; implying that the high levels of haemoglobin in RRL may have adversely affected the efficacy of this purification system. In order to optimise the elution conditions, protein was sequentially eluted off the beads using increasing concentrations of imidazole in the elution buffer (lanes 7-14). This showed that I-Domain protein was successfully isolated by this technique, and 0.6 M imidazole was sufficient to elute ~80% of the target protein from the beads (Figure 3.13, A). It was decided that, despite sacrificing a small amount of protein, 0.6M imidazole represented the optimal conditions for protein elution since it would minimise potential adverse effects caused by higher imidazole concentrations (e.g. 1M) in downstream applications. Given the apparent success of this technique in enriching full-length I-Domain protein, this approach was extended to enriching the other truncated using similar conditions to those described above (Figure 3.13, B).

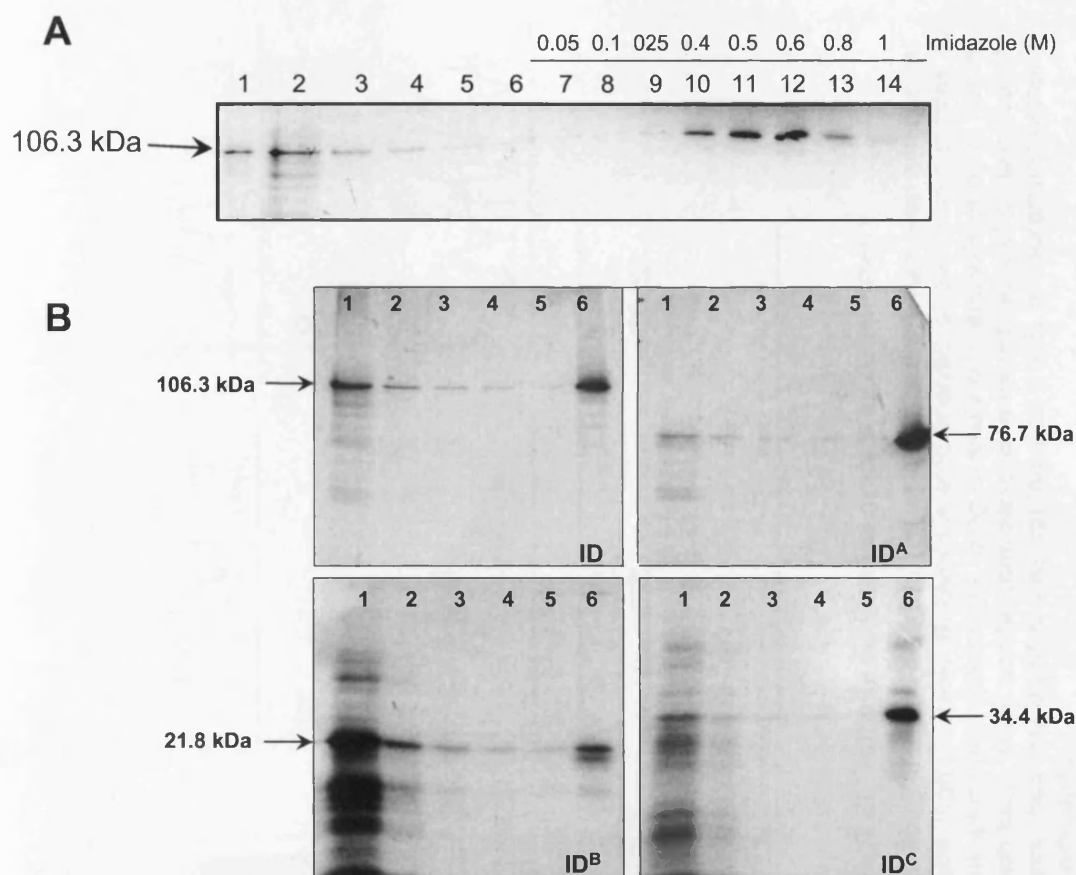


**Figure 3.13. Purification of radiolabelled I-Domain proteins using a zinc-affinity approach.**

**Panel A:** Optimisation of ID protein purification from 50 $\mu$ l RRL using zinc paramagnetic beads. Lane 1 shows 2 $\mu$ l of unpurified RRL expressing ID. Lane 2 shows the unbound product (100 $\mu$ l) following incubation with the Zn<sup>2+</sup> slurry. Lanes 3-6 show the loss following sequential wash-steps (100 $\mu$ l). Lanes 7-14 show the ID protein eluted with increasing concentrations of imidazole. **Panel B:** Purification of ID and truncated ID proteins using optimised Zn<sup>2+</sup>-affinity strategy from RRL (50 $\mu$ l). Lane 1 shows the unbound product (100 $\mu$ l) following incubation with the Zn<sup>2+</sup> slurry; lanes 2-5 show the losses following 4 sequential wash steps. Lane 6 shows the resultant protein eluted with 0.6 M imidazole.

The efficacy of this system was quantified by densitometric analysis of purified and non-purified RRL expressing the I-Domain and truncated I-Domain proteins. Silver staining was used to visualise the proteins remaining after Zn<sup>2+</sup>-based purification, as the amount of protein was below the detection threshold of Imperial protein stain (Section 2.3.4). The silver stained protein profiles were plotted and the area under each curve was calculated by integration, which showed that the MagZ purification system removed ~95% of all background protein (Figure 3.14), thereby enriching the I-Domain proteins.

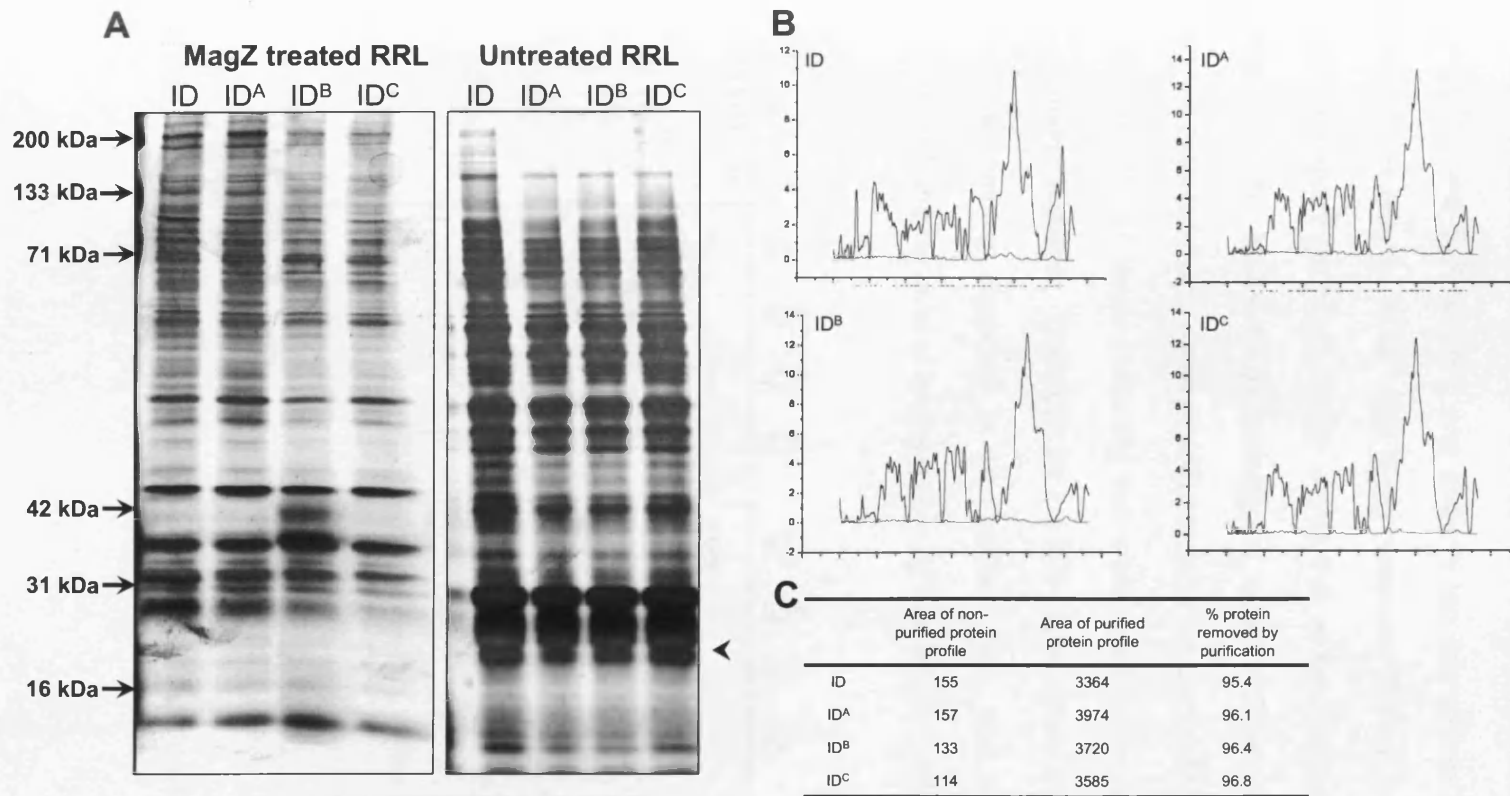


**Figure 3.14. Quantification of the efficacy of the MagZ Zn<sup>2+</sup>-affinity purification system by densitometry**

**Panel A:** Silver staining reveals the protein profiles of MagZ-treated RRL (50µl) in which ID proteins had been synthesised (left) or 2µl of non-purified RRL expressing ID proteins (right). **Panel B:** Densitometric analysis of the protein profiles in MagZ-treated (blue line) and untreated (black line) samples were determined using Quantity one analysis of band density through the lane profile. **Panel C:** The area under each trace, which can be considered as a robust index of protein quantity was obtained by mathematical integration. These figures show that MagZ processing removes > 95% of background proteins. For example, MagZ treatment removes haemoglobin, indicated by ◀.

Next, immunoblot analysis of recombinant I-Domain proteins was performed using S-protein HRP, anti-RyR ab1093, and anti-His tag approaches as previously described. In contrast to the failures of  $\text{Ni}^{2+}$  and S-tag strategies to yield immunodetectable levels of I-Domain proteins, Figure 3.15 clearly shows that all the I-Domain proteins were successfully purified from RRL by the MagZ strategy, at levels sufficient for immunodetection. All the antibodies detected clear, clean protein bands at the correct MW, although the proteins were detected at different levels indicating that enrichment may not have been equivalent for all the I-Domain fragments. Detection by the anti-His antibody showed that the majority of the non-specific binding observed in non-purified RRL had been eliminated, which was consistent with the removal of haemoglobin by zinc affinity purification.

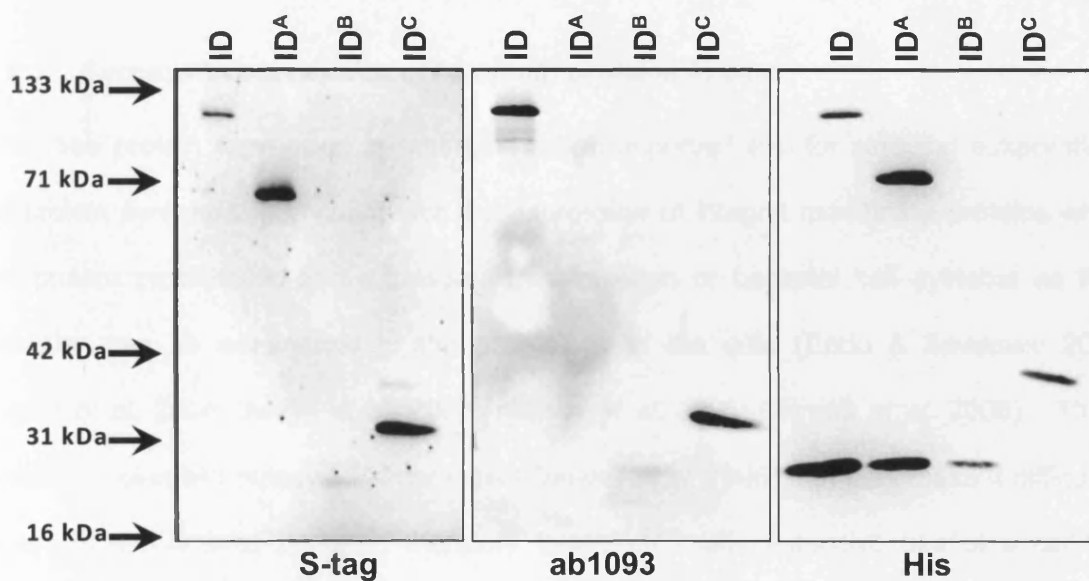


Figure 3.15. Successful immunodetection of MagZ purified I-Domain proteins in RRL

### **3.4 Discussion**

#### **3.4.1 Successful propagation of I-Domain expression cassettes**

Propagation and isolation of the pET-29(b) expression cassettes containing truncated I-Domain templates was successful, when carried out under the conditions optimised for the propagation of hRyR2 DNA that avoid spontaneous recombination or plasmid DNA degradation (George *et al.* 2005). These conditions included a low propagative temperature (typically 30°C), short durations in culture ( $\leq 18$  hours), the use of a specific strain of bacteria adapted for viable transformation with large plasmids, and resin-based DNA purification systems that do not shear the isolated plasmid (George *et al.* 2003a, 2003b).

#### **3.4.2 Successful expression of I-Domain proteins *in vitro***

Cell-free protein expression is emerging as an important tool for studying eukaryotic *in vitro* protein synthesis, particularly for the expression of integral membrane proteins which have proven problematic to synthesise in mammalian or bacterial cell systems as their production can be detrimental to the physiology of the cells (Endo & Sawasaki 2006; Jackson *et al.* 2004; Junge *et al.* 2008; Katzen *et al.* 2005; Klammt *et al.* 2006). The I-Domain contains two putative TM domains (Tunwell *et al.* 1996) that may make it difficult to express in non-*in vitro* systems, therefore this study made extensive use of a cell-free system for recombinant protein. Furthermore, bioinformatic analysis of the full-length I-Domain and the three truncated I-Domain fragments revealed differences in the properties of these proteins, including hydrophobicity, which could affect the way they are expressed in bacterial or mammalian systems. As demonstrated above, cell-free protein expression largely overcomes this problem and the data shows that the *bona fide* I-Domain proteins were consistently synthesised regardless of size, secondary structure, or hydrophobicity. Densitometric analysis of radiolabelled proteins showed that the four I-Domain proteins were successfully expressed, regardless of their size, hydrophathy or secondary structure. This

was further supported by detection using S-protein HRP conjugate, which gave comparable signals for all proteins, indicating broadly equivalent levels of expression.

I-Domain proteins were successfully expressed in a RRL cell free system, and immunodetection using the fusion protein epitopes at either end the protein expression cassette confirmed that full-length recombinant proteins had been produced. Interestingly, expression of the I-Domain proteins in the WG extract was not successful. Only two of the truncated proteins (ID<sup>A</sup> and ID<sup>C</sup>) were expressed by WG extract albeit in lower levels than by RRL, while ID and ID<sup>B</sup> were not expressed at all. This was unexpected, as WG was anticipated to yield proteins in the range of two orders of magnitude higher than those produced in RRL ( Alimov *et al.* 2000; Endo & Sawasaki 2006; Hino *et al.* 2008; Jermutus *et al.* 1998; Katzen *et al.* 2005; Vinarov *et al.* 2006; Zhao *et al.* 2007).

### 3.4.3 The C-terminal hexa-His epitope can be used for isolating I-Domain proteins

Purification of I-Domain proteins from RRL using the S-tag affinity system and the Ni<sup>2+</sup> affinity column proved unsuccessful. It is likely that in both cases, this was due to the small volumes of RRL used and the low levels of expression of the I-Domain proteins which may have been below the effective thresholds of these systems.

The I-Domain proteins were, however, effectively isolated from RRL using a newer strategy based on magnetic zinc beads with a high affinity to poly-His-tagged proteins but not to haem groups, thus allowing the purification of the target protein without co-purification of haemoglobin present in the RRL. This strategy resulted in the removal of 95% of contaminating background proteins, and permitted enrichment of the I-Domain proteins that could be unequivocally identified using immunoblotting techniques.

This chapter has described the robust applicability of cell-free protein synthesis coupled to Zn<sup>2+</sup>-based purification strategies to yield *bona fide* full-length and truncated I-Domain proteins. Ultimately, the aim of this project was to investigate the effects of these fragments on the Ca<sup>2+</sup> handling and phenotype of mammalian cells, and the following chapter

describes the optimisation of microinjection techniques for introducing these recombinant proteins into HL-1 cardiac myocytes.



## ***Chapter 4***

# ***Optimisation of microinjection strategies***

## **4.1 Introduction**

### **4.1.1 HL-1 cells: an immortalised cardiac cell line**

HL-1 cardiomyocytes are the only cardiac cell line that can be serially passaged, while retaining full contractility and differentiated cardiac morphology, biochemical, and electrophysical properties (Claycomb *et al.* 1998; White *et al.* 2004). They are also, to the best of our knowledge, the only cell type that can be cultured into confluent electrically-coupled monolayers that form the basis for the experiments described later in this chapter. The HL-1 cell line was derived from AT-1 cardiac myocytes, which are atrial cardiac muscle cells obtained from transgenic mice in which expression of the SV40 large T antigen was under the control of the atrial natriuretic factor (ANF) promoter (Field 1988). Although AT-1 cells maintain cardiac cell phenotype and contract spontaneously in culture, they cannot be serially passaged *in vitro* or recovered from frozen stocks. AT-1 cells can only be maintained as a subcutaneous tumour lineage in syngenic mice, and myocytes must be prepared from these tumours as primary cells (Delcarpio *et al.* 1991) and thus the utility of the AT-1 cell type is limited. The HL-1 lineage, a derivative of AT-1 cells that could be serially passaged while maintaining a differentiated phenotype, was isolated by Claycomb after more than 100 separate preparations and attempts to passage AT-1 cells under carefully controlled conditions (Claycomb *et al.* 1998). The HL-1 cell line can be serially propagated in culture with an apparently unlimited life span, and retain the ability to contract for at least 240 passages. These characteristics are retained by cells that have been recovered from stocks frozen in liquid nitrogen. In order for HL-1 cells to be passaged repeatedly while maintaining a highly proliferative and differentiated contractile cardiac phenotype, they require a gelatin-fibronectin (GFN) matrix and a specially formulated growth medium containing components such as retinoic acid, norepinephrine, insulin, and essential lipids in addition to factors found in normal foetal calf serum (FCS) (Claycomb *et al.* 1998; White *et al.* 2004).

### 4.1.2 Phenotypic characteristics of HL-1 cells

HL-1 cardiomyocytes have been extensively characterised using microscopic, immunohistochemical, electrophysiological and pharmacological methods to demonstrate that HL-1 cells exhibit properties similar to primary cardiomyocytes *in situ* (Claycomb *et al.* 1998; White *et al.* 2004) as summarised in Figure 4.1.

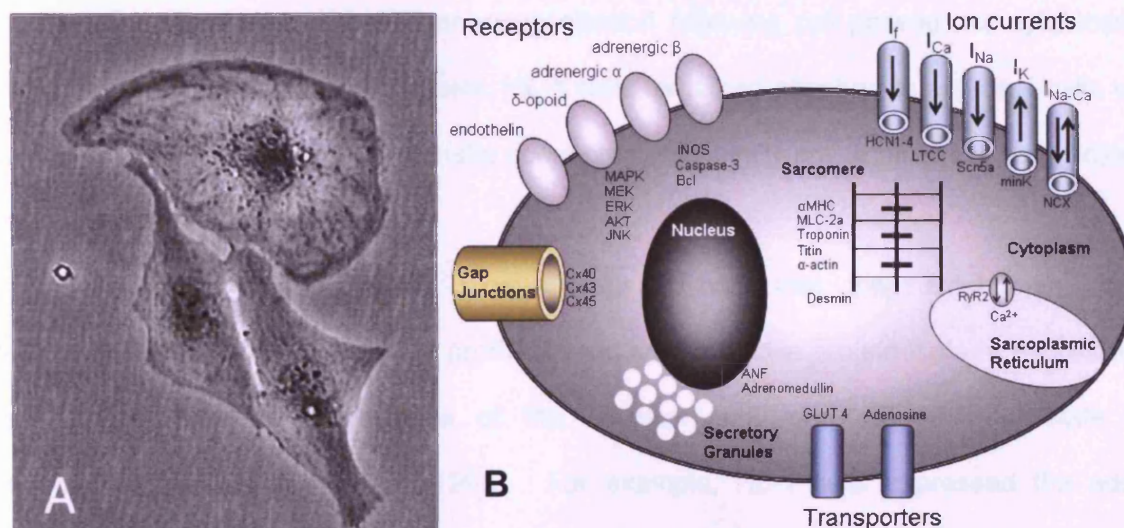


**Figure 4.1. Phenotypic characteristic features of a typical HL-1 cardiomyocyte**

**Panel A:** Shows a phase-contrast image of two HL-1 cardiomyocytes that have just completed cytokinesis adjacent to a contracting myocyte. **Panel B:** A schematic representation of the phenotypic and protein expression characteristics of an HL-1 myocyte. **Abbreviations:** Cx – connexin; iNOS – inducible nitric oxide synthase; MAPK – mitogen-activated protein kinase; ERK – extracellular signal-regulated kinase; MEK – MAPK/ERK kinase; JNK – Jun kinase; MHC – myosin heavy chain; MLC – myosin light chain; GLUT – glucose transporter; RyR – ryanodine receptor; FKBP – FK506 binding protein;  $I_f$  – pacemaking current;  $I_{Ca}$  – calcium current;  $I_{Na}$  – sodium current;  $I_K$  – potassium current;  $I_{Na/Ca}$  – sodium-calcium exchange current. The following genes expressed in HL-1 cells are shown under the current with which they are associated *in vivo*: the hyperpolarisation, cyclic nucleotide-gated channels (HCN), the voltage-gated L-type  $Ca^{2+}$  channel (LTCC), the voltage-gated sodium channel (Scn5a), modulatory  $\beta$ -subunit for the inward rectifier potassium current (mink), and the sodium/calcium exchanger (NCX). Adapted from White *et al.* (2004).

According to both microscopic and immunohistochemical studies, HL-1 cells do not have a classical T-tubular organisation, yet they contain highly organised sarcomeres necessary for mediating contraction and intracellular ANF granules characteristic of atrial myocytes. Morphological characterisation revealed that HL-1 cells resemble AT-1 cells (Moses & Claycomb 1984) and immature mitotic mouse atrial cardiomyocytes *in situ* (Delcarpio *et al.*

1991). As is characteristic of healthy mitotically active cardiomyocytes, the cytoplasm of HL-1 cells contains nascent myofibrils and glycogen-rich areas. The majority of HL-1 cells contain a single centrally-positioned nucleus surrounded by a ring of contracting myofibrils. HL-1 cells also possess perinuclear ANF-containing granules, cardiac-specific myosin, and muscle-specific desmin intermediate filaments. Myofibrillogenesis, a characteristic typical of normal myofibril development in mitotic cardiomyocytes in the developing heart, was also observed in cells undergoing cellular reorganisation following cell passage or cytokinesis (Claycomb *et al.* 1998). During mitosis, HL-1 cells remained attached to adjacent cells via intercalated discs, another characteristic common to mitotically active atrial cardiomyocytes *in situ* (Claycomb *et al.* 1998).

Analysis of gene expression in HL-1 cells reveals that they exhibit an adult cardiomyocyte-like gene expression profile, based on contractile protein isoform expression which is a well established index of the developmental and differentiated state of cardiomyocytes (Claycomb *et al.* 1998). For example, HL-1 cells expressed the adult isoform of MHC ( $\alpha$ -MHC) as well as  $\alpha$ -cardiac actin, ANF and connexin43, similar to adult mouse ventricular cells.

HL-1 cells spontaneously depolarise and express the necessary ion channels required for generating APs characteristic of primary cardiomyocytes. After several days in culture, HL-1 cells exhibited spontaneous APs and synchronous beating in super-confluent cultures. The contractile cells displayed electrophysiological characteristics consistent with those seen in cardiomyocytes *in situ*, including the presence of several voltage-dependent currents typical of a cardiac myocyte phenotype.

Pharmacological studies show that HL-1 cells respond appropriately to inotropic and chronotropic agonists, indicating the expression of functional receptors and intracellular signalling proteins required for these signalling pathways (Claycomb *et al.* 1998).

Overall, the HL-1 cell line represents a hybrid between an embryonic and an adult myocyte. HL-1 cells retain a pattern of gene expression typical of normal adult mouse myocytes, and express genes encoding adult protein isoforms despite the fact that they are

actively dividing. However, as a consequence of their ability to continuously divide in culture, they possess a less differentiated and less organised ultrastructure, which is similar to that of actively dividing embryonic cardiomyocytes (White *et al.* 2004).

#### 4.1.3 HL-1 cells as a model system

HL-1 cardiomyocytes are unique in their capacity to proliferate and be serially passaged without reverting to an embryonic phenotype (Claycomb *et al.* 1998; White *et al.* 2004). Furthermore, HL-1 cells are the only cultured cell line of cardiac origin which can form synchronously coupled beating monolayers suitable for imaging experiments. These properties make them attractive for studies that require expression of adult-specific genes and for studies of cardiomyocyte function, as well as for assessing the activity of pharmacological agents such as modulators of cardiac ion channels.

HL-1 cells have proven useful for studying many aspects of cardiac biology *in vitro*, including hypoxia (Cormier-Regard *et al.* 1998; Nguyen and Claycomb 1999), hyperglycaemia (Collier *et al.* 2002), cellular signalling (McWhinney *et al.* 2000; Kitta *et al.* 2001; Suzuki 2003), electrophysiology (Akhavan *et al.* 2003; Claycomb *et al.* 1998), cell cycle regulation (Lanson *et al.* 2000; Zandstra *et al.* 2003), apoptosis (George *et al.* 2007c) and calcium handling (George *et al.* 2003a, 2006).

Our laboratory routinely uses HL-1 cardiomyocytes to study the effects of altered intracellular Ca<sup>2+</sup> handling in a cardiac cell environment (George *et al.* 2003a). HL-1s also represent a robust system for investigating the effects of ouabain, a pharmacological arrhythmogen which mechanistically mimics the events frequently leading to human arrhythmias (Barberini-Jammaers *et al.* 2008).

#### 4.1.4 Microinjection

Single cell microinjection (MI) has been successfully utilised to deliver exogenous proteins, cDNA constructs, peptides, drugs and particles into transfection-challenged cells. Since it permits the precise control of the amount and timing of delivery, this technique has been used in many studies of primary cultured cells, transgenic animal production, and *in vitro* fertilisation.

Transductions of exogenous cDNAs, proteins, peptides, and drugs are widely used in modern cellular and molecular biology by a variety of different techniques. Chemical transfection of foreign DNAs into the cytosol of mammalian cells is routinely achieved by calcium phosphate or liposome-mediated reagents (Colosimo *et al.* 2000; Zhang & Yu 2008). Viral infection transfers genes of interest through packaging them into a replication-defective viral vector encapsulated within a viral envelope enhancing gene transfer efficiency. Both chemical transfection and viral infection can achieve high levels of transduction once the experimental conditions have been optimised. As an alternative to chemical and viral transduction methods, other more physical methods are available, such as electroporation. Electroporation can directly deliver non-permeable exogenous substances into cells (Orlowski & Mir 1993). During electroporation, a rapid high-voltage electrical pulse results in temporary pore formation in the cell membrane, through which foreign proteins or DNA can enter the cell. Because electroporation eliminates the cytotoxicity caused by chemical transfection or viral infection, it has been widely used to deliver large molecules such as proteins, antibodies, and dextrans. However, electroporation requires relatively large amounts of protein preparation for a single transduction, and has a relatively low efficiency (Orlowski & Mir 1993; Tompers & Labosky 2004). A novel system for protein delivery uses a cationic lipid mixture as a vehicle for the proteins, and releases them into the cell by fusing with the cell membrane. This method is faster and more efficient than the transfection methods discussed above, but has the same limitations with regards to the precise control of timing and the amount of sample being

delivered into the cell. However, none of these methods described above are suited to the experimental approaches described in this thesis since none permit the precise control of timing and amounts of exogenous material introduced into the cells (Zhang & Yu 2008).

A robust mechanical delivery method, MI of single cells, achieves high transduction efficiency in the majority of cell types, including cultured primary cells and oocytes. The greatest advantage of this method is the ability to precisely control the dosage, timing, and location of delivery. Considering a recent study in our laboratory that showed that the effect of I-Domain proteins on cell phenotype occurs less than one day after their recombinant expression in HEK cells (Fry 2008), the technique of MI, that allows control over delivery time, location and amount of exogenous material, is the only feasible way to study the acute effects of these proteins.

In an optimised and well-controlled MI strategy, the exogenous injected material is the only independent variable and therefore the effect of the injected substance can be unequivocally determined. Modern air pressure driven microinjectors allow the fine-tuning of injection pressure, compensation pressure and injection time, which together manipulate the injection volume. The successful application of MI to experiments involving HL-1 myocytes has been demonstrated by Clarke *et al.* (2006) to investigate peptide-based manipulation of gap junction-mediated intercellular communication.

#### **4.1.5 Objectives of this chapter**

This chapter describes the optimisation of a robust MI strategy for the delivery of I-Domain proteins into HL-1 myocytes, while preserving cell viability and ultrastructure. Recent studies in our laboratory (Fry 2008) established that recombinant expression of some I-Domain subfragments ID<sup>A</sup> and ID<sup>C</sup> were profoundly cytotoxic and induced apoptosis in HEK cells after 1 day. In light of these observations, together with the bioinformatics analysis discussed in Chapter 3 and Appendix II, this chapter will focus on investigating the effects of ID<sup>B</sup> on spatio-temporal Ca<sup>2+</sup> handling in HL-1 myocytes.

#### **4.1.6 Specific Hypothesis**

Here, we tested the hypothesis that microinjection of recombinant fragments would enable the phenotypic consequences of ID subfragment, ID<sup>B</sup> to be determined. This chapter describes the characterisation of MI as an appropriate technique for this purpose.



## 4.2 Methods

### 4.2.1 Preparation of HL-1 cells for MI

HL-1 cardiomyocytes were cultured and harvested as described in Chapter 2. The harvested cell pellet was resuspended in supplemented Claycomb media before plating onto glass chambers (14 mm diameter, 0.1 mm thickness, MatTek), which had been coated overnight with a GFN substrate, at a density of  $5 \times 10^5$  cells/chamber. The cells were initially applied to the GFN-coated chambers in a 200 $\mu$ l meniscus, and allowed to adhere to the glass for between 4 and 6 h before the chamber was flooded with an additional 1800 $\mu$ l of supplemented Claycomb media. These were then left to grow for 48 h (37°C, 5% CO<sub>2</sub>, ~80% humidity) with the growth media being replaced daily in order to maintain the cells in a healthy contractile state, before being used for MI experiments.

### 4.2.2 MI apparatus and techniques

All MI experiments were carried out using an Eppendorf NI2 system which provides a reliable and reproducible system for MI of mammalian cells. The system consists of two basic units: the InjectMan NI2 micromanipulator, which electronically controls movement of the microcapillary and the FemtoJet microinjector, which regulates injection parameters. The InjectMan NI2 micromanipulator is controlled by the operator through a joystick and is capable of smooth, coarse, or fine movement, in the x-, y-, and z-axes. Cells were injected by Femtotip microcapillaries (Eppendorf) with a needle diameter of  $0.5 \mu\text{m} \pm 0.2 \mu\text{m}$ , using the axial mode in which the microcapillary penetrates the cells at an angle of 45° (Green *et al.* 2007).

The FemtoJet is programmable and communicates with the micromanipulator to execute standardised injection routines. The injection parameters which can be optimised are injection pressure (Pi), injection time (Ti), and compensation pressure (Pc). The Pi is the pressure which is needed to drive the fluid from the capillary into the cells, and together with

the  $T_i$  determines the volume of sample injected. It is vital to use an optimal  $P_i$ ; using a high  $P_i$  risks damaging the internal structure of the cell while lower  $P_i$  values may result in inefficient injection. The  $P_c$  maintains a low positive pressure inside the capillary to prevent back filling of the needle, and will depend on the viscosity of the sample (Bartoli & Claycomb 1997).

Using defined parameters across different experiments permits the controlled injection of reproducible volumes of injection sample into cells. Once the injection parameters have been set on the FemtoJet microinjector, the capillary is lowered to the focal plane just above the cells. The injection level is then determined by setting the z-limit on the micromanipulator – this is the position on the z-axis at which the microcapillary will enter the cell. The choice of an appropriate z-limit is a critical parameter for successful MI. If set too low it will penetrate through the whole cell and risk breaking the needle, or if positioned too high the needle will not penetrate the cell at all, in both cases resulting in unsuccessful MI. The capillary is then brought back to a focal plane above the cell, and by activating the joystick key, the semi-automatic injection (Figure 4.2, A, B) starts with an axial movement to penetrate the cells. When the capillary has reached the injection level, the microinjector automatically switches from compensation pressure to injection pressure. The injection pressure is applied to the capillary according to the preset injection time. After injection has taken place, the pressure is switched back to the compensation pressure and the capillary returns along the same path (Figure 4.2, C) to its starting position.

All MI experiments were carried out using the set-up described above. The glass culture chambers containing the adherent cells were placed on a heated microscope stage pre-warmed to 37°C, onto which the micromanipulator was mounted.

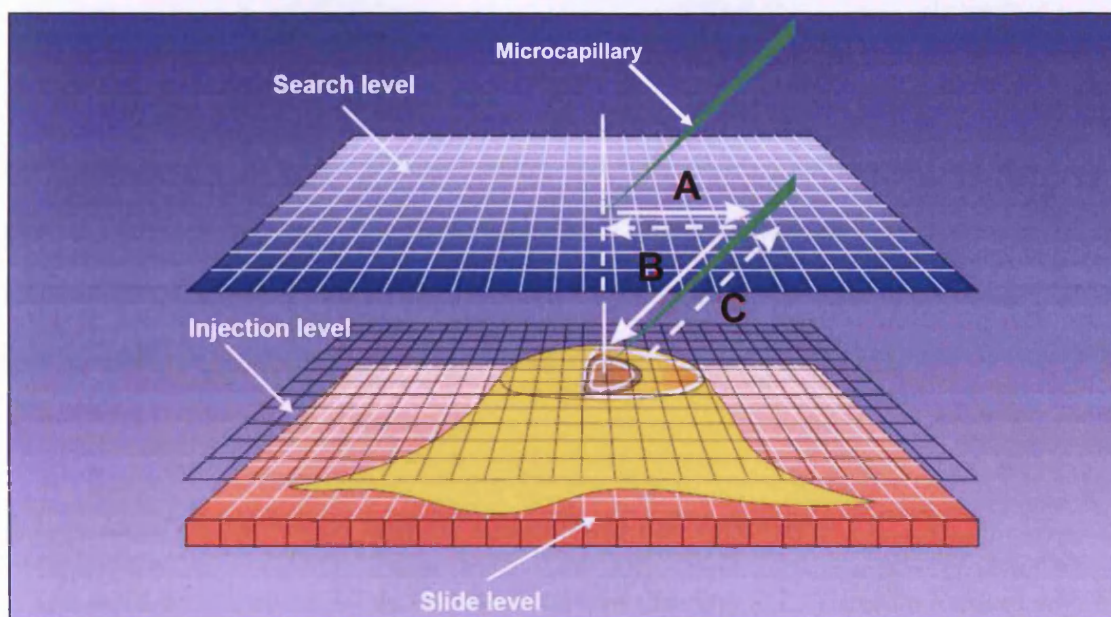


**Figure 4.2. Schematic depicting semi-automated MI into adherent cells**

A, B, and C represent the axial movement of the microcapillary during an injection. Search level is the focal plane above the cell monolayer, and the injection level is the point on the z-axis at which the microcapillary enters the cell (Image reproduced from <http://www.eppendorf.com>)

### 4.2.3 Optimisation of MI parameters

Optimisation of MI parameters was carried out using a Zeiss Axiovert 200 fluorescence microscope. All cDNAs, dyes or peptides to be microinjected were centrifuged at 17,000  $xg$  for 1 h at 4°C prior to loading the MI needle, to remove any small particles which may block its tip. While loading the needle, great care was taken to avoid air bubbles which would prohibit successful injection. MI into the adherent cells was carried out under phase contrast microscopy, initially using ranges of  $P_i$  (50-150 hPa),  $P_c$  (20-120 hPa) and  $T_i$  (0.1-0.5 secs).

Determination of the most suitable MI conditions was carried out in two stages. Firstly, propidium iodide was used as a marker of successful injection, using a range of times and pressures to find the optimal  $P_i$ ,  $P_c$  and  $T_i$  parameters that did not cause cell damage such as bursting or prolonged deformation. Propidium iodide was injected into the cytoplasm of the cells under phase microscopy, and viewed immediately after MI using fluorescence filters 546nm/580-590nm (Zeiss Axiovert). Once the optimal MI parameters had been identified,

cDNA encoding enhanced green fluorescent protein (eGFP, Clontech) (250 µg/ml in 3M Tris, 0.3M EDTA) was injected into the nuclei of HL-1 cells to verify that, under the MI conditions determined above, the cells remained viable and expression-competent for sufficient time to express recombinant eGFP. Following MI, the medium was replaced with fresh supplemented Claycomb media pre-warmed to 37°C, and the cells were viewed after 48 hours using fluorescence filters 345-440nm/460-470nm (Zeiss Axiovert).

#### **4.2.4 MI of recombinant protein and cellular Ca<sup>2+</sup> imaging**

Cells were prepared for MI as described above (Section 4.2.1), before loading with Fluo-4AM (10 µM in 20% (w/v) pluronic acid F-127 dissolved in DMSO) in non-supplemented Claycomb medium pre-warmed to 37°C. The dye-containing solution was added to each chamber as a 200µl meniscus and incubated for 60 minutes (37°C, 5% CO<sub>2</sub>, ~80% humidity). The cells were then immersed in a further 1800µl pre-warmed non-supplemented medium prior to Ca<sup>2+</sup> imaging. Ca<sup>2+</sup> dependent Fluo-4AM fluorescence was imaged using a Leica RS2 confocal microscope with an oil immersion 40x objective lens, using an Argon/Krypton laser (excitation at 488nm, and the fluorescence emission detected at 500nm). 8-bit scaled data were acquired every 200 ms (5 Hz) in a field of view at 512 x 209 pixel resolution. Resting cells were imaged for 1 minute (300 frames) prior to MI in order to obtain a measurement of basal fluorescence levels.

Proteins synthesised and purified as described in Chapter 3 were injected into superconfluent 'beating' HL-1 cells using the optimal conditions determined above. The MagZ purified protein in injection buffer (100 mM potassium chloride, 5 mM potassium phosphate, pH 7.4; using chelex-treated dH<sub>2</sub>O (5g chelex /100ml dH<sub>2</sub>O)), was co-injected with Alexa-647 dye conjugated to a 10,000 MW dextran (1 µg/ml stock) as a non-transferable cellular marker of injection that enables the identification of microinjected cells, in a protein:buffer:dye of 1:2:1 (v/v) ratio. The injection buffer has similar ionic and osmotic properties to those displayed by the intracellular environment, and facilitates complete cell

recovery after MI (Bartoli & Claycomb 1997). Approximately twenty cells per field of view were injected within a time frame of < 2 minutes, and allowed to recover for 5 minutes prior to imaging the cells for a further 60 seconds (300 frames). In every microinjection experiment RRL without I-Domain protein, yet processed using  $Zn^{2+}$ -affinity purification under exactly the same conditions as the RRL samples in which the I-Domain protein was synthesised, was used as a control.

Data were acquired from regions of interest (ROIs) representing global  $Ca^{2+}$  environments, typically approximately  $50 \mu m^2$  in area (~ 200 pixels). These were collected and analysed using Leica confocal software (Leica Microsystems, Heidelberg, Germany). Further analysis was carried out using the SALVO program in Matlab (Section 4.2.5).

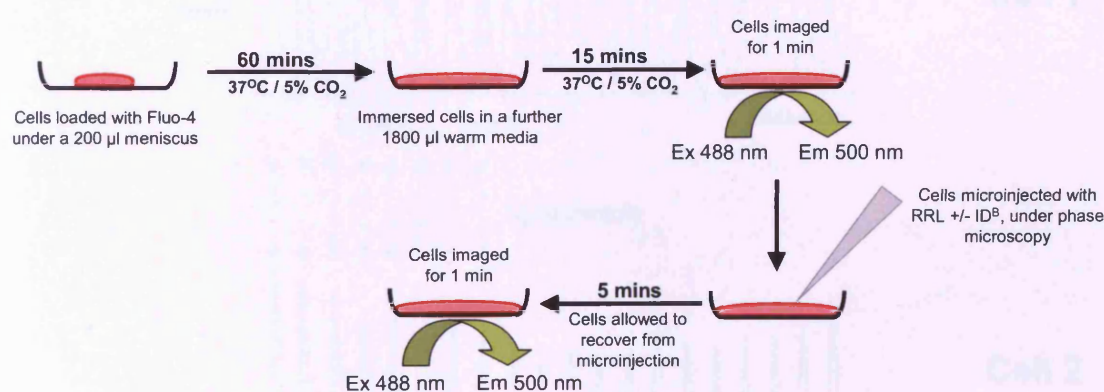


Figure 4.3. Summary of MI and  $Ca^{2+}$  imaging protocol

#### 4.2.5 Analysis of spatio-temporal $Ca^{2+}$ handling in HL-1 myocytes

Spatio-temporal  $Ca^{2+}$  handling in coupled monolayers of fluo-4 loaded HL-1 myocytes was recorded at 5 Hz as described above (Section 4.2.4). Multi-parametric data analysis from 20 ROIs per field of view was performed using the **Synchronicity-Amplitude-Length-Variability of Oscillation (SALVO)** program (Barberini-Jammaers *et al.* 2008); an analytical platform for decoding intracellular  $Ca^{2+}$  handling using high-resolution confocal imaging of spontaneously-beating, coupled HL-1 monolayers. SALVO was programmed in Matlab (The Mathworks Inc.) based on Uhlén's concepts of 'peaks and valleys' (Uhlén 2004) and

enables the robust deciphering of the  $\text{Ca}^{2+}$  handling parameters outlined in Figure 4.4. SALVO provides a quantitative analysis of the release and sequestration processes underlying  $\text{Ca}^{2+}$  fluxes in HL-1 myocytes. By simultaneously measuring a number of inherently inter-linked parameters, it allows a holistic approach to considering the data and provides an indication of the cellular processes that may be involved in shaping  $\text{Ca}^{2+}$  fluxes.

For the purposes of this study, SALVO was used to quantitatively measure ten different parameters of  $\text{Ca}^{2+}$  handling, each of which can be related to specific processes in a cellular context, as summarized below (Table 4.1).

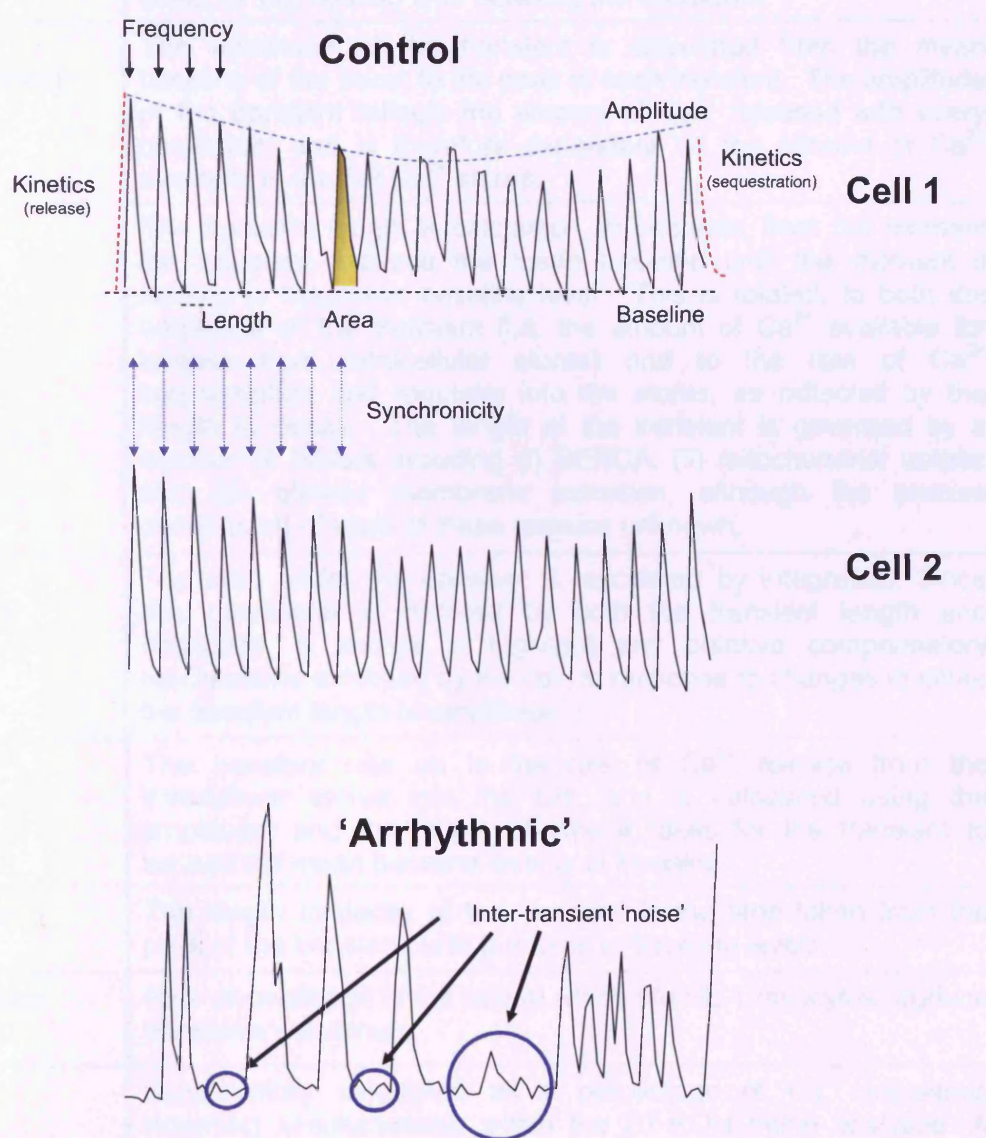


**Figure 4.4. Deciphering intracellular  $\text{Ca}^{2+}$  signalling in HL-1 cardiac cell monolayers**  
Schematic diagram illustrating SALVO analysis parameters (Barberini-Jammaers *et al.* 2008).

SALVO parameter	Description
Total noise (arbitrary units)	This parameter calculates the temporally-resolved $\text{Ca}^{2+}$ fluctuations throughout the entire trace, both within and between the $\text{Ca}^{2+}$ transients. This is an index of how cellular processes regulate $\text{Ca}^{2+}$ release and sequestration.
Inter-transient Noise (arbitrary units)	This parameter calculates all sub-threshold fluctuations in $\text{Ca}^{2+}$ , that are distinct from clearly resolved amplitude and temporal characteristics of $\text{Ca}^{2+}$ "transients" (where a transient is defined as an event exhibiting an amplitude more than 2-fold higher than the mean background signal noise).
Total: Inter-tansient Noise	Ratio of noise in the entire trace versus the inter-transient noise. An increased ratio is suggestive of a reduced inter-transient noise (defined above), indicating either (i) a reduced inter-transient noise, or (ii) reduced time between the transients.
Amplitude (fluorescence units)	The amplitude of the transient is calculated from the mean baseline of the trace, to the peak of each transient. The amplitude of the transient reflects the amount of $\text{Ca}^{2+}$ released with every oscillation, and is therefore dependent on the amount of $\text{Ca}^{2+}$ available in the SR $\text{Ca}^{2+}$ stores.
Transient Length (s)	The transient length is calculated, in seconds, from the moment the transient exceeds the mean baseline until the moment it returns to the mean baseline level. This is related, to both the amplitude of the transient (i.e. the amount of $\text{Ca}^{2+}$ available for release from intracellular stores) and to the rate of $\text{Ca}^{2+}$ sequestration and reuptake into the stores, as reflected by the length to decay. The length of the transient is governed by a number of factors including (i) SERCA, (ii) mitochondrial uptake and (iii) plasma membrane extrusion, although the precise contribution of each of these remains unknown.
Area (arbitrary units)	The area under the transient is calculated by integration. Since this parameter is dictated by both the transient length and amplitude, it serves to highlight any putative compensatory mechanisms exhibited by the cell, in response to changes in either the transient length or amplitude.
Rate Up ( $\text{Fs}^{-1}$ )	The transient rate up is the rate of $\text{Ca}^{2+}$ release from the intracellular stores into the cell, and is calculated using the amplitude, and the length of time it takes for the transient to exceed the mean baseline level until it peaks.
Length to Decay (s)	The length to decay of the transient is the time taken from the peak of the transient, until it returns to baseline levels.
Rate of Oscillation (Hz)	Rate of oscillation is the rate at which the HL-1 myocytes produce transients per minute.
Synchronicity (%)	Synchronicity calculated as a percentage of $\text{Ca}^{2+}$ transients occurring simultaneously within the 20 ROIs being analysed. A value of synchronicity at 100% would show that all transients seen in these regions are occurring simultaneously, all of the time.

Table 4.1. Explanation of SALVO parameters

In the beating syncytium, the most striking phenotype of cellular integrity and intercellular functionality is synchrony. Synchrony is a powerful indicator of intra- and inter-cellular  $\text{Ca}^{2+}$  handling, and was used in this context throughout this thesis. Considering that ID fragments were predicted to functionally modify RyR2/IP<sub>3</sub>R signalling, the phenotypic endpoint of such modulation would logically be expected to be changes in synchrony. The utility of the multi-parametric nature of SALVO allows the user to interrogate the mechanisms underlying alterations in synchrony. Alternatively, in the absence of changes in synchrony, SALVO analysis may resolve cellular mechanisms of plasticity in  $\text{Ca}^{2+}$  handling.



### 4.3 Results

#### 4.3.1 Optimised parameters for MI

Following extensive evaluation of specific MI protocols, optimal conditions for MI efficiency and cell viability were determined at injection pressure (Pi) of 90 hPa, compensation pressure (Pc) of 80 hPa and an injection time (Ti) of 0.3 sec. These conditions gave a MI efficiency of ~95% as observed by injection of propidium iodide, and ~75% of the cells remained viable and able to express recombinant eGFP for at least 48 h (Figure 4.5).

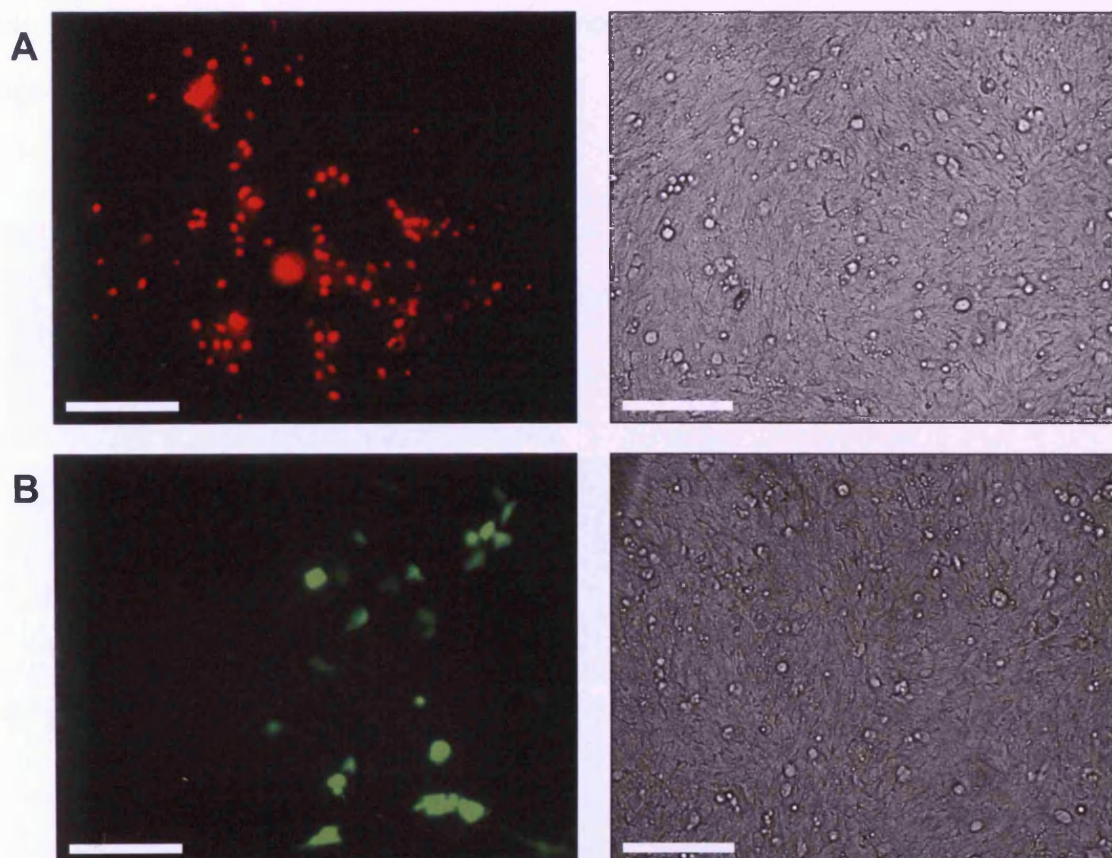


**Figure 4.5. Optimal MI parameters confer efficient injection and cell viability.**

**Panel A:** HL-1 cells injected with propidium iodide visualised by fluorescence microscopy (right) and a phase contrast image of the same field of view (left). **Panel B:** Fluorescence (left) and phase contrast microscopy (right) of HL-1 cells 48h after MI with eGFP cDNA. Scale bar: 100µm

### 4.3.2 MI of recombinant proteins and markers into HL-1 myocytes

I-Domain proteins synthesised and purified as described in Chapter 3, were successfully microinjected into HL-1 myocytes, using the parameters described above. The use of a 647-alexa conjugated dye enabled the easy visual detection of microinjected cells (Figure 4.6, E). Importantly cell phenotype and Fluo-4 fluorescence appeared to be unaltered by MI, indicating that MI conditions were minimally invasive (Figure 4.6, B and D respectively). However, it can also be seen that the intensity of the Alexa 647 signal is not homogenous in all microinjected cells. The differences in signal intensity could be an artefact of the heterogeneity of cell size and shape, but it is also possible that it is an indicator of the amount of sample injected into each of the cells. Nevertheless, similar heterogeneity is evident in all experiments and thus should be normalised by the very large number of cells imaged (15-20 cells per experiment,  $n = 6-10$ ).

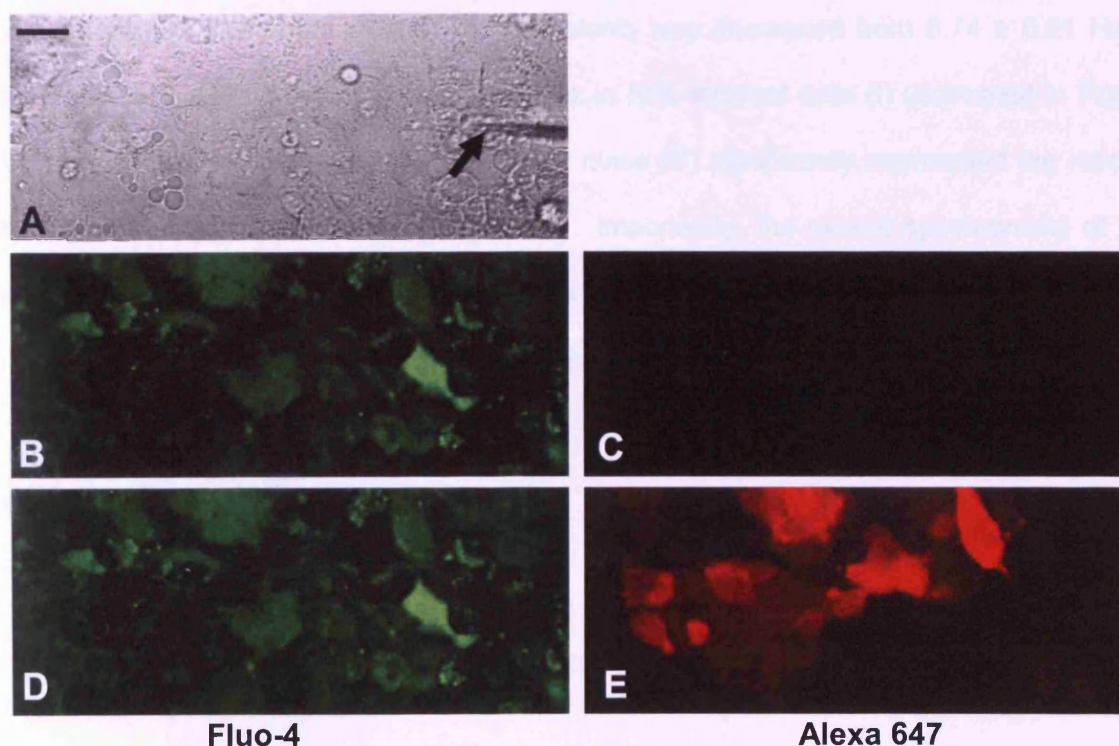


**Figure 4.6.** MI of proteins into HL-1 cells

**Panel A:** Phase contrast image of the field of view, the arrowhead shows the tip of the microcapillary moved to a focal plane above the cells. **Panels B & C:** Fluorescent signals prior to MI. **Panels D & E:** the same field of view 5 minutes after MI with Alexa 647 dextran. The Fluo-4 loaded cells appear unchanged (D) while the microinjected cells are clearly identifiable (E). Scale bar: 25  $\mu\text{m}$

### 4.3.3 MI of RRL affects some aspects of cell $\text{Ca}^{2+}$ -handling phenotype

Although the Fluo-4 data presented above suggested that, under optimised conditions, MI was well tolerated by the cells, the MI procedure itself may modulate some aspects of cellular phenotype and signalling. Consequently, rigorous control experiments were performed to evaluate whether any changes in  $\text{Ca}^{2+}$  handling were attributable to MI. As described above (Section 4.2.4),  $\text{Zn}^{2+}$  affinity processed RRL that had not been used for producing I-Domain protein was microinjected since this sample contains identical 'background' proteins to samples in which the I-Domain protein was synthesised. Control injections of 'naïve' RRL were performed in all MI experiments described in this thesis.

SALVO analysis (Figure 4.7) showed that injection of RRL into beating HL-1 myocytes did not alter the amplitude, length or area of  $\text{Ca}^{2+}$  transients (panels **D**, **E** and **F** respectively). There was also no significant change in the kinetics of  $\text{Ca}^{2+}$  handling (**G** and **H**). However, RRL-injected cells were characterised by significantly increased inter-transient noise (**B**), and the frequency of spontaneous  $\text{Ca}^{2+}$  transients was decreased from  $0.74 \pm 0.01$  Hz in non-microinjected HL-1 cells to  $0.58 \pm 0.02$  Hz in RRL-injected cells (**I**) (illustrated in Figure 4.8). As anticipated, increased inter-transient noise (**B**) significantly augmented the ratio of total signal noise to inter-transient noise (**C**). Importantly, the overall synchronicity of the coupled monolayer, a direct index of the synchronisation of  $\text{Ca}^{2+}$  oscillations between neighbouring cells, was not affected by MI (Figure 4.9).

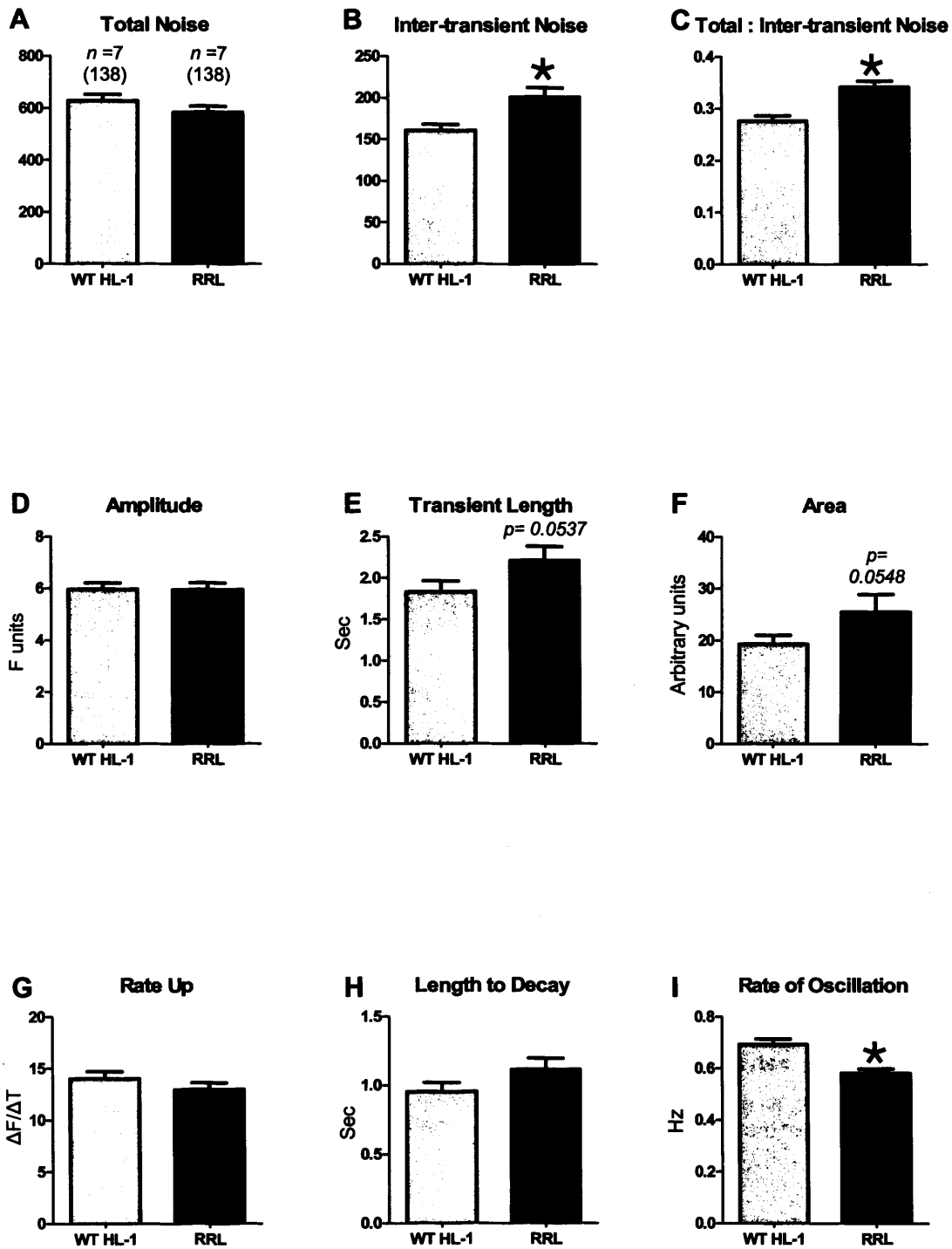


**Figure 4.7. SALVO analysis of the effects of MI on HL-1 myocyte monolayers**

Spatio-temporal  $\text{Ca}^{2+}$  handling parameters in HL-1 myocytes injected with RRL controls (black) compared with non-injected WT HL-1 myocytes (grey), plotted from SALVO analysis of  $\text{Ca}^{2+}$ -dependent Fluo-4 fluorescence (mean  $\pm$  SEM,  $n = 7$ , 15-20 cells per experiment. The total number of cells is indicated in brackets). \* represents  $p < 0.05$  when compared with WT HL-1.

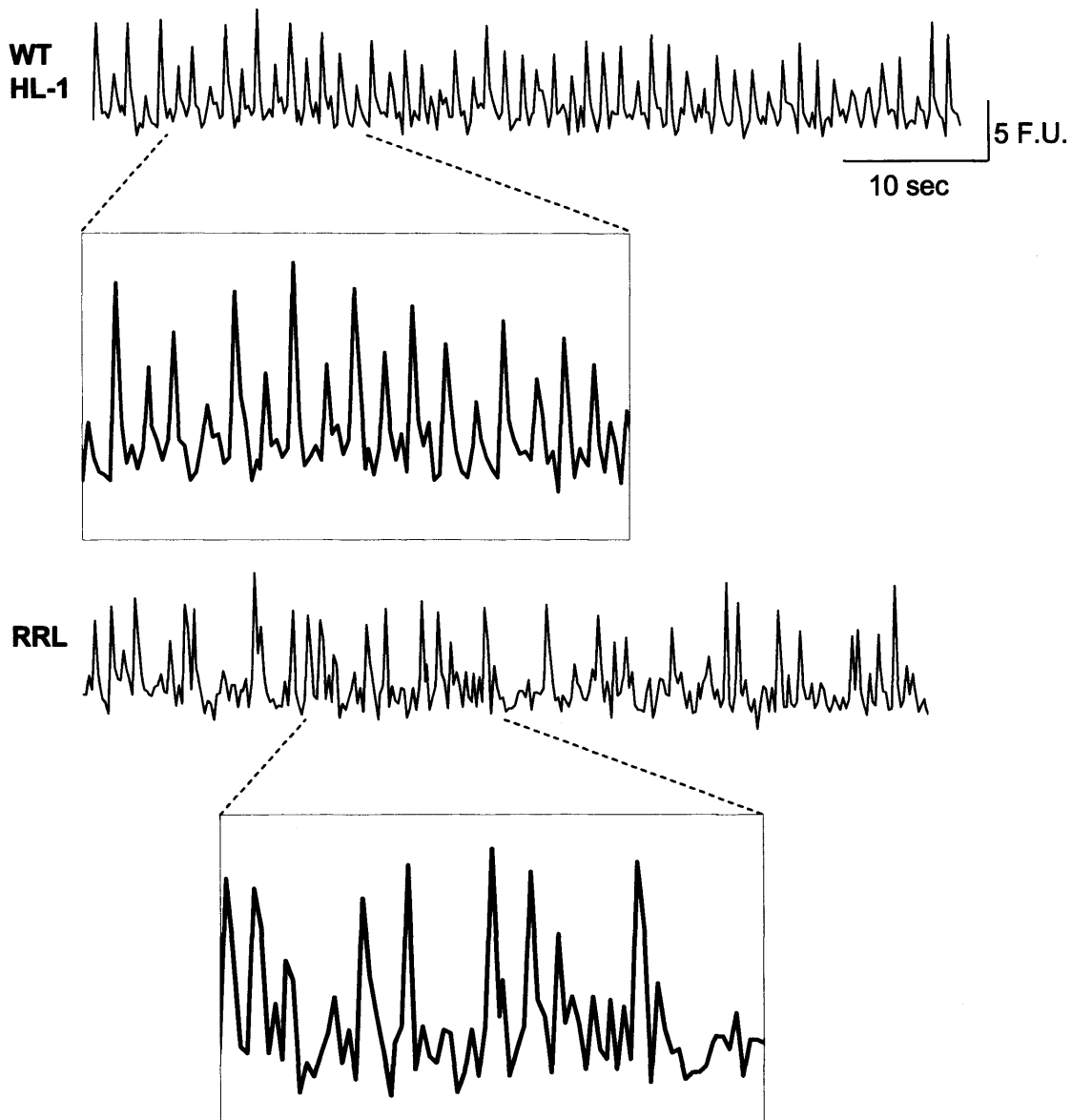


**Figure 4.8. Representative traces of WT and RRL-injected HL-1 myocytes**

Traces show an increased level of inter-transient noise and a lower rate of oscillation in the RRL-injected HL-1 myocytes, compared with WT HL-1 cells. F.U. denotes arbitrary fluorescence units measured in defined regions of interest.

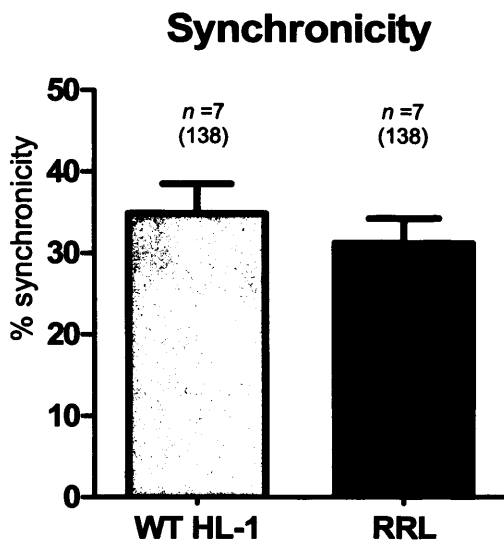


**Figure 4.9. Synchronicity in WT HL-1 cells compared with RRL injected cells**

Synchronicity within HL-1 myocytes monolayers injected with RRL controls (black) compared with non-injected WT HL-1 myocytes (grey), plotted from SALVO analysis of  $\text{Ca}^{2+}$ -dependent Fluo-4 fluorescence (mean  $\pm$  SEM,  $n = 7$ , 15-20 cells per experiment. The total number of cells is indicated in brackets). No significant difference between RRL-injected and WT HL-1 was observed.

#### 4.3.4 MI of $\text{ID}^{\text{B}}$ into HL-1 myocytes

Following the detailed assessment of the changes in HL-1  $\text{Ca}^{2+}$  phenotype induced by MI of RRL proteins (Figure 4.7 and Figure 4.9), it was possible to determine the specific effects of  $\text{ID}^{\text{B}}$  on  $\text{Ca}^{2+}$  handling in HL-1 cardiomyocytes. Figure 4.10 revealed that  $\text{ID}^{\text{B}}$  is associated with a decrease in total signal noise (A) – from  $585 \pm 23.29$  in RRL-injected cells to  $446.6 \pm 9.067$  in cells injected with  $\text{ID}^{\text{B}}$  – which as predicted, was mirrored by an increase in the total:inter-transient noise ratio (C,  $0.3412 \pm 0.0117$  with RRL to  $0.3875 \pm 0.0135$  with  $\text{ID}^{\text{B}}$ ). In addition,  $\text{ID}^{\text{B}}$  injection was linked to a significant decrease in the average rate of  $\text{Ca}^{2+}$  release from  $12.96 \pm 0.6656$  in the RRL-injected control cells to  $8.003 \pm 0.2215$  in  $\text{ID}^{\text{B}}$ -injected cells (G). These  $\text{ID}^{\text{B}}$ -mediated changes did not cause alterations in  $\text{Ca}^{2+}$  transient amplitude (D), length (E), area (F), decay time (H) and frequency of oscillation (I) which remained unchanged. Corroborating the data presented in Figure 4.9 above, cellular synchronicity was not affected (Figure 4.12).

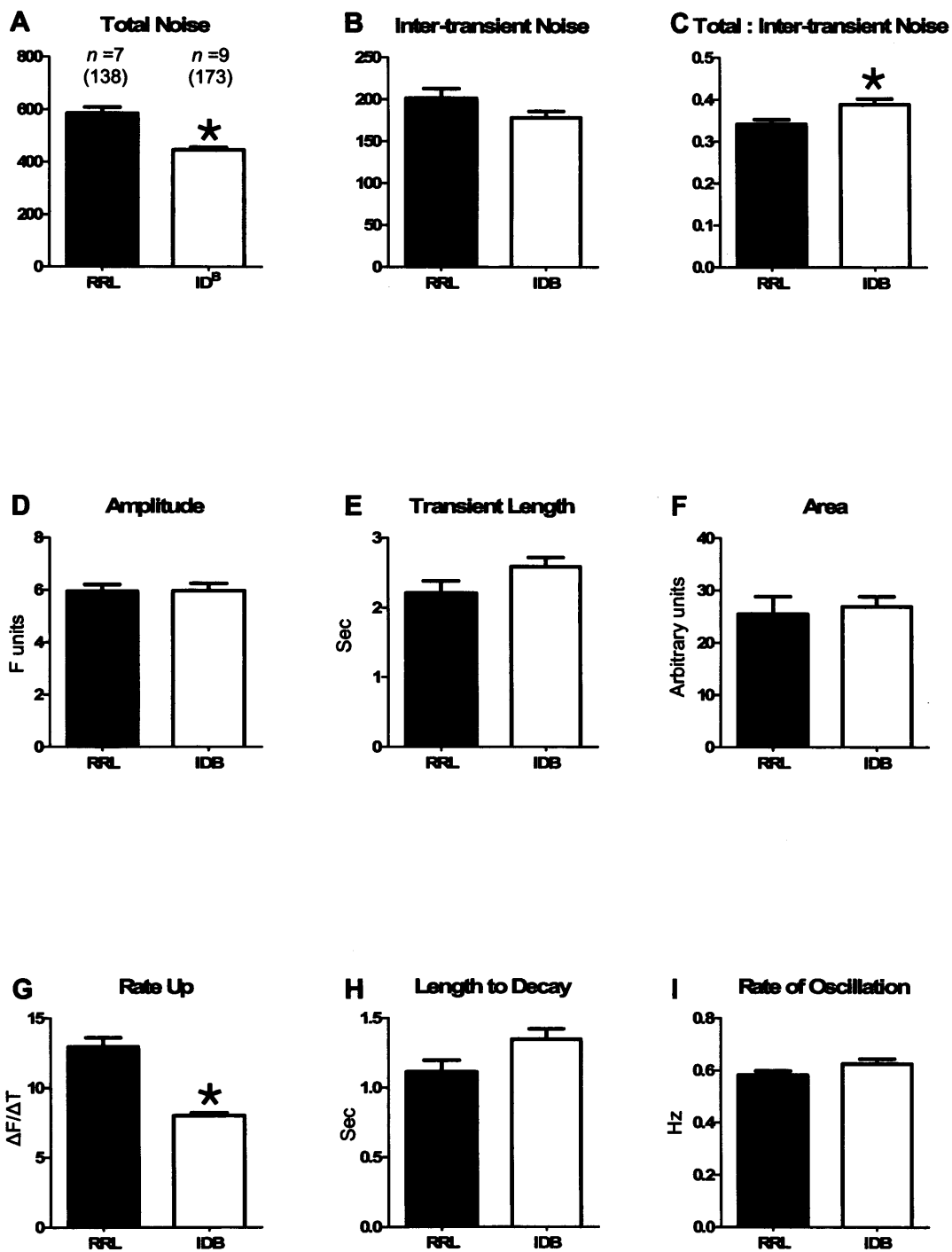


**Figure 4.10. SALVO analysis of the effects of ID<sup>B</sup> on HL-1 myocyte monolayers**

Spatio-temporal Ca<sup>2+</sup> handling parameters in HL-1 myocytes injected with ID<sup>B</sup> protein (white) compared with RRL-injected controls (black), plotted from SALVO analysis of Ca<sup>2+</sup>-dependent Fluo-4 fluorescence (mean  $\pm$  SEM, n = 7-9, 15-20 cells per experiment). \* represents p<0.05 when compared with RRL-injected control cells.

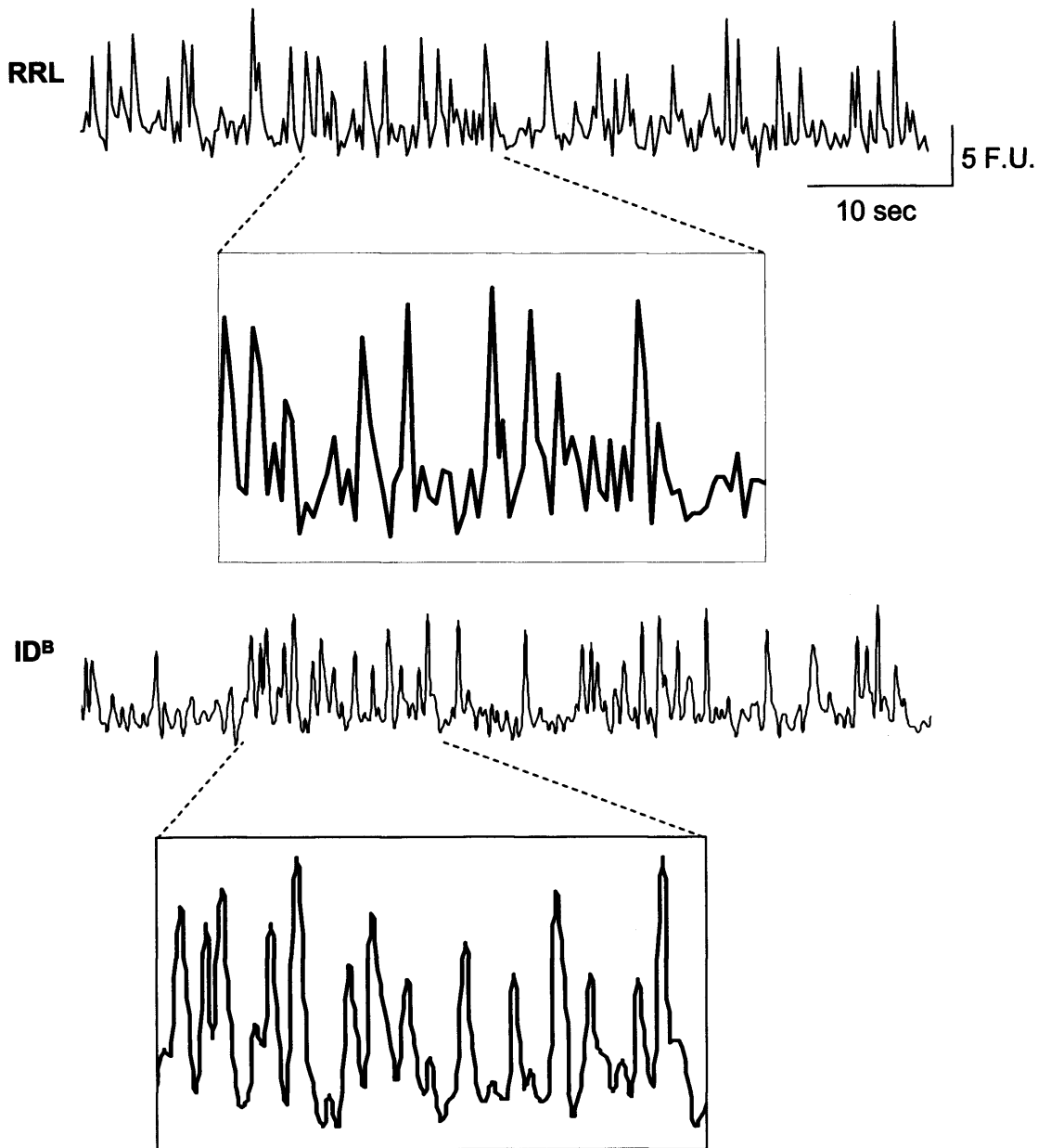


**Figure 4.11. Representative traces of HL-1 myocytes injected with RRL and ID<sup>B</sup>**

Traces show an increased noise in HL-1 myocytes injected with ID<sup>B</sup>, compared with the RRL-injected controls. ID<sup>B</sup>-injected cells also displayed a lower mean transient rate-up. F.U. denotes arbitrary fluorescence units measured in defined regions of interest.



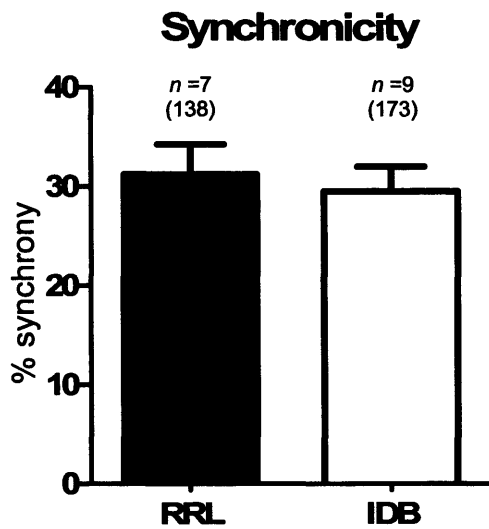


**Figure 4.12. MI of ID<sup>B</sup> does not alter synchronicity**

Synchronicity within HL-1 myocytes monolayers injected with ID<sup>B</sup> protein (white) compared with RRL-injected controls (black), plotted from SALVO analysis of Ca<sup>2+</sup>-dependent Fluo-4 fluorescence (mean  $\pm$  SEM, n = 7-9, 15-20 cells per experiment). No significant difference between HL-1 cells injected with RRL or ID<sup>B</sup> protein was observed.

## 4.4 Discussion

### 4.4.1 Conditions for successful MI

This chapter describes the conditions necessary for the successful MI of HL-1 myocytes while maintaining cellular function and viability. Using the optimised conditions, an injection efficiency of approximately 95% was achieved and more than 75% of cells remained viable for at least two days after MI of cDNA into their nuclei. The successful expression of eGFP after MI of the cDNA is fundamental in the success of this technique, because all gene expression is dependent on appropriately regulated  $\text{Ca}^{2+}$  signals, and shows that cells can tolerate the stress caused by MI without disruption of the tightly regulated cellular  $\text{Ca}^{2+}$  handling. This provided a robust foundation for studying the effects of I-Domain proteins on  $\text{Ca}^{2+}$  handling in functionally- and electrically-coupled HL-1 myocytes and this will be considered in more detail in Chapters 5 and 6.

### 4.4.2 MI affects some aspects of $\text{Ca}^{2+}$ handling in WT HL-1 myocytes

Like gene expression, synchronicity in contractile HL-1 myocytes is entirely dependent on co-ordinated  $\text{Ca}^{2+}$  fluxes. As discussed above, MI did not alter overall cellular  $\text{Ca}^{2+}$  signalling over a 48 hour period. In a shorter time frame, MI of RRL into HL-1 cells under the optimised conditions did not alter the synchronicity of the monolayer five minutes after injection, indicating that the regulation of  $\text{Ca}^{2+}$  fluxes was not sufficiently disrupted by MI to result in asynchrony. In addition, MI did not alter  $\text{Ca}^{2+}$  transient amplitude, length, and area. It did, however, have some effect on the inter-transient noise and transient rate. The increased 'inter-transient noise' which is a measurement of sub-threshold homeostatic  $\text{Ca}^{2+}$  fluctuations, that are distinct from the readily observed  $\text{Ca}^{2+}$  'transients' (see Figure 4.8) was complemented by reduced frequency of  $\text{Ca}^{2+}$  transient oscillations. Whether the decrease in transient rate results in increased inter-transient noise, or vice versa remains to be determined. Interestingly, the increase in the ratio of total:inter-transient noise, along with

the increase in inter-transient noise, suggest that there may be an increase in  $\text{Ca}^{2+}$  fluctuations within the transients themselves. This has also been observed in ongoing studies in our laboratory, though the underlying mechanism has not yet been established. These subtle changes in  $\text{Ca}^{2+}$  handling can only be detected using sophisticated approaches such as SALVO. Less detailed analyses would not distinguish such subtleties, which are well tolerated by the cell and result in no change to the synchronicity of the cell monolayer.

#### **4.4.3 *ID<sup>B</sup> does not affect synchronicity in resting HL-1 myocytes***

The data presented in this chapter emphasise that it is vital to have appropriate controls in order to unequivocally determine the effects of recombinant I-Domain proteins on cell function and phenotype. The findings above clearly show why all data derived from cells injected with I-Domain fragments must be compared with experiments in which the cells were microinjected with “naïve” RRL.

Injection of  $\text{ID}^{\text{B}}$  appeared to have little effect in synchronous resting HL-1 cells and although subtle changes in some  $\text{Ca}^{2+}$  handling parameters, they did not manifest as alterations in synchronicity. Despite the small changes in noise and rate of  $\text{Ca}^{2+}$  release, which may imply some interaction with SERCA, the transient characteristics and synchronicity remained unchanged compared with the control cells. However,  $\text{ID}^{\text{B}}$  may have a more pronounced effect in HL-1 cells in an arrhythmic state, and this will be discussed in the next chapter.

## **Chapter 5**

# ***Investigating the effect of ID<sup>B</sup> in dyssynchronous cardiomyocytes***

## 5.1 Introduction

### 5.1.1 Cardiac glycosides

Cardiac glycosides are a class of plant-derived and animal-derived steroids used clinically to increase contractile force in patients with cardiac disorders (Hauptman *et al.* 1999a; McConkey *et al.* 2000). Their main effect is to inhibit the ubiquitous cell surface enzyme  $\text{Na}^+/\text{K}^+$ -ATPase, which transports  $\text{Na}^+$  ions out of cells and  $\text{K}^+$  ions into cells, thus maintaining the ion gradients between intracellular and extracellular compartments necessary for normal cell function. This results in increased intracellular  $\text{Na}^+$  and  $\text{Ca}^{2+}$ , and decreased intracellular  $\text{K}^+$ . The increased intracellular  $\text{Ca}^{2+}$  promotes muscle contraction and cardiac contractile force (i.e. a positive inotropic effect).  $\text{Na}^+/\text{K}^+$ -ATPase has two subunits, alpha and beta, with the extracellular domain of the alpha subunit containing a stereospecific-binding site for the cardiac glycosides and related steroids (Buckalew 2005).

Cardiac glycosides can be divided into subgroups including cardenolides, compounds identified originally in plants, and bufadienolides, identified in toad venom; both of which have also been found endogenously in humans (Nesher *et al.* 2007). They share a common general structure - a steroid nucleus with a lactone ring at C-17 and a hydroxyl group at C-14 (Figure 5.1). The 5- and 6-membered lactone rings, in cardenolides and bufadienolides, respectively, are considered the most essential functional group of these substances.

The most widely studied cardenolides are digoxin and ouabain, which are derived from the plant genera *Digitalis* and *Strophanthus* respectively, and have also been purified from human plasma and the hypothalamus, and identified by mass spectroscopy (Goto *et al.* 1990; Hamlyn *et al.* 1991; Mathews *et al.* 1991; Qazzaz *et al.* 2004).

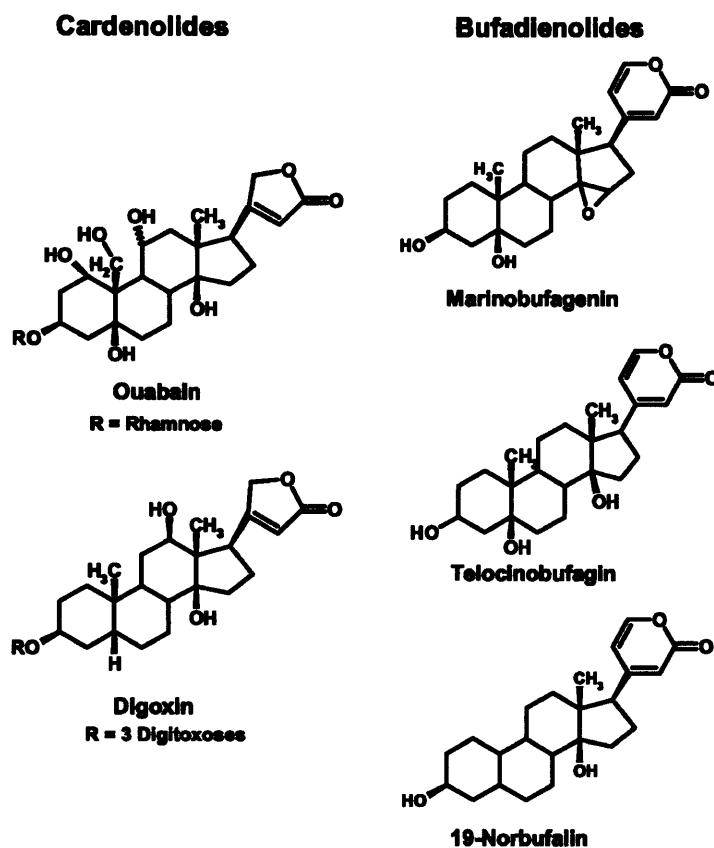


**Figure 5.1. Structures of endogenous cardiac glycosides belonging to the cardenolide and bufadienolide groups.**

Taken from Schoner & Scheiner-Bobis (2007)

### 5.1.1.1 Digoxin

The steroid glycoside digoxin was first isolated from *Digitalis lanata* in 1930, and since then this compound and other similar derivatives have been developed into drugs which are still used to treat HF and atrial fibrillation. The effects of digoxin have been widely studied, and it has a well characterised effect on RyR2. Digoxin is known to increase cardiomyocyte cytosolic  $[Ca^{2+}]$  via its inhibitory action on the  $Na^+/K^+$ -ATPase (Reuter *et al.* 2002), whereby the resulting  $[Na^+]$  increase is removed from the cell by the NCX, resulting in an inward  $Ca^{2+}$  flux. However, digoxin also directly activates RyR2, and therefore its inotropic effect may also reflect its direct effect on RyR2 (McGarry & Williams 1993; Sagawa *et al.* 2002).

### 5.1.1.2 Ouabain

Ouabain is a cardiac glycoside chemically related to the digitalis compound found in foxgloves (Figure 5.1). It has been identified in mammalian tissues and, like other steroids, is synthesised in the adrenal glands, as well as locally produced in other tissues such as the hypothalamus (Kawamura *et al.* 1999, 2001; Schoner 2000, 2001). In humans, ouabain concentrations increase rapidly in blood during physical exercise and decline quickly after rest. About half of people of European descent with hypertension have abnormally high levels of ouabain, as do patients with congestive HF (Arnon *et al.* 2000; Schoner 2001).

Until recently, it was not known how ouabain directly affects heart function at a cellular level. Recent studies by Aizman *et al.* (2001) revealed a new pathway of ouabain signalling through receptors on the plasma membrane, which induce slow oscillations of intracellular  $Ca^{2+}$  levels and thereby activate the transcription factor NF- $\kappa$ B, a key regulator of cell activity. Aizman *et al.* showed that, at low concentrations which only partially inhibit  $Na^+/K^+$ -ATPase, ouabain acts as a hormone and a signal transducer and activator for NF- $\kappa$ B. Slow  $Ca^{2+}$  oscillations are produced through the interactions of other proteins located on the plasma membrane, including store-operated  $Ca^{2+}$  channels (SOCCs) and L-type voltage-gated  $Ca^{2+}$  channels, and  $IP_3$  receptors on the ER/SR. This leads to the translocation of NF- $\kappa$ B into the nucleus where it regulates several genes involved in cardiac physiology.

### 5.1.2 Mechanisms underlying cardiac arrhythmias

Cardiac arrhythmias result from aberrant impulse initiation or impulse conduction or a combination of both. Abnormal impulse initiation is generally believed to originate from either automaticity or triggered activity (Wit & Rosen 1983). Automaticity refers to the ability of myocardial cells to initiate spontaneous depolarisation during the diastolic interval; however it is triggered activity which is thought to be most closely linked to  $Ca^{2+}$ -mediated arrhythmogenesis. Studies using three-dimensional mapping suggest that most VT in non-ischaemic HF is initiated by such mechanisms (Janse 2004; Pogwizd *et al.* 1998, 2004).

Triggered activity is so-called because, unlike the spontaneous depolarisations of automaticity, the impulse can only occur if it follows a previous AP i.e. it is triggered by the previous impulse. Triggered impulses are caused by sub-threshold membrane depolarisations, termed afterdepolarisations. These are second depolarisations that occur either during repolarisation of the previous AP (EADs) or after repolarisation is complete (DADs) as shown in Figure 5.2 (Scoote & Williams 2002).

DADs result from a transient inward current evoked by spontaneous  $\text{Ca}^{2+}$  release from the SR under conditions that favour accumulation of cellular  $\text{Ca}^{2+}$ . If this inward current is sufficient to cause a DAD with an amplitude exceeding the threshold potential, depolarisation will occur. The abnormal impulse generated from this can cause a triggered arrhythmia if surrounding polarised cells propagate the wave, and this is believed to be the underlying cause of bi-directional ventricular tachycardia (VT) (Wit & Rosen 1983; Scoote & Williams 2002). Several factors can increase the amplitude of DADs, and therefore increasing the probability of triggered arrhythmias, including an increase in the rate of the triggering action due to an increased heart rate, and an increase in intracellular  $\text{Ca}^{2+}$  load.

Arrhythmias associated with RyR2-linked channelopathies such as CPVT (see Chapter 1) take the form of bi-directional and/or polymorphic VT, both of which are capable of degenerating into ventricular fibrillation and SCD (Leenhardt *et al.* 1995a; Priori *et al.* 2001, 2002). Bi-directional VT is a rare type of arrhythmia, normally associated with intracellular  $\text{Ca}^{2+}$  overload caused by digoxin toxicity (Ma *et al.* 2001).



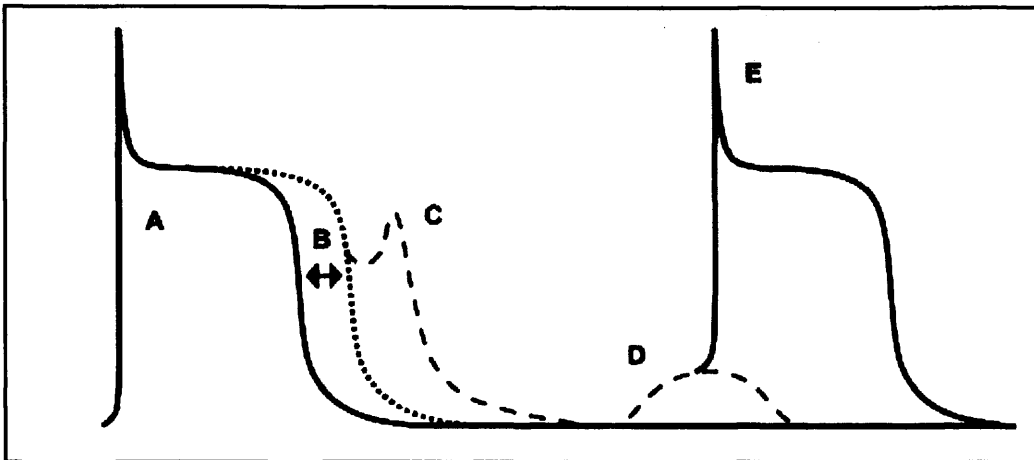


**Figure 5.2. Schematic representation of early and delayed afterdepolarisations with respect to the normal cardiac action potential.**

A normal AP: (A) may be extended in duration (B) such that an EAD is generated (C) during the repolarisation phase. Dispersion of depolarisation time throughout ventricle promotes re-entrant arrhythmia generation. A DAD (D) only occurs after a normal AP (A) is completed and the cell has returned to the resting membrane potential. If the DAD is of sufficient magnitude to reach a depolarising threshold a new AP (E) can occur which itself can initiate a triggered arrhythmia. Taken from Scoote & Williams (2002).

### 5.1.3 Cardiac glycosides in arrhythmia

The mechanism by which cardiac glycosides, such as digoxin and ouabain, cause arrhythmia is known to be via  $\text{Ca}^{2+}$  overload and DAD generation within cardiomyocytes (Hauptman & Kelly 1999b; Rosen & Danilo 1980). This is supported by evidence from isoproterenol induction of arrhythmia in CPVT that DADs occur as a result of this stimulus and lead to the generation of bi-directional VT (Nakajima *et al.* 1997). Cardiac glycosides increase intracellular  $[\text{Ca}^{2+}]$ , and thereby create conditions which favour DAD generation. They inhibit the  $\text{Na}^+/\text{K}^+$  ATPase pump, causing excess cytosolic  $\text{Na}^+$  to be removed by sarcolemmal NCX in exchange for inward bursts of  $\text{Ca}^{2+}$ . CPVT-linked mutations in RyR2 are also associated with bi-directional VT, and this raises the possibility that the mechanism whereby glycosides bring about this arrhythmia is also linked to a direct action on RyR2 (Scoote & Williams 2002). Studies have shown that cardiac glycosides do indeed have a direct action on RyR2 (McGarry & Williams 1993; Sagawa *et al.* 2002), and lead to an increase in channel open probability. It is possible that the bi-directional VT is a

manifestation of DADs, brought about by an increased diastolic release of  $\text{Ca}^{2+}$ , which itself is an indicator of abnormal RyR2 function.

#### **5.1.4 Objectives of this chapter**

The effect of ouabain on HL-1 myocytes has been studied previously in our laboratory (Barberini-Jammaers *et al.* 2008), and has been found to be a robust 'arrhythmogen' perturbing both  $\text{Ca}^{2+}$  handling and synchronous contractility. In this chapter, normal synchronous beating of HL-1 myocytes was disrupted using ouabain and the effects of ID<sup>B</sup> on ouabain-induced  $\text{Ca}^{2+}$  handling dysfunction and dyssynchrony was determined.

#### **5.1.5 Specific Hypothesis**

Following on from the work presented in the previous chapter, where ID<sup>B</sup> was successfully delivered into HL-1 myocytes by microinjection, this chapter now specifically addresses the functional impact of recombinant ID<sup>B</sup> on the  $\text{Ca}^{2+}$  handling phenotype of ouabain-treated HL-1 cardiomyocytes.

## 5.2 Methods

The effect of ID<sup>B</sup> on ouabain-induced intercellular dyssynchrony was investigated by two distinct approaches. The first strategy analysed the effects on ID<sup>B</sup> on cells which had been treated with ouabain prior to MI, and therefore had perturbed intracellular Ca<sup>2+</sup> cycling and reduced intercellular synchrony. The second strategy looked at the effects of ID<sup>B</sup> MI prior to ouabain treatment of the cells.

### 5.2.1 MI of cells before and after incubation in ouabain

Cells were prepared for MI as described in section 4.2.1, before loading with Fluo-4AM (10  $\mu$ M in 20% w/v pluronic acid F-12 / DMSO) in non-supplemented Claycomb media pre-warmed to 37°C. The dye-containing solution was added to each chamber as a 200 $\mu$ l meniscus and incubated for 60 minutes (37°C, 5% CO<sub>2</sub>, ~80% humidity).

For cells incubated in ouabain prior to MI, the cells were then immersed in a further 1800 $\mu$ l pre-warmed non-supplemented media containing 100 nM ouabain 40 mins prior to Ca<sup>2+</sup> imaging, as summarised in Figure 5.3. The cells were imaged for 1 minute (300 frames) as described in section 4.2.1 prior to MI in order to obtain a measurement of basal fluorescence levels.

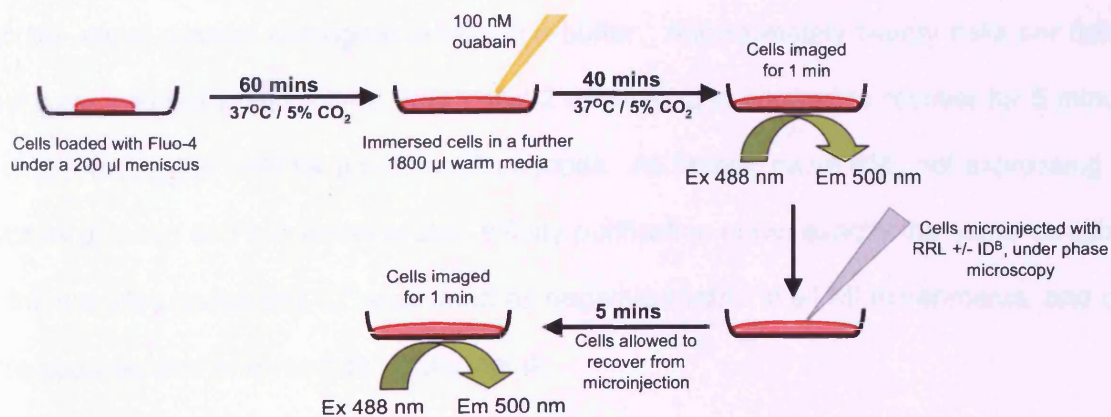


**Figure 5.3. MI of HL-1 myocytes after incubation in ouabain**

For experiments where the cells were microinjected before incubation in 100 nM ouabain, the MagZ purified protein (Chapter 3) was co-injected with the Alexa-dextran conjugate in injection buffer. Twenty cells per field of view were injected within a time frame of < 2 minutes, and allowed to recover for 5 minutes before the addition of 100 nM ouabain. The injected cells were incubated in the ouabain-containing media for 40 mins, and were subsequently imaged for 60 seconds, as shown in Figure 5.4

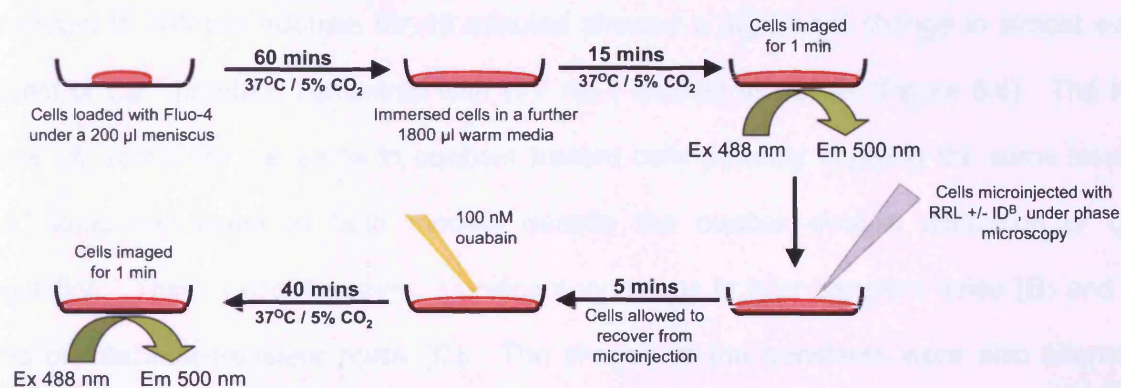


**Figure 5.4. MI of HL-1 myocytes prior to incubation in ouabain**

As in previous experiments, MagZ-enriched ID<sup>B</sup> protein (Chapter 3) was injected into superconfluent, spontaneously oscillating ( $0.74 \pm 0.01$  Hz) HL-1 cells using the optimal conditions determined in Chapter 4. The MagZ purified protein (Chapter 3) was co-injected with the Alexa-dextran conjugate in injection buffer. Approximately twenty cells per field of view were injected within a time frame of < 2 minutes, and allowed to recover for 5 minutes prior to imaging the cells for a further 60 seconds. As before, naïve RRL not expressing any I-Domain protein and subjected to zinc-affinity purification under exactly the same conditions as the samples containing ID<sup>B</sup> was used as negative control in all MI experiments, and data were acquired and analysed as in Chapter 4.

## 5.3 Results

### 5.3.1 Effect of ouabain on beating HL-1 myocytes

The concentration of ouabain used here (100 nM) was determined previously as robustly ablating intercellular  $\text{Ca}^{2+}$  synchrony in cardiac myocytes (George, unpublished). The extent of ouabain-induced disruption is so great, that it was noticeable by eye during confocal microscopy. SALVO analysis of spatio-temporal  $\text{Ca}^{2+}$  handling parameters in HL-1 cells subjected to 100 nM ouabain for 40 minutes showed a significant change in almost every aspect of  $\text{Ca}^{2+}$  handling compared with WT HL-1 cardiac myocytes (Figure 5.6). The total noise (**A**) remained the same in ouabain treated cells possibly implying the same level of  $\text{Ca}^{2+}$  ionic movement in both models despite the ouabain-evoked disruption of  $\text{Ca}^{2+}$  regulation. There were, however, significant increases in inter-transient noise (**B**) and the ratio of total:inter-transient noise (**C**). The shapes of the transients were also altered in ouabain-treated cells (Figure 5.5), displaying significantly increased amplitude, length and area (**D**, **E** and **F** respectively). Ouabain also affected the kinetics of  $\text{Ca}^{2+}$  release and sequestration, manifested as significantly increased rate up (**G**) and length to decay of transients (**H**), as well as a strikingly decreased transient rate (**I**). Together, the changes in these parameters have a marked affect on the synchronicity of the HL-1 monolayer, leading to a significant decrease in the percentage synchronicity observed (Figure 5.7), validating this as a model of  $\text{Ca}^{2+}$ -induced dyssynchrony in coupled HL-1 cell monolayers.

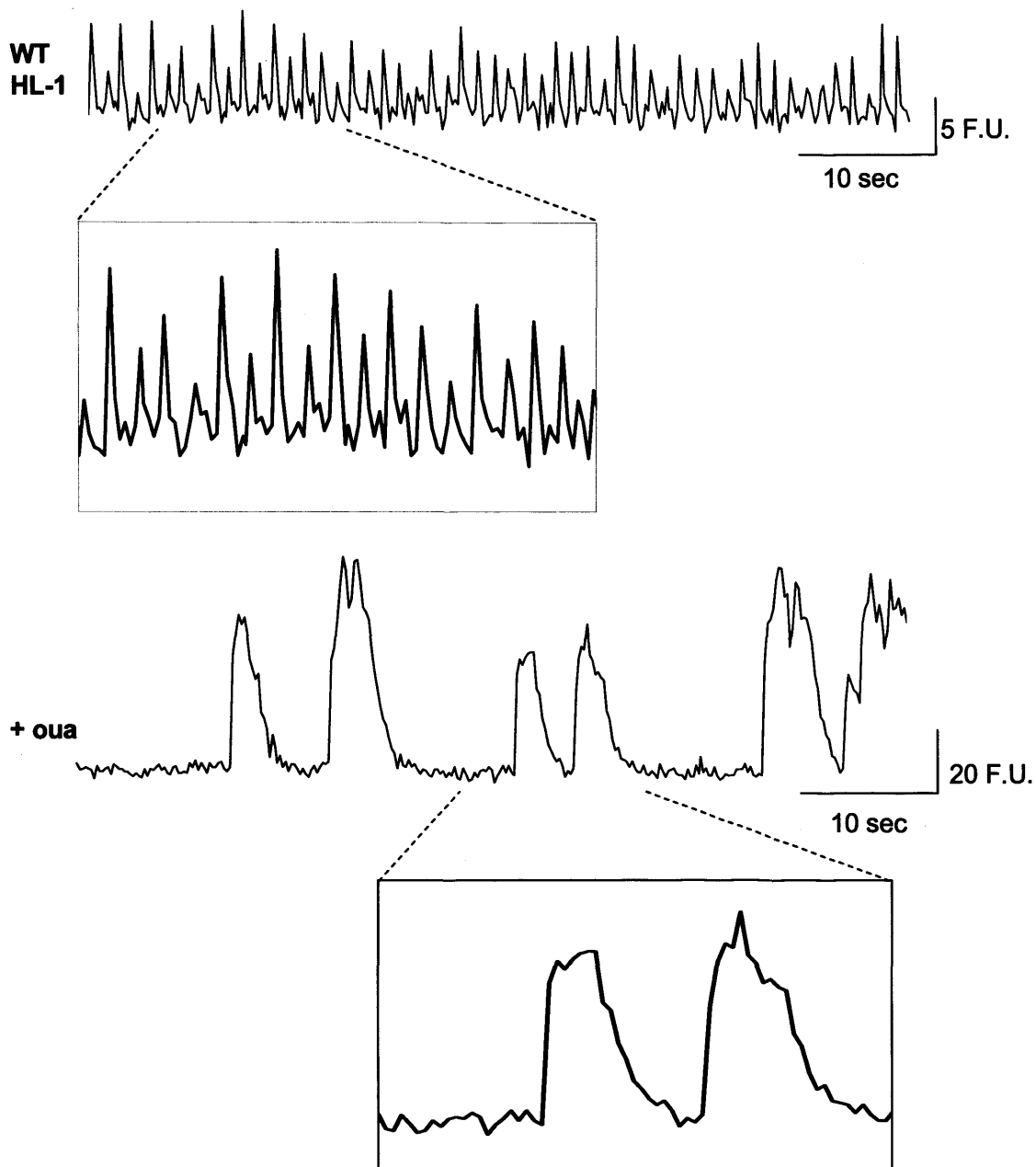


**Figure 5.5. Representative traces of WT and ouabain treated HL-1 myocytes**

These traces illustrate the differences in  $\text{Ca}^{2+}$  observed in WT HL-1 cells, and HL-1 cells treated with ouabain. The ouabain-treated cells exhibit large slow  $\text{Ca}^{2+}$  oscillations, with a profound loss of synchrony compared with the synchronously coupled WT-HL-1 cells. F.U. denotes arbitrary fluorescence units measured in defined regions of interest.

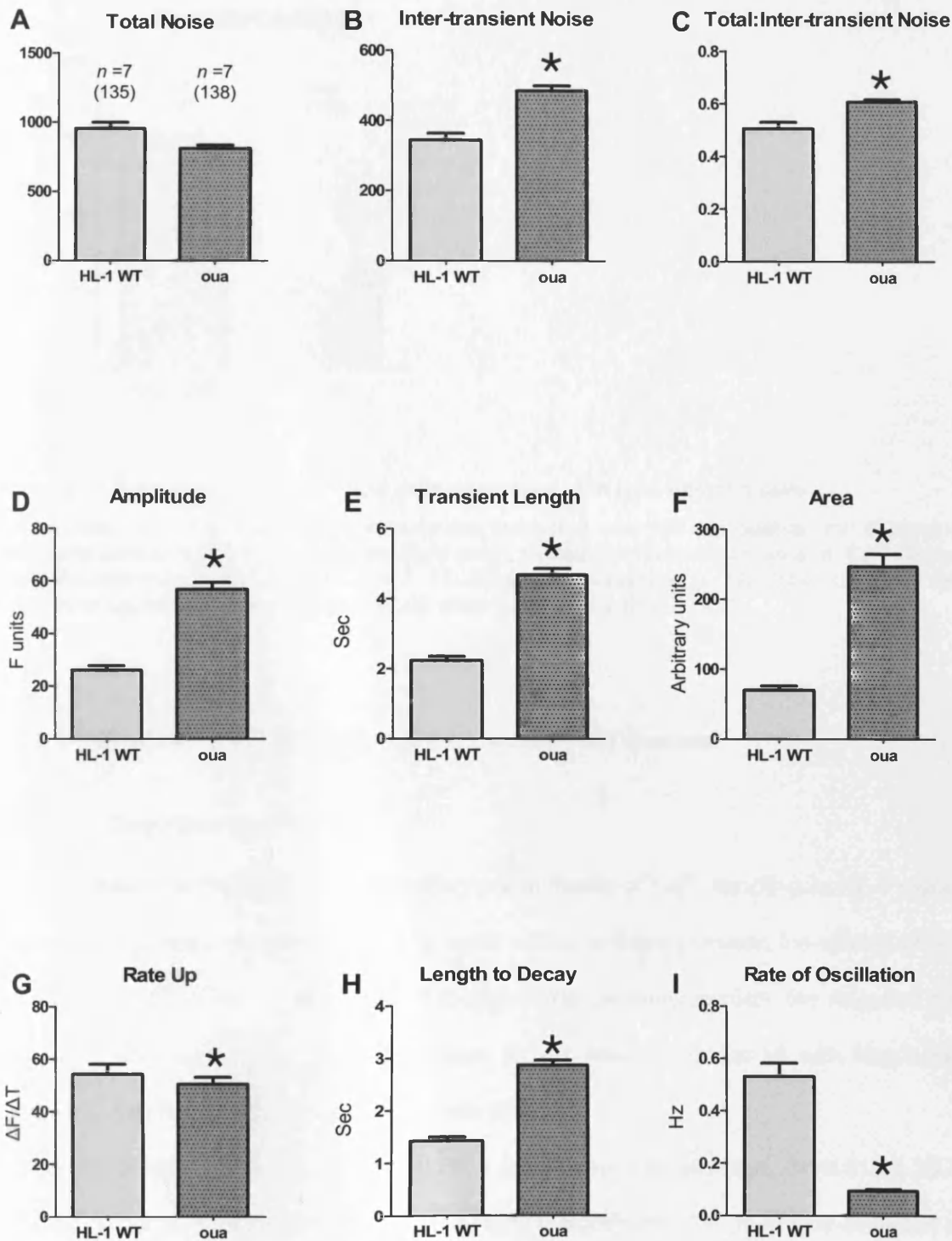


**Figure 5.6. SALVO analysis of the effects of ouabain on HL-1 myocyte monolayers**

Spatio-temporal  $\text{Ca}^{2+}$  handling parameters in HL-1 myocytes incubated with 100 nM ouabain for 40 mins (dark grey) compared with WT HL-1 myocytes (light grey), plotted from SALVO analysis of  $\text{Ca}^{2+}$ -dependent Fluo-4 fluorescence (mean  $\pm$  SEM,  $n = 7$ , 15-20 cells per experiment. The total number of cells is indicated in brackets). \* represents  $p < 0.05$  when compared with WT HL-1.

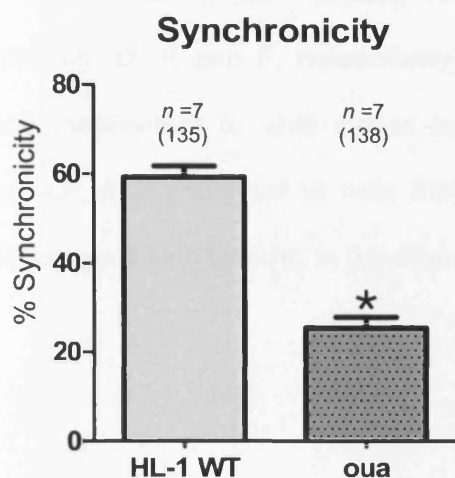


**Figure 5.7. Synchronicity in WT HL-1 cells compared with RRL injected cells**

Synchronicity within HL-1 myocytes monolayers incubated with 100 nM ouabain for 40 mins (dark grey) compared with WT HL-1 myocytes (light grey), plotted from SALVO analysis of  $\text{Ca}^{2+}$ -dependent Fluo-4 fluorescence (mean  $\pm$  SEM,  $n = 7$ , 15-20 cells per experiment. The total number of cells is indicated in brackets). \* represents  $p < 0.05$  when compared with WT HL-1.

### 5.3.2 MI of HL-1 cells following pre-treatment with ouabain

#### 5.3.2.1 Control experiments

As discussed in Chapter 4, MI did affect some facets of  $\text{Ca}^{2+}$  handling in HL-1 myocytes and suitable controls must be in place in order to discriminate between the effects of MI and the effects of  $\text{ID}^{\text{B}}$  in HL-1 myocytes. Throughout the following section, the negative control was HL-1 cells treated with 100 nM ouabain for 40 minutes prior to MI with MagZ-purified naïve RRL (i.e. RRL expressing no I-Domain protein).

Injection of RRL into ouabain-treated HL-1 cells caused an increase, from  $813 \pm 25.48$  to  $1374.4 \pm 67.33$ , in total noise (Figure 5.8, **A**) but no significant change in inter-transient noise (**B**) or the ratio of total:inter-transient noise (**C**) when compared with WT HL-1 cells treated with ouabain. The size of the transients in ouabain-treated HL-1 myocytes was approximately 50% smaller than in WT HL-1 cells, with a decreased amplitude, length and area (**D**, **E**, and **F** respectively). Furthermore, there was a decrease in the length to decay (**H**) and an increased transient rate (**I**).



For some of the  $\text{Ca}^{2+}$ -handling parameters, such as amplitude, length and area of the transients (**D**, **E** and **F**, respectively), injection of RRL into ouabain-treated cells caused these parameters to shift closer to the values observed in untreated WT HL-1 cells. However, it is important to note that despite these changes, there was no restoration of cellular synchrony by RRL in the ouabain-treated HL-1 monolayer (Figure 5.9).

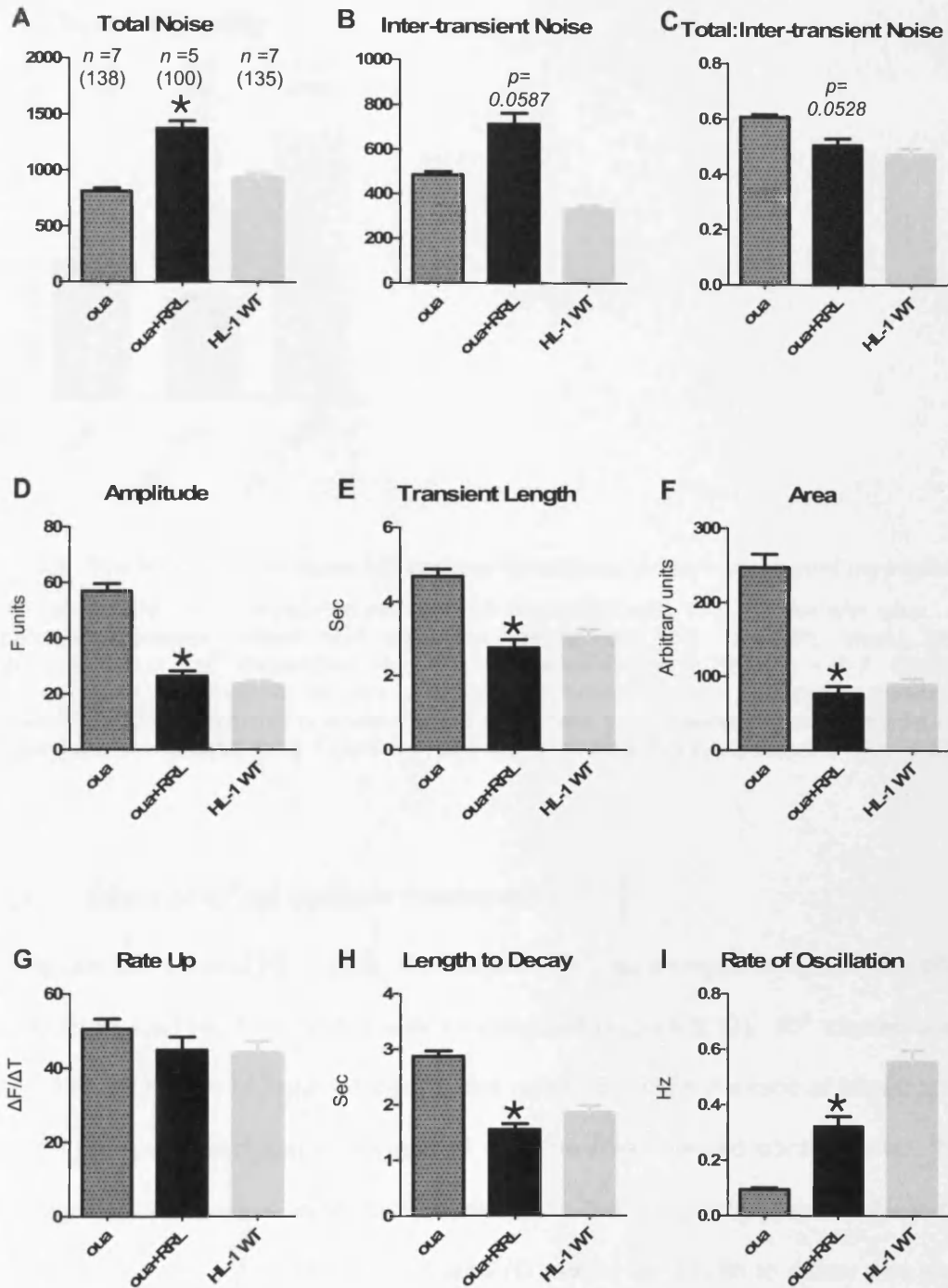


**Figure 5.8. SALVO analysis of the effects of MI on HL-1 myocyte monolayers pre-treated with 100 nM ouabain**

Spatio-temporal  $Ca^{2+}$  handling parameters in non-injected HL-1 myocytes incubated with 100 nM ouabain (oua, dark grey) compared with ouabain-treated HL-1 myocytes injected with RRL (oua+RRL, black), plotted from SALVO analysis of  $Ca^{2+}$ -dependent Fluo-4 fluorescence (mean  $\pm$  SEM, n = 5-7, 15-20 cells per experiment). The total number of cells is indicated in brackets). \* represents  $p < 0.05$  when compared with ouabain-treated HL-1 myocytes. Illustrative values for HL-1 WT cells (light grey) are from Figure 5.6, and were not included in statistical analyses with injected cells.

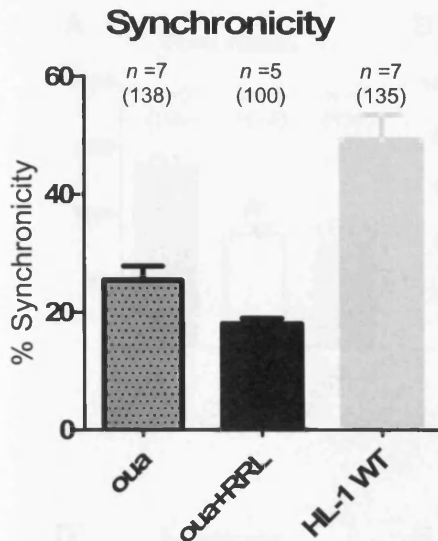


**Figure 5.9. The MI technique does not restore synchrony in ouabain-treated myocytes**

Synchronicity within HL-1 myocytes monolayers incubated with 100 nM ouabain (oua, dark grey) compared with ouabain-treated HL-1 myocytes injected with RRL (oua+RRL, black), plotted from SALVO analysis of  $\text{Ca}^{2+}$ -dependent Fluo-4 fluorescence (mean  $\pm$  SEM,  $n = 5-7$ , 15-20 cells per experiment. The total number of cells is indicated in brackets). No significant difference between RRL-injected and non-injected ouabain-treated HL-1 cells was observed. Values for HL-1 WT cells (light grey) shown here are from Figure 5.7, and were not included in statistical analyses with injected cells.

### 5.3.2.2 Effect of $\text{ID}^{\text{B}}$ on ouabain treated cells

Using ouabain-treated HL-1 cells injected with RRL as a negative control, the effect of  $\text{ID}^{\text{B}}$  on ouabain-treated HL-1 myocytes was investigated (Figure 5.10).  $\text{ID}^{\text{B}}$  caused a significant decrease in total noise (**A**) and inter-transient noise (**B**), while the ratio of total:inter-transient noise (**C**) remained unchanged compared with the RRL-injected control cells. There was also a significant decrease in the amplitude (**D**) of the transients in cells injected with  $\text{ID}^{\text{B}}$ . The rate up was also significantly decreased (**G**), while the length to decay was significantly higher (**H**) and the rate of the transients remained unchanged (**I**). Most strikingly,  $\text{ID}^{\text{B}}$  partially restored the synchrony in the ouabain-treated monolayer, which increased significantly to  $34.6\% \pm 2.4$  in  $\text{ID}^{\text{B}}$ -injected cells from  $18.1\% \pm 0.94$  in the RRL-injected control cells (Figure 5.11). Furthermore, as shown above, synchrony in WT HL-1 cells was  $49.4\% \pm 4.19$  and is comparable to the level of synchrony in ouabain-treated cells injected with  $\text{ID}^{\text{B}}$ .

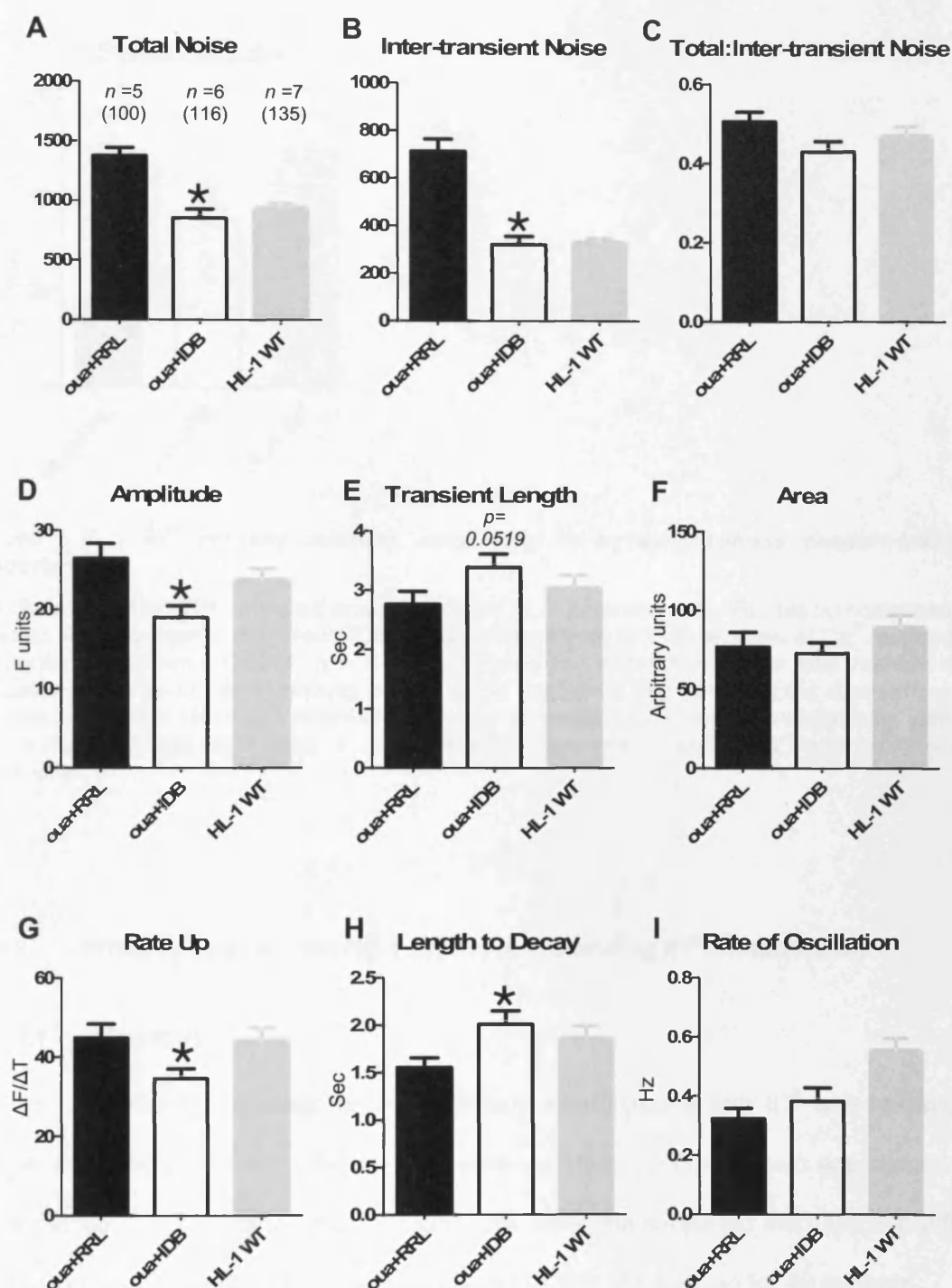


**Figure 5.10. SALVO analysis of the effects of ID<sup>B</sup> on HL-1 myocyte monolayers pre-treated with 100 nM ouabain**

Spatio-temporal Ca<sup>2+</sup> handling parameters in RRL-injected ouabain-treated HL-1 controls (oua<sup>+</sup>RRL, black) compared with ID<sup>B</sup>-injected ouabain-treated HL-1 (oua<sup>+</sup>IDB, white), plotted from SALVO analysis of Ca<sup>2+</sup>-dependent Fluo-4 fluorescence (mean  $\pm$  SEM, n = 5-7, 15-20 cells per experiment. The total number of cells is indicated in brackets). \* represents p < 0.05 when compared with RRL-injected ouabain-treated HL-1 controls. Values for HL-1 WT cells (light grey) shown here are from Figure 5.6, and were not included in statistical analyses with injected cells.

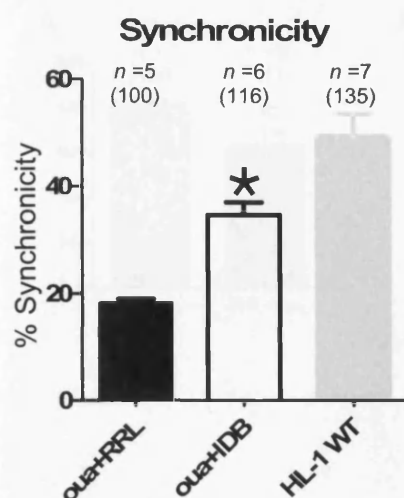


**Figure 5.11.** ID<sup>B</sup> partially restores synchrony in dyssynchronous ouabain-treated HL-1 myocytes.

Synchronicity within RRL-injected ouabain-treated HL-1 controls (oua<sup>+</sup>RRL, black) compared with ID<sup>B</sup>-injected ouabain-treated HL-1 (oua<sup>+</sup>IDB, white), plotted from SALVO analysis of Ca<sup>2+</sup>-dependent Fluo-4 fluorescence (mean  $\pm$  SEM, n = 5-7, 15-20 cells per experiment. The total number of cells is indicated in brackets). \* represents p<0.05 when compared with RRL-injected ouabain-treated HL-1 controls. Although MI of ID<sup>B</sup> restored synchrony to levels which were not statistically different from that in HL-1 WT cells (light grey), a direct statistical comparison between WT and microinjected cells is not valid.

### 5.3.3 Effect of ouabain on HL-1 myocytes following ID<sup>B</sup> transduction

#### 5.3.3.1 Controls

Next, the effect of ouabain on cells already microinjected with ID<sup>B</sup> was investigated, to see whether the stabilising effects seen were maintained. Once again appropriate controls were set up. In this case, the controls cells were microinjected with MagZ-purified RRL containing no I-Domain protein, then subjected to 100 nM ouabain for 40 minutes.

When compared with ouabain-treated WT HL-1 cells, there was a significant difference in all the parameters analysed (Figure 5.12) in cells microinjected with RRL prior to the addition of ouabain. However, once again despite all of these changes, the synchrony within the monolayer remained virtually identical and RRL had no corrective effect on cellular dyssynchrony (Figure 5.13).

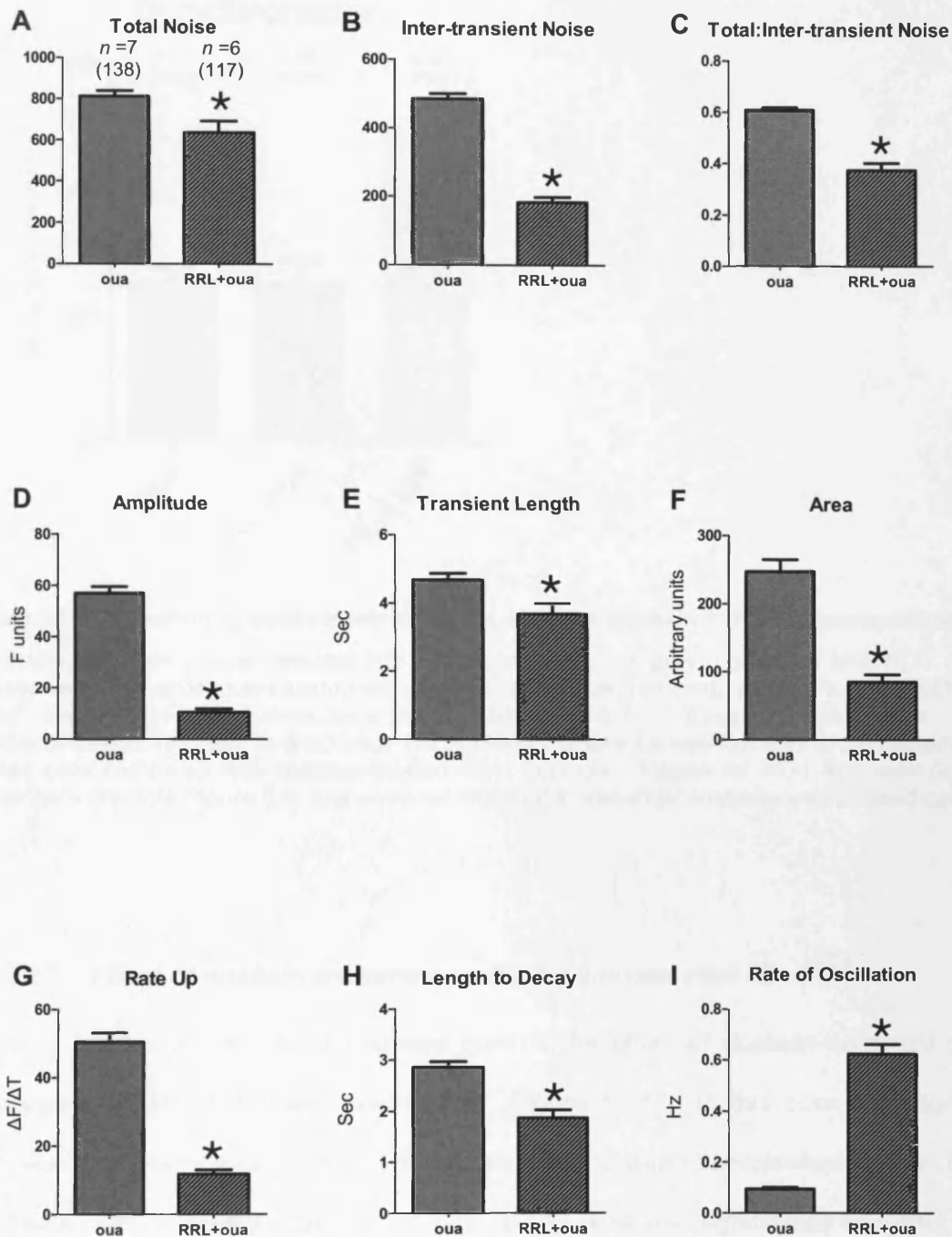


**Figure 5.12. SALVO analysis of the effects of MI on HL-1 myocyte monolayers prior to incubation with 100 nM ouabain**

Spatio-temporal  $\text{Ca}^{2+}$  handling parameters in ouabain-treated HL-1 controls (oua, dark grey) compared with HL-1 myocytes injected with RRL prior to incubation with ouabain (RRL+oua, hatched), plotted from SALVO analysis of  $\text{Ca}^{2+}$ -dependent Fluo-4 fluorescence (mean  $\pm$  SEM,  $n = 6-7$ , 15-20 cells per experiment). \* represents  $p < 0.05$  when compared with ouabain-treated HL-1 controls.

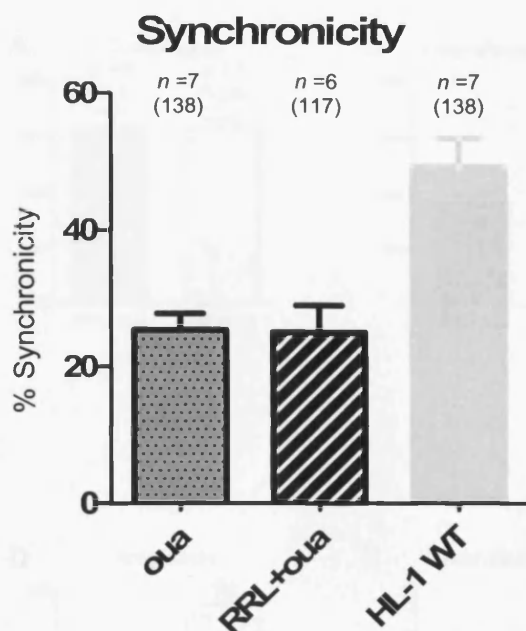


**Figure 5.13. MI before ouabain-treatment does not alter ouabain-induced dyssynchrony**

Synchronicity within ouabain-treated HL-1 controls (oua, dark grey) compared with HL-1 myocytes injected with RRL prior to incubation with ouabain (RRL<sup>+</sup>oua, hatched), plotted from SALVO analysis of Ca<sup>2+</sup>-dependent Fluo-4 fluorescence (mean  $\pm$  SEM, n = 6-7, 15-20 cells per experiment. The total number of cells is indicated in brackets). No significant difference was found in RRL-injected ouabain-treated cells compared with ouabain-treated HL-1 controls. Values for HL-1 WT cells (light grey) shown here are from Figure 5.6, and were not included in statistical analyses with injected cells.

### 5.3.3.2 Effect of ouabain-treatment on HL-1 myocytes after MI of ID<sup>B</sup>

Using the above cells as a negative control, the effect of ouabain-treatment on HL-1 myocytes after MI of ID<sup>B</sup> was investigated (Figure 5.14). In this case, ID<sup>B</sup> significantly increased the inter-transient noise (**B**) and the ratio of total:inter-transient noise (**C**). The amplitude of the transients (**D**) and the rate up (**G**) were also significantly increased in cells containing ID<sup>B</sup>, while the rate of transients (**I**) was significantly slower. The transient length (**E**), area (**F**) and length to decay (**H**) remained unchanged. Under these conditions, ID<sup>B</sup> did not restore synchrony in the cell monolayer (Figure 5.15).

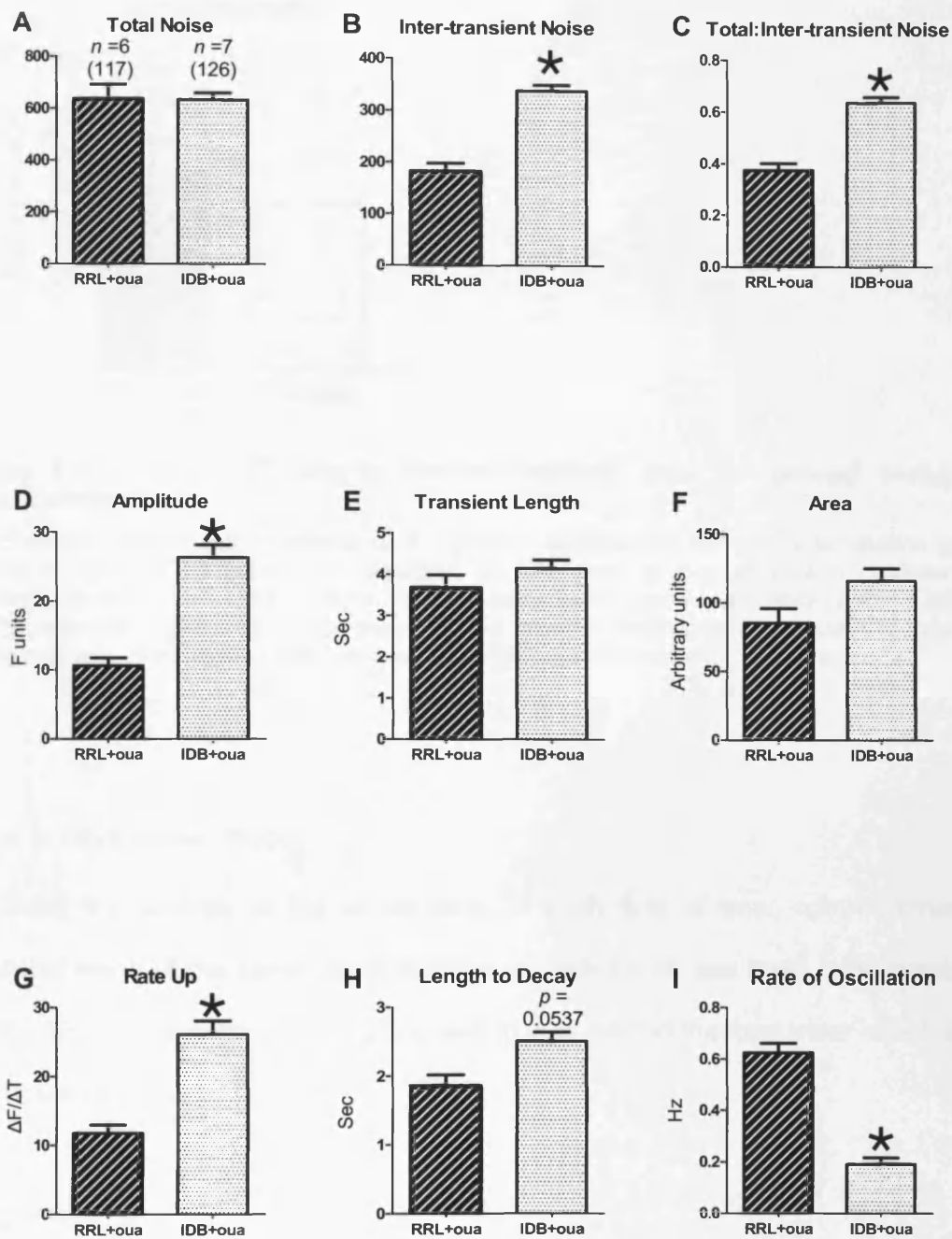


**Figure 5.14. SALVO analysis HL-1 myocytes treated with ouabain after MI with ID<sup>B</sup>**

Spatio-temporal Ca<sup>2+</sup> handling parameters in HL-1 myocytes injected with ID<sup>B</sup> prior to incubation with ouabain (ID<sup>B</sup>+oua, spotted) compared with injection of RRL prior to incubation with ouabain (RRL+oua, hatched), plotted from SALVO analysis of Ca<sup>2+</sup>-dependent Fluo-4 fluorescence (mean  $\pm$  SEM, n = 6-7, 15-20 cells per experiment). \* represents p<0.05 when compared with RRL-injected ouabain-treated HL-1 controls.



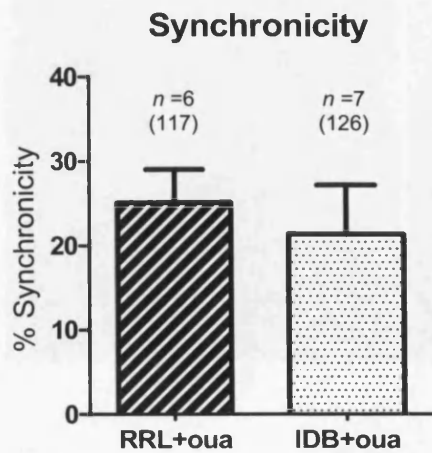


**Figure 5.15. MI of ID<sup>B</sup> prior to ouabain-treatment does not prevent ouabain-induced dyssynchrony**

Synchronicity within ouabain-treated HL-1 myocytes injected with ID<sup>B</sup> prior to incubation with ouabain (IDB<sup>+</sup>oua, spotted) compared with injection of RRL prior to incubation with ouabain (RRL<sup>+</sup>oua, hatched), plotted from SALVO analysis of Ca<sup>2+</sup>-dependent Fluo-4 fluorescence (mean ± SEM, n = 6-7, 15-20 cells per experiment). The total number of cells is indicated in brackets). No significant difference was found between ID<sup>B</sup>-injected and RRL-injected ouabain-treated cells.

#### 5.3.4 Bystander effect

During the analysis of the above data, in each field of view, non-microinjected cells exhibited some of the same characteristics as cells which had been microinjected (Figure 5.16). This unexpected and intriguing finding was termed the 'bystander effect' and will be discussed below.

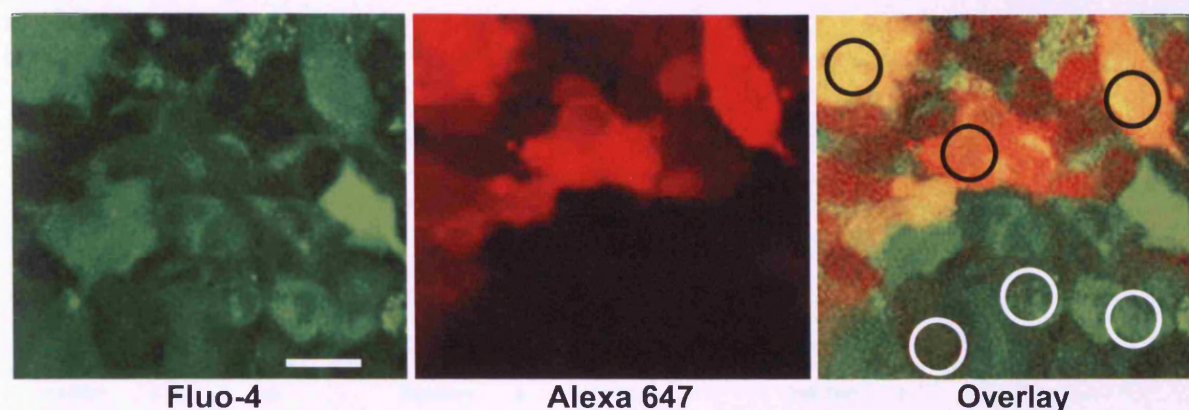
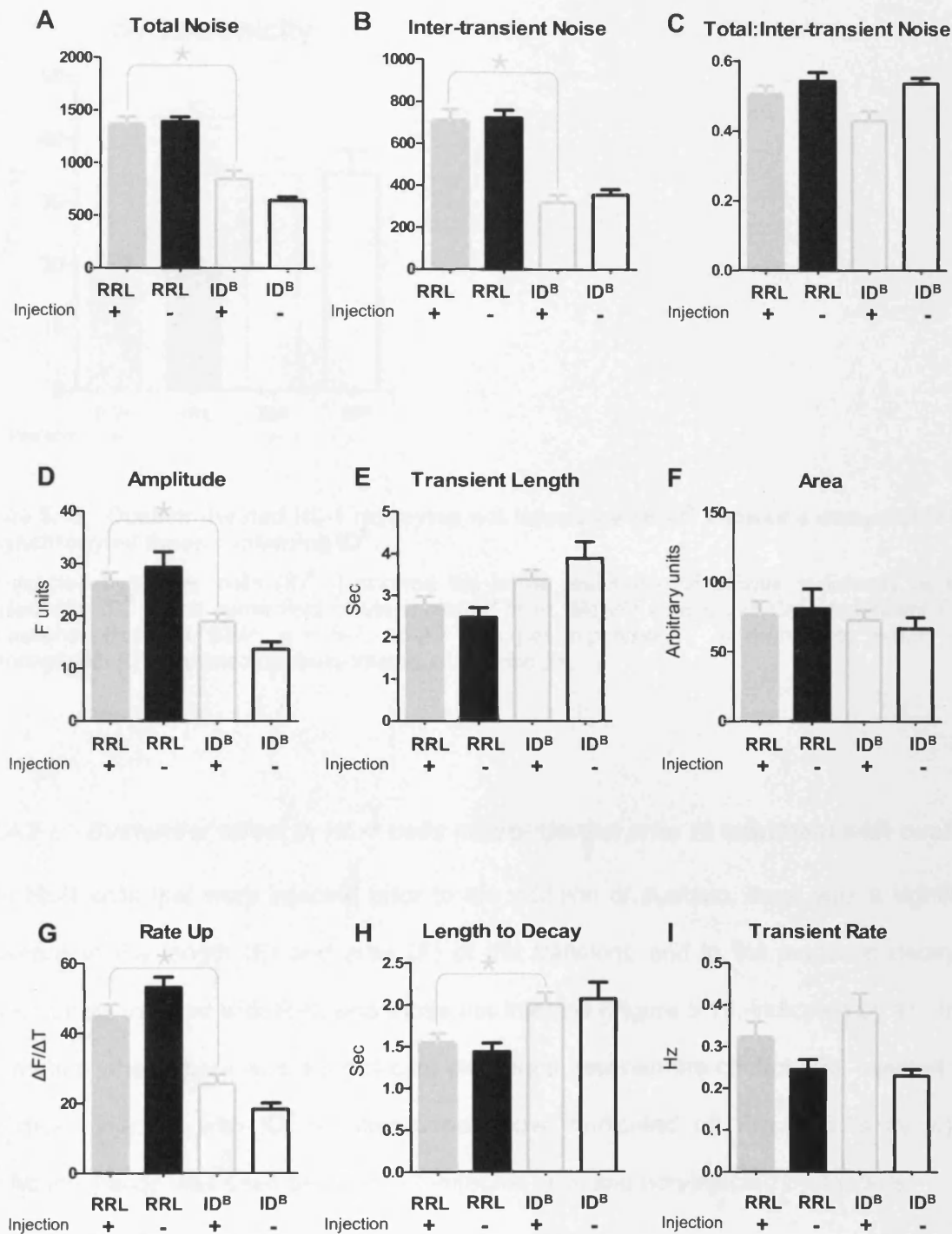


**Figure 5.16. Illustration of non-microinjected bystander cells**

The three panels show confocal images of Fluo-4 loaded cells. Cells containing Alexa 647 have been microinjected. Overlay shows microinjected (black circle) and non-microinjected 'bystander' cells (white circles). Scale bar: 25  $\mu$ m

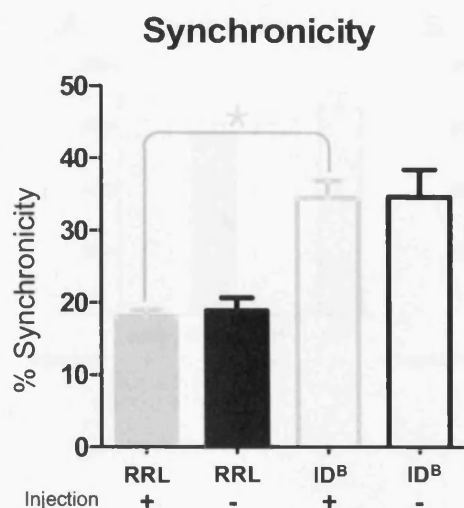
#### 5.3.4.1 *Bystander effect in HL-1 cells microinjected following pre-treatment with ouabain*

Figure 5.17 shows SALVO analysis of ouabain-treated cells which have not been microinjected, compared to those in the same field of view which have been injected. In every case, there is no significant difference between the injected and non-injected cells. This is particularly noticeable in the parameters where there was a significant difference between the control RRL-injected cells and those injected with ID<sup>B</sup> as discussed above (indicated on Figure 5.17 by  $\star$ ). Most importantly, ouabain-induced dyssynchrony was eliminated both in cells which had been injected with ID<sup>B</sup> and in cells in the same field of view which had not been microinjected (Figure 5.18).



**Figure 5.17. SALVO analysis shows a bystander effect in non-injected ouabain-treated HL-1 myocytes**

Non-injected HL-1 myocytes (RRL - and ID<sup>B</sup> -) exhibit the same alterations in most spatio-temporal Ca<sup>2+</sup> handling parameters as those injected with RRL or ID<sup>B</sup> after incubation with 100 nM ouabain (RRL + and ID<sup>B</sup> +, respectively), plotted from SALVO analysis of Ca<sup>2+</sup>-dependent Fluo-4 fluorescence (mean ± SEM, n = 5-7, 15-20 cells per experiment.). \* represents p < 0.05 when compared with RRL-injected ouabain-treated HL-1 controls.



**Figure 5.18. Ouabain-treated HL-1 myocytes not injected with ID<sup>B</sup> showed a comparable level of synchrony as those containing ID<sup>B</sup>.**

Non-injected bystander cells (ID<sup>B</sup> -) showed the same restoration of cellular synchrony as those injected with ID<sup>B</sup> in the same field of view, plotted from SALVO analysis of Ca<sup>2+</sup>-dependent Fluo-4 fluorescence (mean  $\pm$  SEM, n = 5-7, 15-20 cells per experiment). \* represents  $p < 0.05$  when compared with RRL-injected ouabain-treated HL-1 controls.

#### 5.3.4.2 Bystander effect in HL-1 cells microinjected prior to treatment with ouabain

In HL-1 cells that were injected prior to the addition of ouabain, there was a significant difference in the length (E) and area (F) of the transient, and in the length to decay (H) between cells injected with RRL and those not injected (Figure 5.19, indicated by #). In the parameters where there was a significant difference between the control RRL-injected cells and those injected with ID<sup>B</sup> as discussed above (indicated on Figure 5.19 by \*), no significant change was seen between ID<sup>B</sup>-injected cells and non-injected bystanders.

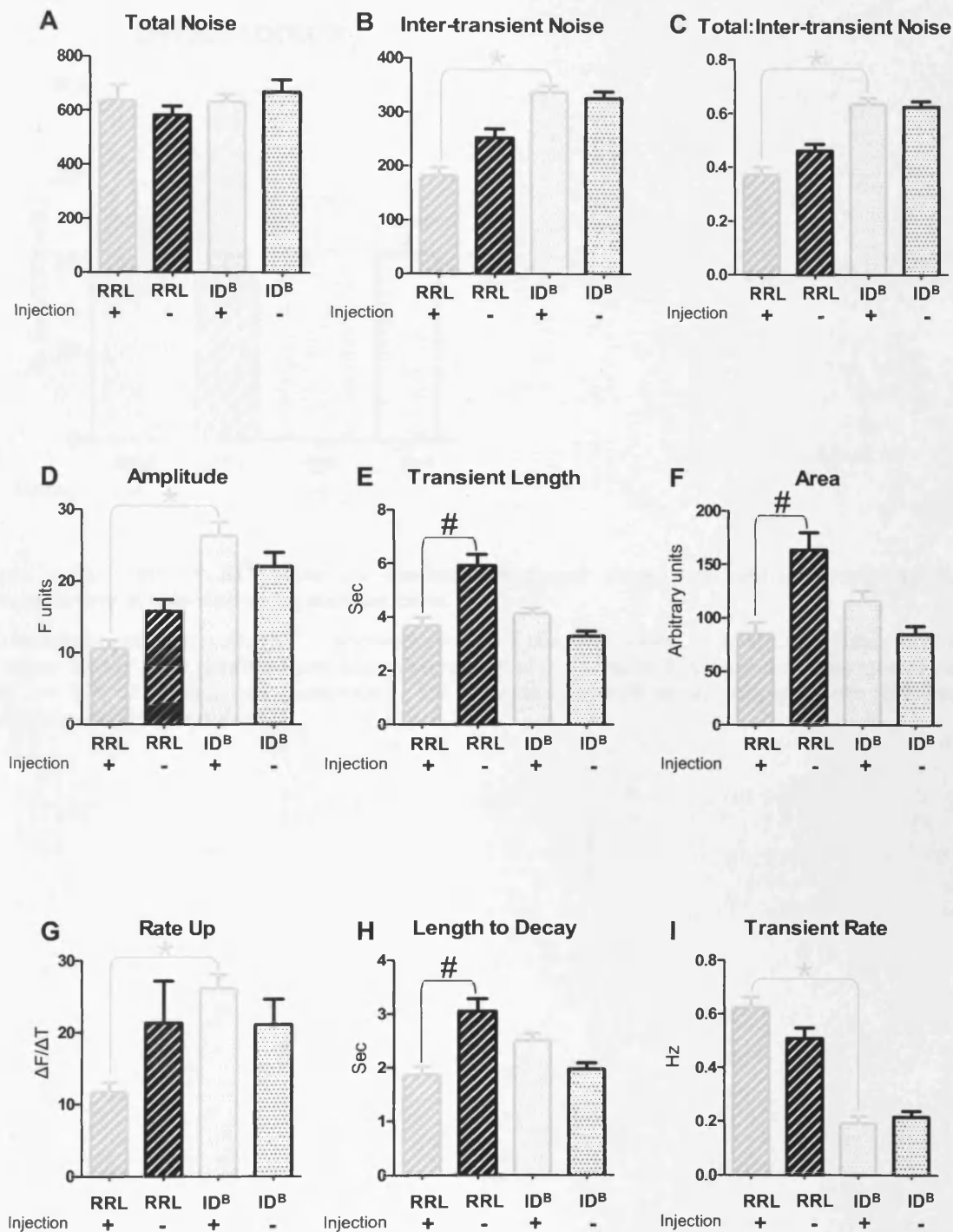


**Figure 5.19. SALVO analysis shows a bystander effect in non-injected ouabain-treated HL-1 myocytes**

Non-injected HL-1 myocytes (RRL - and ID<sup>B</sup> -) exhibit the same alterations in some spatio-temporal Ca<sup>2+</sup> handling parameters as those injected with RRL or ID<sup>B</sup> after incubation with 100 nM ouabain (RRL + and ID<sup>B</sup> +, respectively), plotted from SALVO analysis of Ca<sup>2+</sup>-dependent Fluo-4 fluorescence (mean  $\pm$  SEM, n = 5-7, 15-20 cells per experiment). \* represents p < 0.05 when compared with RRL-injected ouabain-treated HL-1 controls.

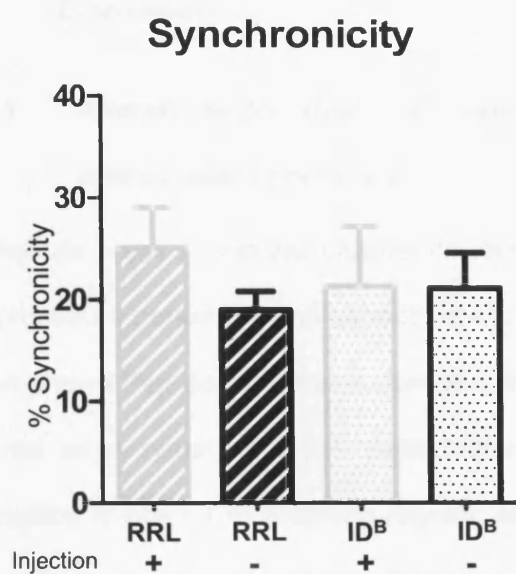


**Figure 5.20. MI of ID<sup>B</sup> prior to ouabain-treatment does not restore ouabain-induced dyssynchrony in injected or bystander cells.**

Non-injected bystander cells (ID<sup>B</sup> -) showed the same level of synchrony as those injected with ID<sup>B</sup> in the same field of view, plotted from SALVO analysis of Ca<sup>2+</sup>-dependent Fluo-4 fluorescence (mean  $\pm$  SEM,  $n = 5-7$ , 15-20 cells per experiment). \* represents  $p < 0.05$  when compared with RRL-injected ouabain-treated HL-1 controls.

## 5.4 Discussion

### 5.4.1 Alterations to some $\text{Ca}^{2+}$ handling parameters do not manifest as altered intercellular synchrony

Results presented in this chapter corroborated those from Chapter 4 and showed that the MI procedure perturbs some aspects of  $\text{Ca}^{2+}$  handling (summarised in Table 5.1). It has also been shown that despite these changes, the synchronicity of the myocyte monolayer is not altered as a result of these perturbations. This indicates that although precise  $\text{Ca}^{2+}$  regulation is vital for maintaining regular, synchronous contractions in cardiac cells, the cells are able to robustly compensate for a surprisingly large degree of disruption in  $\text{Ca}^{2+}$  and still maintain an overall regulated synchronously beating state.

Table 5.1 shows that it is not possible at this stage to pin-point one or a combination of parameters which determine whether or not intercellular synchrony in cardiac cells is perturbed, but further more detailed analyses of each of these parameters may give an insight into the mechanism underlying the regulation of synchronous contraction in cardiac myocytes. Since the experimental work presented in this thesis was completed, new studies are beginning to unravel the relationships between  $\text{Ca}^{2+}$  handling, rhythmicity and synchrony in coupled cardiac monolayers (Silvester *et al.* 2009).

Table 5.1. Summary of alterations of spatio-temporal  $\text{Ca}^{2+}$  handling parameters

	Total Noise	Intertransient Noise	Total: Intertransient Noise	Amplitude	Transient Length	Area	Rate Up	Length to Decay	Rate of Oscillation	Synchronicity
HL-1 + RRL	-	×	×	-	-	-	-	-	×	-
HL-1 + ID <sup>B</sup>	×	-	×	-	-	-	×	-	-	-
HL-1 + oua	-	×	×	×	×	×	×	×	×	↓
HL-1 + oua + RRL	×	-	-	×	×	×	-	×	×	-
HL-1 + oua + ID <sup>B</sup>	×	×	-	×	-	-	×	×	-	↑
HL-1 + RRL + oua	×	×	×	×	×	×	×	×	×	-
HL-1 + ID <sup>B</sup> + oua	-	×	×	×	-	-	×	-	×	-

Table summarising the changes observed in microinjected cells compared with controls, as discussed above. (-) refers to an unchanged parameter; (×) indicates a significant change compared to the appropriate control; (↑) and (↓) indicate a significant increase or decrease in cellular synchronicity.

#### 5.4.2 Effect of ID<sup>B</sup> on arrhythmic HL-1 myocytes

Ouabain-dependent increase in  $[\text{Ca}^{2+}]$  has been shown to occur in cardiac muscle cells (Santana *et al.* 1998), where ouabain binding to  $\text{Na}^+/\text{K}^+$ -ATPase is thought to mediate conformational transitions to adjacent  $\text{Na}^+$  channels, thereby allowing conduction of  $\text{Ca}^{2+}$  and a local increase in  $\text{Ca}^{2+}$  levels. In a model of ouabain-induced  $\text{Ca}^{2+}$ -overload and intercellular dyssynchrony, which from a mechanistic perspective closely mimics the events underlying malignant human arrhythmia, ID<sup>B</sup> reduced the total and inter-transient noise in the cell, which reflects a reduction in sub-threshold  $\text{Ca}^{2+}$  fluctuations. The most striking effect of ID<sup>B</sup> is the restoration of synchrony in the ouabain treated cells, to a level which is



comparable to that seen in WT HL-1 cells.

This effect of ID<sup>B</sup> is corroborated by FRET reporter studies carried out by Dr Chris George, which also showed that ouabain-treated cells had significantly lower signal variability in the presence of ID<sup>B</sup> (Figure 5.21).

Interestingly, the restoration of synchrony by ID<sup>B</sup> was not observed in cells which were microinjected prior to the addition of ouabain, implying that the potential beneficial effects of ID<sup>B</sup> on normalising cellular Ca<sup>2+</sup> cycling may be restricted to those cells in which Ca<sup>2+</sup> cycling is already perturbed. The mechanistic basis of this finding remains to be explored further.

This chapter has shown that MagZ-purified ID<sup>B</sup> synthesised in a cell-free expression system has a 'normalising' effect on intercellular synchrony in ouabain-disrupted HL-1 myocytes. Next, we investigated if this effect could be reproduced using ID<sup>B</sup> protein expressed in other systems, and these findings will be presented in the following chapter.

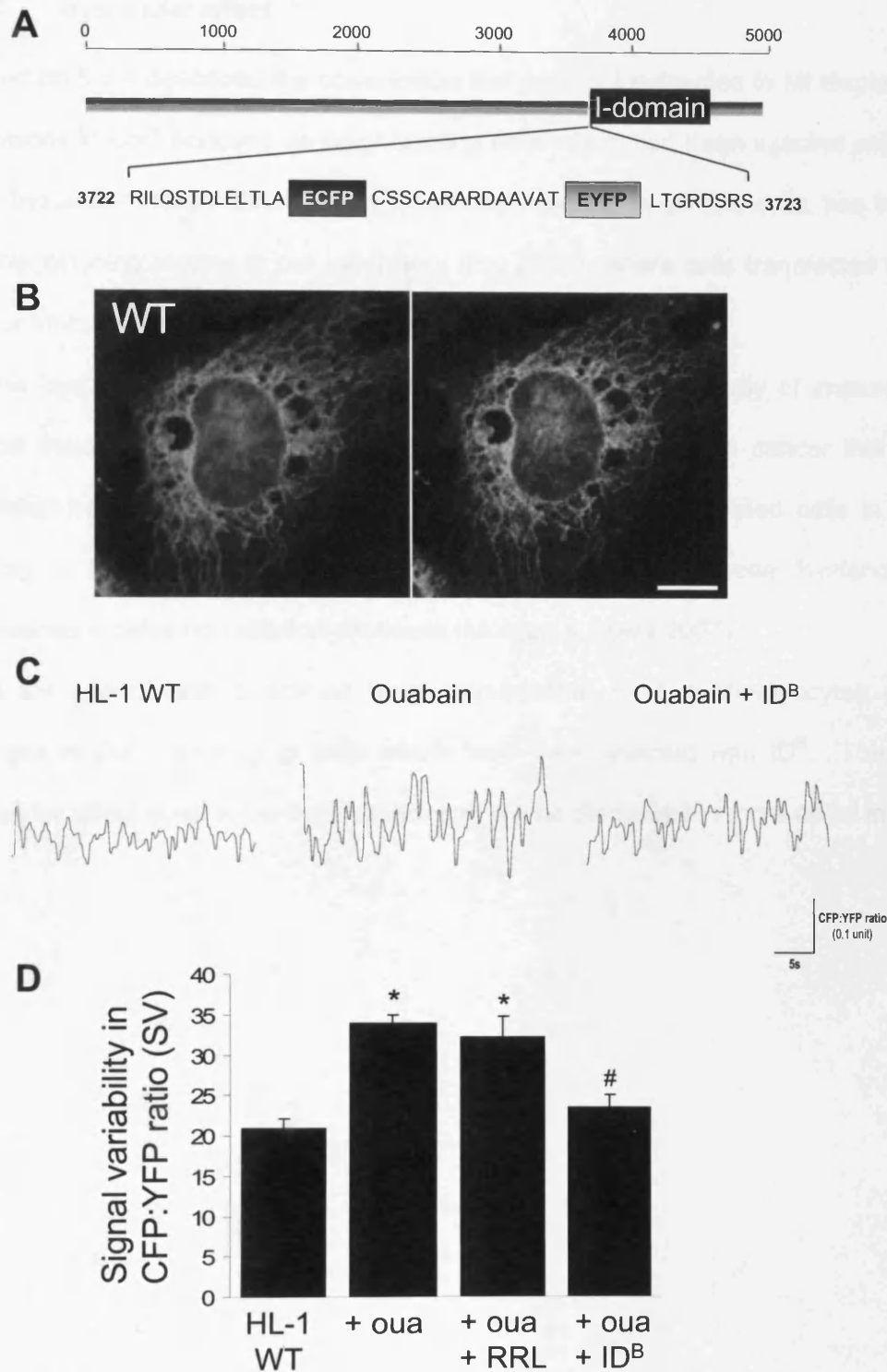


**Figure 5.21. FRET reporter studies of the effect of ID<sup>B</sup> on ouabain-treated HL-1 myocytes.**

Kindly supplied by Dr Chris George. **Panel A:** Schematic showing the FRET linker inserted at the start of the I-Domain. **Panel B:** FAC sorted HL-1 cells expressing the FRET reporter. CFP (left panel) and YFP (right panel) show identical localisation. Scale bare represents 20 $\mu$ m. **Panel C:** Traces showing the ratio of CFP:YFP, where the magnitude of the ratio indicates resting CFP:YFP signal. Signal variability is interpreted as changes in channel stability. **Panel D:** Bar chart showing the quantification of SV (mean  $\pm$  SEM). \* and # represent  $p < 0.05$  when compared to HL-1 WT and ouabain-treated HL-1 myocytes, respectively.

### 5.4.3 *Bystander effect*

Section 5.3.4 described the observation that cells not subjected to MI displayed the same alterations in  $\text{Ca}^{2+}$  handling as neighbouring cells which had been injected with RRL or ID<sup>B</sup>. This 'bystander effect', although not previously reported in cardiac cells, has been observed in other ongoing studies in our laboratory (Fry 2008), where cells transfected with ID<sup>B</sup> show similar traits to neighbouring non-transfected cells.

The 'bystander effect' has been regularly reported in the study of immunology, and in cancer therapy after exposure to ionising radiation treatment in cancer therapy, whereby irradiated cells may also transmit damage signals to non-irradiated cells in a population, leading to the occurrence of the same genetic effects in these 'bystander' cells that themselves receive no radiation exposure (Morgan & Sowa 2007).

In the experiments described here, non-injected HL-1 cardiomyocytes exhibit similar changes in  $\text{Ca}^{2+}$  handling to cells which have been injected with ID<sup>B</sup>. The cause of the bystander effect is yet to be determined, and will be discussed in more detail in Chapter 8.

## **Chapter 6**

# ***Investigating the effect of bacterially synthesised ID<sup>B</sup> in HL-1 cardiomyocytes***

## **6.1 Introduction**

### **6.1.1 *E. coli* as a system for protein expression**

*E. coli* is one of the most successful vehicles for over-expression of both prokaryotic and eukaryotic proteins and remains the most efficient widely-used host for recombinant protein production (Miroux & Walker 1996; Saïda *et al.* 2006). Well-known genetics, high transformation efficiency and inexpensiveness are the main factors that contribute to the selection of this host.

### **6.1.2 Factors affecting protein expression in *E. coli***

Expression of recombinant protein in *E. coli* can be achieved by inserting the target gene into a multi-copy plasmid vector under the transcriptional control of either a constitutive or inducible promoter. Constitutive promoter systems provide a simple means of over-producing a foreign protein in a bacterial cell since the target protein is continually expressed. However, unregulated high level expression of a foreign protein causes a metabolic burden on the bacterial cells' energy resources leading to a reduction or inhibition of cell growth (Glick & Whitney 1987; Bentley *et al.* 1990; Donovan *et al.* 1996). Since the overall yield of the target protein is a function of both the cell yield (number of cells per litre of culture) and the amount of recombinant product expressed per bacterium, the reduced cell growth that generally accompanies constitutive expression results in lower yields of the target protein compared to inducible promoter systems (Donovan *et al.* 1996).

Inducible promoter systems provide the ability to 'switch on' the expression of a foreign gene by varying an environmental factor such as temperature (Remaut *et al.* 1981; Whitney *et al.* 1989; Yabuta *et al.* 1995), or the concentration of a particular component in the growth medium (Carter *et al.* 1992; Neubauer *et al.* 1992). For example, the bacteriophage lambda pL and pR promoters in conjunction with a temperature sensitive repressor gene can be thermally induced when the temperature of the fermentation broth is raised from the growth-

optimum temperature of 30-35°C to 42°C (Murray *et al.* 1979; Whitney *et al.* 1989). The *E. coli trp* and *phoA* promoters are induced following depletion of tryptophan and phosphates, respectively, from the medium (Carter *et al.* 1992; Rockenbach *et al.* 1991), while the *lac* promoter is induced in the presence of lactose or isopropyl-3-D-thiogalactoside (IPTG) (Neubauer *et al.* 1992).

The ability to induce foreign gene expression allows for the separation of cell growth phase from the product synthesis or induction phase of the fermentation. After obtaining a high concentration of cells during an optimised growth phase, the foreign gene can then be induced resulting in higher total yields of the recombinant protein than otherwise could be achieved using constitutive expression. In some cases, the level of transcription of the foreign gene can be regulated by using an appropriate level of the inducing stimulus. This in turn can further improve yields by allowing the level of expression to be optimised during the induction phase (Donovan *et al.* 1996).

The *lac* promoter from the *E. coli* lactose operon is one of the most commonly used promoters for regulating the expression of recombinant genes in bacteria. It is the most widely studied of all bacterial promoters and has been extensively characterised at the molecular level (Donovan *et al.* 1996). This operon will be exclusively used to induce bacterial expression in the experimental system discussed in this chapter.

#### **6.1.2.1 The effect of IPTG concentration**

While a wide range of IPTG concentrations, ranging from 0.005 to 5 mM, have been used for successful protein expression (Chalmers *et al.* 1990; Pack *et al.* 1993; Winograd *et al.* 1993), expression is commonly induced using 1 mM IPTG. It has been shown that high concentrations of inducer that are often used in an effort to fully induce the *lac* promoter do not necessarily lead to maximal expression of a target protein (Glick 1995), and optimal inducer concentration should be chosen to balance the decreasing yields of recombinant cells following induction with increasing cellular levels of target protein (Bentley *et al.* 1991).

Studies have shown that high inducer concentrations (>3 mM IPTG) resulted in a severe reduction in growth rate, which led to an early onset of the stationary phase and cell death. At slightly lower concentrations (~2 mM IPTG), however, the cells partially recovered from the initial shock following induction and established a constant specific growth rate that was 60% lower than pre-induction levels. Thus, the overall level of protein expression in batch culture is a trade-off between increasing product expression in the cell and decreasing cell yields resulting from a lower specific growth rate following induction with IPTG (Bentley *et al.* 1991).

The optimal concentration of IPTG is thus entirely system-dependent and must be empirically determined. However, an intermediate IPTG concentration in the region of 0.5-1.0 mM IPTG usually balances the opposing phenomena of increasing target protein expression and decreasing cell yields to maximise the overall expression of the recombinant product (Donovan *et al.* 1996).

### **6.1.2.2 The effect of temperature**

The maximum growth rate of *E. coli* occurs at a temperature of 37-39°C. Although this is also the temperature at which the *lac* promoter exhibits maximal activity, the use of sub-optimal growth temperatures can in some cases improve the yield and/or solubility of the target protein product (Donovan *et al.* 1996). Reducing the culture temperature from 37°C to 25-30°C can also significantly reduce proteolytic degradation and improve the stability of the target protein (Baneyx *et al.* 1991; Surek *et al.* 1991). Furthermore, studies have shown that ATP-dependent proteolytic activity can decrease more than 2.5-fold as the temperature was decreased from 42°C to 30°C (Kosinski & Bailey 1991). Since it has been suggested that ATP-dependent proteolysis of recombinant proteins may initiate further degradation by ATP-independent proteases, lower culture temperatures may minimise the activity of pathways that lead to product degradation (Kosinski & Bailey 1991). Increased proteolytic degradation of recombinant products above 30°C may also result from conformational changes in the

target protein which may expose sites for proteolytic cleavage (Chesshyre & Hipkiss 1989). Precipitation of over-expressed protein in the form of insoluble aggregates is also less prevalent at lower temperatures (Cabilly 1989).

As with reduced inducer concentrations, lower culture temperatures may enhance functional protein formation by reducing the rate at which the recombinant protein is formed (Donovan *et al.* 1996). Reduced expression rates reduce the concentration of the unfolded recombinant protein in the cell. At lower concentrations, reduced interaction between unfolded intermediates may allow the proteins to react via folding pathways rather than those leading to aggregation (Knappik *et al.* 1993). Improved folding at lower temperatures may also reduce the level of interaction between improperly folded recombinant product and the inner and outer membranes. Since long-term exposure to improperly folded proteins may substantially reduce membrane integrity (Skerra & Plückthun 1991), this may explain why some studies have shown that outer membrane leakiness, cell lysis and death observed at 37°C in response to expression of secreted proteins was reduced or eliminated at 20-30°C (Chalmers *et al.* 1990; Skerra & Plückthun 1991; Somerville *et al.* 1994).

### **6.1.3 Objectives of this chapter**

The previous chapter showed that *in vitro*-generated ID<sup>B</sup> reversed the ouabain-induced intercellular dyssynchrony in HL-1 myocytic monolayers, and restored synchrony to levels comparable with those determined in untreated, natively coupled HL-1 cells. This chapter discusses the validity of these findings and utilises ID<sup>B</sup> synthesised via a distinct mode of expression, namely using a bacterial expression system.

For reasons given above, an inducible system was used and the *E. coli* BL21 strain was chosen to initially optimise the expression of full-length I-Domain. It was anticipated that this would be the most challenging protein to express due to its size and hydrophobicity, and the conditions suitable for the expression of the I-Domain would also be amenable to successful expression of the truncated I-Domain fragments.



This chapter discusses the optimisation of conditions for efficient expression and purification of I-Domain proteins in a bacterial expression system. The resultant protein was used to further investigate the effect of ID<sup>B</sup> on HL-1 myocytes.

#### **6.1.4 Specific Hypothesis**

Having demonstrated in the previous two chapters that *in vitro*-synthesised ID<sup>B</sup> can be successfully microinjected into HL-1 myocytes, and that it restores synchrony in ouabain-treated cells, this chapter now investigates the hypothesis that these observations are independent of the source of the protein, and that microinjection of bacterially-produced ID<sup>B</sup> will produce entirely comparable results.

## 6.2 Methods

### 6.2.1 Bacterial expression of recombinant I-Domain proteins

BL21 competent cells are the most widely used *E. coli* strains for protein expression from the T7 promoter. These strains have been engineered to contain an inducible T7 RNA polymerase gene and contain a mutation in the *ompT* protease gene, which is implicated in the degradation of some recombinant proteins. BL21 cells are derivatives of *E. coli* B and naturally lack the *Lon* protease, which may affect the stability of some recombinant proteins. For the purposes of this study, *E. coli* Rosetta™ 2(DE3) competent cells (Novagen) were used for the expression of recombinant proteins. *E. coli* Rosetta™ 2(DE3) cells are BL21 derivatives designed to enhance the expression of eukaryotic proteins that contain codons rarely used in *E. coli*. For transformation with recombinant plasmid DNA, Rosetta™ 2(DE3) cells (20µl) were thawed on ice before the addition of 5 ng cDNA and subsequent incubation on ice (5 mins), prior to 'heat-shock' treatment at 42°C for exactly 30 seconds then immediate return to ice for 3 minutes. SOC medium (80µl) pre-warmed to RT was added and the suspension was incubated at 37°C for 1 hour with continuous shaking (225 rpm). Following this incubation time, the suspension was plated on LB-Agar medium containing kanamycin (30µg/ml) and chloramphenicol (40µg/ml), which was incubated at 37°C until the appearance of colonies (typically 16-20 hours).

### 6.2.2 Optimisation of culture conditions

#### 6.2.2.1 IPTG-induction of bacterial protein expression

The optimal conditions for the induction of expression of full length I-Domain in *E. coli* Rosetta™ 2(DE3) were investigated using small scale cultures (200ml). In order to find the optimal conditions for protein expression a range of different IPTG concentrations, temperatures and induction times were tested. At each given temperature, four different IPTG concentrations, and four durations of induction were investigated (summarised in

Table 6.1). A total of 39 conditions were tested, and cells not exposed to IPTG were used as a negative control.

**Table 6.1. Summary of bacterial induction conditions**

Temperature:	12°C, 30°C, 37°C
IPTG Concentration:	25µM, 100µM, 500µM, 1mM
Induction Time:	At 12°C: 6, 24, 48 hrs; At 30°C & 37°C: 2, 6, 24 hrs
Negative Control:	Uninduced cells

Isolated colonies from plates grown overnight (as described in Section 6.2.1), were inoculated in 10ml LB broth, containing kanamycin (30µg/ml) and chloramphenicol (40µg/ml) and left to grow overnight on a shaking platform (37°C, 250 rpm, 16-18 h). Following this incubation time, the inoculum was transferred to 190ml LB pre-warmed to 37°C and incubated under the same conditions until an OD<sub>600</sub> was reached. At this stage, the bacterial cells were induced with 0.025, 0.1, 0.5, or 1 mM IPTG, and incubated at 12°C, 30°C or 37°C as described in Table 6.1. After the induction time was complete, the bacterial suspension was pelleted by centrifugation and stored at -80°C until needed for downstream application.

### 6.2.2.2 Protein expression by autoinduction

The Overnight Express™ Autoinduction System (Novagen) is optimised for high-level protein expression with IPTG-inducible pET bacterial expression systems without the need to monitor cell growth and induce protein expression. The method is based on media components that are metabolised differentially to promote growth to high density and automatically induce protein expression from *lac* promoters. In auto-induction media, cultures reliably grow 'uninduced' to relatively high density and then spontaneously induce high levels of target protein without the need to monitor cell density or add IPTG (Studier

2005).

Isolated colonies from plates grown overnight (as described in Section 6.2.1), were inoculated in Overnight Express™ System medium, containing kanamycin (30 µg/ml). A multi-stage inoculation strategy was employed for larger cultures in order to minimise the shock-induced lag phase in growth caused by transfer of a small inoculum to a larger volume of fresh medium and diffusion of vitamins, minerals and cofactors from the cells (Studier 2005). Inoculation of flask cultures greater than 30ml were inoculated in this way using several stages and flasks of increasing size filled with medium (10–20% of the flask volume), by generating a 5% (v/v) inoculum. Typically, the culture was initiated by single colony inoculation of 5ml Overnight Express™ System medium, which was incubated on a shaking platform (37°C, 250 rpm, ~2 h) until an OD<sub>600</sub> of approximately 0.5 was reached. This was then transferred into 95ml of pre-warmed Overnight Express™ System medium, and incubated under the same conditions for a further 2 h. Once this culture had reached an OD<sub>600</sub> of ~0.5, it was divided equally into four flasks, each containing 475ml of pre-warmed Overnight Express™ System medium, to make a total of 2 L bacterial culture, and incubated overnight on a shaking platform (37°C, 250 rpm, 16- 18h).

### 6.2.3 Protein extraction

The goal of protein production and extraction is to maximise the recovery of recombinant protein in the soluble fraction of a bacterial lysate. Five different protein extraction methods were tested to establish which gave the highest yield of soluble protein from the bacterial cells with the least amount of degradation (summarised in Table 6.2). For each method the amount of soluble and insoluble protein was compared by protein staining. The resultant pellet from each method was resuspended in 5ml 10mM Tris/1mM EDTA. This solution containing the insoluble protein fraction was compared to the clarified lysate containing the extracted soluble proteins by SDS-PAGE electrophoresis and protein staining (See Chapter 2).

Table 6.2. Summary of protein extraction methods.

Extraction Method	Mechanism of protein extraction
French Press	Lysis by forcing the cells through a narrow space at high pressure that breaks down inclusion bodies
Sonication	Pulsed, high frequency sound waves to agitate and lyse cells.
B-PER Popper <sup>®</sup> reagent (Pierce)	Bacterial cell lysis by mild, non-ionic detergent
BugBuster Master Mix (Novagen)	Disruption of cell wall by a detergent mix
8M urea total protein extraction buffer	Total cell lysis and denaturation of proteins

### 6.2.3.1 Protein extraction by pressure lysis

The French press mechanically disrupts the bacterial cell membrane by passing the bacterial solution through a narrow valve under high pressure. The press uses an external hydraulic pump to drive a piston within a larger cylinder that contains the sample. The highly pressurised solution is then squeezed past a needle valve. Once past the valve, the pressure drops to atmospheric pressure and generates shear stress that disrupts the cells (Vanderheiden *et al.* 1970).

The bacterial cells were pelleted by centrifugation (6,000  $xg$ , 10 mins), and the resultant pellet was resuspended in 30ml 10mM Tris/1mM EDTA solution by gentle pipetting until a homogeneous cell suspension was achieved. The bacterial suspension was passed through a French press at 20,000 p.s.i. in a drop-wise manner into a pre-chilled tube on ice. The lysate was then centrifuged (16,000  $xg$ , 20 min, 4°C) to separate the soluble and insoluble protein fractions.

### 6.2.3.2 Protein extraction by sonication

Sonication applies ultrasound energy to agitate the bacterial cells and disrupt cell membranes in order to release the cellular contents. For this method, the bacterial cells

were centrifuged (6,000  $xg$ , 10 mins), and the resultant pellet was resuspended in 5ml 10mM Tris/1mM EDTA solution by gentle pipetting until a homogeneous cell suspension was achieved. This was then placed on ice and subjected to sonication (4 x 30 sec pulses). The lysate was pelleted by centrifugation (16,000  $xg$ , 20 min, 4°C) to remove any insoluble cell debris.

#### **6.2.3.3 Protein extraction by B-PER<sup>®</sup>**

Bacterial Protein Extraction Reagent (B-PER<sup>®</sup>, Pierce) utilises a proprietary, mild, non-ionic detergent in 20 mM Tris-HCl (pH 7.5) for lysis of the bacterial cells and eliminates the need for mechanical disruption by sonication or French press techniques.

The bacterial suspension was treated with B-PER<sup>®</sup> according to the manufacturer's guidelines. The bacterial cells were pelleted by centrifugation (5,000  $xg$ , 10 mins), and the resultant pellet was resuspended in 2.5ml of B-PER<sup>®</sup> Reagent by gentle pipetting until a homogeneous cell suspension was achieved. The cell suspension was then incubated on a shaking platform (20 min, RT) before centrifugation (27,200  $xg$ , 15 mins) to separate the soluble and insoluble protein fractions.

#### **6.2.3.4 Protein extraction by BugBuster**

Like B-PER<sup>®</sup>, BugBuster Protein Extraction Reagent (Novagen) is formulated for the gentle disruption of the cell wall of *E. coli* to liberate active proteins. It provides a simple, rapid, low-cost alternative to mechanical methods such as French Press or sonication for releasing expressed target protein in preparation for purification or other applications. The proprietary formulation utilises a detergent mix that is capable of cell wall perforation without protein denaturation.

The bacterial suspension was treated according to the manufacturer's protocol. Briefly, the bacterial cells were harvested from liquid culture by centrifugation (10,000  $xg$ , 10 min).

The supernatant was then decanted, and the pellet was weighed to determine its wet weight. The pellet was resuspended in BugBuster reagent pre-warmed to RT by pipetting, using 5ml reagent per gram of wet cell paste. At this stage, Benzonase Nuclease (Novagen) was added to reduce the viscosity of the lysate (25U per ml Bugbuster). The cell suspension was incubated on a slow rotating mixer (20 min, RT) before centrifugation (16,000  $xg$ , 20 min, 4°C) to remove any insoluble cell debris.

#### **6.2.3.5 Protein extraction by urea**

Protein extraction by urea completely lyses the bacterial cells and results in near total protein extraction. However, proteins extracted by this method are generally not suitable for downstream applications, due to the chaotropic effects of urea on the proteins' structure. Since this method should result in total protein extraction, it was used as a positive control to which the other methods were compared.

The bacterial cells were harvested from liquid culture by centrifugation (6,000  $xg$ , 10 min). The supernatant was then decanted, and the wet weight of the pellet was determined. The pellet was resuspended in urea extraction buffer (100 mM NaH<sub>2</sub>PO<sub>4</sub>, 10 mM Tris, 8 M urea) using 5ml reagent per gram of wet cell paste, and incubated on a rotating mixer (RT, 3 hrs), before centrifugation (16,000  $xg$ , 20 min, 4°C) to remove any insoluble cell debris.

#### **6.2.4 Microinjection of bacterially produced ID<sup>B</sup> into HL-1 cells**

Bacterially-produced ID<sup>B</sup> was microinjected into resting and ouabain-treated HL-1 cells following exactly the same protocol as previously described for *in vitro* synthesised proteins (Sections 4.2.4. and 5.2.1, respectively). Following microinjection, the cells were imaged and the ROIs analysed by SALVO, as described in previous chapters.

## **6.3 Results**

### **6.3.1 Selection of a suitable protein extraction technique**

Untransformed bacterial cells were induced according to the manufacturer's recommended protocol, and five different protein extraction methods were investigated to establish which method gave the highest yield of soluble protein with the least amount of degradation. Urea extraction was used as the positive control as it completely lyses the bacterial cells and results in near total protein extraction. However, urea is not suitable for the extraction of proteins which will be used in downstream applications due to its chaotropic effects which would disrupt the three-dimensional structure of the protein and prevent protein re-folding.

The reagents had varying efficacy, indicated by the yield and the amount of soluble versus insoluble protein extracted (Figure 6.1). B-PER<sup>®</sup> and Bugbuster were not suitable for this extraction, as the soluble lysate contained no proteins >71 kDa. Sonication did extract high molecular weight protein, but a high level of insoluble protein persisted. The French press gave the highest yield of soluble protein and had the additional advantage of eliminating the use of any detergent which may affect downstream processes. Based on these results, the French Press was chosen as the method of choice for extracting the I-Domain protein from the large scale bacterial cultures.



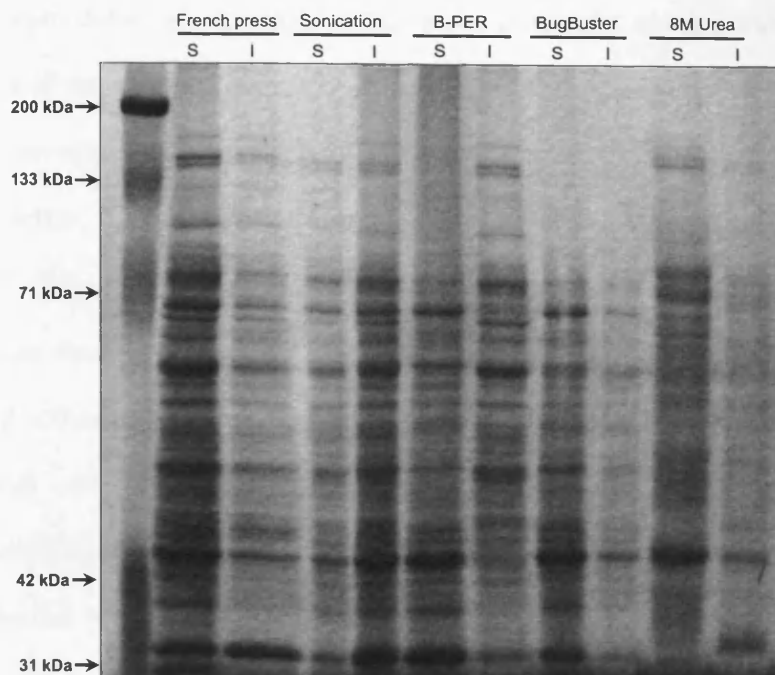


**Figure 6.1. Optimisation of protein extraction from bacterial cells**

SDS-PAGE gel (10%) stained with Imperial Protein Stain, showing the amount of soluble (S) and insoluble (I) extracted by five different protein extraction techniques. The protein samples were normalised for cell number, and each lane contains 1/20 of the resuspension volume for each extraction method (equivalent to 10ml of original bacterial culture).

### 6.3.2 Protein Induction by IPTG

The full-length I-Domain was transformed into *E. coli* BL21 derivatives, Rosetta™ 2(DE3) bacterial cells, which are optimised for the expression of large or ‘difficult-to-express’ proteins. Single colonies were isolated and inoculated into 10ml of LB and induced as described above (Section 6.2.2.1). Although French Press lysis was optimal, since these small scale cultures were required purely for diagnostic purposes to test and optimise IPTG induction, and not required any downstream applications, the proteins were extracted from the bacterial cells by urea lysis (Section 6.2.3.5).

Induction of bacterial protein expression by IPTG failed to produce any significant amounts of full-length I-Domain protein, under any of the 39 conditions tested (Figure 6.2). The Imperial-stained gels showed that there was no visible protein product at 106 kDa, the anticipated molecular weight of the recombinant I-Domain. Furthermore, the S-tag blots

failed to detect any product at 106 kDa, but under some conditions the S-tag showed a high level of degradation product. To eliminate the possibility that these proteins were an artefact of non-specific expression of endogenous bacterial proteins or due to non-specific S-tag detection, bacterial cells expressing the I-Domain were compared with cells expressing only pET-29(b). It was found that in cells expressing pET-29(b), S-tag detection produced a single discrete band at 18 kDa, with no degradation or non-specific binding (Figure 6.3).

Another possibility was that the protein degradation observed in Figure 6.2 was due to the harsh cell lysis conditions imposed by the urea extraction buffer. To investigate this possibility, the induction conditions giving the best protein yield at each temperature were selected (denoted by ★ on Figure 6.2). These were chosen as the optimal conditions at each temperature, based on the amount of protein produced and detected, with the least degradation. The inductions were repeated, and 2 L bacterial culture was pelleted and resuspended in 200ml 10mM Tris/1mM EDTA, before the cells were lysed by passing through the French press as described in Section 6.2.3.1. Once again, Imperial-stained SDS-PAGE gels failed to show any protein product at 106 kDa, corresponding to the I-Domain, and S-tag-based techniques continued to show a high level of degradation product but no intact product at 106 kDa (Figure 6.4).

A number of alterations to this strategy were investigated, including the addition of a range of different protease inhibitors, all of which failed to eliminate the substantial levels of protein degradation. It was therefore concluded that IPTG was not a suitable inducer for full length I-Domain protein, as it resulted in multiple truncated fragments but does not produce any detectable levels of full-length protein.

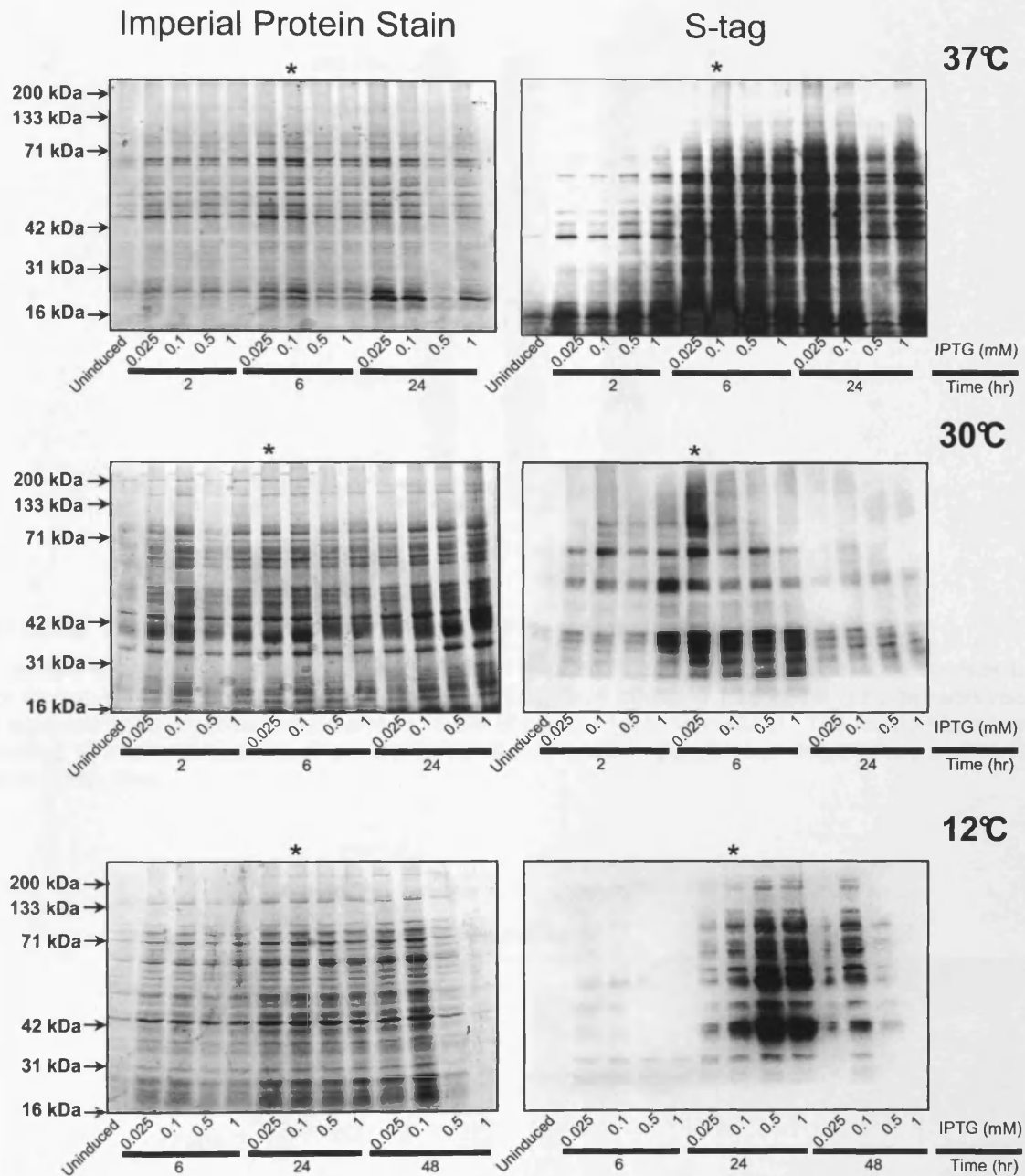


**Figure 6.2. Testing the induction conditions to optimise the production of I-Domain protein in an IPTG-induced bacterial system.**

A total of 39 conditions were tested in an attempt to identify the optimal set of conditions for the production of I-Domain protein in *E. coli*. **Left-hand panels** – Imperial-stained SDS-PAGE gels (10%) of full length I-Domain extracted from bacterial culture, showing the optimal induction conditions at each of the temperatures tested. **Right-hand panels** – S-Tag blots of an equivalent gel; shows that although the protein profiles may be similar despite varying conditions the level of detectable protein produced is variable. Each lane contains 1/20 of the resuspension volume for each extraction method (equivalent to 100ml of original bacterial culture). Lanes marked with \* were selected for further investigation, as shown in Figure 6.4.

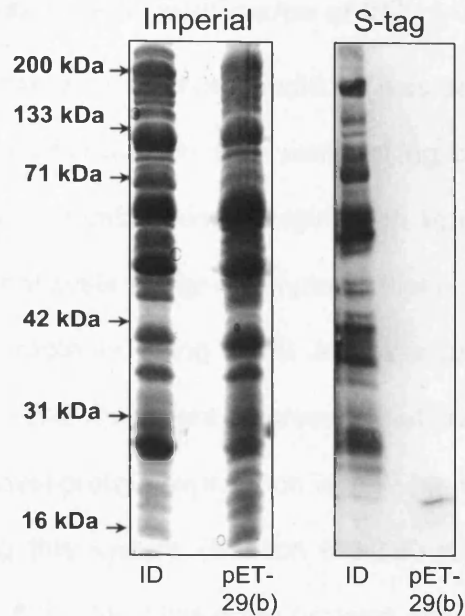


**Figure 6.3. Expression of I-Domain and pET29-(b) in Rosetta™ 2(DE3) cells**

Bacterially expressed I-Domain (ID) and pET29-(b) proteins pET29-(b) produces one discrete band with no non-specific binding by S-tag detection. Each lane contains 1/20 of the resuspension volume for each extraction method (equivalent to 100ml of original bacterial culture). The multiple bands seen following ID expression are thus an artefact of the ID protein, possibly via degradation or alternative transcription sites.

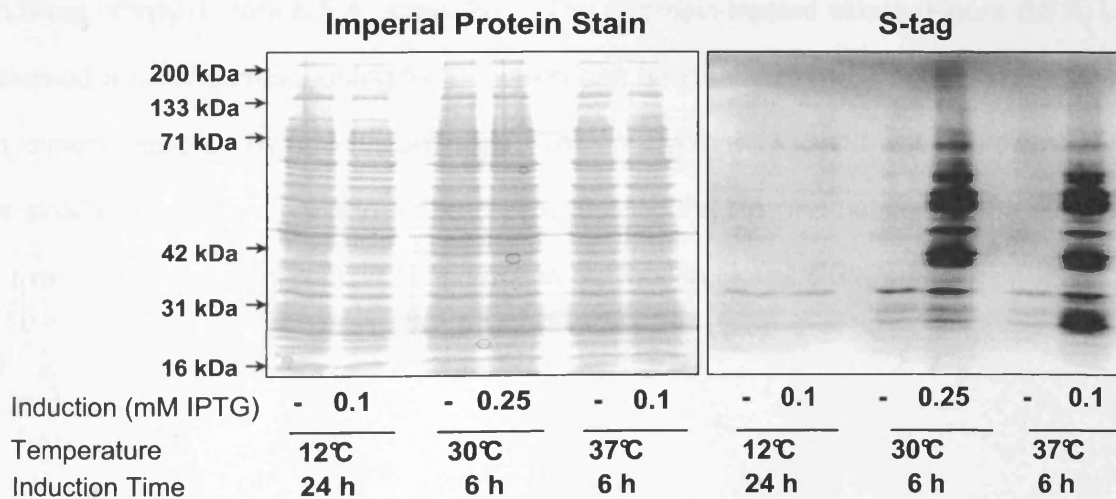


**Figure 6.4. IPTG induction conditions selected for large-scale culture**

**Left panel** – Protein stained 10% SDS-PAGE gel of full length I-Domain extracted from bacterial culture, showing the optimal induction conditions at each of the temperatures tested (100µl). **Right panel** – S-Tag blot of an equivalent gel; shows that although the protein profiles may be similar despite varying conditions, the level of detectable protein produced varies. Each lane contains 1/20 of the resuspension volume for each extraction method (equivalent to 100ml of original bacterial culture)

### 6.3.3 Successful expression and purification of ID<sup>B</sup>

While the optimisation of protein induction conditions was being carried out, simultaneous studies of I-Domain proteins produced *in vitro* were taking place (Chapters 3-5) and the marked effects of ID<sup>B</sup> in cardiac cells was emerging. In light of this, the expression and purification of ID<sup>B</sup> in a bacterial system was attempted. Since the expression of full-length I-Domain showed potential problems using IPTG as an inducer, an alternative induction system was used for this – The Overnight Express™ Autoinduction System (Novagen) – which is optimised for high-level protein expression with IPTG-inducible pET vectors.

ID<sup>B</sup> was expressed using this system (Section 6.2.2.2) and subsequently extracted by French Press lysis (Section 6.2.3.1). Unlike the proteins synthesised *in vitro* in Chapter 3, the resultant lysate was then purified using the His-GraviTrap Ni<sup>2+</sup>-affinity method followed by S-tag cleavage (Chapter 2 Sections 2.3.7 and 2.3.8) rather than with Mag-Z beads. The MagZ purification system is optimised for the purification of target His-tagged proteins from RRL, and is not suitable for purification of large volumes of bacterial lysate. The eluate from His-GraviTrap Ni<sup>2+</sup>-affinity purification (Figure 6.5 A, lane 1) was subjected to purification with S-tag affinity (Figure 6.5 A, lanes 2-7). The thrombin-treated eluate (Figure 6.5 A, Lane 8) showed a band corresponding to ID<sup>B</sup> which can be clearly seen by both Imperial staining and immunodetection by anti-His antibody. The finding that this band was approximately 1.7 kDa smaller than those seen in lanes 1-7, was encouraging and pointed to the successful removal of the S-tag by thrombin cleavage, as outlined in Figure 6.5 (Panel B).

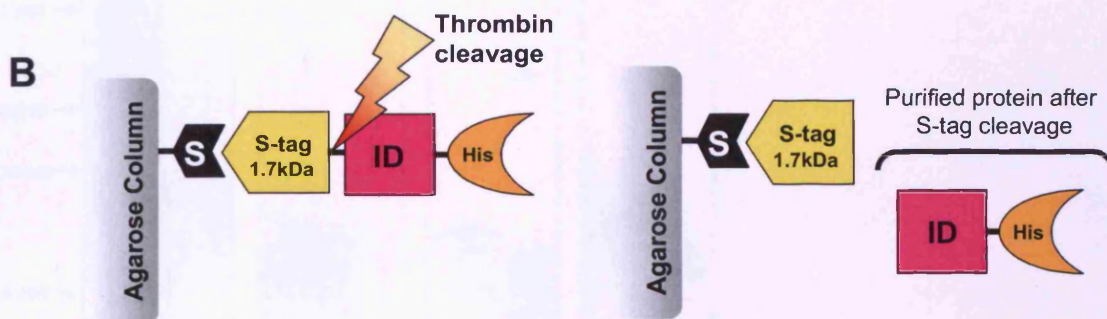
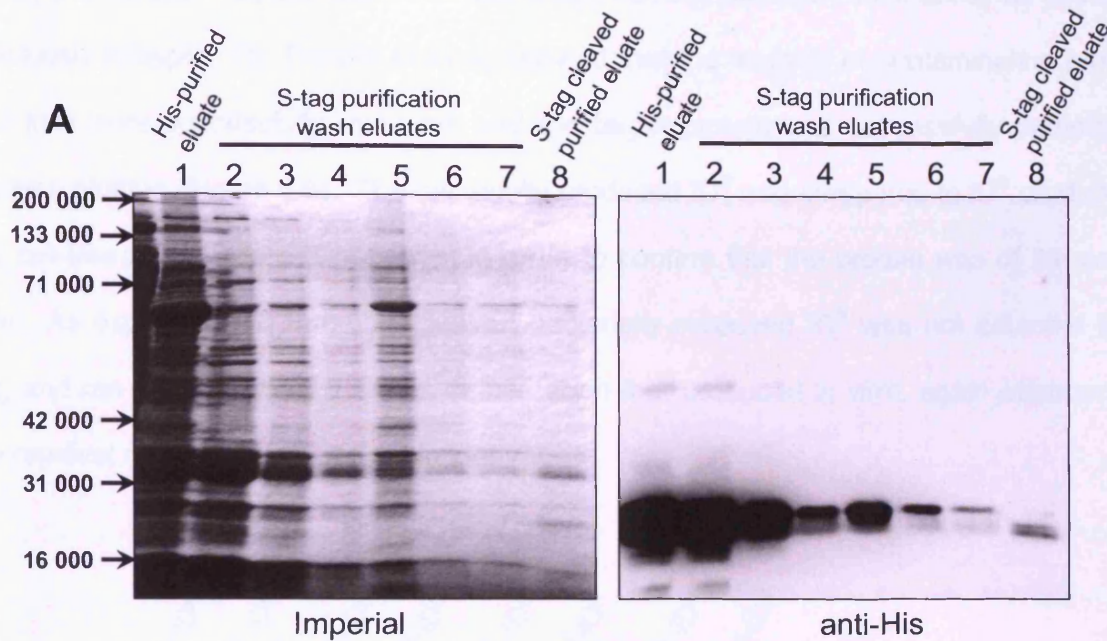


**Figure 6.5. Purification of ID<sup>B</sup> from bacterial cells**

**Panel A:** Eluates from the Ni<sup>2+</sup> affinity and S-protein affinity systems were separated by SDS-PAGE (10% (v/v)), and visualised with Imperial protein stain and His-tag detection. Each lane contains 1/20 of the resuspension volume for each extraction method (equivalent to 100ml of original bacterial culture). **Panel B:** Schematic depicting the mechanism of protein purification by S-tag affinity and thrombin cleavage. As seen by His-tag detection, the purified protein is ~1.7 kDa smaller than the uncleaved protein, due to the loss of the S-tag.

Imperial staining of the thrombin-treated eluate shows that there was a small amount of 'non-target' proteins present in addition to the thrombin-cleaved ID<sup>B</sup>. To eliminate these contaminating proteins the eluate was run through size-exclusion filter (Microcon) with a cut-off of 30,000 MW, so only proteins below this size remained in the purified eluate. The purified eluate was then loaded onto an SDS-PAGE gel to confirm the presence of purified

ID<sup>B</sup> by protein staining, and detection with S-tag, ab1093 and anti-His antibody as described previously (Chapter 2). Protein staining showed that the majority of contaminating proteins >30 kDa were successfully removed, and the target protein was successfully detected by western blotting (Figure 6.6). The bacterially produced ID<sup>B</sup> was compared to ID<sup>B</sup> produced in the cell-free RRL system (Chapter 3) in order to confirm that the protein was of the correct size. As expected, the thrombin-cleaved bacterially-produced ID<sup>B</sup> was not detected by S-tag, and ran approximately 1.7 kDa smaller than that produced *in vitro*, again corroborating the removal of the S-tag by thrombin cleavage.

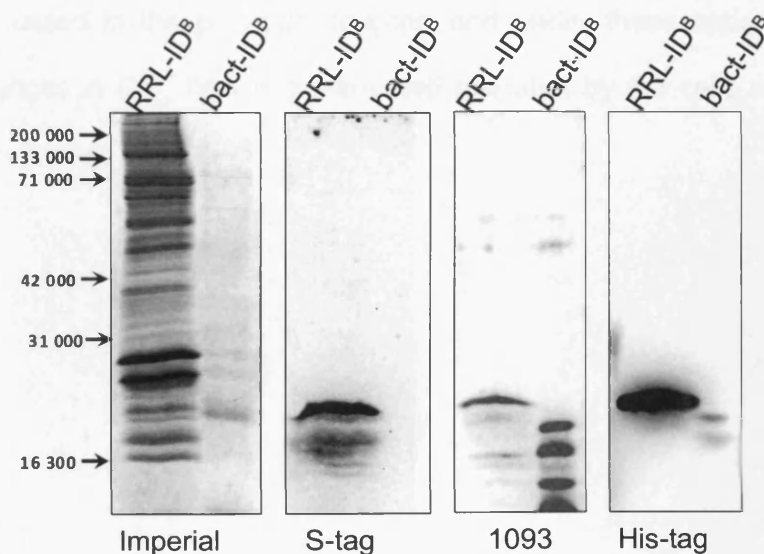


**Figure 6.6. Successful purification and detection of bacterially produced ID<sup>B</sup>**

ID<sup>B</sup> (right-hand lanes) purified from bacterial culture by Ni<sup>2+</sup> affinity followed by S-protein affinity systems were separated by SDS-PAGE (10% (v/v)), and visualised with Imperial protein stain and detected by S-tag, ab1093 and His-tag detection. Non-purified *in vitro*-synthesised ID<sup>B</sup> (Left-hand lanes) was used to illustrate the size difference in bacterially-produced ID<sup>B</sup> after S-tag cleavage. Each lane contains 1/20 of the resuspension volume for each extraction method (equivalent to 100ml of original bacterial culture).

#### 6.3.4 Effect of bacterially-produced ID<sup>B</sup> on resting cells

Following the assessment of the changes in HL-1 Ca<sup>2+</sup> handling phenotype induced by microinjection of ID<sup>B</sup> protein produced in a cell-free RRL system (Chapter 4), the effect of bacterially produced ID<sup>B</sup> was also investigated to validate the results discussed previously. SALVO analysis (Figure 6.7) revealed that bacterially-produced ID<sup>B</sup> caused a significant change in every parameter measured, when compared with the effects of RRL (★) or ID<sup>B</sup> produced *in vitro* (#). However, despite these marked alterations in cellular Ca<sup>2+</sup>-handling parameters, the synchrony remained comparable to that seen in cells injected with RRL, *in vitro* synthesised ID<sup>B</sup> and WT HL-1 cells (Figure 6.8). These findings support the results discussed in the previous chapter, and under these experimental conditions, substantial changes in Ca<sup>2+</sup> handling were well tolerated by the cells and did not abolish intercellular synchrony.



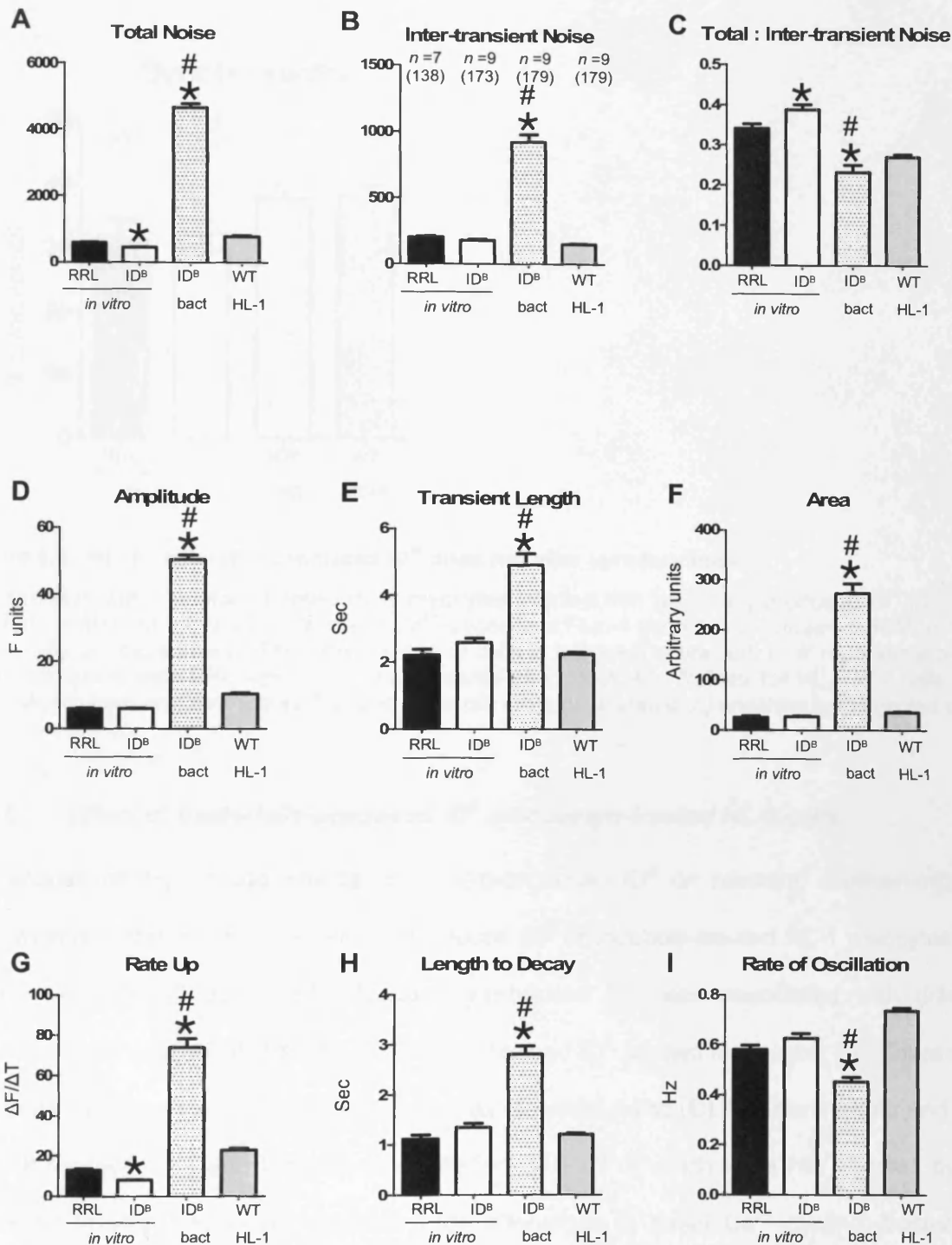


**Figure 6.7. SALVO analysis of the effects of bacterially produced ID<sup>B</sup> on HL-1 myocyte monolayers.**

Spatio-temporal Ca<sup>2+</sup> handling parameters in HL-1 myocytes injected with bacterially-produced ID<sup>B</sup> (ID<sup>B</sup> bact, spotted), plotted from SALVO analysis of Ca<sup>2+</sup>-dependent Fluo-4 fluorescence (mean  $\pm$  SEM, n = 7-9, 15-20 cells per experiment). The total number of cells is indicated in brackets). \* represents p<0.05 when compared with RRL-injected ouabain-treated HL-1 myocytes. # represents p<0.05 when compared with ouabain-treated HL-1 cells injected with ID<sup>B</sup> produced *in vitro*. Values for HL-1 WT cells (light grey), and *in vitro* proteins (RRL black, ID<sup>B</sup> white) shown here from the results shown in Chapter 5.

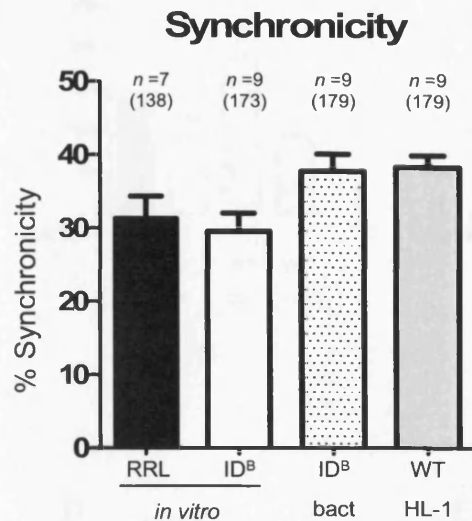


**Figure 6.8. MI of bacterially-produced ID<sup>B</sup> does not alter synchronicity**

Synchronicity within ouabain-treated HL-1 myocytes injected with bacterially-produced ID<sup>B</sup> (ID<sup>B</sup> bact, spotted), plotted from SALVO analysis of Ca<sup>2+</sup>-dependent Fluo-4 fluorescence (mean  $\pm$  SEM, n = 7-9, 15-20 cells per experiment). The total number of cells is indicated in brackets). \* represents p<0.05 when compared with RRL-injected ouabain-treated HL-1 controls. Values for HL-1 WT cells (light grey) shown here are from Figure 5.6, and were not included in statistical analyses with injected cells.

### 6.3.5 Effect of bacterially-produced ID<sup>B</sup> on ouabain-treated HL-1 cells

Because of the striking effects of *in vitro*-produced ID<sup>B</sup> on rescuing ouabain-induced dyssynchrony, the effect of bacterially-produced ID<sup>B</sup> on ouabain-treated HL-1 myocytes was also investigated (Figure 6.9). Bacterially-produced ID<sup>B</sup> was associated with different alterations to those observed with *in vitro* synthesised ID<sup>B</sup> (shown in Chapter 5). There were pronounced differences in the ratio of total:inter-transient noise (C), transient length and area (E & F respectively), and the rate of oscillation (I) – all of which were not affected by ID<sup>B</sup> produced *in vitro*. However, despite large alterations in basal Ca<sup>2+</sup> cycling, bacterially-produced ID<sup>B</sup> restored the synchrony in the ouabain-treated monolayer to 55.14%  $\pm$  4.80, which was comparable to both cells containing *in vitro* produced ID<sup>B</sup> (34.6%  $\pm$  2.43) and WT HL-1s (49.4%  $\pm$  4.19). These compelling findings further corroborated the results seen in Chapter 5, and showed the potential utility of ID<sup>B</sup> in normalising intercellular coupling and synchrony.

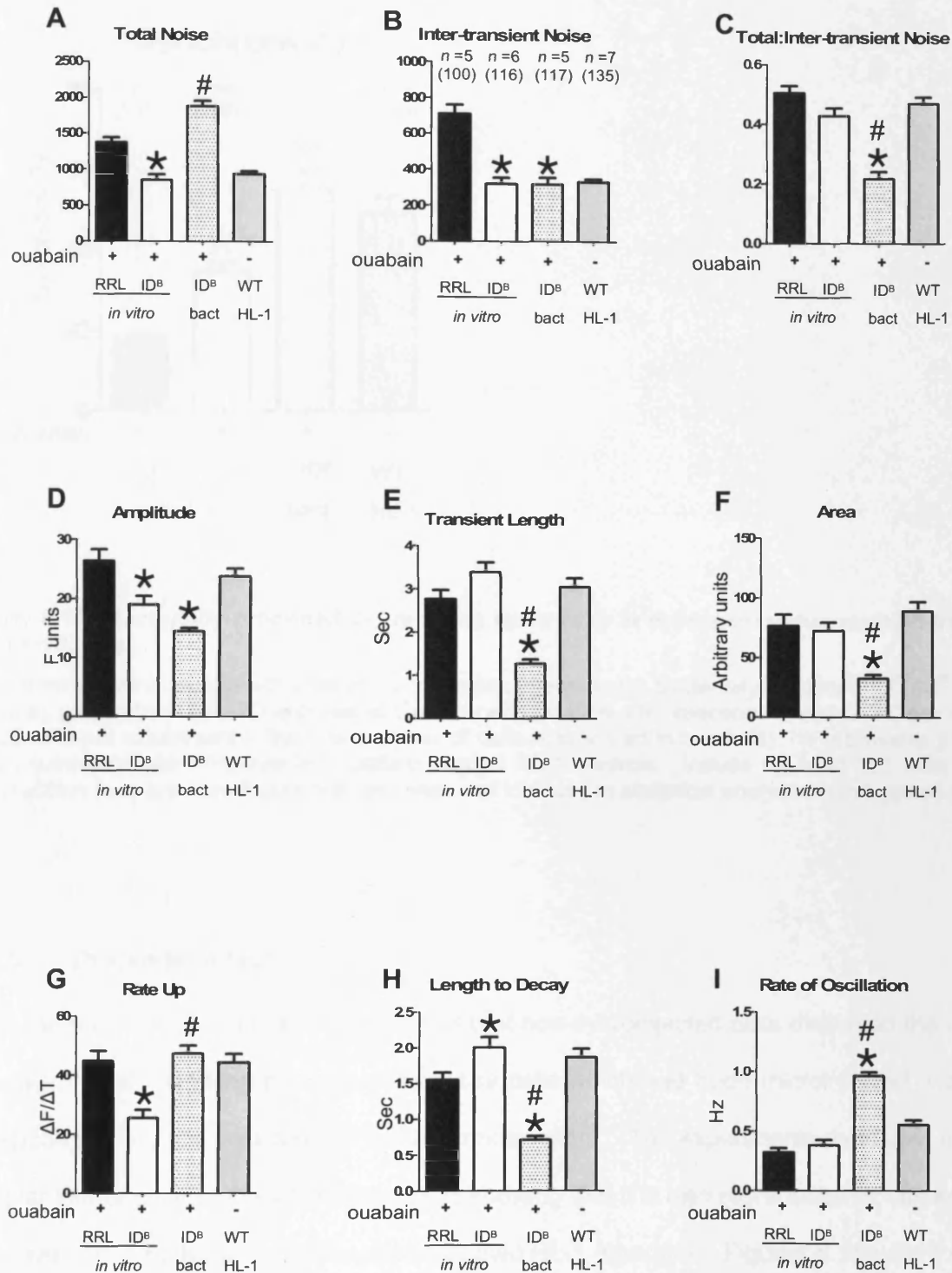


**Figure 6.9. SALVO analysis of the effects of bacterially produced ID<sup>B</sup> on HL-1 myocyte monolayers pre-treated with 100 nM ouabain**

Spatio-temporal Ca<sup>2+</sup> handling parameters in ouabain-treated HL-1 myocytes injected with bacterially-produced ID<sup>B</sup> (ID<sup>B</sup> bact, spotted), plotted from SALVO analysis of Ca<sup>2+</sup>-dependent Fluo-4 fluorescence (mean ± SEM, n = 5-7, 15-20 cells per experiment. The total number of cells is indicated in brackets). \* represents p<0.05 when compared with RRL-injected ouabain-treated HL-1 myocytes. # represents p<0.05 when compared with ouabain-treated HL-1 cells injected with ID<sup>B</sup> produced *in vitro*. Values for HL-1 WT cells (light grey), and *in vitro* proteins (RRL black, ID<sup>B</sup> white) shown here from the results shown in Chapter 5.

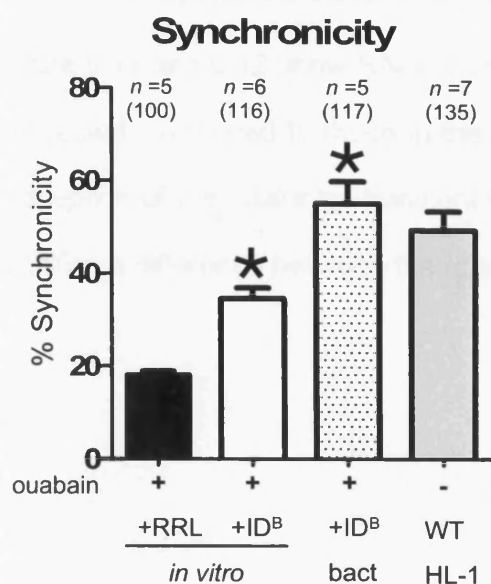


**Figure 6.10. Bacterially-produced ID<sup>B</sup> restores synchrony in dyssynchronous ouabain-treated HL-1 myocytes.**

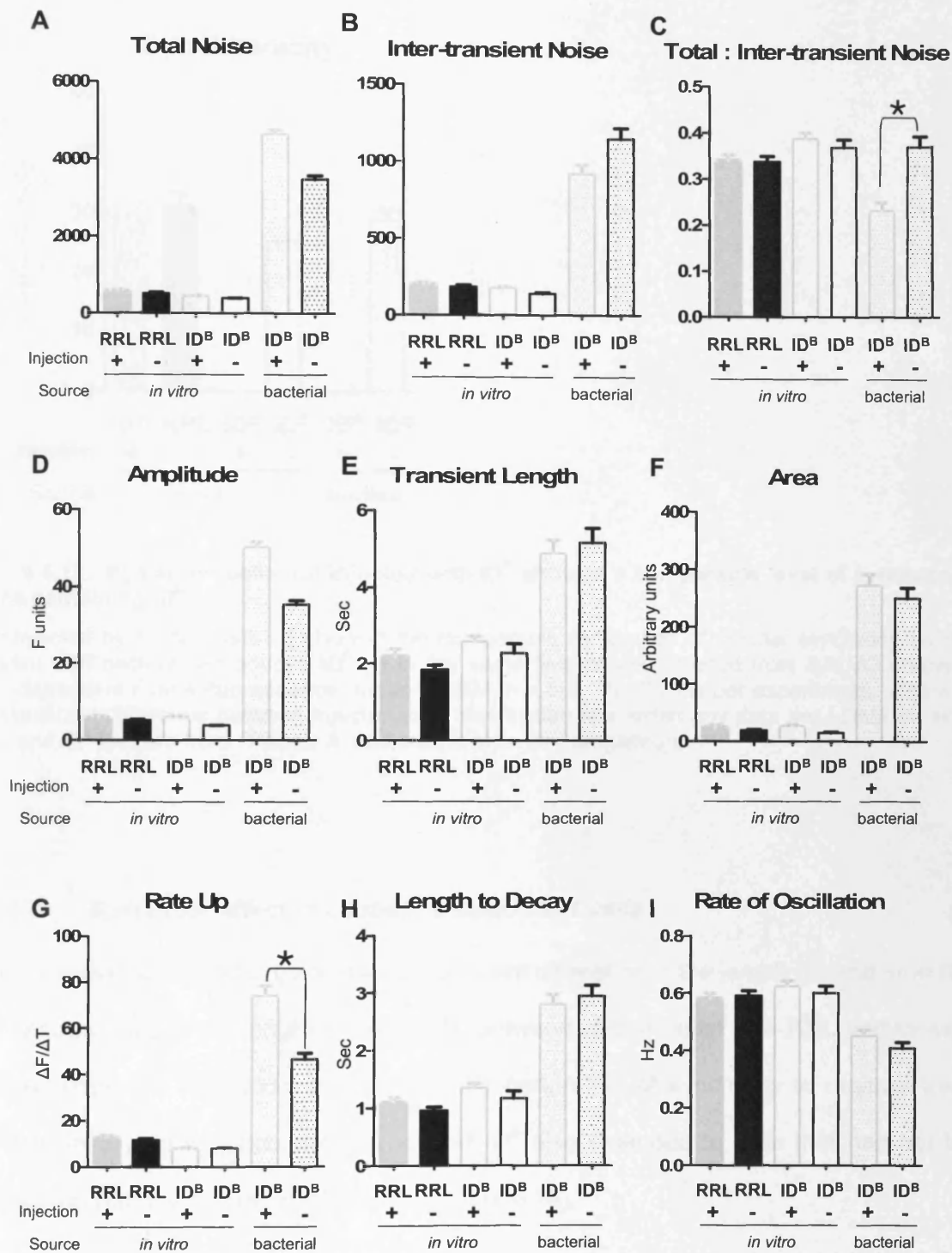
Synchronicity within ouabain-treated HL-1 myocytes injected with bacterially-produced ID<sup>B</sup> (ID<sup>B</sup> bact, spotted), plotted from SALVO analysis of Ca<sup>2+</sup>-dependent Fluo-4 fluorescence (mean  $\pm$  SEM, n = 5-7, 15-20 cells per experiment). The total number of cells is indicated in brackets). \* represents p < 0.05 when compared with RRL-injected ouabain-treated HL-1 controls. Values for HL-1 WT cells (light grey) shown here are from Figure 5.6, and were not included in statistical analyses with injected cells.

### 6.3.6 Bystander effect

In the previous chapter, it was observed that non-microinjected cells displayed the same changes in Ca<sup>2+</sup>-handling phenotype as those cells which had been microinjected with ID<sup>B</sup> produced *in vitro*, and was termed the 'bystander effect'. The experiments described in this chapter further support this phenomenon by showing that it is also reproduced by bacterially-produced ID<sup>B</sup> in both resting and ouabain-treated HL-1 myocytes. Figures 6.11 – 6.14 show that in the majority of the parameters, including synchrony, any change exhibited by microinjected cells is mirrored in non-injected cells in the same field of view.

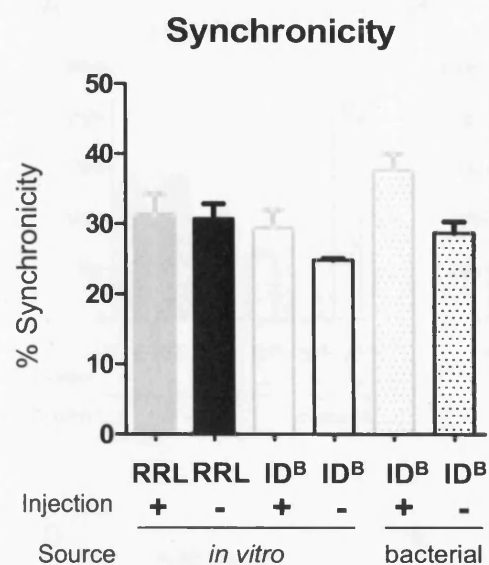
**6.3.6.1 The bystander effect in HL-1 cells**

Figure 6.11 and 6.12 show SALVO analysis of HL-1 myocytes cells which have not been microinjected, compared to those in the same field of view which have been injected. With the exception of the total:inter-transient noise ratio (C) and transient rate up (G), there was no significant difference between the injected and non-injected cells.



**Figure 6.11. SALVO analysis shows a bystander effect in non-injected HL-1 myocytes**

Non-injected HL-1 myocytes (-) exhibit the same alterations in most spatio-temporal  $\text{Ca}^{2+}$  handling parameters as those injected with bacterially-produced ID<sup>B</sup> (+), plotted from SALVO analysis of  $\text{Ca}^{2+}$ -dependent Fluo-4 fluorescence (mean  $\pm$  SEM,  $n = 5-9$ , 15-20 cells per experiment). \* represents  $p < 0.05$  between injected cells and non-injected bystander cells. Data for *in vitro* RRL and ID<sup>B</sup> is taken from Chapter 4, and shown here for comparison.



**Figure 6.12. Bystander cells not injected with ID<sup>B</sup> showed a comparable level of synchrony as those containing ID<sup>B</sup>**

Non-injected bystander cells (-) showed the comparable restoration of cellular synchrony as those injected with bacterially-produced ID<sup>B</sup> (+) in the same field of view, plotted from SALVO analysis of Ca<sup>2+</sup>-dependent Fluo-4 fluorescence (mean  $\pm$  SEM, n = 5-9, 15-20 cells per experiment). There was no significant difference between injected cells and bystanders within any data set. Data for *in vitro* RRL and ID<sup>B</sup> is taken from Chapter 4, and shown here for comparison.

### 6.3.6.2 Bystander effect in ouabain-treated HL-1 cells

In ouabain-treated cells, there was a significant difference in the length (E) and area (F) of the transient, and in the length to decay (H) between cells injected with RRL and those not injected (Figure 6.13). Most importantly, the restoration of synchrony in ouabain-treated cells microinjected with bacterially-produced ID<sup>B</sup> also extended to cells that had not been transduced with the recombinant protein (Figure 6.14).

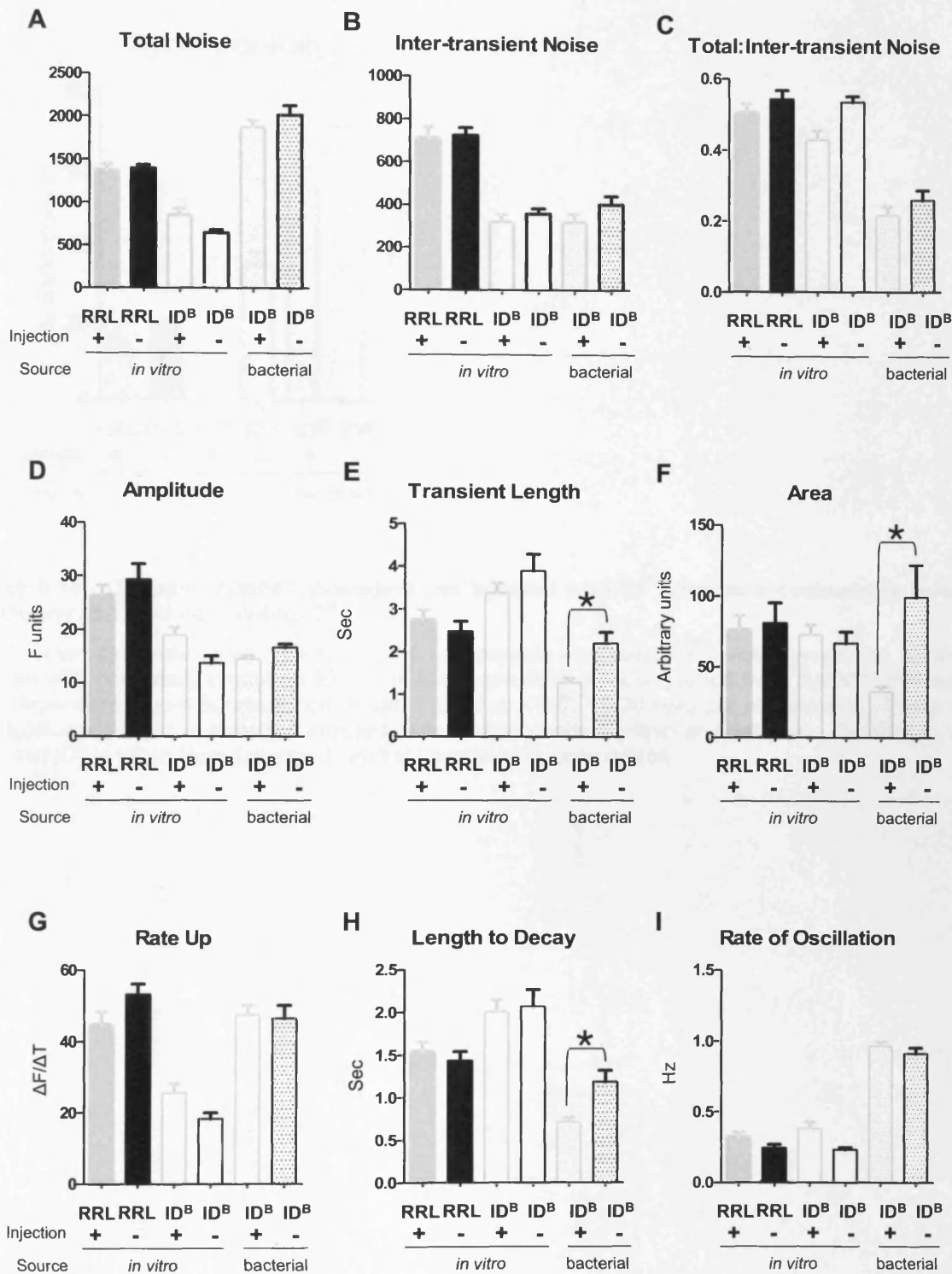


**Figure 6.13. SALVO analysis shows a bystander effect in non-injected ouabain-treated HL-1 myocytes**

Non-injected HL-1 myocytes (-) exhibit the same alterations in most spatio-temporal  $\text{Ca}^{2+}$  handling parameters as those injected with bacterially-produced ID<sup>B</sup> after incubation with 100 nM ouabain (+), plotted from SALVO analysis of  $\text{Ca}^{2+}$ -dependent Fluo-4 fluorescence (mean  $\pm$  SEM,  $n = 5-7$ , 15-20 cells per experiment). \* represents  $p < 0.05$  between injected cells and non-injected bystander cells. Data for *in vitro* RRL and ID<sup>B</sup> is taken from Chapter 4, and shown here for comparison.



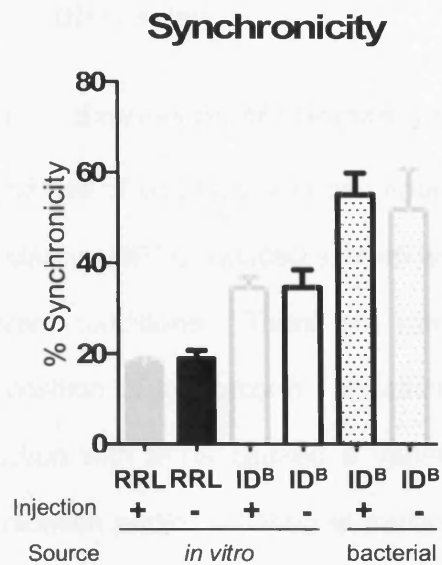


**Figure 6.14. Ouabain-treated bystanders not injected with ID<sup>B</sup> showed a comparable level of synchrony as those containing ID<sup>B</sup>**

Non-injected bystander cells (-) showed the comparable restoration of cellular synchrony as those injected with bacterially-produced ID<sup>B</sup> (+) in the same field of view, plotted from SALVO analysis of Ca<sup>2+</sup>-dependent Fluo-4 fluorescence (mean  $\pm$  SEM, n = 5-7, 15-20 cells per experiment). There was no significant difference between injected cells and bystanders within any data set. Data for *in vitro* RRL and ID<sup>B</sup> is taken from Chapter 4, and shown here for comparison.

## **6.4 Discussion**

### **6.4.1 Expression of I-Domain proteins in a bacterial expression system**

The use of BL21-derived bacterial cells for the expression of full-length I-Domain protein in a classical IPTG-induced system was unsuccessful despite the investigation of an array of different conditions. There are many possible reasons for this, including the size and composition of the protein. In addition to this, our data suggested that in this instance, induction with IPTG caused a variety of stress responses in the cell such as proteolytic degradation and/or initiation at multiple sites of transcription (Donovan *et al.* 1996; Kosinski & Bailey 1991).

The use of an autoinduction system was better suited for the expression of I-Domain proteins, and successfully expressed ID<sup>B</sup> which was subsequently purified and used for microinjection into HL-1 myocytes.

### **6.4.2 Bacterially-produced ID<sup>B</sup> modifies cellular Ca<sup>2+</sup> handling differently to ID<sup>B</sup> produced *in vitro* without altering synchrony**

This chapter has provided further support for the observations of Chapters 4 and 5, by showing that perturbation of various aspects of Ca<sup>2+</sup> handling, at least under the conditions tested, did not ablate intercellular synchrony (summarised in

Table 6.3). However, it is intriguing that in ouabain-treated cells, alteration of these parameters was associated with a restoration of synchrony. This validates the observations discussed in previous chapters and suggests that the extent of intercellular synchrony is controlled by the complex interplay between an array of Ca<sup>2+</sup> signalling parameters. Further work is necessary here to delineate the mechanistic basis of these findings.

Figures 6.7, 6.8, 6.9 and 6.10 profound differences in the bioactivity of ID<sup>B</sup> fragments generated *in vitro* or bacterial expression methodologies. This could be due to a number of reasons. The bacterially synthesised proteins have undergone S-tag cleavage as part of the

large-scale purification process, and this may enhance the bioactivity of the proteins. Additionally, bacterial expression systems allow for secondary modification of proteins, which does not occur in cell free systems. Furthermore, the bacterially-produced sample contains detectable amounts of several truncated ID species which were detected by ab1093 (Figure 6.6). These truncated fragments may be bioactive, and therefore may cumulatively increase the ID<sup>B</sup> phenotype observed in microinjected cells.

Some or all of the considerations may contribute to the stark differences observed on Ca<sup>2+</sup> handling parameters. Notably, the restoration of synchrony is equivalent in both methodologies. Further work will be necessary to determine how discrepant mechanisms can result in a comparable effect on synchrony - a robust index of intra- and inter-cellular Ca<sup>2+</sup> handling - and indeed, how this is determined by the source of the protein.

Table 6.3. Summary of alterations of spatio-temporal Ca<sup>2+</sup> handling parameters

	Total Noise	Intertransient Noise	Total: Intertransient Noise	Amplitude	Transient Length	Area	Rate Up	Length to Decay	Rate of Oscillation	Synchronicity
HL-1 + RRL	-	-	×	-	-	-	-	-	×	-
HL-1 + ID <sup>B</sup>	×	-	×	-	-	-	×	-	-	-
HL-1 + bact ID <sup>B</sup>	×	×	×	×	×	×	×	×	×	-
HL-1 + oua +RRL	×	-	-	×	×	×	-	×	×	-
HL-1 + oua +ID <sup>B</sup>	×	×	-	×	-	-	×	×	-	↑
HL-1 + oua + bact ID <sup>B</sup>	×	×	×	×	×	×	×	×	×	↑

Table summarising the changes observed in microinjected cells compared with controls, as discussed above. (-) refers to an unchanged parameter; (×) indicates a significant change compared to the appropriate control; (↑) indicates a significant increase in cellular synchronicity.

### 6.4.3 Effect of bacterially-produced ID<sup>B</sup> on arrhythmic HL-1 myocytes

The previous chapter reported the striking effect of ID<sup>B</sup> produced *in vitro* on the restoration of synchrony in dyssynchronous ouabain-treated HL-1 cells, to a level which is comparable to that seen in WT HL-1 cells. This observation was validated by the demonstration here that bacterially-produced ID<sup>B</sup> also restored synchrony and provided further support that this phenomenon was not an artefact of the expression system used to produce the protein.

### 6.4.4 Bystander effect

Chapter 5 reported that cells not subjected to microinjection displayed the same alterations in Ca<sup>2+</sup> handling as neighbouring cells which had been injected with ID<sup>B</sup> produced *in vitro*. Importantly, this observation was also reproduced here using bacterially produced ID<sup>B</sup>, and showed that the existence of a 'bystander' effect in our experiments is robust and not dependent on the source of the injected protein. A strong bystander effect has significant implications for the therapeutic modulation of synchrony in the intact myocardium and this will be discussed in more detail in Chapter 8.

The results presented here persuasively show that microinjection of a discrete and identifiable cell population triggered changes in neighbouring cells (a phenomenon termed the bystander effect). This phenomenon is more fully appraised in Chapter 8. It should be noted that in all experiments presented in this thesis, the findings must be interpreted in the knowledge of an existing bystander effect. Despite several experimental manipulations, we were not able to block this effect (see Chapter 8). Consequently, it is accepted that a limitation of the conclusions presented in this thesis is that we did not separate out the distinct effects of recombinant RyR2 fragments in isolated populations of microinjected cells, versus those results obtained in the presence of a bystander effect. Ongoing experiments are presently addressing this issue.

## ***Chapter 7***

***Determining the effects of ID<sup>B</sup> on IP<sub>3</sub>R-  
dependent Ca<sup>2+</sup> signalling in HEK cells***

## 7.1 Introduction

### 7.1.1 Inositol 1,4,5-trisphosphate receptors

Inositol 1,4,5-trisphosphate receptors (IP<sub>3</sub>R) are large tetrameric channels (approximately 250-300 kDa) that belong to a superfamily of ion channels with six TM domains. They are unique in exhibiting dual regulation of channel opening by two second messengers, IP<sub>3</sub> and Ca<sup>2+</sup> and are responsible for the generation and control of diverse and complex Ca<sup>2+</sup> signals (Dawson 1997; Taylor 1998).

Although RyRs are the principal Ca<sup>2+</sup> release channels within cardiomyocytes, they are not the only route for Ca<sup>2+</sup> to be mobilised from intracellular stores. Cardiac myocytes also express IP<sub>3</sub>Rs, albeit at ~100-fold lower levels than RyRs. Although IP<sub>3</sub>Rs absolutely require InsP<sub>3</sub> for activation, they can also be considered as CICR channels, since cytosolic Ca<sup>2+</sup> has a bimodal effect on IP<sub>3</sub>R open probability similar to its actions on RyR (Roderick *et al.* 2003). IP<sub>3</sub>Rs are structurally and functionally similar to RyRs. They have the same tetrameric quatrefoil structure and similarly possess carboxy-terminal transmembrane helices that form the ion pore and a large cytoplasmic amino-terminal portion (Bootman & Roderick 2008) (Figure 7.1). Like RyRs, three isoforms of IP<sub>3</sub>R have been identified (Blondel *et al.* 1994; Iwai *et al.* 2005; Newton *et al.* 1994; Yamada *et al.* 1994; Yamamoto-Hino *et al.* 1994). Although each isoform has a different affinity to IP<sub>3</sub>, biochemical analysis showed a similar affinity of the IP<sub>3</sub>-binding core to IP<sub>3</sub> for each of the isoforms thus revealing that the IP<sub>3</sub>-binding suppressor domain linked to the N-terminal side of the binding core may be responsible for the isoform-specific tuning of IP<sub>3</sub>-binding affinity (Iwai *et al.* 2007).

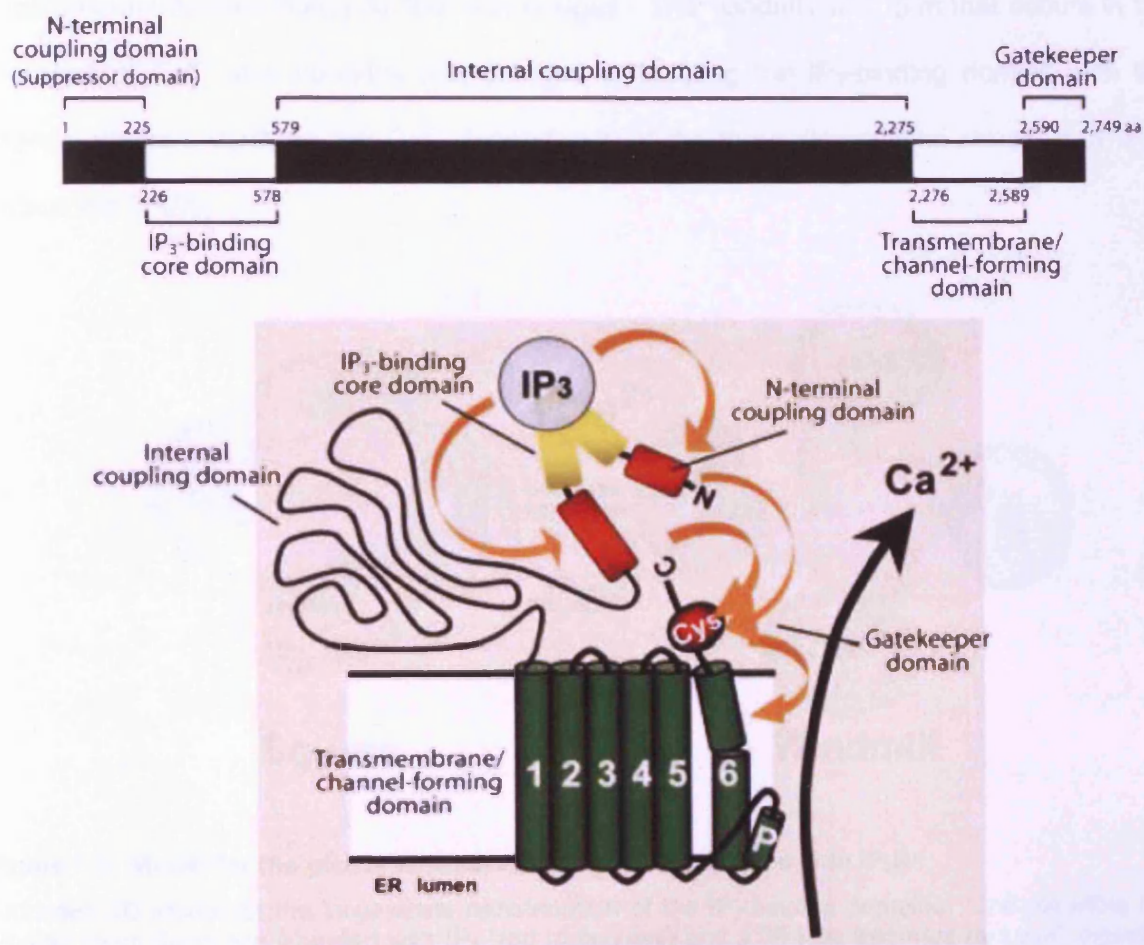


**Figure 7.1. Five-domain structural model IP<sub>3</sub>R**

The structure of IP<sub>3</sub>R (depicted here as IP<sub>3</sub>R1) is divided into five functional domains. The binding of IP<sub>3</sub> is transduced by the N-terminal and internal coupling domains to the gatekeeper domain, which triggers a conformational change in the activation gate formed within the transmembrane/ channel-forming domain (Mikoshiba 2007).

The three-dimensional structure of IP<sub>3</sub>R1 has been visualised by several groups using EM (da Fonseca *et al.* 2003; Hamada *et al.* 2002, 2003; Jiang *et al.* 2002b; Sato *et al.* 2004; Serysheva *et al.* 2003) that revealed a reversible transition between two distinct structures with four-fold symmetry – a ‘windmill’ structure and a ‘square’ structure (Figure 7.2). Supporting biochemical studies suggested that transition from the ‘square’ to the ‘windmill’ conformation was promoted by Ca<sup>2+</sup> via the relocation of four peripheral IP<sub>3</sub>-binding domains. The structure in the absence of Ca<sup>2+</sup>, as reconstructed using EM, shows a ‘mushroom-like’ appearance, similar to RyR, consisting of a large square-shaped head and a

small channel domain linked by four thin bridges. The 'windmill-like' form that occurs in the presence of  $\text{Ca}^{2+}$  also contains four bridges connecting the  $\text{IP}_3$ -binding domain with the channel domain, verifying the  $\text{Ca}^{2+}$ -dependence of the three-dimensional structure of  $\text{IP}_3\text{R}$  (Mikoshiba 2007).

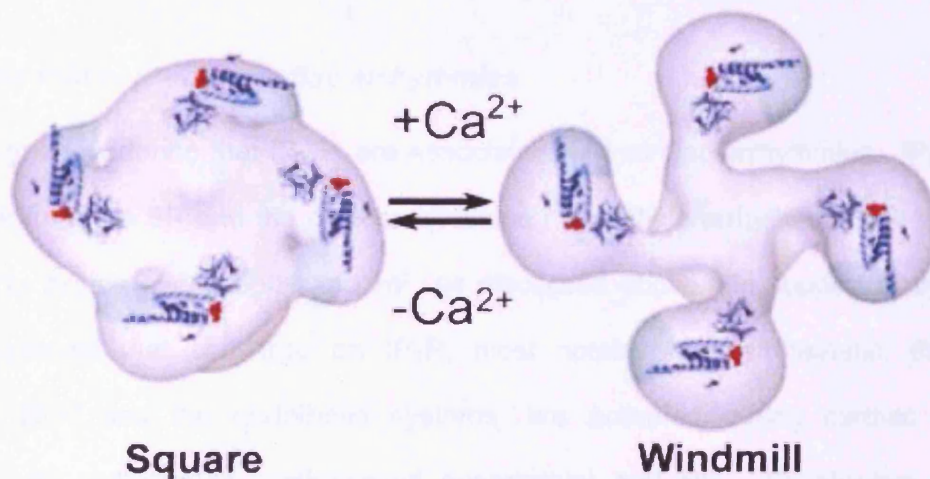


**Figure 7.2. Model for the global structural changes that occur within  $\text{IP}_3\text{R1}$**

Proposed 3D model for the large-scale redistribution of the  $\text{IP}_3$ -binding domains. The plausible  $\text{IP}_3$ -binding cores (blue) are liganded with  $\text{IP}_3$  (red molecules) and a 38-kDa fragment by Lys-C digestion (green) (Mikoshiba 2007).

The previous chapters showed that  $\text{ID}^{\text{B}}$  modulated  $\text{RyR2}$   $\text{Ca}^{2+}$  release, presumably by altering intra-molecular rearrangement – a mechanistic feature common to both  $\text{RyR2}$  and  $\text{IP}_3\text{R}$ . Like  $\text{RyR}$ , the structure of  $\text{IP}_3\text{R}$  has traditionally been divided into functional domains: the N-terminal ligand-binding domain; the modulatory/coupling domain; and the C-terminal transmembrane/channel-forming domain (Furuichi *et al.* 1989, 1994). Studies have suggested that the channel-forming domain of  $\text{IP}_3\text{R1}$  is necessary to keep the channel closed, and that the binding of  $\text{IP}_3$  is transduced by long-range modulation of N-terminal and internal coupling domains to the gatekeeper domain, which triggers a conformational change the transmembrane channel-forming domain (Mikoshiba 2007).

As discussed in Chapter 3, bioinformatic comparisons revealed striking structural homology between sub-fragments of the  $\text{RyR2}$  I-Domain and I-Domain-like regions of  $\text{IP}_3\text{R}$ ,



despite the absence of any notable primary sequence homology between these two  $\text{Ca}^{2+}$  release channels (Appendix II). In light of this, the study of RyR2 I-Domain fragments, that exhibited profound effects on RyR2-dependent  $\text{Ca}^{2+}$  handling, was extended to investigate their effects on  $\text{IP}_3\text{R}$  channel regulation.

### **7.1.2 *The role of $\text{IP}_3\text{R}$ in cardiac arrhythmias***

There is good evidence that  $\text{IP}_3\text{Rs}$  are associated with cardiac arrhythmias.  $\text{IP}_3$ -induced  $\text{Ca}^{2+}$  release from the SR and the nuclear envelope may initiate arrhythmias and alter gene expression to induce hypertrophy and HF, as discussed above. In support of this, many signalling systems that converge on  $\text{IP}_3\text{R}$ , most notably the sympathetic, the renin-angiotensin (RA) and the endothelin systems, are activated during cardiac diseases associated with arrhythmias, pathological hypertrophy and HF. Substantive evidence suggests that  $\text{IP}_3$  signalling may be involved in the development and/or maintenance of atrial fibrillation, reperfusion arrhythmias, ankyrin-B-related arrhythmias, diabetic cardiomyopathy, hypertrophy and HF (summarised in Figure 7.3).

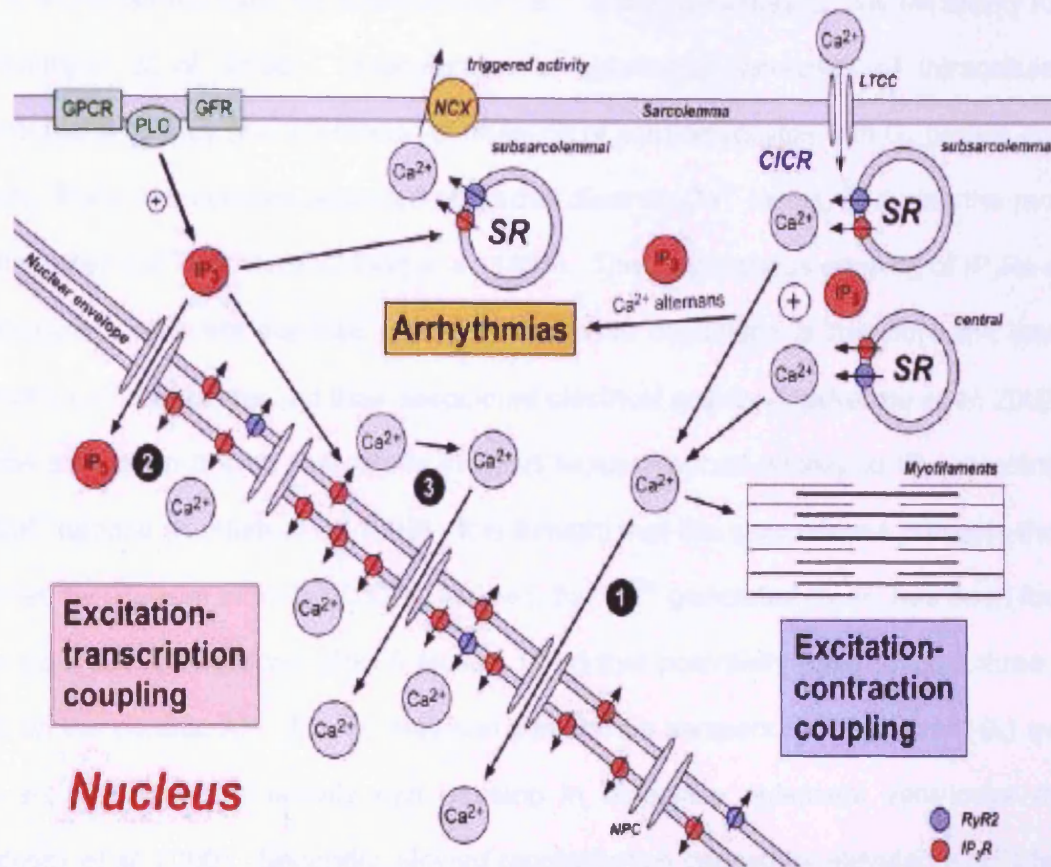


**Figure 7.3. Overview of cardiac IP<sub>3</sub>R signalling and its involvement in EC coupling, excitation-transcription (ET) coupling and arrhythmias.**

Schematic drawing of an adult cardiac myocyte showing parts of the sarcolemma, the nucleus, the SR and the myofilaments. G protein-coupled receptors (GPCR) increase cytoplasmic IP<sub>3</sub> concentration via activation of phospholipase C (PLC). EC-coupling is mediated by CICR from the SR through RyR2. Cytoplasmic Ca<sup>2+</sup> binds to the myofilaments and initiates contraction. IP<sub>3</sub>-induced Ca<sup>2+</sup> release from the SR through IP<sub>3</sub>R may contribute to EC-coupling by increasing the Ca<sup>2+</sup> transient and thus contraction. On the other hand, IP<sub>3</sub>-induced Ca<sup>2+</sup> release from the SR may trigger further Ca<sup>2+</sup> release through neighbouring RyR2 with subsequent activation of sarcolemmal NCX. This induces arrhythmias via generation of DADs and triggered activity. IP<sub>3</sub>-induced SR Ca<sup>2+</sup> release also generates pro-arrhythmic Ca<sup>2+</sup> alternans (Kockskämper *et al.* 2008).

Furthermore, a recent study by Domeier *et al.* (2008) reported that InsP<sub>3</sub>R activation underlies the positive inotropic action of endothelin-1 (ET-1) on ventricular myocytes. ET-1 is a potent vasoconstrictive hormone that has been shown to have inotropic, arrhythmic, and hypertrophic effects on cardiomyocytes. Despite the relatively low levels of InsP<sub>3</sub>R in cardiac cells, they can influence cardiac Ca<sup>2+</sup> signalling by contributing to systolic Ca<sup>2+</sup> increases because of the ability to act as 'feed-forward' CICR channels (Figure 7.3). Binding

of IP<sub>3</sub> to IP<sub>3</sub>Rs primes them for activation by Ca<sup>2+</sup>, and also increases their sensitivity to Ca<sup>2+</sup> (Kockskämper *et al.* 2008). Therefore, with substantial increases of intracellular IP<sub>3</sub> concentrations as may occur following stimulation of cardiomyocytes with G<sub>q</sub> protein-coupled agonists, IP<sub>3</sub>Rs can become activated at normal diastolic Ca<sup>2+</sup> levels, or during the recovery of a stimulated Ca<sup>2+</sup> transient (Gilbert *et al.* 1991). The promiscuous opening of IP<sub>3</sub>Rs during the otherwise quiescent diastolic period under these conditions is therefore the cause of arrhythmic Ca<sup>2+</sup> transients and their associated electrical activity (Mackenzie *et al.* 2002).

It has also been shown that IP<sub>3</sub>Rs in heart tissue respond weakly to IP<sub>3</sub>, resulting in a slow Ca<sup>2+</sup> release (Kentish *et al.* 1990). It is thought that this slow release prevents the Ca<sup>2+</sup> generated by IP<sub>3</sub> from inducing CICR. Instead, the Ca<sup>2+</sup> generated by IP<sub>3</sub> has been found to initiate slow Ca<sup>2+</sup> oscillations (Zhu & Nosek 1991) that potentially have at least three acute effects on the cardiac AP. Firstly, they can stimulate a transient inward current (I<sub>ti</sub>) evoking DADs so that triggered activity can develop in otherwise quiescent ventricular muscle (Woodcock *et al.* 2000). Secondly, slowed repolarisation caused by elevated [Ca<sup>2+</sup>]<sub>i</sub> favours conditions for Ca<sup>2+</sup> re-entry (Kleber & Fast 1997); and thirdly, it can cause intercellular uncoupling with conduction slowing (Woodcock *et al.* 2000). Any of these alterations in myocardial electrical activity are potentially pro-arrhythmic. Furthermore, IP<sub>3</sub> has been reported to activate NCX (Gilbert *et al.* 1991), which may also be arrhythmogenic.

### 7.1.3 HEK293 cells as a model system

The HEK cell line has been extensively used as an expression tool for recombinant proteins since it was generated over 25 years ago by Graham *et al.* (1977). The transformation of human embryonic kidney (HEK) cells following exposure to sheared fragments of human adenovirus type 5 (Ad5) DNA generated the widely used HEK293 cell line. This permanently transformed cell line has incorporated Ad5 into chromosome 19 of the host genome, a modification used subsequently for the generation of transcription incompetent human adenoviral vectors (Thomas & Smart 2005). The current commercially

available source of HEK cell is from the original transformation (Graham *et al.* 1977). Although of epithelial origin, its biochemical machinery is capable of carrying out most of the post-translational folding and processing required to generate functional, mature protein from a wide spectrum of both mammalian and non-mammalian nucleic acids.

The principal attributes which have made the HEK cell a popular choice of model system to study receptor channels include its quick and easy reproduction and maintenance; amenability to transfection using a wide variety of methods; high efficiency of transfection and protein production; faithful translation and processing of proteins; and small cell size with minimal processes appropriate for voltage-clamp experimentation. These, and other attributes, also mean that complementary biochemical/cell biological evaluations of expressed proteins can be performed in parallel with functional analyses to establish detailed pharmacological and biophysical profiles for the action of new drugs and their targets (Thomas & Smart 2005).

Though popular as a transient expression system, this cell type has also been widely employed in stable transfection studies, and has been utilised for functional and biochemical studies on ionic channel proteins. Given its RyR-null status, HEK cells have proven useful in expressing all three isoforms of RyR for structure-function studies (Rossi *et al.* 2002; Xiao *et al.* 2002). Consequently, in this thesis HEK293 cells were used as a well-characterised, IP<sub>3</sub>R sufficient, RyR2-deficient model in which to investigate the effects of I-Domain sub-fragment proteins on IP<sub>3</sub>R-dependent cellular Ca<sup>2+</sup> handling.

#### **7.1.4 The use of 'noise' analysis to analyse Ca<sup>2+</sup> transients**

Unlike HL-1 cell monolayers, HEK cells do not exhibit large, spontaneous intercellular Ca<sup>2+</sup> release and thus the mode of data analysis used extensively for HL-1 cells experiments (SALVO) was not a suitable analysis tool for the analysis of agonist-evoked Ca<sup>2+</sup> signalling in HEK cells. Instead cellular noise was analysed by looking at signal variability (SV), which quantifies subtle changes in cellular Ca<sup>2+</sup> cycling and can be used to determine cell-to-cell

signal variability, in addition to agonist-induced changes within the same cell (George *et al.* 2006).

#### 7.1.4.1 Relative signal variability (RSV)

George *et al.* (2006) developed a novel calculation to assess relative changes in  $\text{Ca}^{2+}$  signal variability (SV) within a cell following the administration of  $\text{Ca}^{2+}$  channel agonists, termed the relative signal variability (RSV). The SV is calculated by the sum of point-to-point differences in  $\text{Ca}^{2+}$ -dependent fluorescence signals and as such is not influenced by agonist-induced gradients or background 'drift' in the data.

RSV (see Figure 7.4) is calculated by comparing the SV in a signal trace following cellular activation (i.e. by  $\text{Ca}^{2+}$  channel openers) ( $\text{SV}_B$ ) to the pre-activation SV in the same trace ( $\text{SV}_A$ ) i.e.

$$\text{RSV} = \text{SV}_B / \text{SV}_A$$

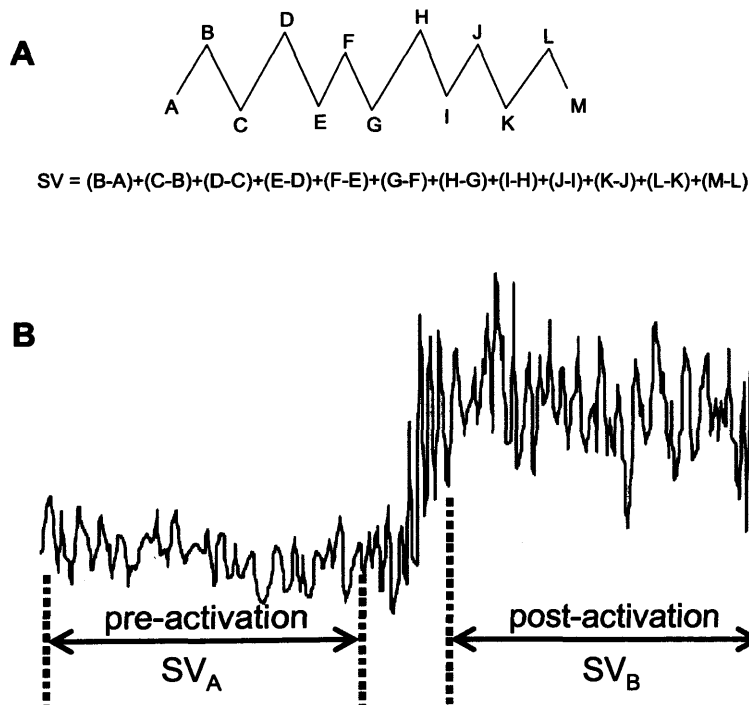


**Figure 7.4. Calculation of SV and RSV**

**Panel A:** Schematic illustration for calculating signal variability (SV), where SV is the sum of point-to-point differences in  $\text{Ca}^{2+}$  signals over a set time. **Panel B:** Schematic illustration for calculating relative signal variability (RSV) as a change in cellular  $\text{Ca}^{2+}$  handling before ( $\text{SV}_A$ ) and after ( $\text{SV}_B$ ) agonist administration in the same cell.

### 7.1.4.2 Indicators of signal variability

Studies in our laboratory have clearly demonstrated the limited utility of some commonly used indices of signal variability, including the F-ratio, coefficient of variance (CoV) and standard deviation (Fry 2008) since all of these indices of signal variability are significantly influenced by the inherent gradient or 'drift' frequently present in our confocal experiments (Figure 7.5).

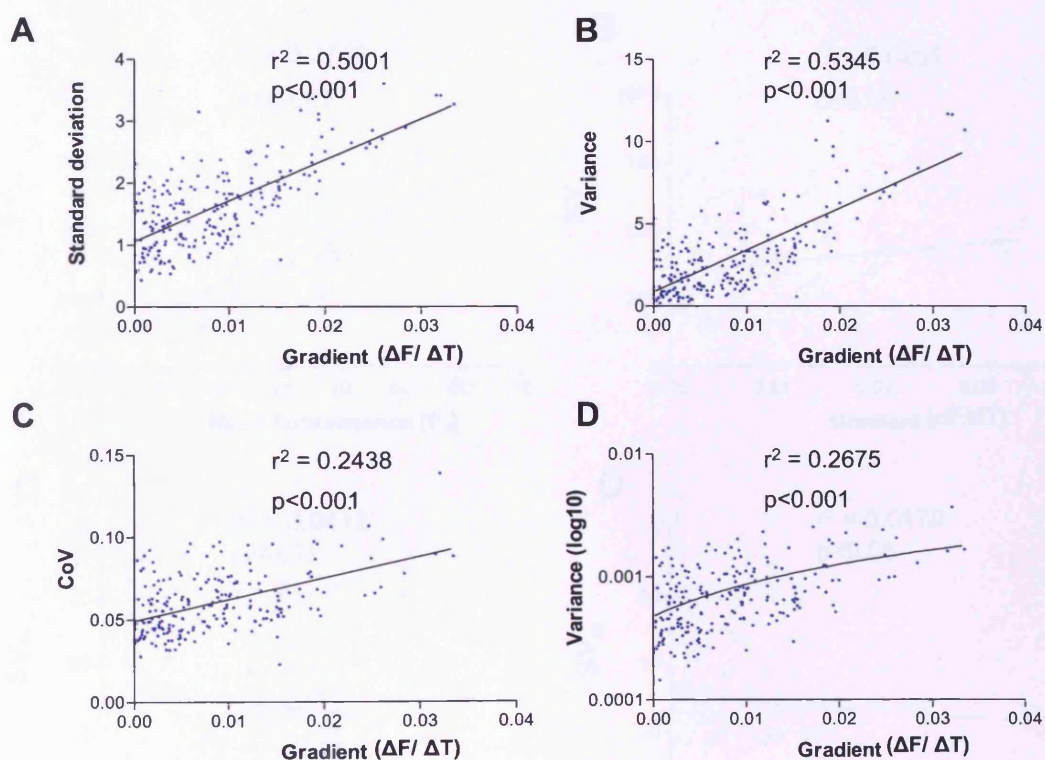


**Figure 7.5. Correlation between common indices of signal variability and gradient**

Gradient in the fluorescent signal was associated with an increase in signal variability as determined by standard deviation (A), variance (B), CoV (C) and log transformed variance (D).  $r^2$  refers to the gradient of the slope calculated by linear regression;  $p$  is the probability that the slope is significantly different to zero. Data are taken from fluo4-loaded HEK cells and was kindly supplied by Debra Fry (Fry 2008).

Analysis of  $\text{Ca}^{2+}$  traces from different non-stimulated cells was therefore performed using signal variability (SV) normalised to mean fluorescence ( $\text{SV}_m$ ), a novel indicator of signal variability. As shown in Figure 7.6,  $\text{SV}_m$  is largely independent of gradient and the signal intensity of the Fluo-4 loaded cells (mean fluorescence), and therefore provides a suitable and robust indicator of signal variability in this experimental system.

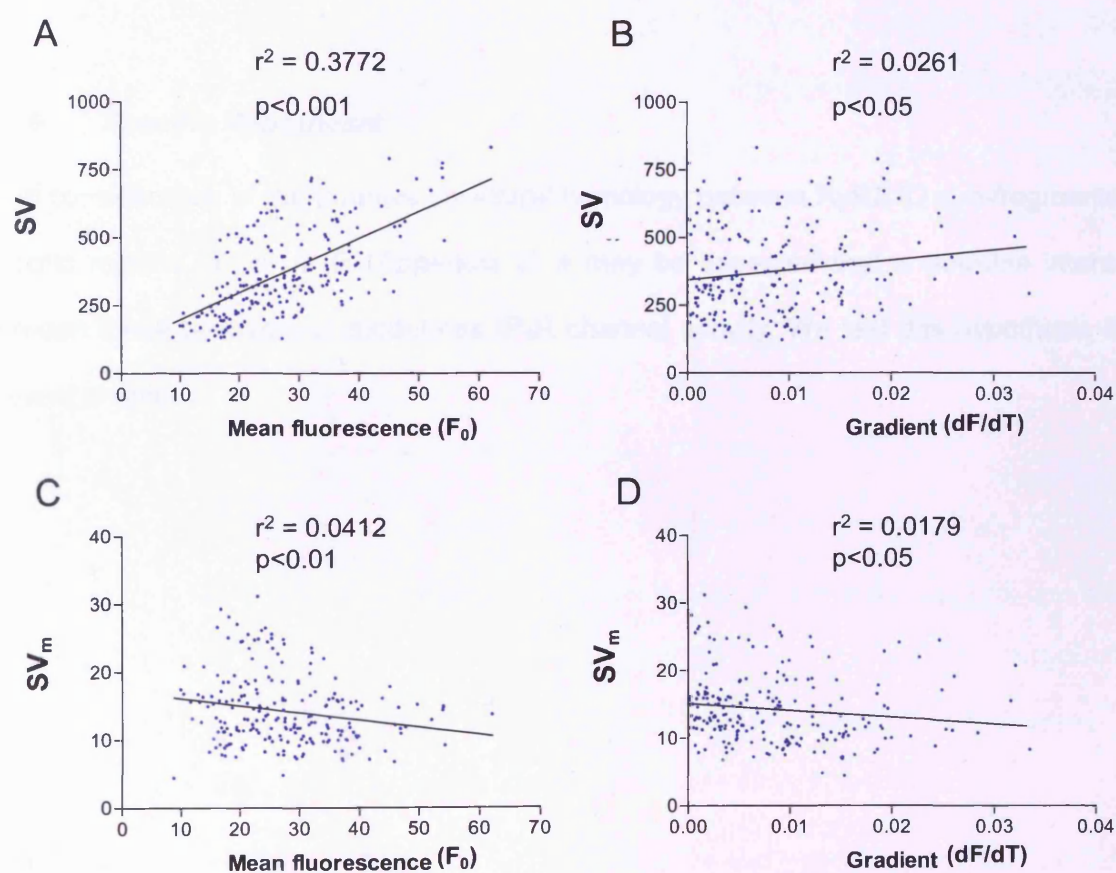


**Figure 7.6. Signal variability (SV) normalised to mean fluorescence ( $\text{SV}_m$ ) is independent of fluorescence and gradient.**

Scatter plots of data obtained from HEK cells ( $n=221$ ) showing the relationship between SV with mean fluorescence (A) and gradient (B), and  $\text{SV}_m$  with mean fluorescence (C) and gradient (D).  $r^2$  refers to the gradient of the slope calculated by linear regression;  $p$  is the probability that the slope significantly different to zero. Data were taken from fluo4-loaded HEK cells and was supplied by Debra Fry (Fry 2008).

### **7.1.5 Objectives of this chapter**

This chapter investigated the effect of MI of I-Domain proteins into HEK cells, by studying changes in agonist-evoked IP<sub>3</sub>R-dependent Ca<sup>2+</sup> transients, as opposed to the spontaneously oscillating Ca<sup>2+</sup> signals in HL-1 cardiac cells. This chapter aimed to determine whether recombinant ID<sup>B</sup> can modulate IP<sub>3</sub>R as would be predicted from bioinformatic analysis. The study was also extended to investigate the effects ID<sup>A</sup> and ID<sup>C</sup> on IP<sub>3</sub>R-dependent signalling using the fragments synthesised *in vitro* (Chapter 3).

### **7.1.6 Specific Hypothesis**

In consideration of the putative structural homology between RyR2 ID sub-fragments and specific regions of the IP<sub>3</sub>R (Appendix 2) it may be expected that a possible interaction between these two regions modulates IP<sub>3</sub>R channel activity. We test this hypothesis in the present chapter.



## 7.2 Methods

### 7.2.1 Preparation of HEK293 cells for MI

HEK293 cells were cultured and harvested as described in Chapter 2. The harvested cell pellet was resuspended in supplemented DMEM (Invitrogen) before plating onto poly-lysine coated glass chambers (14 mm diameter, 0.1 mm thickness, MatTek) at a density of  $5 \times 10^4$  cells/chamber. The cells were initially applied to the poly-lysine-coated chambers under a 200 $\mu$ l meniscus, and allowed to adhere to the glass for between 4 and 6 h before the chamber was flooded with an additional 1800 $\mu$ l of supplemented DMEM. These were left to adhere to the glass for 24 hours (37°C, 5% CO<sub>2</sub>, ~80% humidity) before being used for MI experiments. It is important that HEK cells are not allowed to grow beyond 50-60% confluency, as at this stage the loss of adhesion makes MI more difficult.

### 7.2.2 MI of recombinant protein and cellular Ca<sup>2+</sup> imaging

Cells were prepared for MI as described above, before loading with Fluo-4AM (10  $\mu$ M in 20% (w/v) pluronic acid F-127 dissolved in DMSO) in non-supplemented DMEM pre-warmed to 37°C. The dye-containing solution was added to each chamber as a 200  $\mu$ l meniscus and incubated for 30 minutes (37°C, 5% CO<sub>2</sub>, ~80% humidity). The cells were then immersed in a further 1800 $\mu$ l pre-warmed non-supplemented media 15 minutes prior to Ca<sup>2+</sup> imaging. Ca<sup>2+</sup> dependent Fluo-4AM fluorescence was imaged using a Leica RS2 confocal microscope with an oil immersion 40x objective lens, using an Argon/Krypton laser (excitation at 488nm, and the fluorescence emission detected at 500nm). 8-bit scaled data were acquired every 200 ms (5 Hz) in a field of view at 512 x 209 pixel resolution. Resting cells were imaged for 1 minute (300 frames) prior to MI in order to obtain a measurement of basal fluorescence levels.

Proteins synthesised and purified as described in Chapter 3 were injected into HEK293 cells using the optimal conditions determined in Chapter 4. The MagZ-purified protein

(Chapter 3) in injection buffer (100mM potassium chloride, 5mM potassium phosphate, pH 7.4; using chelex-treated dH<sub>2</sub>O), was co-injected with Alexa-647 dye conjugated to a 10,000 MW dextran (1µg/ml stock) as a non-transferable cellular marker of injection that enables the identification of microinjected cells, in a protein:buffer:dye of 1:2:1 (v/v) ratio. Approximately twenty cells per field of view were injected within a time frame of < 2 minutes, and allowed to recover for 5 minutes. After this time cells were imaged for 60 seconds (300 frames) before the addition of caffeine or carbachol, followed by imaging for a further 60 seconds (300 frames) as summarised in Figure 7.7. In every MI experiment, RRL without I-Domain protein, yet processed using MagZ-purification under exactly the same conditions as the RRL samples in which the I-Domain protein was synthesised, was used as a control for the reasons discussed previously (Chapter 4).

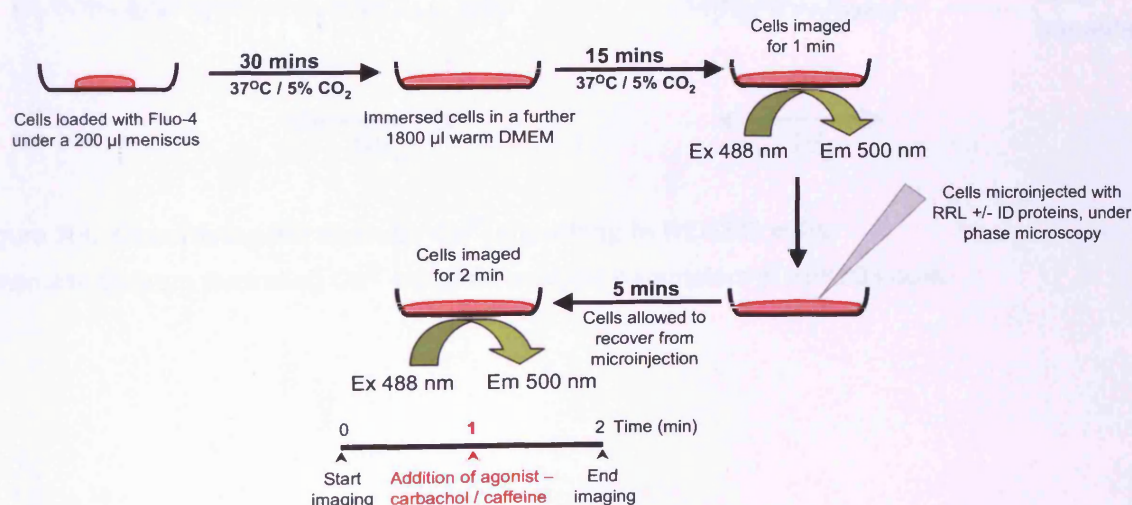
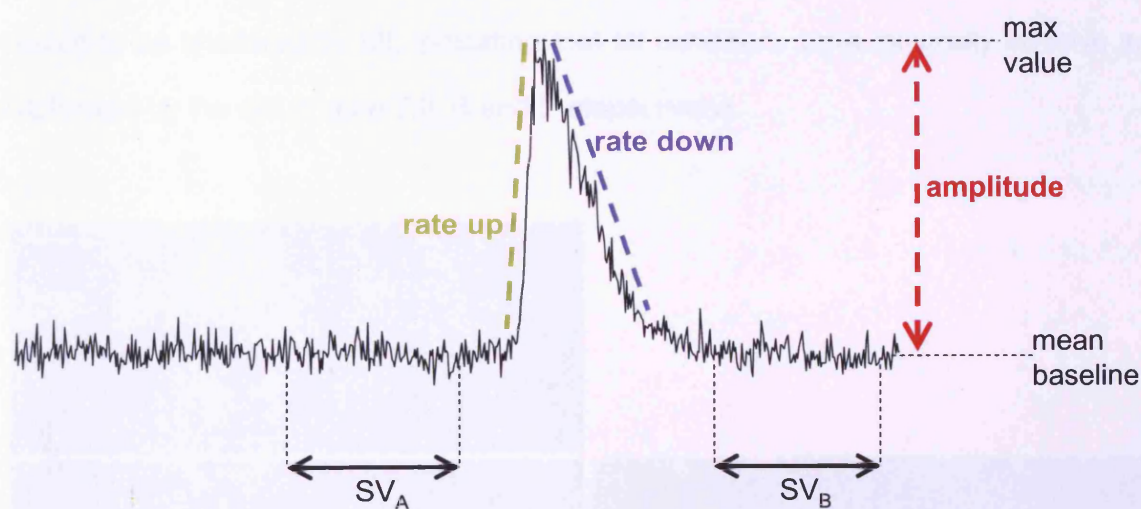


Figure 7.7. Schematic of MI experiments with HEK293 cells.

Data were acquired from regions of interest (ROIs) representing global  $\text{Ca}^{2+}$  environments, typically approximately  $50 \mu\text{m}^2$  in area ( $\sim 200$  pixels). These were collected and analysed using Leica confocal software (Leica Microsystems, Heidelberg, Germany). Further analysis was carried out using Microsoft Excel software and Graphpad Prism, in order to quantify the transient parameters outlined in Figure 7.8.



**Figure 7.8. Quantifying intracellular  $\text{Ca}^{2+}$  signalling in HEK293 cells**

Schematic diagram illustrating  $\text{Ca}^{2+}$  transient analysis parameters in HEK293 cells.

### 7.3 Results

#### 7.3.1 MI of recombinant proteins and markers in HEK293 cells

I-Domain proteins synthesised and purified as described in Chapter 3, were successfully microinjected into HEK293 cells, using the parameters optimised previously (Chapter 4). The use of a 647-alexa conjugated dye enabled the easy visual detection of microinjected cells (Figure 7.9, E). As with HL-1 myocytes, cell phenotype and Fluo-4 fluorescence appeared to be unaltered by MI, indicating that MI conditions were minimally invasive and well-tolerated by the cell (Figure 7.9, B and D respectively).

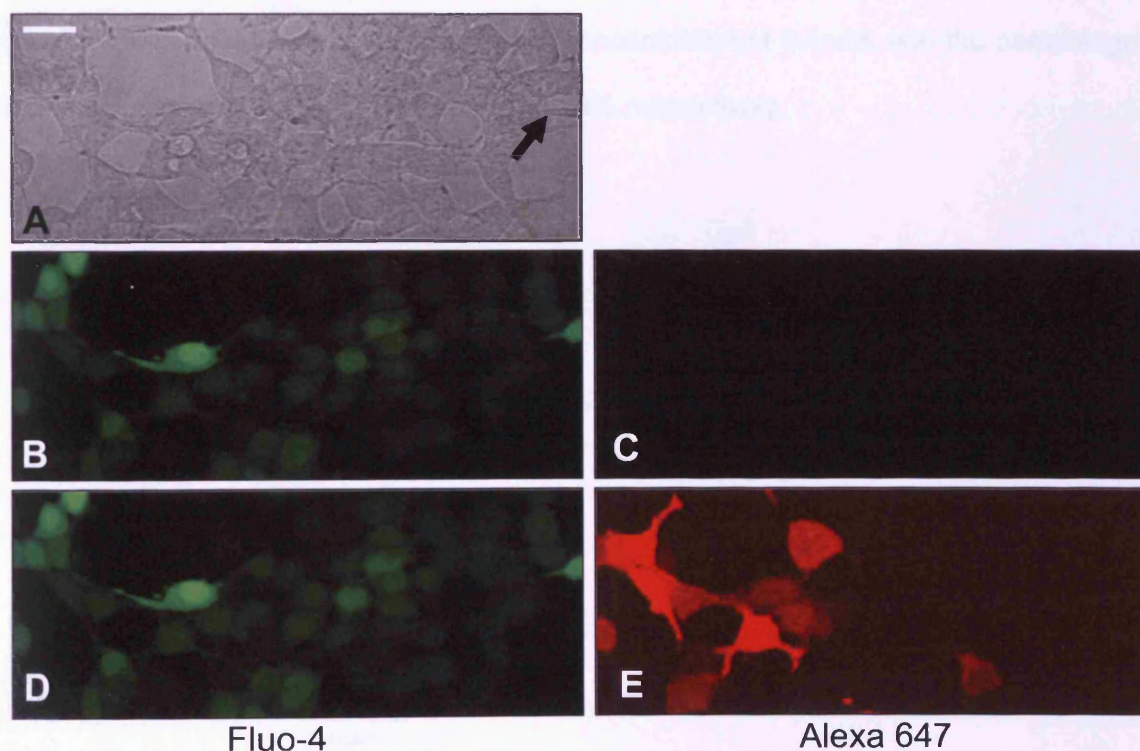


**Figure 7.9. MI of proteins into HEK293 cells**

**Panel A:** Phase contrast image of the field of view, the arrowhead shows the tip of the microcapillary moved to a focal plane above the cells. **Panels B & C:** Fluorescent signals prior to MI. **Panels D & E:** the same field of view 5 minutes after MI with Alexa 547 dextran. The Fluo-4 loaded cells appear unchanged (D) while the microinjected cells are clearly identifiable (E). Scale bar: 25  $\mu$ m

### 7.3.2 Effect of I-Domain proteins on $IP_3R$ carbachol-induced $Ca^{2+}$ transients

Although the data presented above suggested that, under optimised conditions, MI was well tolerated by HEK cells, I previously showed that MI procedure modulated cellular phenotype and signalling (Chapters 4 and 5). Therefore, as before, a number of rigorous controls, including the use of MagZ-treated RRL that had not been used for producing I-Domain protein, were performed.

It was found that MI of RRL or ID fragments altered the proportion of cells responding to carbachol compared to WT HEK cells (Figure 7.10). The number of cells responding to 0.1mM carbachol was reduced from 86% in WT HEK cells to 60% in those injected with RRL containing no recombinant protein. MI of ID<sup>B</sup> or ID<sup>C</sup> into the HEK cells markedly reduced carbachol-evoked  $Ca^{2+}$ -release at carbachol concentration of 0.1mM, and the percentage of responding cells was decreased to 25% and 19% respectively.

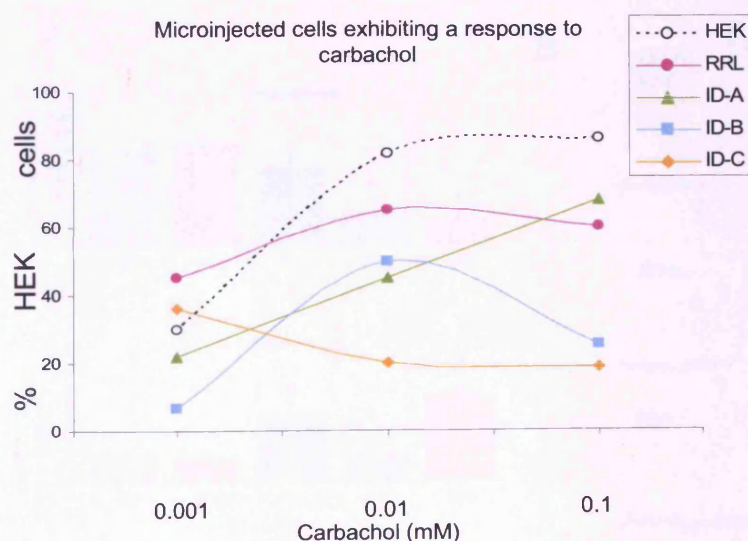


**Figure 7.10. MI of I-Domain proteins reduces the percentage of cells responding to 0.1 mM carbachol.**

Line chart depicting the proportion of cells responding to carbachol as a percentage of the total cells imaged, before (HEK) or after microinjection with RRL or ID proteins.  $n > 100$  cells per data point.

### 7.3.2.1 Effect of I-Domain proteins on $Ca^{2+}$ transient characteristics

As discussed above,  $Ca^{2+}$  transient modulation was investigated using noise analysis. Analysis of carbachol-induced  $Ca^{2+}$  transient characteristics in those cells which did respond to 0.1mM carbachol showed that injection of RRL into HEK cells did not alter the amplitude, rate up, or rate down of the transients (Figure 7.11). In contrast, MI of the I-Domain fragments, in most cases, significantly changed these parameters compared to the RRL-injected controls. Injection of ID<sup>A</sup> significantly increased both the rate up and rate down of the transients. ID<sup>B</sup> and ID<sup>C</sup> both significantly decreased the amplitude of the carbachol-induced  $Ca^{2+}$  transient. ID<sup>C</sup> was also linked to a significant increase in rate up and rate down of the transient. The rate down in ID<sup>B</sup> could not be determined, partially because of the very small number of ID<sup>B</sup>-injected cells which responded to 0.1mM carbachol, but also because in those cells which did respond, only a small fraction displayed a  $Ca^{2+}$  transient which returned to basal  $Ca^{2+}$  levels (Figure 7.11, B).

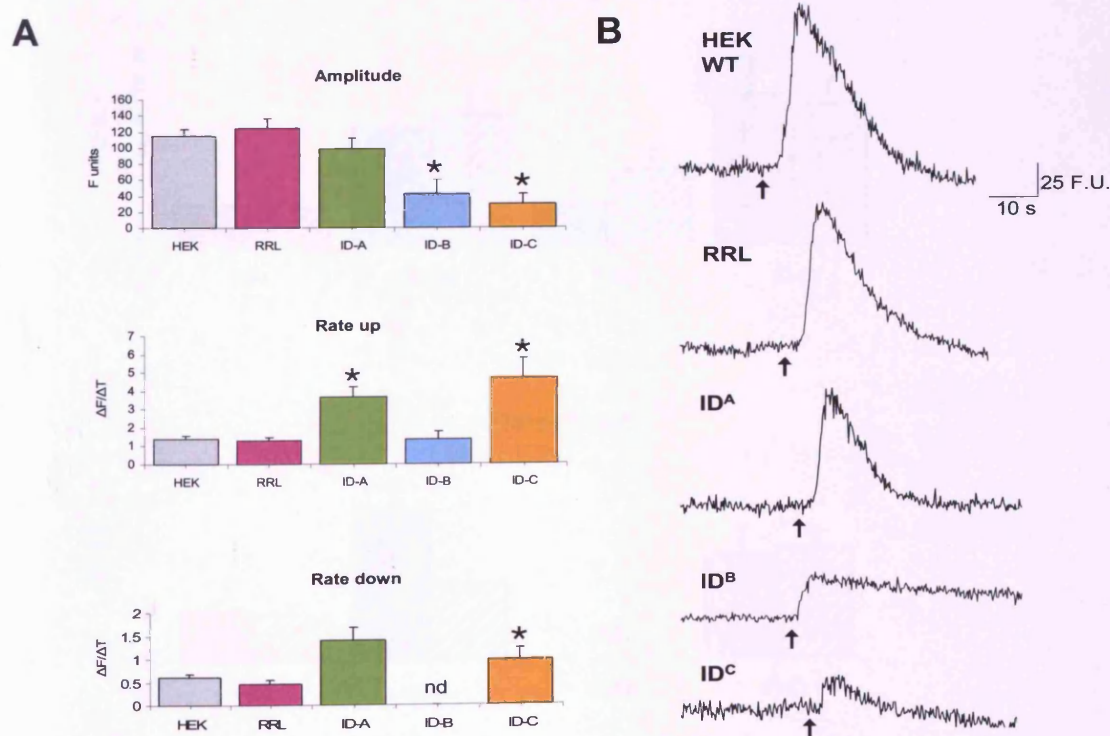


**Figure 7.11. I-Domain proteins blunt carbachol-evoked  $Ca^{2+}$  transients**

**Panel A:** Changes in carbachol-induced  $Ca^{2+}$  transients after MI of ID fragments (mean  $\pm$  SEM,  $n=5-7$ , 15-20 cells per experiment).  $\star$  represents  $p<0.001$  when compared with RRL-injected HEK cells; nd: not determined **Panel B:** Representative traces of carbachol-induced  $Ca^{2+}$  transients in WT and injected HEK cells. Arrow heads indicate point of carbachol addition.

Interestingly, as observed in HL-1 myocytes, non-injected HEK cells ('bystanders') in the same field of view showed similarly altered  $\text{Ca}^{2+}$  transients to those which had been injected with ID proteins (Figure 7.12). In every case, there is no significant difference between the injected and non-injected cells, and this finding further corroborated the results obtained in HL-1 myocytes after injection of bacterial- or *in vitro*-synthesised ID<sup>B</sup>.

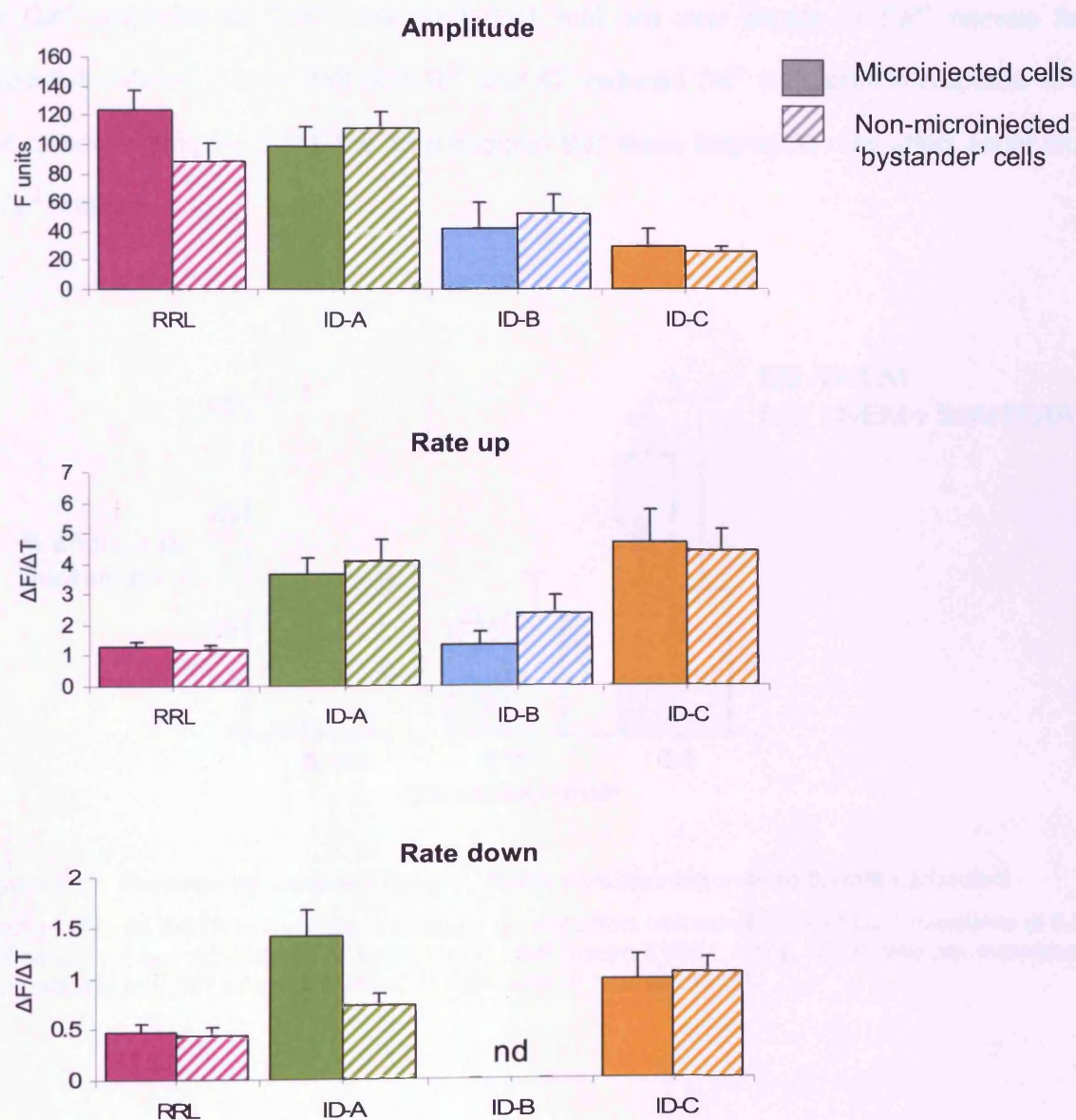


**Figure 7.12. Changes in carbachol-evoked  $\text{Ca}^{2+}$  transients were also seen in non-injected cells**

Changes in carbachol-induced  $\text{Ca}^{2+}$  transients after MI of ID fragments were seen in bystander cells (striped bars) as well as microinjected cells (solid bars) (mean  $\pm$  SEM,  $n=5-7$ , 15-20 cells per experiment). Data for microinjected cells is taken from Figure 7.11. There was no significant difference between microinjected and bystander cells for any ID fragment.

The addition of 5 mM EGTA, a  $\text{Ca}^{2+}$  chelator, to cell medium prior to the addition of carbachol (0.001 – 0.1 mM), reduced the magnitude of carbachol-evoked  $\text{Ca}^{2+}$  release to similar levels in cells exposed to 0.1 mM and 0.01 mM carbachol (Figure 7.13). Contrastingly, cells bathed in normal medium (containing approximately 1.3mM  $\text{Ca}^{2+}$ ), exhibited a significantly increased  $\text{Ca}^{2+}$  release evoked by 0.1mM carbachol compared to 0.01mM. These data indicate that the addition of 0.1mM carbachol triggers  $\text{Ca}^{2+}$  influx, while the  $\text{Ca}^{2+}$  response at 0.001 mM and 0.01 mM are due largely to  $\text{Ca}^{2+}$  release from intracellular stores. Given that both  $\text{ID}^{\text{B}}$  and  $\text{ID}^{\text{C}}$  reduced  $\text{Ca}^{2+}$  transients in response to 0.1 mM carbachol (Figure 7.11), the data suggest that these fragments may affect some mode of  $\text{Ca}^{2+}$  influx.

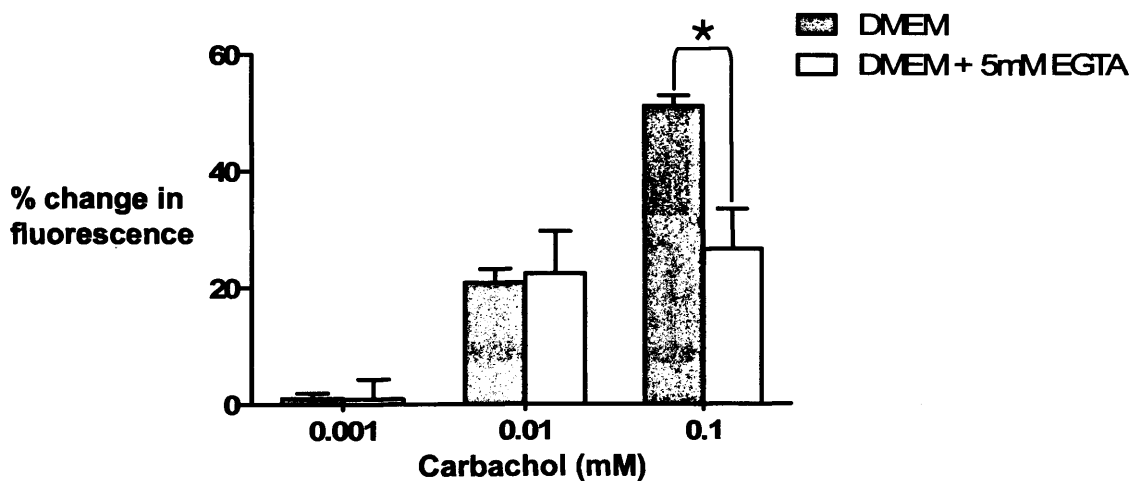


**Figure 7.13. Removal of extracellular  $\text{Ca}^{2+}$  limits cellular response to 0.1mM carbachol**

Addition of 5mM EGTA to the culture medium did not affect carbachol-evoked  $\text{Ca}^{2+}$  transients at 0.001 mM carbachol, but significantly reduced it at 0.1mM (mean  $\pm$  SEM,  $n = 4$ , 15-20 cells per experiment). \* represents  $p < 0.001$  when compared to HEK cells in normal DMEM.

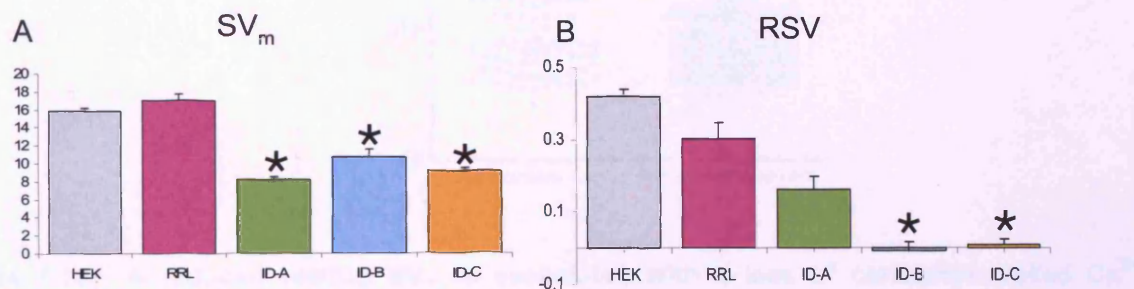
### 7.3.2.2 Effect of I-Domain proteins on cell 'noise' in carbachol-responsive cells

SALVO analysis of HL-1 cells shows a modification of cellular noise in cells exposed to  $\text{ID}^{\text{B}}$ . This was also investigated in HEK cells by calculating the  $\text{SV}_m$  and relative signal RSV



as described in the Methods section above. Basal and agonist-evoked signal variability ( $SV_m$  and RSV respectively) in RRL-injected control cells was not significantly different to that determined in WT HEK cells (Figure 7.14). Injection of I-Domain proteins, however, significantly reduced the RSV in cells injected with ID<sup>B</sup> and ID<sup>C</sup> (Figure 7.14, B) in carbachol-responsive cells, while the  $SV_m$  was significantly reduced with injection of all three truncated I-Domain proteins (Figure 7.14, A). As before, these changes were mirrored in the surrounding non-injected cells (Figure 7.14, C & D), as was the markedly reduced proportion of responding cells (ID<sup>B</sup> - 45%; ID<sup>C</sup> - 30%) compared to WT HEK cells (86%), though they remained more responsive than microinjected cells (ID<sup>B</sup> - 25%; ID<sup>C</sup> - 19%).

### Microinjected cells



### Microinjected cells compared with non-injected 'bystander' cells

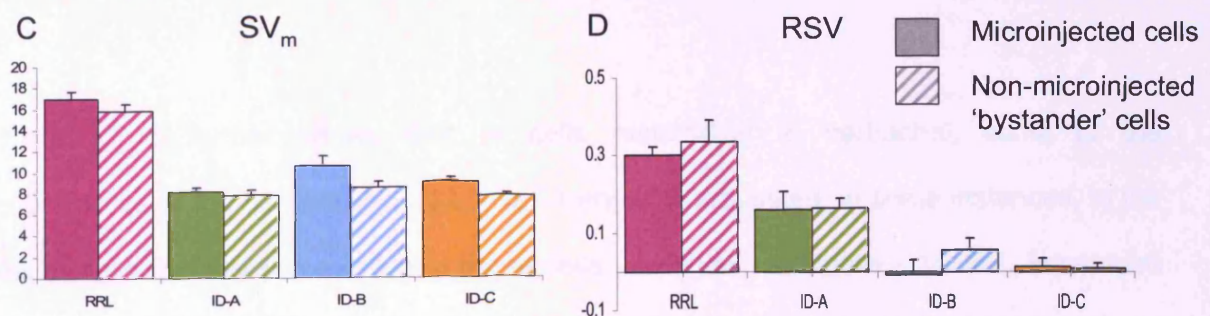


**Figure 7.14. MI of I-Domain fragments reduces cellular 'noise' in carbachol-responsive HEK cells**

**Panels A & B:** MI of ID fragments significantly reduced signal variability. **Panels C & D:** changes in cellular signal variability after MI of ID fragments were seen in both microinjected (solid bars) and (mean ± SEM, n=5-7, 15-20 cells per experiment). \* represents  $p < 0.05$  when compared with RRL-injected HEK cells. There was no significant difference between microinjected and bystander cells for any ID fragment.

### 7.3.2.3 Carbachol-induced $\text{Ca}^{2+}$ -transients are modulated by cellular noise

Interestingly, a comparison of the  $\text{SV}_m$  in carbachol-responsive and non-responsive HEK cells showed a relationship between the  $\text{SV}_m$  and whether or not a carbachol-induced  $\text{Ca}^{2+}$  transient was triggered by the addition of 0.1mM carbachol. It was found that, in general, carbachol-responsive HEK cells had a mean resting  $\text{SV}_m$  that was significantly higher than that measured in non-responsive cells ( $16.22 \pm 0.34$  versus  $10.90 \pm 0.32$ ,  $p < 0.05$ ) (Figure 7.15).

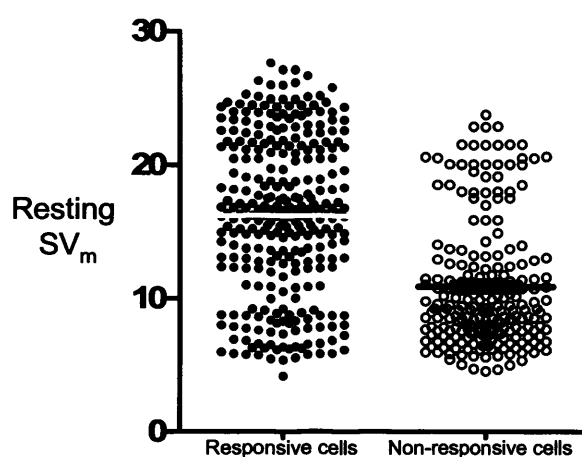


**Figure 7.15. A reduced resting  $\text{SV}_m$  is associated with a lack of carbachol-evoked  $\text{Ca}^{2+}$  response in HEK cells**

Resting  $\text{SV}_m$  in carbachol-responsive cells is significantly higher than that in non-responsive cells,  $p < 0.001$ . Bars indicate mean  $\pm$  SEM,  $n > 500$  cells.

Figure 7.16 further shows that in cells responding to carbachol, some of the characteristics of the carbachol-evoked  $\text{Ca}^{2+}$  transients are linked, in some instances, to the basal signal variability pre-existing in those cells. As shown in Figure 7.14,  $\text{SV}_m$  is reduced following exposure to ID fragments and this appears to modulate the amplitude and temporal kinetics of the  $\text{Ca}^{2+}$  transients, and the data presented in Figure 7.15 suggests that there is a link between reduced  $\text{SV}_m$  and the absence of a carbachol-evoked  $\text{Ca}^{2+}$  in the cell. This observation was extended by the data shown in Figure 7.16, which shows that a reduced  $\text{SV}_m$  may modulate certain aspects of the transients, and this is seen to different extents after exposure to different ID fragments, as summarised in .

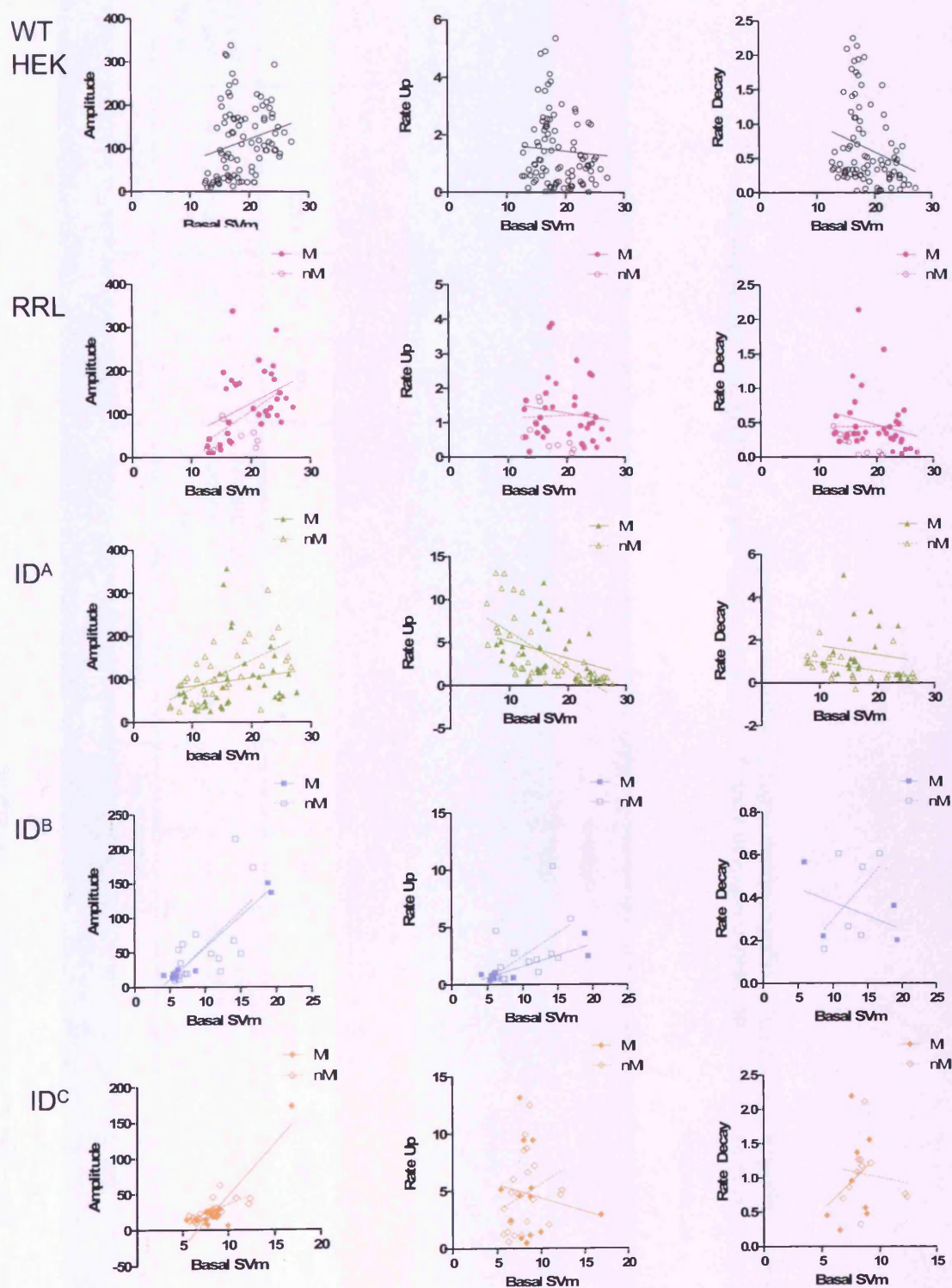


Figure 7.16. The relationship of  $SV_m$  with amplitude and kinetic properties of carbachol induced  $Ca^{2+}$  response

$r^2$  and  $p$  values for each scatterplot are summarised in Table 7.1

Table 7.1. Correlation of SV<sub>m</sub> with carbachol-evoked Ca<sup>2+</sup> transients

	Amplitude vs SV <sup>m</sup>					Rate Up vs SV <sup>m</sup>					Rate Decay vs SV <sup>m</sup>				
	Microinjected		Bystander		Correlation significantly different?	Microinjected		Bystander		Correlation significantly different?	Microinjected		Bystander		Correlation significantly different?
	r <sup>2</sup>	p	r <sup>2</sup>	p		r <sup>2</sup>	p	r <sup>2</sup>	p		r <sup>2</sup>	p	r <sup>2</sup>	p	
HEK WT	n/a	n/a	0.051	*	n/a	n/a	n/a	0.004	ns	n/a	n/a	n/a	0.062	*	n/a
RRL	0.156	*	0.219	**	ns	0.019	ns	0.001	ns	ns	0.056	ns	0.001	***	ns
ID <sup>A</sup>	0.019	ns	0.385	***	ns	0.121	*	0.428	***	*	0.021	ns	0.188	*	ns
ID <sup>B</sup>	0.964	***	0.459	*	ns	0.775	**	0.363	**	ns	0.276	ns	0.254	ns	ns
ID <sup>C</sup>	0.809	***	0.512	***	***	0.026	ns	0.078	ns	ns	0.094	ns	0.195	ns	*

Abbreviations: r<sup>2</sup> indicates the extent of correlation between x and y; p is the probability that r<sup>2</sup> is significantly different to zero; ns – not significant; \* significant at p<0.05; \*\* significant at p<0.01; \*\*\* significant at p<0.001

#### **7.3.2.4 Effect of I-Domain proteins on cell 'noise' in non-responding cells**

Notably, a significant proportion of cells transduced with ID fragments did not respond to carbachol, even at a concentration of 0.1mM. We investigated whether this surprising finding was underpinned by changes in the homeostatic Ca<sup>2+</sup> handling in these cells. 'Noise' analysis was chosen as an appropriate analytical tool since previous studies have shown the broad applicability of detailed signal variability analysis to Ca<sup>2+</sup> cycling (George *et al.* 2006). In cells that did not exhibit carbachol-evoked Ca<sup>2+</sup> transients, there was no significant difference between post- and pre-carbachol signals in WT HEK cells and the RRL-injected controls. However, consistent with the observations in carbachol-responsive cells, we determined a significant decrease in post-carbachol signals in cells microinjected with any of the three I-Domain fragments. Notably, this suppression of Ca<sup>2+</sup> trace variability following carbachol addition was also evident in cells that had not been transduced with the I-Domain fragments and provided further evidence of the 'bystander' effect.

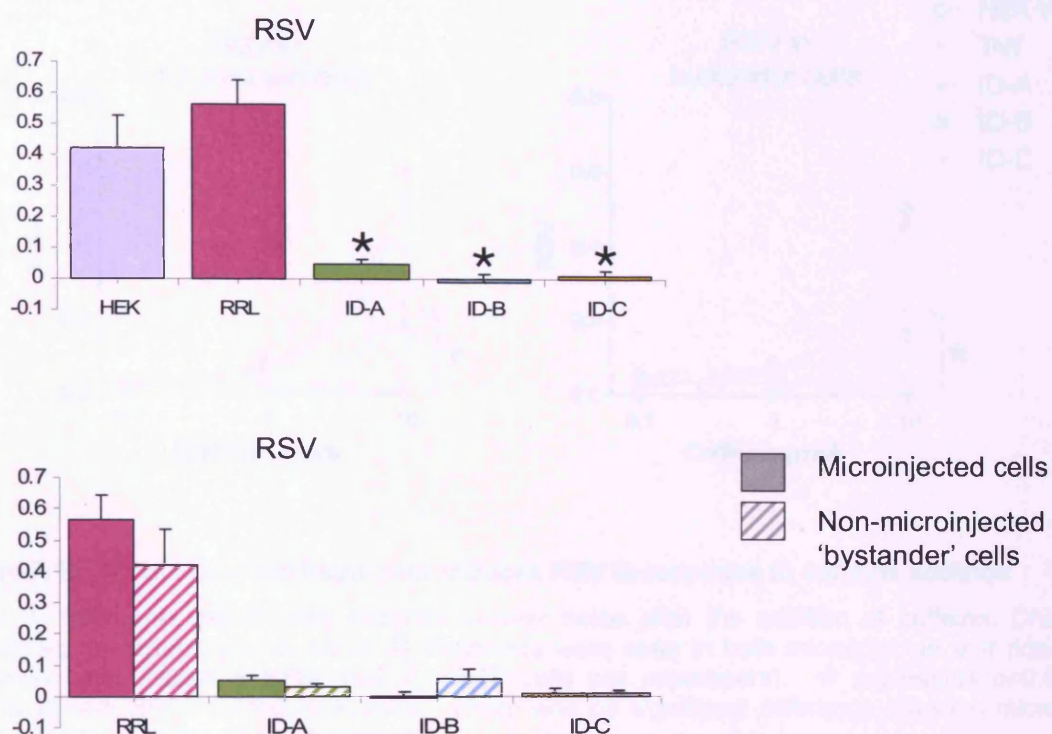


**Figure 7.17. MI of I-Domain fragments reduces RSV in carbachol non-responsive HEK cells**

MI of ID fragments significantly reduced cellular noise after the addition of carbachol. Changes in cellular signal variability after MI of ID fragments were seen in both microinjected (solid bars) and (mean  $\pm$  SEM,  $n=5-7$ , 15-20 cells per experiment). \* represents  $p < 0.05$  when compared with RRL-injected HEK cells. There was no significant difference between microinjected and bystander cells for any ID fragment.

### 7.3.3 Effect of I-Domain proteins on $IP_3R$ caffeine-modulated $Ca^{2+}$ handling

Next, we investigated the effect of the I-Domain proteins on cellular  $Ca^{2+}$  handling in response to the addition of caffeine, which does not induce a  $Ca^{2+}$  transient via  $IP_3R$ . MI of RRL did not alter the post-caffeine signals compared to WT HEK cells, but cells injected with  $ID^A$ ,  $ID^B$  or  $ID^C$  displayed a dramatically decreased  $Ca^{2+}$  signal variability following addition of 10mM (Figure 7.18).

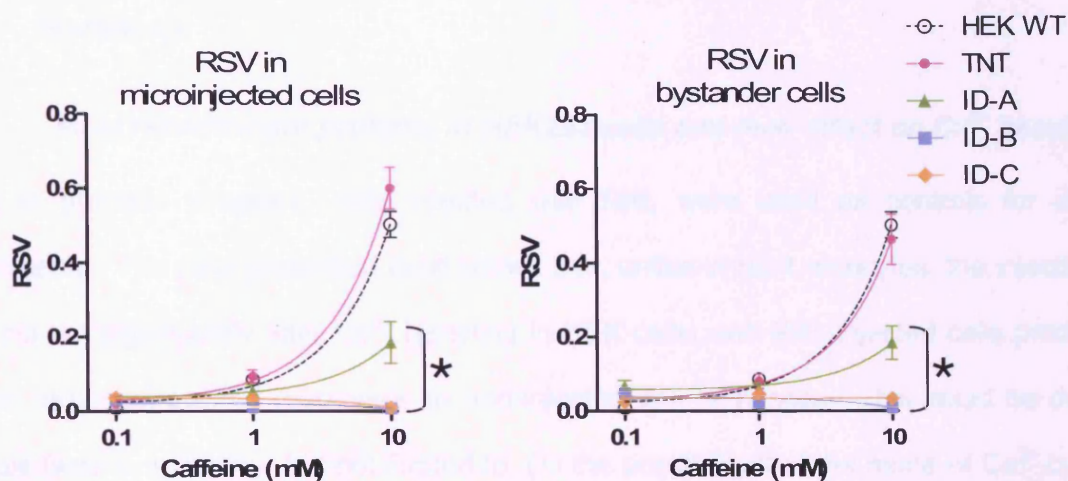


**Figure 7.18. MI of I-Domain fragments reduces RSV in response to caffeine addition**

MI of ID fragments significantly reduced cellular noise after the addition of caffeine. Changes in cellular signal variability after MI of ID fragments were seen in both microinjected and non-injected bystander cells (mean  $\pm$  SEM,  $n=5-7$ , 15-20 cells per experiment). \* represents  $p < 0.05$  when compared with RRL-injected HEK cells. There was no significant difference between microinjected and bystander cells for any ID fragment.

## 7.4 Discussion

### 7.4.1 MI of recombinant proteins in HEK293 cells and their effect on Ca<sup>2+</sup> handling

As in previous chapters, cells injected with RRL were used as controls for all MI experiments. The data presented here shows that, unlike in HL-1 myocytes, the injection of RRL did not significantly alter Ca<sup>2+</sup> handling in HEK cells, and RRL-injected cells produced similar carbachol-evoked responses to non-injected WT HEK cells. This could be due to multiple factors, including, but not limited to, (1) the possibility that the mode of Ca<sup>2+</sup> cycling in HEK cells is fundamentally different than that occurring in HL-1 myocytes, or (2) given the large global Ca<sup>2+</sup> oscillations characteristic of HL-1 cells, it may be easier for our experimental system to dissect alterations in HL-1 cell Ca<sup>2+</sup> handling.

Even noting the above considerations, the injection of ID proteins into HEK cells did profoundly affect cellular Ca<sup>2+</sup> handling phenotype. Specifically, it reduced IP<sub>3</sub>R-dependent Ca<sup>2+</sup> responses evoked by stimulation with 0.1mM carbachol. This surprising finding confirmed and extended studies (Chapters 4, 5 and 6) that showed the modulatory effects of ID on RyR2-dependent signalling. In the present chapter, the effects of ID on IP<sub>3</sub>R-dependent Ca<sup>2+</sup> signalling are determined, entirely consistent with our bioinformatic analysis that revealed significant structural homology between ID and ID-like regions of IP<sub>3</sub>R. Furthermore, the demonstration that ID-mediated Ca<sup>2+</sup> modulation exists between different cell types (non-excitabile and excitable) suggests that their effects are unlikely to be artefacts of the experimental conditions and techniques used.

It was also evident that Ca<sup>2+</sup> transient 'shape', which reflects the balance between ER efflux and sequestration mechanisms and a contributory role of PM Ca<sup>2+</sup> fluxes, was altered following MI of ID fragments. Whether this occurs directly as a result of modulating IP<sub>3</sub>R, or as a downstream consequence of ID-mediated IP<sub>3</sub>R Ca<sup>2+</sup> signalling remains to be determined. We also cannot exclude the possibility that the ID fragments associate with, and modulate, other facets of HEK Ca<sup>2+</sup> handling machinery.

It is interesting that other work in our laboratory has recently shown that chronic



expression of ID<sup>B</sup> causes a profound downregulation of IP<sub>3</sub>R activity (Fry *et al.* 2007). In keeping with this finding, the small fraction of ID<sup>B</sup>-injected HEK cells which did respond to carbachol mostly exhibited a decreased amplitude followed by a sustained increase in intracellular Ca<sup>2+</sup>, where the transient did not return to basal levels. This decreased amplitude is concordant with a downregulation of IP<sub>3</sub>R, though the sustained increased Ca<sup>2+</sup> levels may implicate ID<sup>B</sup>-linked inhibition of Ca<sup>2+</sup> sequestration machinery, such as SERCA.

The contribution of influx of Ca<sup>2+</sup> from the extracellular medium to carbachol-evoked Ca<sup>2+</sup> transients was also shown by experiments where the Ca<sup>2+</sup>-chelator, EGTA was added to the culture medium prior to carbachol addition. The dampened Ca<sup>2+</sup> response observed in cells pre-exposed to EGTA suggested that Ca<sup>2+</sup> influx contributed to the amplitude of agonist-induced Ca<sup>2+</sup> release at 0.1 mM carbachol. Clearly, the mechanistic basis of our findings in this context requires further investigation.

#### **7.4.2 Effect of I-Domain proteins on cell 'noise'**

Subtle changes in cellular Ca<sup>2+</sup> cycling in HEK cells were investigated and quantified by calculation of the signal variability due to agonist-induced changes within the same cell. Basal and agonist-evoked signal variability (SV<sub>m</sub> and RSV, respectively) in RRL-injected control cells were not significantly different to that determined in WT HEK cells. Contrastingly, MI of I-Domain proteins significantly reduced the RSV in cells injected with ID<sup>B</sup> and ID<sup>C</sup> in carbachol-responsive cells, and the SV<sub>m</sub> was significantly reduced with injection of all three truncated I-Domain proteins. Since the SV<sub>m</sub> is an index of basal Ca<sup>2+</sup> handling, derived from the actions of multiple Ca<sup>2+</sup> signalling moieties (e.g. SERCA and IP<sub>3</sub>R), the observation that ID-fragments suppressed these fluxes may be a robust indicator that ID-targeted approaches may be useful in suppressing abnormally high levels of intracellular Ca<sup>2+</sup> flux that frequently characterises cellular pathology (e.g. necrosis). Interestingly, a comparison of the SV<sub>m</sub> in carbachol-responsive and non-responsive HEK cells showed that, in general, mean resting SV<sub>m</sub> was significantly higher in carbachol-responsive HEK cells.

This implies that the amplitude variability of resting  $\text{Ca}^{2+}$  fluxes is proportionally linked with the propensity of the cell to respond to 0.1mM carbachol. It is tempting to speculate that the association between cellular 'noise' and agonist response may be a reflection of the relative stability of the  $\text{Ca}^{2+}$  release channels involved. This concept is supported by the observations that molecular instability of RyR2 correlates with increased intracellular  $\text{Ca}^{2+}$  fluxes (George *et al.* 2006; Yano *et al.* 2006).

### **7.4.3 Bystander effect in HEK cells**

In agreement with the data presented in Chapters 5 and 6, a bystander effect was observed in non-injected HEK cells after MI of any of the three truncated ID proteins. These observations together showed that the existence of a 'bystander' effect in our experiments is robust and not dependent on the source of the injected protein, or the cell type into which they are injected. In order to further corroborate this finding, the mechanisms underlying the bystander effect will be investigated in the context of cell-to-cell communication, and via the extracellular release of soluble factors. This will be discussed in more detail in Chapter 8.

## ***Chapter 8***

# ***Insights into the mechanistic basis of the bystander effect***

## 8.1 Introduction

### 8.1.1 The bystander effect

This thesis has provided compelling evidence for a bystander effect, whereby non-injected cells showed the same  $\text{Ca}^{2+}$ -handling phenotypes as adjacent cells that had been microinjected with I-Domain fragments. The bystander effect was corroborated in different cell types (HL-1 and HEK cells) and using recombinant proteins produced via distinct synthetic routes (bacterial expression and *in vitro* synthesis).

The 'bystander effect' is a phenomenon which has also regularly been reported in cells after exposure to ionising radiation treatment in cancer therapy, where irradiated cells may also transmit damage signals to non-irradiated cells in a population, leading to the occurrence of genetic damage effects in these 'bystander' cells that in themselves receive no radiation exposure (Chaudhry 2006; Little 2006; Morgan 2003; 2007). The recent interest in this phenomenon was stimulated by the findings of Nagasawa and Little (1992), who demonstrated that when cell monolayers were exposed to mean  $\alpha$ -particle doses where as few as <1% of the nuclei were traversed by a single  $\alpha$ -particle track, more than 30% of the non-irradiated cells exhibited effects associated with direct ionising radiation (Nagasawa & Little 1992). Since this study, numerous laboratories have reported *in vivo* and *in vitro* bystander effects in a wide variety of cell types, and following exposure to both particulate and electromagnetic radiation (Hamada *et al.* 2007b).

It has been proposed that there may be two basic mechanisms by which 'damage' signals may be transmitted from irradiated to non-irradiated cells. The first is by direct cell-to-cell contact often mediated by gap junction intercellular communication (GJIC) (Azzam *et al.* 2001; Shao *et al.* 2003), whereas the second is by means of soluble factors released into the surrounding medium by irradiated cells (Azzam *et al.* 1998; Prise *et al.* 1998). There is substantial evidence that irradiated individuals may release clastogenic factors into their plasma that can induce chromosomal damage when transferred to cultured cells from normal donors (Emerit *et al.* 1994; Gemignani *et al.* 1999; Lloyd & Moquet 1985). Similar

phenomena have been shown in rodent models, although in all cases the nature of these clastogenic factors has proven elusive (Morgan & Sowa 2007; Pant & Kamada 1977).

### **8.1.2 Objectives of this chapter**

As discussed above, a bystander effect was reproducibly observed following the microinjection of I-Domain proteins into HEK293 and HL-1 cells. This chapter presents preliminary investigations into two mechanisms (GJIC and via extracellular transmission of soluble factors) that may potentially underlie the bystander effect observed in the experiments described in the preceding chapters.

### **8.1.3 Specific Hypothesis**

The bystander effect is thought to be caused by two potential mechanisms – GJIC and extracellular transfer of soluble substrates (i.e. a paracrine mechanism). Here, it is proposed that the injection of a dye into a single cell will identify GJIC as a potential mechanism if the dye is transferred from cell to cell. Similarly, the phenotypic effects of transferring the media surrounding microinjected cells onto physically separate non-microinjected cells can potentially identify the contribution of extracellular mechanisms to the observed phenomenon. This chapter specifically examines the hypothesis that a paracrine mechanism mediated by intercellular transfer of soluble effectors fundamentally contributes to the bystander effect.

## **8.2 Methods**

### **8.2.1 Lucifer Yellow**

Lucifer Yellow (LY, 5% (w/v) in 0.3 M LiCl) was injected into the cytoplasm of a single cell in HL-1 or HEK cell monolayers prepared as described previously using the conditions optimised previously (Chapter 4). Direct intercellular transfer of dye that is absolutely dependent on GJIC, was viewed on the Zeiss Axiovert microscope using fluorescence filters 450-490nm/510-520nm (HEK cells), or on the Leica RS2 confocal microscope using an Argon/Krypton laser (488nm/500nm) (HL-1 cells).

### **8.2.2 Medium transfer**

#### **8.2.2.1 HEK293 cells**

HEK293 cells were cultured and harvested (Chapter 2) and prepared for microinjection as described in Section 7.2.1. Two chambers containing cells were set up and loaded with Fluo-4AM, as summarised in Figure 8.1. The cells in Chamber 1 were microinjected under the conditions optimised previously, and the medium surrounding them was transferred to Chamber 2 immediately after microinjection. The effects of different dilutions of transferred media were investigated as summarised in Table 8.1.

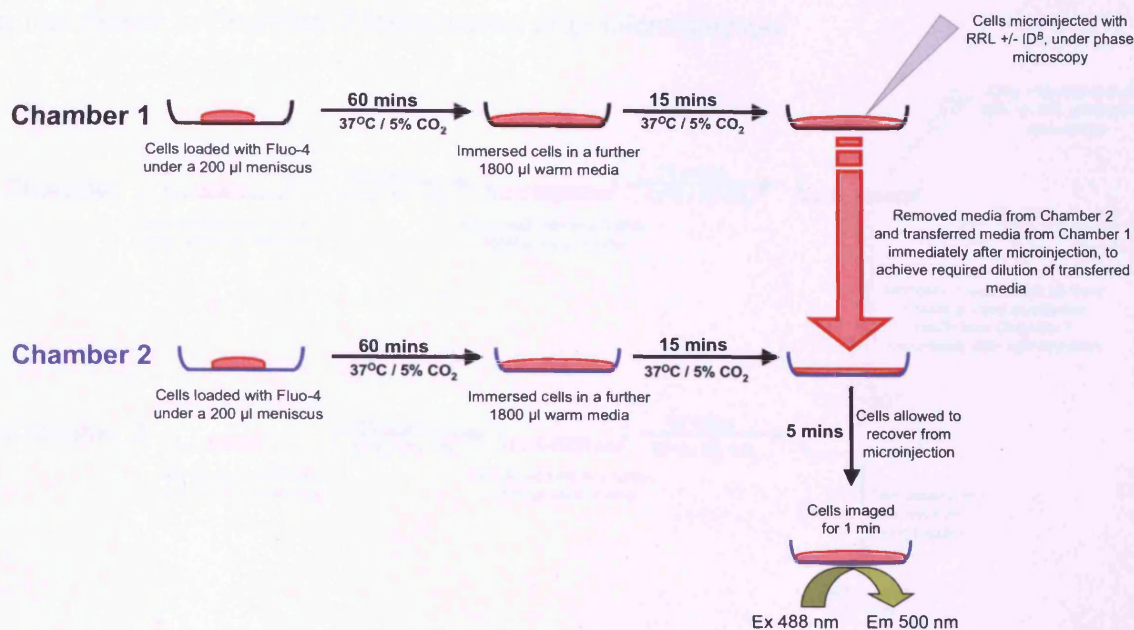


Figure 8.1. Summary of medium transfer experiment protocol with HEK293 cells

Table 8.1. Summary of medium dilution strategy

Required concentration of transferred medium	Volume of medium in Chamber 2 (µl)	Volume of medium transferred from Chamber 1 (µl)	Total volume of medium surrounding imaged cells (µl)
100 %	0	2000	2000
75 %	500	1500	2000
50 %	1000	1000	2000
20 %	1600	400	2000
10 %	1800	200	2000
0 %	2000	0	2000

### 8.2.2.2 HL-1 myocytes

HL-1 cells were cultured and harvested (Chapter 2) and prepared for microinjection as described in Section 4.2.1. As above, two chambers containing cells were set up and loaded with Fluo-4AM, as summarised in Figure 8.2. The cells in Chamber 1 were microinjected under the conditions optimised previously, and the medium surrounding them

was transferred to Chamber 2 immediately after microinjection.

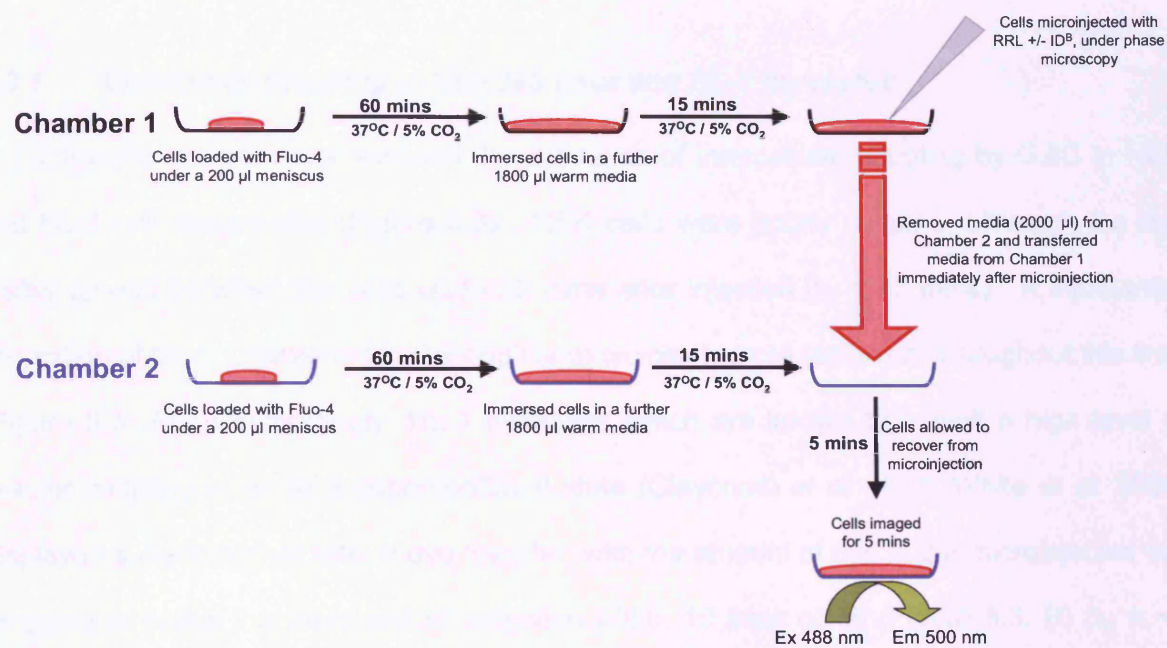


**Figure 8.2. Summary of medium transfer experiment protocol with HL-1 cardiomyocytes**



## 8.3 Results

### 8.3.1 Cell-to-cell coupling in HEK293 cells and HL-1 myocytes

LY transfer experiments revealed the presence of intercellular coupling by GJIC in HEK and HL-1 cell monolayers (Figure 8.3). HEK cells were poorly coupled, although the dye visibly spread between the cells up to 20 mins after injection ( $t_{1/2} = \sim 7$  mins). A substantial proportion of the LY remained in the original microinjected cell (arrowed) throughout this time (Figure 8.3, A). Contrastingly, HL-1 myocytes which are known to exhibit a high level of cellular coupling when in a superconfluent state (Claycomb *et al.* 1998; White *et al.* 2004) displayed a much higher rate of dye transfer, with the amount of dye in the microinjected cell dropping to below the threshold of detection within 10 secs of MI (Figure 8.3, B) ( $t_{1/2} = \sim 2$  secs).

HEK293 cells were found to have a  $t_{1/2}$  of approximately 7 minutes, while the  $t_{1/2}$  of HL-1 myocytes was dramatically lower, at  $\sim 2$  secs (Figure 8.3, C & D respectively). The finding of GJIC, albeit at greatly different extents in HEK and HL-1 cells, suggests that cell-to-cell contact is one possible mechanism for the bystander effect in HEK293 cells. However, ongoing work in our laboratory has also shown the I-Domain linked bystander effect in spatially distinct cells, suggesting that cell-to-cell contact can not be the only means of communication between cells. Furthermore, cell-to-cell contact in HEK cells is limited due to their low confluency (50-60%), which may affect the speed of dye transfer. Higher confluencies could not practically be investigated, as HEK cells lose adherence properties at confluency  $>60\%$ . However, even at higher cell densities, it is not anticipated that the speed of dye transfer in HEK cells could match that observed in HL-1 myocytes.

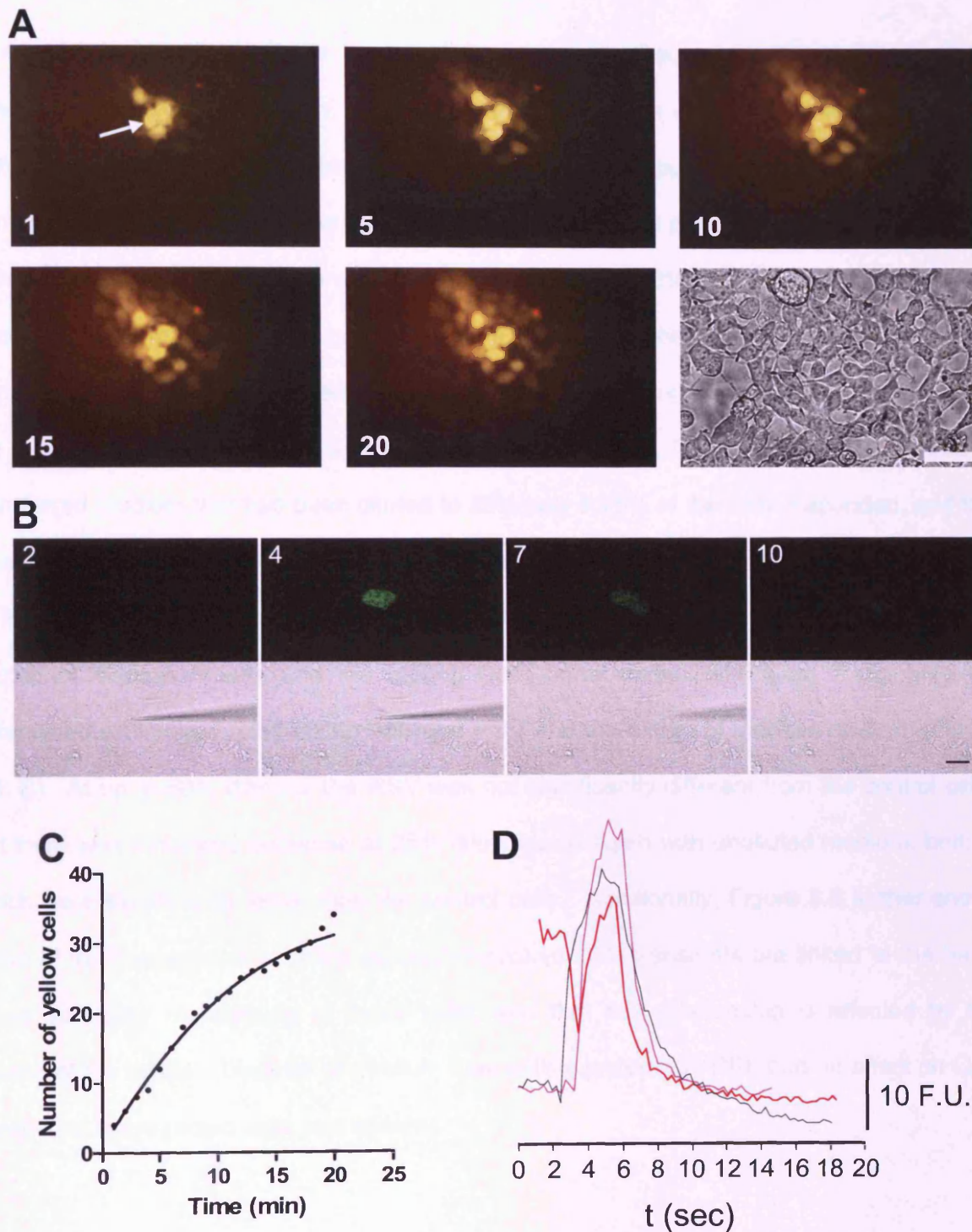


**Figure 8.3. Differential extents of cell-to-cell communication in HEK and HL-1 cells**

**Panel A:** Fluorescence microscopy images showing dye transfer in HEK cells after MI of a single cell (arrowed). Numbers indicate time after MI (mins). Scale bar 50  $\mu\text{m}$ . **Panel B:** Confocal microscopy images showing dye transfer in HL-1 myocytes after MI of a single cell. Numbers indicate time after MI (secs). Scale bar 10  $\mu\text{m}$ . **Panels C & D:** Line graphs showing dye transfer in HEK and HL-1 cells respectively.

### 8.3.2 Medium transfer in HEK cells

In order to investigate if the trans-cellular exchange of soluble factors is triggered by injecting cells with ID fragments, the medium from chambers containing cells microinjected with ID<sup>B</sup> was removed immediately after microinjection and applied to a chamber containing non-injected WT HEK cells. The strategy was augmented by performing these experiments with undiluted medium and also with medium diluted by 25-90% (with fresh medium). There was a relationship between the proportion of HEK cells that responded to 0.1 mM carbachol and the dilution of the transferred medium. At dilutions ranging from 10- 50% dilution, all of the cells (100%) responded to 0.1 mM carbachol. Strikingly, following exposure of cells to transferred medium that had been diluted to 25% only 8.75% of the cells responded, and this was decreased further with undiluted medium (4% carbachol responsive) (Figure 8.4, A).

Following on from data presented in Chapter 7 in which we revealed a link between carbachol responsiveness and the resting Ca<sup>2+</sup> signal variability (Figure 7.15), here we determined an inverse relationship between RSV and the extent of medium dilution (Figure 8.4, B). At up to 50% dilution, the RSV was not significantly different from the control cells, but there was a marked decrease at 25% dilution and again with undiluted medium, both of which were significantly lower than the control cells. Additionally, Figure 8.5 further shows some of the characteristics of the carbachol-evoked Ca<sup>2+</sup> transients are linked to the basal signal variability pre-existing in those cells, and that this relationship is affected by the dilution of the media. Transfer of medium from cells injected with RRL had no effect on Ca<sup>2+</sup> handling in non-injected cells (not shown).

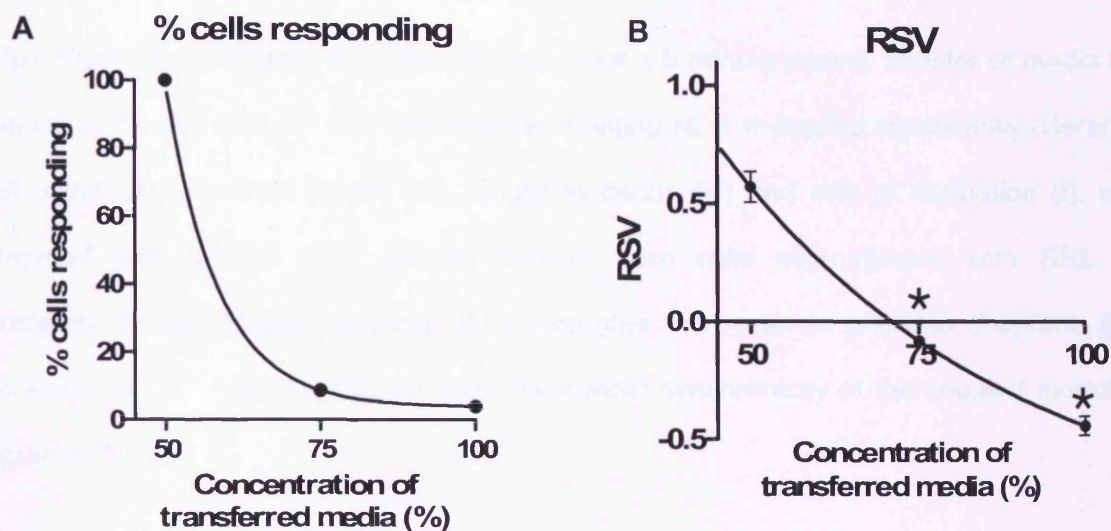


Figure 8.4. Dilution of transferred medium affects  $\text{Ca}^{2+}$  handling in carbachol-stimulated HEK cells.

**Panel A:** Line chart depicting the proportion of cells responding to carbachol as a percentage of the total cells imaged, after transfer of medium from HEK cells injected with  $\text{ID}^{\text{B}}$ .  $n > 70$  cells per data point. **Panel B:** Transfer of medium from HEK cells injected with  $\text{ID}^{\text{B}}$  caused a significant decrease in RSV, as the concentration of transferred medium increased (mean  $\pm$  SEM,  $n=4$ , 15-20 cells per experiment). \* represents  $p < 0.001$  when compared with WT HEK cells.

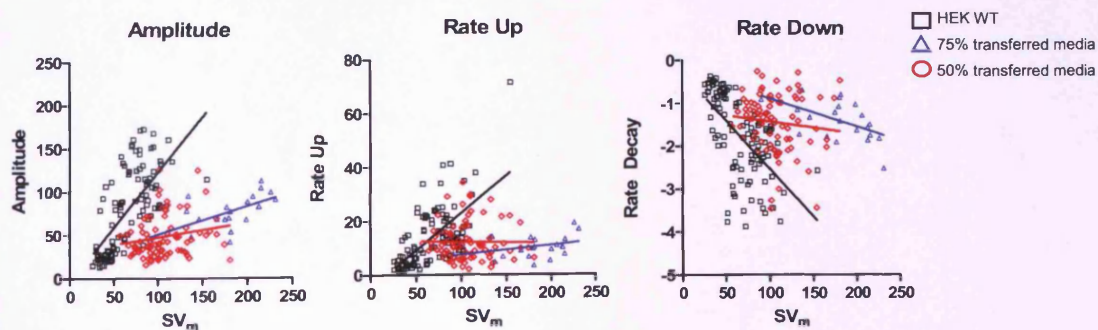
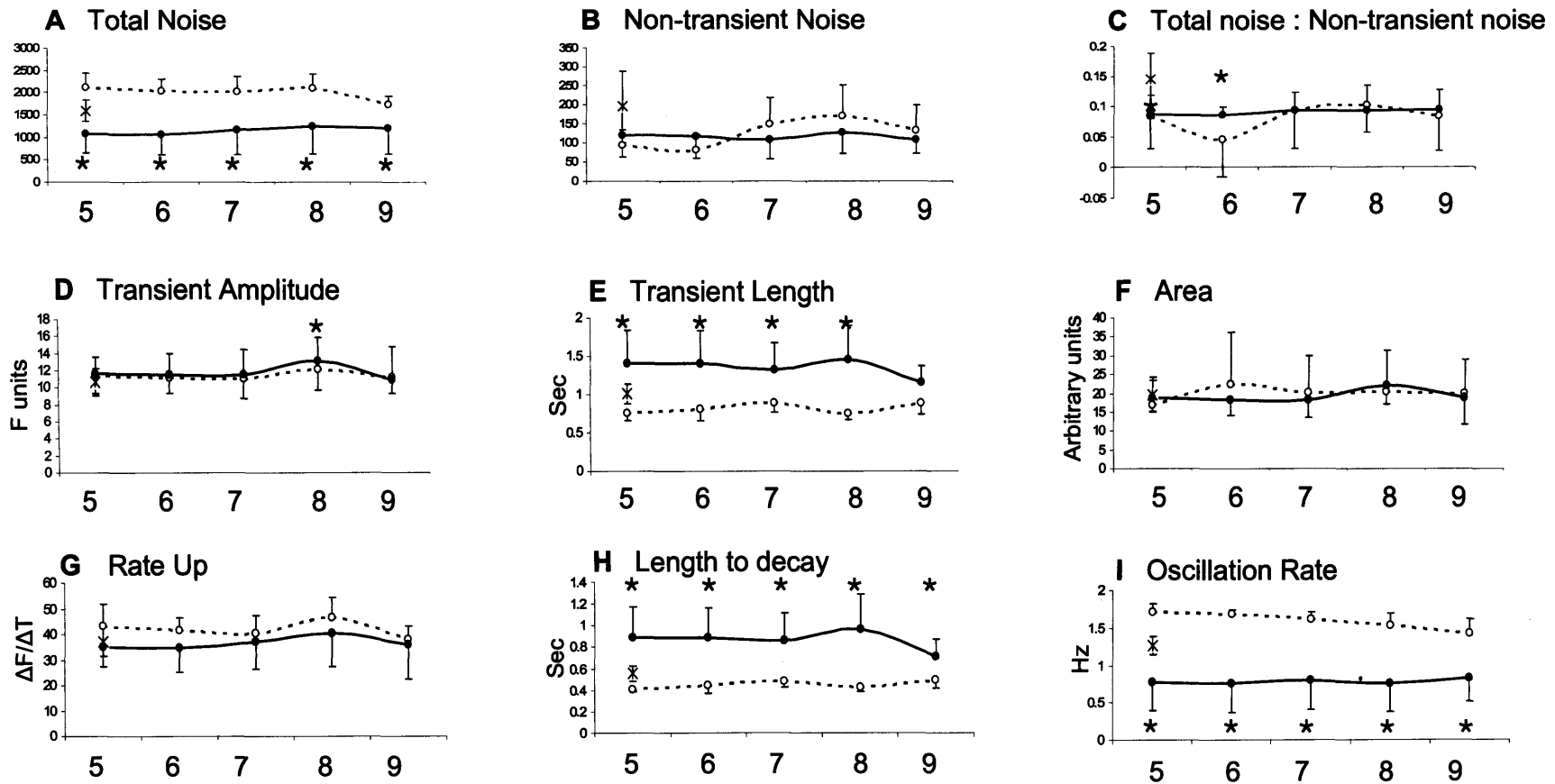


Figure 8.5. The relationship between resting  $\text{SV}_m$  and carbachol-evoked  $\text{Ca}^{2+}$  transients in HEK cells is affected by transferred medium concentration

### 8.3.3 *Medium transfer in HL-1 myocytes*

SALVO analysis (Figure 8.6) showed that, over a 5 minute period, transfer of media from cells microinjected with ID<sup>B</sup> onto non-injected beating HL-1 myocytes significantly altered the total noise (A), transient length (E), length to decay (H) and rate of oscillation (I), when compared with control cells where medium from cells microinjected with RRL was transferred to non-injected beating HL-1 myocytes. As seen in previous chapters, these alterations in Ca<sup>2+</sup> handling did not alter the overall synchronicity of the coupled monolayer (Figure 8.7).



**Figure 8.6. SALVO analysis of the effects of media transfer on HL-1 myocyte monolayers.**

Spatio-temporal  $Ca^{2+}$  handling parameters in HL-1 myocytes exposed to media from cells injected with RRL (dashed line) or *in vitro*-produced ID<sup>B</sup> (solid line), plotted from SALVO analysis of  $Ca^{2+}$ -dependent Fluo-4 fluorescence (mean  $\pm$  SEM, n = 4, 15-20 cells per experiment) \* represents p < 0.01 when compared with cells exposed to media from RRL-injected HL-1 myocytes. Values for HL-1 WT cells (X), shown here from the results shown in Chapter 4.

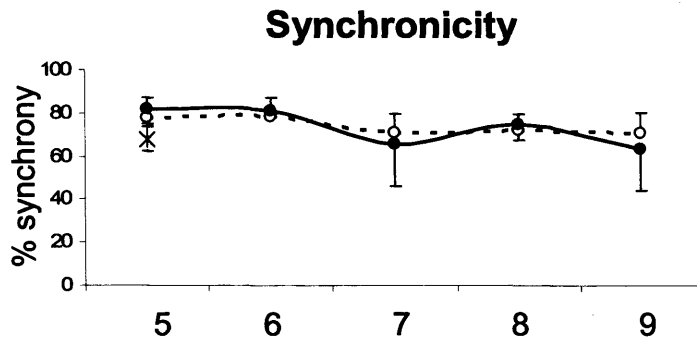


**Figure 8.7. Synchronicity is not affected by medium transfer**

Synchronicity within HL-1 monolayers exposed to medium from cells injected with RRL (dashed line) or *in vitro*-produced ID<sup>B</sup> (solid line), plotted from SALVO analysis of Ca<sup>2+</sup>-dependent Fluo-4 fluorescence (mean  $\pm$  SEM, n = 4, 15-20 cells per experiment). Values for HL-1 WT cells ( $\times$ ), shown here from the results. No significant difference between RRL- or ID<sup>B</sup>- injected and WT HL-1 was observed.

#### 8.4 Discussion

This thesis has provided compelling evidence for a bystander effect, whereby non-injected cells showed comparable  $\text{Ca}^{2+}$ -handling phenotypes as adjacent cells that had been microinjected with I-Domain fragments. The bystander effect was corroborated in different cell types (HL-1 and HEK cells) and using recombinant proteins produced via distinct synthetic routes (bacterial expression versus *in vitro* synthesis). It has been proposed that there may be two basic mechanisms by which 'damage' signals may be transmitted from irradiated to non-irradiated cells. Firstly by direct cell-to-cell contact often mediated by gap junction intercellular communication (GJIC) (Azzam *et al.* 2001; Shao *et al.* 2003), and secondly by means of soluble factors released into the surrounding medium by transduced cells (Azzam *et al.* 1998; Prise *et al.* 1998).

The first mechanism was investigated by the transfer of dye between coupled cells, and it was found that although the extent of coupling in HEK and HL-1 cells varied greatly between the two cell lines, cell-to-cell contact represents a mechanism that probably underpins intercellular communication in HEK and HL-1 cell population and likely contributes to the bystander effect in both instances. However, further in-depth analyses of connexin expression levels in both of these cell lines, as well as comprehensive control experiments using gap-junction blockers are required before GJIC can be considered as a *bona fide* mechanism underlying the bystander effect.

Studies that investigated the trans-cellular exchange of soluble factors revealed the possible involvement of an alternative pathway underlying the bystander effect. Media transferred from cells injected with ID<sup>B</sup> onto non-microinjected cells had a profound effect on cellular  $\text{Ca}^{2+}$  handling in naïve HEK and HL-1 cells. In HL-1 cells, the transfer of media from cells microinjected with ID<sup>B</sup> onto non-injected beating HL-1 myocytes significantly altered multiple aspects of cellular  $\text{Ca}^{2+}$  handling behaviour, but not the synchronicity of the coupled monolayer. This supports the data presented in previous chapters, whereby HL-1 myocytes exhibited a robust plasticity that resulted in the preservation of cellular synchrony despite



subtle changes in numerous facets of cellular  $\text{Ca}^{2+}$ -handling. In HEK cells, the transfer of media markedly reduced the number of cells responding to 0.1mM carbachol as well as significantly reducing the  $\text{Ca}^{2+}$  signal variability following carbachol stimulation. Furthermore, it was found that the dilution of the transferred media increased the proportion of cells that exhibited carbachol-evoked  $\text{Ca}^{2+}$  release and restored  $\text{Ca}^{2+}$  signal variability. The finding that the phenotypic effects of trans-media exchange were dependent on the extent of the dilution adds further support to our hypothesis that factors released from micro-injected cells could modulate  $\text{Ca}^{2+}$  signalling events in adjacent, non-microinjected cells. There are numerous candidate molecules that could be considered in this context (including ATP, reactive oxygen species, GSH), and their unequivocal identification is key to delineating the mechanisms underlying the bystander effect.

As discussed previously, the results presented throughout the thesis persuasively show that microinjection of a discrete population of cells is associated with a bystander effect, whereby it initiates similar phenotypic changes in neighbouring non-microinjected cells. So far, we were not able to block this effect, so it is accepted that the conclusions presented in this thesis require further evaluation in experiments that ultimately succeed in separating distinct effects in microinjected cells, versus those in the persistent presence of a bystander effect. Thus, that the findings from all experiments presented in this thesis must be interpreted in the context of an existing bystander effect.

## ***Chapter 9***

### ***General discussion***

The aim of this thesis was to further elucidate the precise roles of functional motifs within the I-Domain. Specifically, I addressed their effects on cellular  $\text{Ca}^{2+}$  cycling using a peptide probe-based approach. My findings reveal novel insights into the mechanisms by which disruption of interdomain interactions via the I-Domain could result in abnormal  $\text{Ca}^{2+}$  handling (e.g. HF). Conversely in a therapeutic context, these studies present compelling evidence that targeting this region could normalise these abnormal interactions in cardiac disease.

### 9.1 Expression of I-Domain proteins

Propagation and isolation of the pET-29(b) expression cassettes containing truncated ID templates was successful, when carried out under the conditions optimised for the propagation of hRyR2 DNA that avoid spontaneous recombination or plasmid DNA degradation (George *et al.* 2005).

These expression cassettes were then used for the successful synthesis of ID proteins in a cell free RRL system, regardless of size, secondary structure, or hydrophobicity, which may have been difficult to achieve in a bacterial system. According to densitometric analysis of radiolabelled proteins and S-protein HRP conjugate detection, the four I-Domain proteins displayed broadly equivalent levels of expression, and immunodetection using the fusion protein epitopes at either end of the protein expression cassette confirmed that full-length recombinant proteins had been produced. However, expression of the I-Domain proteins in the WG extract was not successful, with only two of the proteins ( $\text{ID}^{\text{A}}$  and  $\text{ID}^{\text{C}}$ ) being expressed by WG extract albeit in lower levels than by RRL, while  $\text{ID}^{\text{D}}$  and  $\text{ID}^{\text{B}}$  were not expressed at all. This was unexpected, as WG was anticipated to yield proteins in the range of two orders of magnitude higher than those produced in RRL (Alimov *et al.* 2000; Endo & Sawasaki 2006; Hino *et al.* 2008; Jermutus *et al.* 1998; Katzen *et al.* 2005; Vinarov *et al.* 2006; Zhao *et al.* 2007), and may suggest an inherent incompatibility of the I-Domain proteins with the WG extract expression system (Chapter 3).

The *in vitro*-synthesised I-Domain proteins were effectively isolated from RRL using a strategy based on magnetic zinc beads with a high affinity to poly-His-tagged proteins but not to haem groups, thus allowing the purification of the target protein without co-purification of haemoglobin present in the RRL. This strategy resulted in the removal of ~95% of contaminating background proteins, and permitted enrichment of the I-Domain proteins that could be unequivocally identified using immunoblotting techniques.

The I-Domain proteins were more difficult to express in a BL21-derived bacterial system. The expression of full-length I-Domain protein in a classical IPTG-induced system was unsuccessful despite the investigation of an array of different conditions, and resulted in numerous incomplete protein fragments with high levels of degradation, and no detectable full-length protein. As shown in Chapter 6, the use of an auto-induction system was found to be better suited for the expression of I-Domain proteins, and effectively expressed ID<sup>B</sup> which was subsequently purified using sequential Ni<sup>2+</sup>-affinity and S-protein affinity to selectively bind the His- and S-tag, respectively.

Further work is required to set up rigorous control experiments, in order to accurately elucidate the effects of bacterially produced ID<sup>B</sup>. The bacterially produced protein potentially differs to the *in vitro* protein by (i) lacking the S-tag, which was cleaved during purification, (ii) being subject to secondary modification, (iii) containing truncated ID proteins in the purified sample, each of which could alter the proteins bioactivity in HL-1 cells (Figure 6.6).

The bacterially synthesised proteins have undergone S-tag cleavage as part of the large-scale purification process, and this may enhance the bioactivity of the proteins. Additionally, bacterial expression systems allow for secondary modification of proteins, which does not occur in cell free systems. Furthermore, the bacterially-produced sample contains several truncated ID species which were detected by ab1093 (Figure 6.6). These truncated fragments may be bioactive, and therefore may cumulatively increase the ID<sup>B</sup> phenotype observed in microinjected cells.

Some or all of the considerations may contribute to the stark differences observed on Ca<sup>2+</sup> handling parameters. Notably, the restoration of synchrony is equivalent in both

methodologies. Further work will be necessary to determine how discrepant mechanisms can result in a comparable effect on synchrony - a robust index of intra- and inter-cellular  $\text{Ca}^{2+}$  handling - and indeed, how this is determined by the source of the protein.

## 9.2 *Microinjection technique*

Single cell MI is a robust and reproducible technique which permits the precise control of the amount and timing of delivery, and was used in this thesis to deliver exogenous proteins to adherent HL-1 cardiomyocytes and HEK293 cells. It was accepted that the MI procedure itself had altered some facets of cellular  $\text{Ca}^{2+}$  handling phenotype, but this was addressed by the use of robust control experiments. This is a limitation of the MI approach, but we believe that in the context of this thesis, this disadvantage is far outweighed by the advantages of MI, which including having precise control of the location and duration of sample delivery, as well as obtaining a clearly identifiable population of MI cells, which may not be possible with other conventional sample delivery technologies such as transfection (e.g. Bioporter reagent) or electroporation.

Using carefully optimised conditions (see Chapter 4), MI proved to be a minimally invasive delivery method which was well tolerated by cells without disruption of the tightly regulated cellular  $\text{Ca}^{2+}$  handling. This was corroborated by MI of both cDNA, and protein fragments, in synchronously oscillating HL-1 myocytes and in non-excitabile HEK cells.

Interestingly, MI had differential effects on HEK and HL-1 cells, whereby MI was not found to alter any of the  $\text{Ca}^{2+}$  handling parameters measured in HEK cells (Chapter 7), but did alter several parameters in HL-1 myocytes (Chapter 4). This may indicate an inherent difference in the modes of  $\text{Ca}^{2+}$  cycling between the two cell types, or that the absence of spontaneous oscillations in HEK cells indicates a simpler  $\text{Ca}^{2+}$  handling mechanism which is less easily perturbed. Importantly, although MI was found to affect some facets of  $\text{Ca}^{2+}$  handling in HL-1 myocytes, it consistently did not alter the synchronicity of the HL-1 monolayers, suggesting that  $\text{Ca}^{2+}$  fluxes were not sufficiently disrupted by MI to result in dyssynchrony. This

indicates that although precise  $\text{Ca}^{2+}$  regulation is vital for maintaining regular, synchronous contractions in cardiac cells, the cells exhibit pronounced functional plasticity and are able to robustly compensate for a surprisingly large degree of disruption in  $\text{Ca}^{2+}$  while still maintaining an overall regulated synchronously beating state. At this stage, it is not possible to identify which parameter(s) determine the state of cell synchronicity, and more detailed analyses of each of these interdependent parameters are required to provide an insight into the mechanism underlying the regulation of synchronous contraction in cardiac myocytes. Ongoing studies in our laboratory are currently addressing this, and are already unravelling the complex and interdependent relationships between  $\text{Ca}^{2+}$  handling, rhythmicity and synchrony in coupled cardiac monolayers (Silvester *et al.* 2009).

### 9.3 The effect of $\text{ID}^{\text{B}}$ in HL-1 cardiomyocytes

Injection of  $\text{ID}^{\text{B}}$  appeared to have little effect in synchronous resting HL-1 cells and although subtle changes in some  $\text{Ca}^{2+}$  handling parameters were observed, they did not manifest as alterations in synchronicity (discussed in Chapter 5). Despite the small changes in noise and rate of  $\text{Ca}^{2+}$  release, which may imply some interaction with SERCA or altered modes of  $\text{Ca}^{2+}$  influx and/or efflux, the transient characteristics and synchronicity remained unchanged compared with the control cells.

In a model of ouabain-induced  $\text{Ca}^{2+}$ -overload and intercellular dyssynchrony, which from a mechanistic perspective mimics the events underlying some forms of malignant human arrhythmia (i.e. chronic  $\text{Ca}^{2+}$  overload),  $\text{ID}^{\text{B}}$  restored synchrony in ouabain pre-treated cells, to a level which is comparable to that seen in WT HL-1 cells. This was observed after the injection of both *in vitro*- and bacterially-produced  $\text{ID}^{\text{B}}$  (Chapters 5 and 6, respectively)

Interestingly, the restoration of synchrony by  $\text{ID}^{\text{B}}$  was not observed in cells which contained  $\text{ID}^{\text{B}}$  prior to the addition of ouabain, implying that the potential beneficial effects of  $\text{ID}^{\text{B}}$  on normalising cellular  $\text{Ca}^{2+}$  cycling may be restricted to those cells in which  $\text{Ca}^{2+}$  cycling is already perturbed. The present data provides a platform for further investigating the

therapeutic utility of specific intra-RyR2 epitopes e.g. as novel anti-arrhythmic moieties.

HL-1 cells provide a unique experimental system, which is ideal for a proof of concept study, as presented in this thesis. HL-1 cardiomyocytes are distinctive in their capacity to proliferate and be serially passaged without reverting to an embryonic phenotype (Claycomb et al. 1998; White et al. 2004), and are the only cultured cell line of cardiac origin which can form synchronously coupled beating monolayers suitable for imaging experiments. Further studies will need to address the physiological applicability of the results observed in HL-1 cells, and if they can be reproduced in other experimental systems, such as computational modelling systems, canine wedge preparations, and animal models.

#### **9.4 The effect of the I-Domain on IP<sub>3</sub>R-dependent Ca<sup>2+</sup> handling**

The ID<sup>B</sup>-mediated restoration of synchrony in dyssynchronous HL-1 cells is likely to be associated with favourable intra-molecular conformational changes (Figure 5.21) – a mechanistic feature common to both RyR2 and IP<sub>3</sub>R. Since bioinformatic comparisons revealed striking structural homology between sub-fragments of the RyR2 I-Domain and I-Domain-like regions of IP<sub>3</sub>R, the study of the I-Domain fragments was extended to investigate their effects on IP<sub>3</sub>R channel regulation, as described in Chapter 7.

ID proteins had a profound effect on cellular Ca<sup>2+</sup> handling phenotype in HEK cells following IP<sub>3</sub>R stimulation by 0.1mM carbachol. Transduction with I-Domain fragments altered both the extent of carbachol-evoked Ca<sup>2+</sup> transient as well as the transient shape. Although this suggests the direct (and possibly indirect) involvement of components regulating intracellular Ca<sup>2+</sup> it also suggests that these alterations in Ca<sup>2+</sup> behaviour may be due to the ID fragments modulating some mode of Ca<sup>2+</sup> influx, as indicated by the findings of experiments in which a chelator of extracellular Ca<sup>2+</sup> (EGTA) was added to the culture media (Figure 7.13). This requires further investigation.

Additionally, a comparison of the SV<sub>m</sub> in carbachol-responsive and non-responsive HEK cells found a link between SV<sub>m</sub> and the propensity of cell to respond to carbachol. In

general, carbachol-responsive HEK cells had a higher mean resting  $SV_m$ , a finding that points towards an intriguing link between basal  $Ca^{2+}$  fluxes and agonist-evoked  $Ca^{2+}$  release. The concept that homeostatic  $Ca^{2+}$  fluxes 'tunes' the amplitude and temporal characteristics of agonist-evoked  $Ca^{2+}$  mobilisation is rapidly emerging (George *et al.* 2006; Silvester *et al.* 2009).

### 9.5 *The bystander effect*

This thesis provides persuasive evidence for the existence of a 'bystander effect', whereby non-injected cells showed the same  $Ca^{2+}$ -handling phenotypes as nearby cells that had been microinjected with I-Domain fragments. The 'bystander effect' has been regularly reported in the study of immunology, and in cancer therapy after exposure to ionising radiation treatment in cancer therapy, whereby irradiated cells may also transmit damage signals to non-irradiated cells in a population, leading to the occurrence of the same genetic effects in these 'bystander' cells that themselves receive no radiation exposure (Morgan & Sowa 2007), but to the best of our knowledge, this is the first report of a bystander effect in cardiac cells.

The bystander effect was observed in different cell types (HL-1 and HEK cells) and using recombinant proteins produced via distinct synthetic routes (bacterial expression and *in vitro* synthesis), and importantly, has also been observed in other distinct studies in our laboratory (Fry 2008). Taken together, these indicate that the bystander effect, that probably involves both direct intercellular communication (via GJIC) and an extracellular transfer route, is not simply an artefact of the cell-line, delivery technique or experimental conditions. Such a bystander effect may have important implications in arrhythmogenesis, whereby a relatively small number of asynchronous cells may be sufficient to underlie disruption of synchronicity in the heart. In addition, it may provide the conceptual basis for the therapeutic targeting of small, discrete cellular populations within the myocardium. To this end, a recent study by Marban and colleagues highlighted the therapeutic consequences of a bystander effect in



the context of arrhythmia. Kashiwakura (Circulation 2006 114 1682-1686) showed a remarkable restoration of normal heart rhythm following the transduction of <2% of the myocardium with an adenovirus encoding a recombinant ion channel.

## ***Bibliography***

- Ahern, G.P., Junankar, P.R. & Dulhunty, A.F. (1994) Single channel activity of the ryanodine receptor calcium release channel is modulated by FK-506. *Federation of Biochemical Societies Letters*, 352 (3), pp.369-74.
- Ahern, G.P., Junankar, P.R. & Dulhunty, A.F. (1997) Subconductance states in single-channel activity of skeletal muscle ryanodine receptors after removal of FKBP12. *Biophysical Journal*, 72 (1), pp.146-62.
- Aizman, O., Uhlén, P., Lal, M., Brismar, H. & Aperia, A. (2001) Ouabain, a steroid hormone that signals with slow calcium oscillations. *Proceedings of the National Academy of Sciences of the United States of America*, 98 (23), pp.13420-4.
- Akhavan, A., Atanasiu, R. & Shrier, A. (2003) Identification of a COOH-terminal Segment Involved in Maturation and Stability of Human Ether-a-go-go-related Gene Potassium Channels. *Journal of Biological Chemistry*, 278 (41), pp.40105-40112.
- Alimov, A.P., Khmel'nitsky, A.Y., Simonenko, P.N., Spirin, A.S. & Chetverin, A.B. (2000) Cell-free synthesis and affinity isolation of proteins on a nanomole scale. *Biotechniques*, 28 (2), pp.338-44.
- Anderson, C.W., Atkins, J.F. & Dunn, J.J. (1976) Bacteriophage T3 and T7 early RNAs are translated by eukaryotic 80S ribosomes: active phage T3 coded S-adenosylmethionine cleaving enzyme is synthesized. *Proceedings of the National Academy of Sciences of the United States of America*, 73 (8), pp.2752-6.
- Antoons, G. & Sipido, K.R. (2008) Targeting calcium handling in arrhythmias. *Europace: European Pacing, Arrhythmias, and Cardiac Electrophysiology: Journal of the Working Groups on Cardiac Pacing, Arrhythmias, and Cardiac Cellular Electrophysiology of the European Society of Cardiology*, 10 (12), pp.1364-9.
- Antos, C.L., Frey, N., Marx, S.O., Reiken, S., Gaburjakova, M., Richardson, J.A., Marks, A.R. & Olson, E.N. (2001) Dilated cardiomyopathy and sudden death resulting from constitutive activation of protein kinase a. *Circulation Research*, 89 (11), pp.997-1004.
- Arnon, A., Hamlyn, J.M. & Blaustein, M.P. (2000) Ouabain augments Ca<sup>2+</sup> transients in arterial smooth muscle without raising cytosolic Na<sup>(+)</sup>. *American Journal of Physiology. Heart and Circulatory Physiology*, 279 (2), pp.H679-91.
- Ausubel, F.M., Brent, R. & Kingston, R.E. (2002) *Short Protocols in Molecular Biology: A Compendium of Methods from Current*, Wiley.
- Azzam, E.I., de Toledo, S.M., Gooding, T. & Little, J.B. (1998) Intercellular communication is involved in the bystander regulation of gene expression in human cells exposed to very low fluences of alpha particles. *Radiation Research*, 150 (5), pp.497-504.
- Azzam, E.I., de Toledo, S.M. & Little, J.B. (2001) Direct evidence for the participation of gap junction-mediated intercellular communication in the transmission of damage signals from alpha -particle irradiated to nonirradiated cells. *Proceedings of the National Academy of Sciences of the United States of America*, 98 (2), pp.473-8.
- Baneyx, F., Ayling, A., Palumbo, T., Thomas, D. & Georgiou, G. (1991) Optimization of growth conditions for the production of proteolytically-sensitive proteins in the periplasmic space of Escherichia coli. *Applied Microbiology and Biotechnology*, 36 (1), pp.14-20.

- Barberini-Jammaers, S.R., Ashton, P.M., Claycomb, W.C., Lai, F.A. & George, C.H. (2008) SALVO - A new analytical platform for decoding intracellular Ca<sup>2+</sup> fluxes and evaluating anti-arrhythmic compounds. *Biophysical Journal Supplement*, 104a.
- Barg, S., Copello, J.A. & Fleischer, S. (1997) Different interactions of cardiac and skeletal muscle ryanodine receptors with FK-506 binding protein isoforms. *The American Journal of Physiology*, 272 (5 Pt 1), pp.C1726-33.
- Bartoli, M. & Claycomb, W.C. (1997) Transfer of macromolecules into living adult cardiomyocytes by microinjection. *Molecular and Cellular Biochemistry*, 172 (1), pp.103-109.
- Bassani, J.W., Yuan, W. & Bers, D.M. (1995) Fractional SR Ca release is regulated by trigger Ca and SR Ca content in cardiac myocytes. *The American Journal of Physiology*, 268 (5 Pt 1), pp.C1313-9.
- Bassani, R.A., Bassani, J.W. & Bers, D.M. (1994) Relaxation in ferret ventricular myocytes: unusual interplay among calcium transport systems. *The Journal of Physiology*, 476 (2), pp.295-308.
- Beard, N.A., Casarotto, M.G., Wei, L., Varsányi, M., Laver, D.R. & Dulhunty, A.F. (2005) Regulation of ryanodine receptors by calsequestrin: effect of high luminal Ca<sup>2+</sup> and phosphorylation. *Biophysical Journal*, 88 (5), pp.3444-54.
- Benkusky, N.A., Farrell, E.F. & Valdivia, H.H. (2004) Ryanodine receptor channelopathies. *Biochemical and Biophysical Research Communications*, 322 (4), pp.1280-1285.
- Bentley, W., Davis, R. & Kompala, D. (1991) Dynamics of induced cat expression in *Escherichia coli*. *Biotechnology and Bioengineering*, 38 (7), pp.749-760.
- Bentley, W., Mirjalili, N., Andersen, D., Davis, R. & Kompala, D. (1990) Plasmid-encoded protein - The principal factor in the metabolic burden associated with recombinant bacteria. *Biotechnology and Bioengineering*, 35 (7), pp.668-681.
- Berridge, M.J. (1997) Elementary and global aspects of calcium signalling. *Journal of Physiology*, (499.2), pp.291-306.
- Berridge, M.J., Lipp, P. & Bootman, M.D. (2000) The versatility and universality of calcium signalling. *Nature Reviews; Molecular Cell Biology*, 1, pp.11-21.
- Berridge, M.J., Bootman, M.D. & Roderick, H.L. (2003) Calcium signalling: dynamics, homeostasis and remodelling. *Nature reviews. Molecular cell biology*, 4 (7), pp.517-29.
- Bers, D.M. (2002) Cardiac excitation-contraction coupling. *Nature*, 415 (6868), pp.198-205.
- Bers, D.M. (2006) Cardiac ryanodine receptor phosphorylation: target sites and functional consequences. *The Biochemical Journal*, 396 (1), pp.e1-3.
- Bers, D.M., Eisner, D.A. & Valdivia, H.H. (2003) Sarcoplasmic reticulum Ca<sup>2+</sup> and heart failure: roles of diastolic leak and Ca<sup>2+</sup> transport. *Circulation Research*, 93 (6), pp.487-90.

- Bers, D.M. (2001) *Excitation-Contraction Coupling and Cardiac Contractile Force*. 2nd ed., Dodrecht (Netherlands): Kluwer academic publishers.
- Bers, D.M. (2004) Macromolecular complexes regulating cardiac ryanodine receptor function. *Journal of Molecular and Cellular Cardiology*, 37 (2), pp.417-429.
- Blayney, L.M., Zissimopoulos, S., Ralph, E., Abbot, E., Matthews, L. & Lai, F.A. (2004) Ryanodine receptor oligomeric interaction: identification of a putative binding region. *The Journal of Biological Chemistry*, 279 (15), pp.14639-48.
- Blondel, O., Moody, M.M., Depaoli, A.M., Sharp, A.H., Ross, C.A., Swift, H. & Bell, G.I. (1994) Localization of inositol trisphosphate receptor subtype 3 to insulin and somatostatin secretory granules and regulation of expression in islets and insulinoma cells. *Proceedings of the National Academy of Sciences of the United States of America*, 91 (16), pp.7777-81.
- Bootman, M.D. & Roderick, H.L. (2008) Why, where, and when do cardiac myocytes express inositol 1,4,5-trisphosphate receptors? *American Journal of Physiology. Heart and Circulatory Physiology*, 294 (2), pp.H579-81.
- Bootman, M.D., Berridge, M.J. & Lipp, P. (1997) Cooking with Calcium: The Recipes for Composing Global Signals from Elementary Events. *Cell*, 91 (3), pp.367-373.
- Braunwald, E. & Bristow, M.R. (2000) Congestive heart failure: fifty years of progress. *Circulation*, 102 (20 Suppl 4), pp.IV14-23.
- Brillantes, A.B., Ondrias, K., Scott, A., Kobrinsky, E., Ondriasová, E., Moschella, M.C., Jayaraman, T., Landers, M., Ehrlich, B.E. & Marks, A.R. (1994) Stabilization of calcium release channel (ryanodine receptor) function by FK506-binding protein. *Cell*, 77 (4), pp.513-23.
- Brini, M. (2004) Ryanodine receptor defects in muscle genetic diseases. *Biochemical and Biophysical Research Communications*, 322 (4), pp.1245-1255.
- Buckalew, V.M. (2005) Endogenous digitalis-like factors. An historical overview. *Frontiers in Bioscience: A Journal and Virtual Library*, 10, pp.2325-34.
- Bultynck, G., Ross, D., Callewaert, G., Missiaen, L., Sorrentino, V., Parys, J.B. & De Smedt, H. (2001) The conserved sites for FK506-binding proteins in ryanodine receptors and inositol 1,4,5-triphosphate receptors are structurally and functionally different. *Journal of Biological Chemistry*, 276 (50), pp.47715-47724.
- Cabilly, S. (1989) Growth at sub-optimal temperatures allows the production of functional, antigen-binding Fab fragments in *Escherichia coli*. *Gene*, 85 (2), pp.553-7.
- Cadwell, J.J. & Caswell, A.H. (1982) Identification of a constituent of the junctional feet linking terminal cisternae to transverse tubules in skeletal muscle. *The Journal of Cell Biology*, 93 (3), pp.543-50.
- Cameron, A.M., Nucifora, F.C., Fung, E.T., Livingston, D.J., Aldape, R.A., Ross, C.A. & Snyder, S.H. (1997) FKBP12 binds the inositol 1,4,5-trisphosphate receptor at leucine-proline (1400-1401) and anchors calcineurin to this FK506-like domain. *The Journal of Biological Chemistry*, 272 (44), pp.27582-8.

- Carter, P., Kelley, R.F., Rodrigues, M.L., Snedecor, B., Covarrubias, M., Velligan, M.D., Wong, W.L., Rowland, A.M., Kotts, C.E. & Carver, M.E. (1992) High level *Escherichia coli* expression and production of a bivalent humanized antibody fragment. *Bio/Technology*, 10 (2), pp.163-7.
- Carter, S., Colyer, J. & Sitsapesan, R. (2006) Maximum phosphorylation of the cardiac ryanodine receptor at serine-2809 by protein kinase a produces unique modifications to channel gating and conductance not observed at lower levels of phosphorylation. *Circulation Research*, 98 (12), pp.1506-13.
- Chalmers, J.J., Kim, E., Telford, J.N., Wong, E.Y., Tacon, W.C., Shuler, M.L. & Wilson, D.B. (1990) Effects of temperature on *Escherichia coli* overproducing beta-lactamase or human epidermal growth factor. *Applied and Environmental Microbiology*, 56 (1), pp.104-11.
- Chaudhry, M.A. (2006) Bystander effect: biological endpoints and microarray analysis. *Mutation Research*, 597 (1-2), pp.98-112.
- Chelu, M.G., Danila, C.I., Gilman, C.P. & Hamilton, S.L. (2004) Regulation of Ryanodine Receptors by FK506 Binding Proteins. *Trends in Cardiovascular Medicine*, 14 (6), pp.227-234.
- Cheng, H., Lederer, M.R., Lederer, W.J. & Cannell, M.B. (1996) Calcium sparks and  $[Ca^{2+}]_i$  waves in cardiac myocytes. *The American Journal of Physiology*, 270 (1 Pt 1), pp.C148-59.
- Chesshyre, J. & Hipkiss, A. (1989) Low temperatures stabilize interferon-alpha-2 against proteolysis in *Methylophilus-methylotrophus* and *Escherichia-coli*. *Applied Microbiology and Biotechnology*, 31 (2), pp.158-162.
- Ching, L.L., Williams, A.J. & Sitsapesan, R. (2000) Evidence for  $Ca^{2+}$  activation and inactivation sites on the luminal side of the cardiac ryanodine receptor complex. *Circulation Research*, 87 (3), pp.201-6.
- Chu, A., Fill, M., Stefani, E. & Entman, M.L. (1993) Cytoplasmic  $Ca^{2+}$  does not inhibit the cardiac muscle sarcoplasmic reticulum ryanodine receptor  $Ca^{2+}$  channel, although  $Ca^{2+}$ -induced  $Ca^{2+}$  inactivation of  $Ca^{2+}$  release is observed in native vesicles. *The Journal of Membrane Biology*, 135 (1), pp.49-59.
- Clapham, D.E. (2007) Calcium signaling. *Cell*, 131 (6), pp.1047-58.
- Clarke, T.C., Thomas, D., Petersen, J.S., Evans, W.H. & Martin, P.E.M. (2006) The antiarrhythmic peptide rotigaptide (ZP123) increases gap junction intercellular communication in cardiac myocytes and HeLa cells expressing connexin 43. *British Journal of Pharmacology*, 147 (5), pp.486-95.
- Claycomb, W., Lanson, N., Stallworth, B., Egeland, D., Delcarpio, J., Bahinski, A. & Izzo, N. (1998) HL-1 cells: a cardiac muscle cell line that contracts and retains phenotypic characteristics of the adult cardiomyocyte. *Proceedings of the National Academy of Sciences of the United States of America*, 95 (6), pp.2979-2984.
- Cohn, J.N. (1995) Plasma norepinephrine and mortality. *Clinical Cardiology*, 18 (3 Suppl 1), pp.I9-12.

- Cohn, J.N., Levine, T.B., Olivari, M.T., Garberg, V., Lura, D., Francis, G.S., Simon, A.B. & Rector, T. (1984) Plasma norepinephrine as a guide to prognosis in patients with chronic congestive heart failure. *The New England Journal of Medicine*, 311 (13), pp.819-23.
- Collier, J., White, S., William, C. & Scott, S. (2002) Insulin represses and chronic hyperglycemia stimulates adrenomedullin gene expression in HL-1 cultured cardiac myocytes. *Diabetes*, 51, pp.A590-A590.
- Colosimo, A., Goncz, K.K., Holmes, A.R., Kunzelmann, K., Novelli, G., Malone, R.W., Bennett, M.J. & Gruenert, D.C. (2000) Transfer and expression of foreign genes in mammalian cells. *BioTechniques*, 29 (2), pp.314-8.
- Copello, J.A., Barg, S., Sonnleitner, A., Porta, M., Diaz-Sylvester, P., Fill, M., Schindler, H. & Fleischer, S. (2002) Differential activation by  $Ca^{2+}$ , ATP and caffeine of cardiac and skeletal muscle ryanodine receptors after block by  $Mg^{2+}$ . *The Journal of Membrane Biology*, 187 (1), pp.51-64.
- Cormier-Regard, S., Nguyen, S.V. & Claycomb, W.C. (1998) Adrenomedullin gene expression is developmentally regulated and induced by hypoxia in rat ventricular cardiac myocytes. *The Journal of Biological Chemistry*, 273 (28), pp.17787-92.
- Currie, S., Loughrey, C.M., Craig, M. & Smith, G.L. (2004) Calcium/calmodulin-dependent protein kinase I $\delta$  associates with the ryanodine receptor complex and regulates channel function in rabbit heart. *The Biochemical Journal*, 377 (Pt 2), pp.357-66.
- Dawson, A.P. (1997) Calcium signalling: How do IP<sub>3</sub> receptors work? *Current Biology*, 7 (9), pp.544-547.
- Delcarpio, J.B., Lanson, N.A., Field, L.J. & Claycomb, W.C. (1991) Morphological characterization of cardiomyocytes isolated from a transplantable cardiac tumor derived from transgenic mouse atria (AT-1 cells). *Circulation Research*, 69 (6), pp.1591-600.
- Domeier, T.L., Zima, A.V., Maxwell, J.T., Huke, S., Mignery, G.A. & Blatter, L.A. (2008) IP<sub>3</sub> receptor-dependent  $Ca^{2+}$  release modulates excitation-contraction coupling in rabbit ventricular myocytes. *American Journal of Physiology. Heart and Circulatory Physiology*, 294 (2), pp.H596-604.
- Donovan, R.S., Robinson, C.W. & Glick, B.R. (1996) Review: optimizing inducer and culture conditions for expression of foreign proteins under the control of the lac promoter. *Journal of Industrial Microbiology*, 16 (3), pp.145-54.
- Du, G.G., Khanna, V.K. & MacLennan, D.H. (2000) Mutation of divergent region 1 alters caffeine and  $Ca^{2+}$  sensitivity of the skeletal muscle  $Ca^{2+}$  release channel (ryanodine receptor). *The Journal of Biological Chemistry*, 275 (16), pp.11778-83.
- Du, G.G., Sandhu, B., Khanna, V.K., Guo, X.H. & MacLennan, D.H. (2002) Topology of the  $Ca^{2+}$  release channel of skeletal muscle sarcoplasmic reticulum RyR1. *Proceedings of The National Academy of Sciences of The United States of America*, 99 (26), pp.16725-16730.

- Du, G.G., Avila, G., Sharma, P., Khanna, V.K., Dirksen, R.T. & MacLennan, D.H. (2004) Role of the sequence surrounding predicted transmembrane helix M4 in membrane association and function of the Ca<sup>2+</sup> release channel of skeletal muscle sarcoplasmic reticulum (ryanodine receptor isoform 1). *The Journal of Biological Chemistry*, 279 (36), pp.37566-74.
- Dulhunty, A.F. & Pouliquin, P. (2003) What we don't know about the structure of ryanodine receptor calcium release channels. *Clinical and Experimental Pharmacology & Physiology*, 30 (10), pp.713-23.
- El-Hayek, R., Saiki, Y., Yamamoto, T. & Ikemoto, N. (1999) A postulated role of the near amino-terminal domain of the ryanodine receptor in the regulation of the sarcoplasmic reticulum Ca<sup>2+</sup> channel. *The Journal of Biological Chemistry*, 274 (47), pp.33341-7.
- Emerit, I., Levy, A., Cernjavski, L., Arutyunyan, R., Oganessian, N., Pogolian, A., Mejlumian, H., Sarkisian, T., Gulkandian, M. & Quastel, M. (1994) Transferable clastogenic activity in plasma from persons exposed as salvage personnel of the Chernobyl reactor. *Journal of Cancer Research and Clinical Oncology*, 120 (9), pp.558-61.
- Endo, Y. & Sawasaki, T. (2006) Cell-free expression systems for eukaryotic protein production. *Current Opinion in Biotechnology*, 17 (4), pp.373-380.
- Field, L.J. (1988) Atrial natriuretic factor-SV40 T antigen transgenes produce tumors and cardiac arrhythmias in mice. *Science (New York, N.Y.)*, 239 (4843), pp.1029-33.
- Fill, M. & Copello, J.A. (2002) Ryanodine receptor calcium release channels. *Physiological Reviews*, 82 (4), pp.893-922.
- Flucher, B.E. & Franzini-Armstrong, C. (1996) Formation of junctions involved in excitation-contraction coupling in skeletal and cardiac muscle. *Proceedings of the National Academy of Sciences of the United States of America*, 93 (15), pp.8101-6.
- da Fonseca, P.C.A., Morris, S.A., Nerou, E.P., Taylor, C.W. & Morris, E.P. (2003) Domain organization of the type 1 inositol 1,4,5-trisphosphate receptor as revealed by single-particle analysis. *Proceedings of the National Academy of Sciences of the United States of America*, 100 (7), pp.3936-41.
- Franzini, C. (1970) Studies of triad 1: Structure of junction in frog twitch fibers. *Journal of Cell Biology*, 47 (2), pp.488-&.
- Franzini-Armstrong, C. (1973) Studies of the triad. IV. Structure of the junction in frog slow fibers. *The Journal of Cell Biology*, 56 (1), pp.120-8.
- Franzini-Armstrong, C. & Protasi, F. (1997) Ryanodine receptors of striated muscles: a complex channel capable of multiple interactions. *Physiological Reviews*, 77 (3), pp.699-729.
- Franzini-Armstrong, C., Protasi, F. & Ramesh, V. (1999) Shape, size, and distribution of Ca<sup>2+</sup> release units and couplons in skeletal and cardiac muscles. *Biophysical Journal*, 77 (3), pp.1528-39.
- Fry, D.L., Jundi, H., Thomas, N.L., Lai, F.A. & George, C.H. (2007) Modulating intracellular Ca<sup>2+</sup> signaling using recombinant fragments of the human cardiac ryanodine receptor (RyR2). *Biophysical Journal*, (Suppl. S), p.260A.



- Fry, D.L. (2008) Modulating intracellular Ca<sup>2+</sup> handling using recombinant fragments of the human cardiac ryanodine receptor (RyR2). *Cardiff University Thesis*.
- Furuichi, T., Kohda, K., Miyawaki, A. & Mikoshiba, K. (1994) Intracellular channels. *Current Opinion in Neurobiology*, 4 (3), pp.294-303.
- Furuichi, T., Yoshikawa, S., Miyawaki, A., Wada, K., Maeda, N. & Mikoshiba, K. (1989) Primary structure and functional expression of the inositol 1,4,5-trisphosphate-binding protein P400. *Nature*, 342 (6245), pp.32-8.
- Gaburjakova, M., Gaburjakova, J., Reiken, S., Huang, F., Marx, S.O., Rosembliit, N. & Marks, A.R. (2001) FKBP12 binding modulates ryanodine receptor channel gating. *The Journal of Biological Chemistry*, 276 (20), pp.16931-5.
- Gao, L., Tripathy, A., Lu, X. & Meissner, G. (1997) Evidence for a role of C-terminal amino acid residues in skeletal muscle Ca<sup>2+</sup> release channel (ryanodine receptor) function. *Federation of Biochemical Societies Letters*, 412 (1), pp.223-226.
- Gemignani, F., Ballardini, M., Maggiani, F., Rossi, A.M., Antonelli, A. & Barale, R. (1999) Chromosome aberrations in lymphocytes and clastogenic factors in plasma detected in Belarus children 10 years after Chernobyl accident. *Mutation Research*, 446 (2), pp.245-53.
- George, C.H. (2008a) Sarcoplasmic reticulum Ca<sup>2+</sup> leak in heart failure: mere observation or functional relevance? *Cardiovascular Research*, 77, pp.302-314.
- George, C.H., Barberini-Jammaers, S.R. & Muller, C.T. (2008b) Refocussing therapeutic strategies for cardiac arrhythmias: defining viable molecular targets to restore cardiac ion flux. *Expert Opinion on Therapeutic Patents*, 18 (1), pp.1-19.
- George, C.H., Higgs, G.V. & Lai, F.A. (2003a) Ryanodine receptor mutations associated with stress-induced ventricular tachycardia mediate increased calcium release in stimulated cardiomyocytes. *Circulation Research*, 93 (6), pp.531-40.
- George, C.H., Higgs, G.V., Mackrill, J.J. & Lai, F.A. (2003b) Dysregulated ryanodine receptors mediate cellular toxicity: restoration of normal phenotype by FKBP12.6. *The Journal of Biological Chemistry*, 278 (31), pp.28856-64.
- George, C.H., Jundi, H., Thomas, N.L., Fry, D.L. & Lai, F.A. (2007a) Ryanodine receptors and ventricular arrhythmias: emerging trends in mutations, mechanisms and therapies. *Journal of Molecular and Cellular Cardiology*, 42 (1), pp.34-50.
- George, C.H., Jundi, H., Thomas, N.L., Scoote, M., Walters, N., Williams, A.J. & Lai, F.A. (2004) Ryanodine receptor regulation by intramolecular interaction between cytoplasmic and transmembrane domains. *Molecular Biology of the Cell*, 15 (6), pp.2627-38.
- George, C.H., Jundi, H., Walters, N., Thomas, N.L., West, R.R. & Lai, F.A. (2006) Arrhythmogenic mutation-linked defects in ryanodine receptor autoregulation reveal a novel mechanism of Ca<sup>2+</sup> release channel dysfunction. *Circulation Research*, 98 (1), pp.88-97.

- George, C.H. & Lai, F.A. (2007b) Developing new anti-arrhythmics: clues from the molecular basis of cardiac ryanodine receptor (RyR2) Ca<sup>2+</sup>-release channel dysfunction. *Current Pharmaceutical Design*, 13 (31), pp.3195-211.
- George, C.H., Rogers, S.A., Bertrand, B.M.A., Tunwell, R.E.A., Thomas, N.L., Steele, D.S., Cox, E.V., Pepper, C., Hazeel, C.J., Claycomb, W.C. & Lai, F.A. (2007c) Alternative splicing of ryanodine receptors modulates cardiomyocyte Ca<sup>2+</sup> signaling and susceptibility to apoptosis. *Circulation Research*, 100 (6), pp.874-83.
- George, C.H., Sorathia, R., Bertrand, B.M.A. & Lai, F.A. (2003c) In situ modulation of the human cardiac ryanodine receptor (hRyR2) by FKBP12.6. *The Biochemical Journal*, 370 (Pt 2), pp.579-89.
- George, C.H., Yin, C.C. & Lai, F.A. (2005) Toward a molecular understanding of the structure-function of ryanodine receptor Ca<sup>2+</sup> release channels: perspectives from recombinant expression systems. *Cell Biochemistry and Biophysics*, 42 (2), pp.197-222.
- Giannini, G., Clementi, E., Ceci, R., Marziali, G. & Sorrentino, V. (1992) Expression of a ryanodine receptor-Ca<sup>2+</sup> channel that is regulated by TGF-beta. *Science (New York, N.Y.)*, 257 (5066), pp.91-4.
- Giannini, G., Conti, A., Mammarella, S., Scrobogna, M. & Sorrentino, V. (1995) The ryanodine receptor/calcium channel genes are widely and differentially expressed in murine brain and peripheral tissues. *The Journal of Cell Biology*, 128 (5), pp.893-904.
- Gilbert, J.C., Shirayama, T. & Pappano, A.J. (1991) Inositol trisphosphate promotes Na-Ca exchange current by releasing calcium from sarcoplasmic reticulum in cardiac myocytes. *Circulation Research*, 69 (6), pp.1632-9.
- Glick, B.R. (1995) Metabolic load and heterologous gene expression. *Biotechnology Advances*, 13 (2), pp.247-61.
- Glick, B.R. & Whitney, G. (1987) Factors affecting the expression of foreign proteins in *Escherichia coli*. *Journal of Industrial Microbiology*, 1 (5), pp.277-282.
- Goto, A., Yamada, K., Ishii, M. & Sugimoto, T. (1990) Digitalis-like activity in human plasma - relation to blood-pressure and sodium-balance. *American Journal of Medicine*, 89 (4), pp.420-426.
- Graham, F.L., Smiley, J., Russell, W.C. & Nairn, R. (1977) Characteristics of a human cell line transformed by DNA from human adenovirus type 5. *The Journal of General Virology*, 36 (1), pp.59-74.
- Green, M., Thorburn, A., Kern, R. & Loewenstein, P.M. (2007) The Use of Cell Microinjection for the In Vivo Analysis of Viral Transcriptional Regulatory Protein Domains. , 131.
- Györke, I. & Györke, S. (1998) Regulation of the cardiac ryanodine receptor channel by luminal Ca<sup>2+</sup> involves luminal Ca<sup>2+</sup> sensing sites. *Biophysical Journal*, 75 (6), pp.2801-10.
- Györke, I., Hester, N., Jones, L.R. & Györke, S. (2004) The role of calsequestrin, triadin, and junctin in conferring cardiac ryanodine receptor responsiveness to luminal calcium. *Biophysical Journal*, 86 (4), pp.2121-8.

- Hachida, M., Lu, H., Kaneko, N., Horikawa, Y., Ohkado, A., Gu, H., Zhang, X.L., Hoshi, H., Nonoyama, M., Nakanishi, T. & Koyanagi, H. (1999) Protective effect of JTV519 (K201), a new 1,4-benzothiazepine derivative, on prolonged myocardial preservation. *Transplantation Proceedings*, 31 (1-2), pp.996-1000.
- Haghighi, K., Kolokathis, F., Gramolini, A.O., Waggoner, J.R., Pater, L., Lynch, R.A., Fan, G., Tsiapras, D., Parekh, R.R., Dorn, G.W., MacLennan, D.H., Kremastinos, D.T. & Kranias, E.G. (2006) A mutation in the human phospholamban gene, deleting arginine 14, results in lethal, hereditary cardiomyopathy. *Proceedings of the National Academy of Sciences of the United States of America*, 103 (5), pp.1388-93.
- Hakamata, Y., Nakai, J., Takeshima, H. & Imoto, K. (1992) Primary structure and distribution of a novel ryanodine receptor/calcium release channel from rabbit brain. *Federation of Biochemical Societies Letters*, 312, pp.229-235.
- Hamada, K., Miyata, T., Mayanagi, K., Hirota, J. & Mikoshiba, K. (2002) Two-state conformational changes in inositol 1,4,5-trisphosphate receptor regulated by calcium. *The Journal of Biological Chemistry*, 277 (24), pp.21115-8.
- Hamada, K., Terauchi, A. & Mikoshiba, K. (2003) Three-dimensional rearrangements within inositol 1,4,5-trisphosphate receptor by calcium. *The Journal of Biological Chemistry*, 278 (52), pp.52881-9.
- Hamada, N., Matsumoto, H., Hara, T. & Kobayashi, Y. (2007b) Intercellular and intracellular signaling pathways mediating ionizing radiation-induced bystander effects. *Journal of Radiation Research*, 48 (2), pp.87-95.
- Hamada, T., Bannister, M.L. & Ikemoto, N. (2007a) Peptide probe study of the role of interaction between the cytoplasmic and transmembrane domains of the ryanodine receptor in the channel regulation mechanism. *Biochemistry*, 46 (14), pp.4272-9.
- Hamilton, S.L. & Serysheva, I. (2008) Ryanodine receptor structure: Progress and challenges. *The Journal of Biological Chemistry*. In press; d.o.i R800054200.
- Hamilton, S.L. (2005) Ryanodine receptors. *Cell Calcium*, 38 (3-4), pp.253-260.
- Hamlyn, J., Blaustein, M., Bova, S., Ducharme, D., Harris, D., Mandel, F., Mathews, W. & Ludens, J. (1991) Identification and characterization of a ouabain-like compound from human plasma. *Proceedings of the National Academy of Sciences of the United States of America*, 88 (14), pp.6259-6263.
- Hasenfuss, G. & Pieske, B. (2002) Calcium cycling in congestive heart failure. *Journal of Molecular and Cellular Cardiology*, 34 (8), pp.951-69.
- Hauptman, P.J., Garg, R. & Kelly, R.A. (1999a) Cardiac glycosides in the next millennium. *Progress in Cardiovascular Diseases*, 41 (4), pp.247-54.
- Hauptman, P.J. & Kelly, R.A. (1999b) Digitalis. *Circulation*, 99 (9), pp.1265-70.
- Hedman, A., Hartikainen, J., Vanninen, E., Laitinen, T., Jääskeläinen, P., Laakso, M., Peuhkurinen, K. & Kuusisto, J. (2004) Inducibility of life-threatening ventricular arrhythmias is related to maximum left ventricular thickness and clinical markers of sudden cardiac death in patients with hypertrophic cardiomyopathy attributable to the Asp175Asn mutation in the alpha-tropomyosin gene. *Journal of Molecular and Cellular Cardiology*, 36 (1), pp.91-9.

- Hino, M., Kataoka, M., Kajimoto, K., Yamamoto, T., Kido, J., Shinohara, Y. & Baba, Y. (2008) Efficiency of cell-free protein synthesis based on a crude cell extract from *Escherichia coli*, wheat germ, and rabbit reticulocytes. *Journal of Biotechnology*, 133 (2), pp.183-189.
- Houser, S.R., Piacentino, V. & Weisser, J. (2000) Abnormalities of calcium cycling in the hypertrophied and failing heart. *Journal of Molecular and Cellular Cardiology*, 32 (9), pp.1595-607.
- Huke, S. & Bers, D.M. (2008) Ryanodine receptor phosphorylation at Serine 2030, 2808 and 2814 in rat cardiomyocytes. *Biochemical and Biophysical Research Communications*, 376 (1), pp.80-5.
- Hunt, D.J., Jones, P.P., Wang, R., Chen, W., Bolstad, J., Chen, K., Shimoni, Y. & Chen, S.R.W. (2007) K201 (JTV519) suppresses spontaneous  $\text{Ca}^{2+}$  release and [3H]ryanodine binding to RyR2 irrespective of FKBP12.6 association. *The Biochemical Journal*, 404 (3), pp.431-8.
- Hymel, L., Inui, M., Fleischer, S. & Schindler, H. (1988) Purified ryanodine receptor of skeletal muscle sarcoplasmic reticulum forms  $\text{Ca}^{2+}$ -activated oligomeric  $\text{Ca}^{2+}$  channels in planar bilayers. *Proceedings of the National Academy of Sciences of the United States of America*, 85 (2), pp.441-5.
- Ikemoto, N. & Yamamoto, T. (2000) Postulated role of inter-domain interaction within the ryanodine receptor in  $\text{Ca}^{2+}$  channel regulation. *Trends in Cardiovascular Medicine*, 10 (7), pp.310-316.
- Ikemoto, N. & Yamamoto, T. (2002) Regulation of calcium release by interdomain interaction within ryanodine receptors. *Frontiers in Bioscience*, 7, pp.671-683.
- Imagawa, T., Smith, J.S., Coronado, R. & Campbell, K.P. (1987) Purified ryanodine receptor from skeletal muscle sarcoplasmic reticulum is the  $\text{Ca}^{2+}$ -permeable pore of the calcium release channel. *The Journal of Biological Chemistry*, 262 (34), pp.16636-43.
- Inui, M., Saito, A. & Fleischer, S. (1987a) Isolation of the ryanodine receptor from cardiac sarcoplasmic reticulum and identity with the feet structures. *The Journal of Biological Chemistry*, 262 (32), pp.15637-42.
- Inui, M., Saito, A. & Fleischer, S. (1987b) Purification of the ryanodine receptor and identity with feet structures of junctional terminal cisternae of sarcoplasmic reticulum from fast skeletal muscle. *The Journal of Biological Chemistry*, 262 (4), pp.1740-7.
- Iwai, M., Michikawa, T., Bosanac, I., Ikura, M. & Mikoshiba, K. (2007) Molecular basis of the isoform-specific ligand-binding affinity of inositol 1,4,5-trisphosphate receptors. *The Journal of Biological Chemistry*, 282 (17), pp.12755-64.
- Iwai, M., Tateishi, Y., Hattori, M., Mizutani, A., Nakamura, T., Futatsugi, A., Inoue, T., Furuichi, T., Michikawa, T. & Mikoshiba, K. (2005) Molecular cloning of mouse type 2 and type 3 inositol 1,4,5-trisphosphate receptors and identification of a novel type 2 receptor splice variant. *The Journal of Biological Chemistry*, 280 (11), pp.10305-17.
- Jackson, A.M., Boutell, J., Cooley, N. & He, M. (2004) Cell-free protein synthesis for proteomics. *Briefings in Functional Genomics & Proteomics*, 2 (4), pp.308-19.

- Janczewski, A.M., Spurgeon, H.A., Stern, M.D. & Lakatta, E.G. (1995) Effects of sarcoplasmic reticulum  $Ca^{2+}$  load on the gain function of  $Ca^{2+}$  release by  $Ca^{2+}$  current in cardiac cells. *The American Journal of Physiology*, 268 (2 Pt 2), pp.H916-20.
- Janse, M.J. (2004) Electrophysiological changes in heart failure and their relationship to arrhythmogenesis. *Cardiovascular Research*, 61 (2), pp.208-17.
- Jayaraman, T., Brillantes, A.M., Timerman, A.P., Fleischer, S., Erdjument-Bromage, H., Tempst, P. & Marks, A.R. (1992) FK506 binding protein associated with the calcium release channel (ryanodine receptor). *The Journal of Biological Chemistry*, 267 (14), pp.9474-7.
- Jenden, D.J. & Fairhurst, A.S. (1969) The pharmacology of ryanodine. *Pharmacological Reviews*, 21 (1), pp.1-25.
- Jermutus, L., Ryabova, L.A. & Plückthun, A. (1998) Recent advances in producing and selecting functional proteins by using cell-free translation. *Current Opinion in Biotechnology*, 9 (5), pp.534-48.
- Jeyakumar, L.H., Copello, J.A., O'Malley, A.M., Wu, G.M., Grassucci, R., Wagenknecht, T. & Fleischer, S. (1998) Purification and characterization of ryanodine receptor 3 from mammalian tissue. *The Journal of Biological Chemistry*, 273 (26), pp.16011-20.
- Jiang, M.T., Lokuta, A.J., Farrell, E.F., Wolff, M.R., Haworth, R.A. & Valdivia, H.H. (2002a) Abnormal  $Ca^{2+}$  release, but normal ryanodine receptors, in canine and human heart failure. *Circulation Research*, 91 (11), pp.1015-22.
- Jiang, Q., Thrower, E.C., Chester, D.W., Ehrlich, B.E. & Sigworth, F.J. (2002b) Three-dimensional structure of the type 1 inositol 1,4,5-trisphosphate receptor at 24 Å resolution. *The EMBO Journal*, 21 (14), pp.3575-81.
- Junge, F., Schneider, B., Reckel, S., Schwarz, D., Dötsch, V. & Bernhard, F. (2008) Large-scale production of functional membrane proteins. *Cellular and Molecular Life Sciences (CMLS)*, 65 (11), pp.1729-1755.
- Kaftan, E., Marks, A.R. & Ehrlich, B.E. (1996) Effects of rapamycin on ryanodine receptor/ $Ca^{2+}$ -release channels from cardiac muscle. *Circulation Research*, 78 (6), pp.990-7.
- Kaneko, N. (1994) New 1,4-benzothiazepine derivative, K201, demonstrates cardioprotective effects against sudden cardiac cell-death and intracellular calcium blocking action. *Drug Development Research*, 33 (4), pp.429-438.
- Kass, R.S. (2005) The channelopathies: novel insights into molecular and genetic mechanisms of human disease. *The Journal of Clinical Investigation*, 115 (8), pp.1986-9.
- Katzen, F., Chang, G. & Kudlicki, W. (2005) The past, present and future of cell-free protein synthesis. *Trends in Biotechnology*, 23 (3), pp.150-6.
- Kawamura, A., Abrell, L.M., Maggiali, F., Berova, N., Nakanishi, K., Labutti, J., Magil, S., Hauptert, G.T. & Hamlyn, J.M. (2001) Biological implication of conformational flexibility in ouabain: observations with two ouabain phosphate isomers. *Biochemistry*, 40 (19), pp.5835-44.

- Kawamura, A., Guo, J.S., Itagaki, Y., Bell, C., Wang, Y., Hauptert, G.T., Magil, S., Gallagher, R.T., Berova, N. & Nakanishi, K. (1999) On the structure of endogenous ouabain. *Proceedings of the National Academy of Sciences of the United States of America*, 96 (12), pp.6654-6659.
- Kay, J.E. (1996) Structure-function relationships in the FK506-binding protein (FKBP) family of peptidylprolyl cis-trans isomerases. *The Biochemical Journal*, 314 ( Pt 2), pp.361-85.
- Keating, M.T. & Sanguinetti, M.C. (2001) Molecular and cellular mechanisms of cardiac arrhythmias. *Cell*, 104 (4), pp.569-80.
- Kentish, J.C., Barsotti, R.J., Lea, T.J., Mulligan, I.P., Patel, J.R. & Ferenczi, M.A. (1990) Calcium release from cardiac sarcoplasmic reticulum induced by photorelease of calcium or Ins(1,4,5)P<sub>3</sub>. *The American Journal of Physiology*, 258 (2 Pt 2), pp.H610-5.
- Kimura, J., Kawahara, M., Sakai, E., Yatabe, J. & Nakanishi, H. (1999) Effects of a novel cardioprotective drug, JTV-519, on membrane currents of guinea pig ventricular myocytes. *Japanese Journal of Pharmacology*, 79 (3), pp.275-81.
- Kitta, K., Clément, S.A., Remeika, J., Blumberg, J.B. & Suzuki, Y.J. (2001) Endothelin-1 induces phosphorylation of GATA-4 transcription factor in the HL-1 atrial-muscle cell line. *Biochemical Journal*, 359 (Pt 2), pp.375-380.
- Klabunde, R.E. (2005) *Cardiovascular Physiology Concepts*,
- Klammt, C., Schwarz, D., Löhr, F., Schneider, B., Dötsch, V. & Bernhard, F. (2006) Cell-free expression as an emerging technique for the large scale production of integral membrane protein. *The Federation of Biochemical Societies Journal*, 273 (18), pp.4141-53.
- Kleber, A.G. & Fast, V. (1997) Molecular and cellular aspects of re-entrant arrhythmias. *Basic Research in Cardiology*, 92 Suppl 1, pp.111-9.
- Knappik, A., Krebber, C. & Plückthun, A. (1993) The effect of folding catalysts on the in vivo folding process of different antibody fragments expressed in *Escherichia coli*. *Bio/Technology (Nature Publishing Company)*, 11 (1), pp.77-83.
- Kobayashi, S., Yamamoto, T., Parness, J. & Ikemoto, N. (2004) Antibody probe study of Ca<sup>2+</sup> channel regulation by interdomain interaction within the ryanodine receptor. *The Biochemical Journal*, 380 (Pt 2), pp.561-9.
- Kockskämper, J., Zima, A.V., Roderick, H.L., Pieske, B., Blatter, L.A. & Bootman, M.D. (2008) Emerging roles of inositol 1,4,5-trisphosphate signaling in cardiac myocytes. *Journal of Molecular and Cellular Cardiology*, 45 (2), pp.128-47.
- Kosinski, M.J. & Bailey, J.E. (1991) Temperature and induction effects on the degradation rate of an abnormal beta-galactosidase in *Escherichia coli*. *Journal of Biotechnology*, 18 (1-2), pp.55-68.
- Kozak, M. (1987) An analysis of 5'-noncoding sequences from 699 vertebrate messenger RNAs. *Nucleic Acids Research*, 15 (20), pp.8125-48.

- Kuwajima, G., Futatsugi, A., Niinobe, M., Nakanishi, S. & Mikoshiba, K. (1992) Two types of ryanodine receptors in mouse brain: Skeletal muscle type exclusively in Purkinje cells and cardiac muscle type in various neurons. *Neuron*, 9 (6), pp.1133-1142.
- Lahat, H., Pras, E., Olender, T., Avidan, N., Ben-Asher, E., Man, O., Levy-Nissenbaum, E., Khoury, A., Lorber, A., Goldman, B., Lancet, D. & Eldar, M. (2001) A missense mutation in a highly conserved region of CASQ2 is associated with autosomal recessive catecholamine-induced polymorphic ventricular tachycardia in Bedouin families from Israel. *American Journal of Human Genetics*, 69 (6), pp.1378-84.
- Lahat, H., Pras, E. & Eldar, M. (2004) A missense mutation in CASQ2 is associated with autosomal recessive catecholamine-induced polymorphic ventricular tachycardia in Bedouin families from Israel. *Annals of Medicine*, 36 Suppl 1, pp.87-91.
- Lai, F.A., Anderson, K., Rousseau, E., Liu, Q.Y. & Meissner, G. (1988a) Evidence for a Ca<sup>2+</sup> channel within the ryanodine receptor complex from cardiac sarcoplasmic reticulum. *Biochemical and Biophysical Research Communications*, 151 (1), pp.441-9.
- Lai, F.A., Erickson, H., Block, B.A. & Meissner, G. (1987) Evidence for a junctional feet-ryanodine receptor complex from sarcoplasmic reticulum. *Biochemical and Biophysical Research Communications*, 143 (2), pp.704-9.
- Lai, F.A., Erickson, H.P., Rousseau, E., Liu, Q.Y. & Meissner, G. (1988b) Purification and reconstitution of the calcium release channel from skeletal muscle. *Nature*, 331, pp.315-319.
- Lai, F.A. & Meissner, G. (1989a) The muscle ryanodine receptor and its intrinsic Ca<sup>2+</sup> channel activity. *Journal of Bioenergetics and Biomembranes*, 21 (2), pp.227-46.
- Lai, F.A., Misra, M., Xu, L., Smith, H.A. & Meissner, G. (1989b) The ryanodine receptor-Ca<sup>2+</sup> release channel complex of skeletal muscle sarcoplasmic reticulum. Evidence for a cooperatively coupled, negatively charged homotetramer. *The Journal of Biological Chemistry*, 264 (28), pp.16776-85.
- Lanson, N.A., Egeland, D.B., Royals, B.A. & Claycomb, W.C. (2000) The MRE11-NBS1-RAD50 pathway is perturbed in SV40 large T antigen-immortalized AT-1, AT-2 and HL-1 cardiomyocytes. *Nucleic Acids Research*, 28 (15), pp.2882-2892.
- Laver, D.R., Baynes, T.M. & Dulhunty, A.F. (1997) Magnesium inhibition of ryanodine-receptor calcium channels: evidence for two independent mechanisms. *The Journal of Membrane Biology*, 156 (3), pp.213-29.
- Laver, D.R., Roden, L.D., Ahern, G.P., Eager, K.R., Junankar, P.R. & Dulhunty, A.F. (1995) Cytoplasmic Ca<sup>2+</sup> inhibits the ryanodine receptor from cardiac muscle. *The Journal of Membrane Biology*, 147 (1), pp.7-22.
- Laver, D.R., O'Neill, E.R. & Lamb, G.D. (2004) Luminal Ca<sup>2+</sup>-regulated Mg<sup>2+</sup> inhibition of skeletal RyRs reconstituted as isolated channels or coupled clusters. *The Journal of General Physiology*, 124 (6), pp.741-58.
- Lee, S.B., Várnai, P., Balla, A., Jalink, K., Rhee, S. & Balla, T. (2004) The pleckstrin homology domain of phosphoinositide-specific phospholipase Cdelta4 is not a critical determinant of the membrane localization of the enzyme. *The Journal of Biological Chemistry*, 279 (23), pp.24362-71.

- Leenhardt, A., Lucet, V., Denjoy, I., Grau, F., Ngoc, D.D. & Coumel, P. (1995) Catecholaminergic polymorphic ventricular tachycardia in children. A 7-year follow-up of 21 patients. *Circulation*, 91 (5), pp.1512-9.
- Lehnart, S.E., Wehrens, X.H.T. & Marks, A.R. (2005a) Defective ryanodine receptor interdomain interactions may contribute to intracellular Ca<sup>2+</sup> leak: a novel therapeutic target in heart failure. *Circulation*, 111 (25), pp.3342-6.
- Lehnart, S.E., Wehrens, X.H.T., Reiken, S., Warriar, S., Belevych, A.E., Harvey, R.D., Richter, W., Jin, S.C., Conti, M. & Marks, A.R. (2005b) Phosphodiesterase 4D deficiency in the ryanodine-receptor complex promotes heart failure and arrhythmias. *Cell*, 123 (1), pp.25-35.
- Lehnart, S.E., X, Wehrens, E.H. & Marks, A.R. (2004) Calstabin deficiency, ryanodine receptors, and sudden cardiac death. *Biochemical and Biophysical Research Communications*, 322 (4), pp.1267-1279.
- Levitan, I.B. (1999) It is calmodulin after all! Mediator of the calcium modulation of multiple ion channels. *Neuron*, 22 (4), pp.645-8.
- Li, Y., Kranias, E.G., Mignery, G.A. & Bers, D.M. (2002) Protein kinase A phosphorylation of the ryanodine receptor does not affect calcium sparks in mouse ventricular myocytes. *Circulation Research*, 90 (3), pp.309-16.
- Lindner, M., Erdmann, E. & Beuckelmann, D.J. (1998) Calcium content of the sarcoplasmic reticulum in isolated ventricular myocytes from patients with terminal heart failure. *Journal of Molecular and Cellular Cardiology*, 30 (4), pp.743-9.
- Lipp, P. & Niggli, E. (1998) Fundamental calcium release events revealed by two-photon excitation photolysis of caged calcium in guinea-pig cardiac myocytes. *The Journal of Physiology*, 508 (Pt 3), pp.801-809.
- Little, J.B. (2006) Cellular radiation effects and the bystander response. *Mutation Research*, 597 (1-2), pp.113-8.
- Litwin, S.E. (2006) "Ryanogate": who leaked the calcium? *Circulation Research*, 98 (2), pp.165-8.
- Liu, N., Colombi, B., Memmi, M., Zissimopoulos, S., Rizzi, N., Negri, S., Imbriani, M., Napolitano, C., Lai, F.A. & Priori, S.G. (2006) Arrhythmogenesis in catecholaminergic polymorphic ventricular tachycardia: insights from a RyR2 R4496C knock-in mouse model. *Circulation Research*, 99 (3), pp.292-8.
- Liu, N., Ruan, Y. & Priori, S.G. (2008) Catecholaminergic polymorphic ventricular tachycardia. *Progress in Cardiovascular Diseases*, 51 (1), pp.23-30.
- Liu, Z., Zhang, J., Li, P., Chen, S.R.W. & Wagenknecht, T. (2002) Three-dimensional reconstruction of the recombinant type 2 ryanodine receptor and localization of its divergent region 1. *Journal of Biological Chemistry*, 277 (48), pp.46712-46719.
- Liu, Z., Zhang, J., Wang, R., Chen, S.R.W. & Wagenknecht, T. (2004) Location of Divergent Region 2 on the Three-dimensional Structure of Cardiac Muscle Ryanodine Receptor/Calcium Release Channel. *Journal of Molecular Biology*, 338 (3), pp.533-545.



- Lloyd, D.C. & Moquet, J.E. (1985) The clastogenic effect of irradiated human plasma. *International Journal of Radiation Biology and Related Studies in Physics, Chemistry, and Medicine*, 47 (4), pp.433-44.
- Ludtke, S.J., Serysheva, I.I., Hamilton, S.L. & Chiu, W. (2005) The pore structure of the closed RyR1 channel. *Structure*, 13 (8), pp.1203-11.
- Ma, G., Brady, W.J., Pollack, M. & Chan, T.C. (2001) Electrocardiographic manifestations: digitalis toxicity. *The Journal of Emergency Medicine*, 20 (2), pp.145-52.
- Mackenzie, L., Bootman, M.D., Laine, M., Berridge, M.J., Thuring, J., Holmes, A., Li, W. & Lipp, P. (2002) The role of inositol 1,4,5-trisphosphate receptors in Ca<sup>2+</sup> signalling and the generation of arrhythmias in rat atrial myocytes. *The Journal of Physiology*, 541 (Pt 2), pp.395-409.
- MacKinnon, R. (2003) Potassium channels. *Federation of Biochemical Societies Letters*, 555 (1), pp.62-5.
- Mackrill, J.J. (1999) Protein-protein interactions in intracellular Ca<sup>2+</sup>-release channel function. *Biochemical Journal*, 337, pp.345-361.
- Marks, A.R. (2003) A guide for the perplexed towards an understanding of the molecular basis of heart failure. *Circulation*, 107, pp.1456-1459.
- Marks, A.R. (2000) Cardiac intracellular calcium release channels: role in heart failure. *Circulation Research*, 87 (1), pp.8-11.
- Marks, A.R. (2001) Ryanodine receptors/calcium release channels in heart failure and sudden cardiac death. *Journal of Molecular and Cellular Cardiology*, (33), pp.615-624.
- Marks, A.R., Tempst, P., Hwang, K.S., Taubman, M.B., Inui, M., Chadwick, C., Fleischer, S. & Nadal-Ginard, B. (1989) Molecular cloning and characterization of the ryanodine receptor/junctional channel complex cDNA from skeletal muscle sarcoplasmic reticulum. *Proceedings of the National Academy of Sciences of the United States of America*, 86 (22), pp.8683-7.
- Marks, A.R., Marx, S.O. & Reiken, S. (2002) Regulation of Ryanodine Receptors via Macromolecular Complexes : A Novel Role for Leucine/Isoleucine Zippers. *Trends in Cardiovascular Medicine*, 12 (4), pp.166-170.
- Marx, S.O., Gaburjakova, J., Gaburjakova, M., Henrikson, C., Ondrias, K. & Marks, A.R. (2001a) Coupled gating between cardiac calcium release channels (ryanodine receptors). *Circulation Research*, 88, pp.1151-1158.
- Marx, S.O., Reiken, S., Hisamatsu, Y., Gaburjakova, M., Gaburjakova, J., Yang, Y.M., Rosemblyt, N. & Marks, A.R. (2001b) Phosphorylation-dependent regulation of ryanodine receptors: a novel role for leucine/ isoleucine zippers. *The Journal of Cell Biology*, 153 (4), pp.699-708.
- Marx, S.O., Reiken, S., Hisamatsu, Y., Jayaraman, T., Burkhoff, D., Rosemblyt, N. & Marks, A.R. (2000) PKA phosphorylation dissociates FKBP12.6 from the calcium release channel (ryanodine receptor): defective regulation in failing hearts. *Cell*, 101 (4), pp.365-76.

- Marx, S.O., Ondrias, K. & Marks, A.R. (1998a) Coupled Gating Between Individual Skeletal Muscle  $Ca^{2+}$  Release Channels (Ryanodine Receptors). *Science*, 281 (5378), pp.818-821.
- Marx, S.O., Ondrias, K. & Marks, A.R. (1998b) Coupled Gating Between Individual Skeletal Muscle  $Ca^{2+}$  Release Channels (Ryanodine Receptors). *Science*, 281 (5378), pp.818-821.
- Maryon, E.B., Coronado, R. & Anderson, P. (1996) unc-68 encodes a ryanodine receptor involved in regulating *C. elegans* body-wall muscle contraction. *The Journal of Cell Biology*, 134 (4), pp.885-93.
- Masumiya, H., Zhang, R.W.J., Xiao, B. & Chen, S.R.W. (2003) Localization of the 12.6kDa FK506-binding protein (FKBP12.6) binding site to the  $NH_2$ -terminal domain of the cardiac  $Ca^{2+}$  release channel (ryanodine receptor). *Journal of Biological Chemistry*, 278 (6), pp.3786-3792.
- Mathews, W., Ducharme, D., Hamlyn, J., Harris, D., Mandel, F., Clark, M. & Ludens, J. (1991) Mass-spectral characterization of an endogenous-digitalis-like-factor from human plasma. *Hypertension*, 17 (6, Suppl. S), pp.930-935.
- McCall, E., Li, L., Satoh, H., Shannon, T.R., Blatter, L.A. & Bers, D.M. (1996) Effects of FK-506 on contraction and  $Ca^{2+}$  transients in rat cardiac myocytes. *Circulation Research*, 79 (6), pp.1110-21.
- McConkey, D.J., Lin, Y., Nutt, L.K., Ozel, H.Z. & Newman, R.A. (2000) Cardiac glycosides stimulate  $Ca^{2+}$  increases and apoptosis in androgen-independent, metastatic human prostate adenocarcinoma cells. *Cancer Research*, 60 (14), pp.3807-12.
- McDonald, T.F., Pelzer, S., Trautwein, W. & Pelzer, D.J. (1994) Regulation and modulation of calcium channels in cardiac, skeletal, and smooth muscle cells. *Physiological Reviews*, 74 (2), pp.365-507.
- McGarry, S.J. & Williams, A.J. (1993) Digoxin activates sarcoplasmic reticulum  $Ca^{2+}$ -release channels: a possible role in cardiac inotropy. *British Journal of Pharmacology*, 108 (4), pp.1043-50.
- McWhinney, C.D., Hansen, C. & Robishaw, J.D. (2000) Alpha-1 adrenergic signaling in a cardiac murine atrial myocyte (HL-1) cell line. *Molecular and Cellular Biochemistry*, 214 (1), pp.111-119.
- Meisler, M.H. & Kearney, J.A. (2005) Sodium channel mutations in epilepsy and other neurological disorders. *The Journal of Clinical Investigation*, 115 (8), pp.2010-7.
- Meissner, G. (1994) Ryanodine receptor/ $Ca^{2+}$  release channels and their regulation by endogenous effectors. *Annual Review of Physiology*, 56, pp.485-508.
- Meissner, G., Rios, E., Tripathy, A. & Pasek, D.A. (1997) Regulation of skeletal muscle  $Ca^{2+}$  release channel (ryanodine receptor) by  $Ca^{2+}$  and monovalent cations and anions. *The Journal of Biological Chemistry*, 272 (3), pp.1628-38.
- Meissner, G. (2004) Molecular regulation of cardiac ryanodine receptor ion channel. *Cell Calcium*, 35 (6), pp.621-628.

- Mikoshiba, K. (2007) IP3 receptor/Ca<sup>2+</sup> channel: from discovery to new signaling concepts. *Journal of Neurochemistry*, 102 (5), pp.1426-46.
- Milnes, J.T. & MacLeod, K.T. (2001) Reduced ryanodine receptor to dihydropyridine receptor ratio may underlie slowed contraction in a rabbit model of left ventricular cardiac hypertrophy. *Journal of Molecular and Cellular Cardiology*, 33 (3), pp.473-85.
- Miroux, B. & Walker, J.E. (1996) Over-production of proteins in Escherichia coli: mutant hosts that allow synthesis of some membrane proteins and globular proteins at high levels. *Journal of Molecular Biology*, 260 (3), pp.289-98.
- Morgan, W.F. & Sowa, M.B. (2007) Non-targeted bystander effects induced by ionizing radiation. *Mutation Research*, 616 (1-2), pp.159-64.
- Morgan, W.F. (2003) Non-targeted and delayed effects of exposure to ionizing radiation: ii. radiation-induced genomic instability and bystander effects in vivo, clastogenic factors and transgenerational effects. *Radiation Research*, 159 (5), pp.581-596.
- Moses, R.L. & Claycomb, W.C. (1984) Ultrastructure of cultured atrial cardiac muscle cells from adult rats. *The American Journal of Anatomy*, 171 (2), pp.191-206.
- Moss, A.J. & Kass, R.S. (2005) Long QT syndrome: from channels to cardiac arrhythmias. *The Journal of Clinical Investigation*, 115 (8), pp.2018-24.
- Murayama, T. & Ogawa, Y. (2002) Roles of Two Ryanodine Receptor Isoforms Coexisting in Skeletal Muscle. *Trends in Cardiovascular Medicine*, 12 (7), pp.305-311.
- Murray, N.E., Bruce, S.A. & Murray, K. (1979) Molecular cloning of the DNA ligase gene from bacteriophage T4. II. Amplification and preparation of the gene product. *Journal of Molecular Biology*, 132 (3), pp.493-505.
- Nagasawa, H. & Little, J.B. (1992) Induction of sister chromatid exchanges by extremely low doses of alpha-particles. *Cancer Research*, 52 (22), pp.6394-6.
- Nakai, J., Imagawa, T., Hakamat, Y., Shigekawa, M., Takeshima, H. & Numa, S. (1990) Primary structure and functional expression from cDNA of the cardiac ryanodine receptor/calcium release channel. *Federation of Biochemical Societies Letters*, 271 (1-2), pp.169-77.
- Nakajima, T., Kaneko, Y., Taniguchi, Y., Hayashi, K., Takizawa, T., Suzuki, T. & Nagai, R. (1997) The mechanism of catecholaminergic polymorphic ventricular tachycardia may be triggered activity due to delayed afterdepolarization. *European Heart Journal*, 18 (3), pp.530-1.
- Nakaya, H., Furusawa, Y., Ogura, T., Tamagawa, M. & Uemura, H. (2000) Inhibitory effects of JTV-519, a novel cardioprotective drug, on potassium currents and experimental atrial fibrillation in guinea-pig hearts. *British Journal of Pharmacology*, 131 (7), pp.1363-72.
- Nava, A., Canciani, B., Daliento, L., Miraglia, G., Buja, G., Fasoli, G., Martini, B., Scognamiglio, R. & Thiene, G. (1988) Juvenile sudden death and effort ventricular tachycardias in a family with right ventricular cardiomyopathy. *International Journal of Cardiology*, 21 (2), pp.111-26.

- Nesher, M., Shpolansky, U., Rosen, H. & Lichtstein, D. (2007) The digitalis-like steroid hormones: new mechanisms of action and biological significance. *Life sciences*, 80 (23), pp.2093-107.
- Neubauer, P., Hofmann, K., Holst, O., Mattiasson, B. & Kruschke, P. (1992) Maximizing the expression of a recombinant gene in *Escherichia coli* by manipulation of induction time using lactose as inducer. *Applied Microbiology and Biotechnology*, 36 (6), pp.739-44.
- Newton, C.L., Mignery, G.A. & Südhof, T.C. (1994) Co-expression in vertebrate tissues and cell lines of multiple inositol 1,4,5-trisphosphate (InsP3) receptors with distinct affinities for InsP3. *The Journal of Biological Chemistry*, 269 (46), pp.28613-9.
- Nguyen, S.V. & Claycomb, W.C. (1999) Hypoxia regulates the expression of the adrenomedullin and HIF-1 genes in cultured HL-1 cardiomyocytes. *Biochemical and Biophysical Research Communications*, 265 (2), pp.382-6.
- Nimer, L.R., Needleman, D.H., Hamilton, S.L., Krall, J. & Movsesian, M.A. (1995) Effect of ryanodine on sarcoplasmic reticulum  $Ca^{2+}$  accumulation in nonfailing and failing human myocardium. *Circulation*, 92 (9), pp.2504-10.
- Nirenberg, M.W. & Matthaei, J.H. (1961) The dependence of cell-free protein synthesis in *E. coli* upon naturally occurring or synthetic polyribonucleotides. *Proceedings of the National Academy of Sciences of the United States of America*, 47, pp.1588-602.
- Oda, T., Yano, M., Yamamoto, T., Tokuhisa, T., Okuda, S., Doi, M., Ohkusa, T., Ikeda, Y., Kobayashi, S., Ikemoto, N. & Matsuzaki, M. (2005) Defective regulation of interdomain interactions within the ryanodine receptor plays a key role in the pathogenesis of heart failure. *Circulation*, 111 (25), pp.3400-10.
- Ono, K., Yano, M., Ohkusa, T., Kohno, M., Hisaoka, T., Tanigawa, T., Kobayashi, S., Kohno, M. & Matsuzaki, M. (2000) Altered interaction of FKBP12.6 with ryanodine receptor as a cause of abnormal  $Ca^{2+}$  release in heart failure. *Cardiovascular Research*, 48 (2), pp.323-31.
- Orlova, E.V., Serysheva, I.I., van Heel, M., Hamilton, S.L. & Chiu, W. (1996) Two structural configurations of the skeletal muscle calcium release channel. *Nature Structural Biology*, 3 (6), pp.547-52.
- Orlowski, S. & Mir, L.M. (1993) Cell electroporation: a new tool for biochemical and pharmacological studies. *Biochimica Et Biophysica Acta*, 1154 (1), pp.51-63.
- Otsu, K., Willard, H.F., Khanna, V.K., Zorzato, F., Green, N.M. & MacLennan, D.H. (1990) Molecular cloning of cDNA encoding the  $Ca^{2+}$  release channel (ryanodine receptor) of rabbit cardiac muscle sarcoplasmic reticulum. *The Journal of Biological Chemistry*, 265 (23), pp.13472-83.
- Ottini, L., Marziali, G., Conti, A., Charlesworth, A. & Sorrentino, V. (1996) Alpha and beta isoforms of ryanodine receptor from chicken skeletal muscle are the homologues of mammalian RyR1 and RyR3. *The Biochemical Journal*, 315 ( Pt 1), pp.207-16.
- Oyamada, H., Murayama, T., Takagi, T., Iino, M., Iwabe, N., Miyata, T., Ogawa, Y. & Endo, M. (1994) Primary structure and distribution of ryanodine-binding protein isoforms of the bullfrog skeletal muscle. *The Journal of Biological Chemistry*, 269 (25), pp.17206-14.

- Pack, P., Kujau, M., Schroeckh, V., Knüpfer, U., Wenderoth, R., Riesenber, D. & Plückthun, A. (1993) Improved bivalent miniantibodies, with identical avidity as whole antibodies, produced by high cell density fermentation of *Escherichia coli*. *Bio/Technology (Nature Publishing Company)*, 11 (11), pp.1271-7.
- Pant, G.S. & Kamada, N. (1977) Chromosome aberrations in normal leukocytes induced by the plasma of exposed individuals. *Hiroshima Journal of Medical Sciences*, 26 (2-3), pp.149-54.
- Pessah, I.N., Waterhouse, A.L. & Casida, J.E. (1985) The calcium-ryanodine receptor complex of skeletal and cardiac muscle. *Biochemical and Biophysical Research Communications*, 128 (1), pp.449-56.
- Pogwizd, S.M., McKenzie, J.P. & Cain, M.E. (1998) Mechanisms underlying spontaneous and induced ventricular arrhythmias in patients with idiopathic dilated cardiomyopathy. *Circulation*, 98 (22), pp.2404-14.
- Pogwizd, S.M. & Bers, D.M. (2004) Cellular basis of triggered arrhythmias in heart failure. *Trends in Cardiovascular Medicine*, 14 (2), pp.61-6.
- Pogwizd, S.M., Schlotthauer, K., Li, L., Yuan, W. & Bers, D.M. (2001) Arrhythmogenesis and Contractile Dysfunction in Heart Failure : Roles of Sodium-Calcium Exchange, Inward Rectifier Potassium Current, and Residual  $\beta$ -Adrenergic Responsiveness. *Circulation Research*, 88 (11), pp.1159-1167.
- Postma, A.V., Denjoy, I., Hoorntje, T.M., Lupoglazoff, J., Da Costa, A., Sebillon, P., Mannens, M.M.A.M., Wilde, A.A.M. & Guicheney, P. (2002) Absence of caldesmon 2 causes severe forms of catecholaminergic polymorphic ventricular tachycardia. *Circulation Research*, 91 (8), pp.e21-6.
- Priori, S.G., Napolitano, C., Memmi, M., Colombi, B., Drago, F., Gasparini, M., DeSimone, L., Coltorti, F., Bloise, R., Keegan, R., Filho, C., Vignati, G., Benatar, A. & DeLogu, A. (2002) Clinical and molecular characterization of patients with catecholaminergic polymorphic ventricular tachycardia. *Circulation*, 106, pp.69-74.
- Priori, S.G., Napolitano, C., Tiso, N., Memmi, M., Vignati, G., Bloise, R., Vincenzo, S. & Danieli, G.A. (2001) Mutations in the cardiac ryanodine receptor gene (hRyR2) underlie catecholaminergic polymorphic ventricular tachycardia. *Circulation*, (103), pp.196-200.
- Prise, K.M., Belyakov, O.V., Folkard, M. & Michael, B.D. (1998) Studies of bystander effects in human fibroblasts using a charged particle microbeam. *International Journal of Radiation Biology*, 74 (6), pp.793-8.
- Protasi, F., Sun, X.H. & Franzini-Armstrong, C. (1996) Formation and maturation of the calcium release apparatus in developing and adult avian myocardium. *Developmental Biology*, 173 (1), pp.265-78.
- Qazzaz, H., Cao, Z.M., Bolanowski, D.D., Clark, B.J. & Valdes, R. (2004) De Novo Biosynthesis and Radiolabeling of Mammalian Digitalis-Like Factors. *Clinical Chemistry*, 50 (3), pp.612-620.

- Radermacher, M., Rao, V., Grassucci, R., Frank, J., Timerman, A.P., Fleischer, S. & Wagenknecht, T. (1994) Cryo-electron microscopy and three-dimensional reconstruction of the calcium release channel/ryanodine receptor from skeletal muscle. *Journal of Cell Biology*, 127, pp.411-423.
- Reid, D.S., Tynan, M., Braidwood, L. & Fitzgerald, G.R. (1975) Bidirectional tachycardia in a child. A study using His bundle electrography. *British Heart Journal*, 37 (3), pp.339-44.
- Reiken, S., Lacampagne, A., Kherani, A., Lehnart, S.E., Ward, C., Huang, F., Gaburjakova, M., Gaburjakova, J., Rosemblyt, N., Warren, M.S., He, K., Yi, G., Wang, J., Burkhoff, D., Vassort, G. & Marks, A.R. (2003) PKA phosphorylation activated the calcium release channel (ryanodine receptor) in skeletal muscle: defective regulation in heart failure. *Journal of Cell Biology*, 160 (6), pp.919-928.
- Remaut, E., Stanssens, P. & Fiers, W. (1981) Plasmid vectors for high-efficiency expression controlled by the PL promoter of coliphage lambda. *Gene*, 15 (1), pp.81-93.
- Reuter, H., Henderson, S.A., Han, T., Ross, R.S., Goldhaber, J.I. & Philipson, K.D. (2002) The Na<sup>+</sup>-Ca<sup>2+</sup> Exchanger Is Essential for the Action of Cardiac Glycosides. *Circulation Research*, 90 (3), pp.305-8.
- Rockenbach, S.K., Dupuis, M.J., Pitts, T.W., Marschke, C.K. & Tomich, C.S. (1991) Secretion of active truncated CD4 into Escherichia coli periplasm. *Applied Microbiology and Biotechnology*, 35 (1), pp.32-7.
- Roderick, H.L., Berridge, M.J. & Bootman, M.D. (2003) Calcium-induced calcium release. *Current Biology: CB*, 13 (11), p.R425.
- Rodriguez, P., Bhogal, M.S. & Colyer, J. (2003) Stoichiometric phosphorylation of cardiac ryanodine receptor on serine 2809 by calmodulin-dependent kinase II and protein kinase A. *The Journal of Biological Chemistry*, 278 (40), pp.38593-600.
- Rosamond, W., Flegal, K., Furie, K., Go, A., Greenlund, K., Haase, N., Hailpern, S.M., Ho, M., Howard, V., Kissela, B., Kittner, S., Lloyd-Jones, D., McDermott, M., Meigs, J., Moy, C., Nichol, G., O'Donnell, C., Roger, V., Sorlie, P., Steinberger, J., Thom, T., Wilson, M. & Hong, Y. (2008) Heart disease and stroke statistics--2008 update: a report from the American Heart Association Statistics Committee and Stroke Statistics Subcommittee. *Circulation*, 117 (4), pp.e25-146.
- Rosen, M.R. & Danilo, P. (1980) Effects of tetrodotoxin, lidocaine, verapamil, and AHR-2666 on Ouabain-induced delayed afterdepolarizations in canine Purkinje fibers. *Circulation Research*, 46 (1), pp.117-24.
- Rossi, D., Simeoni, I., Micheli, M., Bootman, M.D., Lipp, P., Allen, P.D. & Sorrentino, V. (2002) RyR1 and RyR3 isoforms provide distinct intracellular Ca<sup>2+</sup> signals in HEK 293 cells. *Journal of Cell Science*, 115 (12), pp.2497-2504.
- Rousseau, E. & Meissner, G. (1989) Single cardiac sarcoplasmic reticulum Ca<sup>2+</sup>-release channel: activation by caffeine. *The American Journal of Physiology*, 256 (2 Pt 2), pp.H328-33.
- Ruehr, M.L., Russell, M.A. & Bond, M. (2004) A-kinase anchoring protein targeting of protein kinase A in the heart. *Journal of Molecular and Cellular Cardiology*, 37 (3), pp.653-65.

- Sagawa, T., Sagawa, K., Kelly, J.E., Tsushima, R.G. & Wasserstrom, J.A. (2002) Activation of cardiac ryanodine receptors by cardiac glycosides. *American Journal of Physiology. Heart and Circulatory Physiology*, 282 (3), pp.H1118-26.
- Saïda, F., Uzan, M., Odaert, B. & Bontems, F. (2006) Expression of highly toxic genes in *E. coli*: special strategies and genetic tools. *Current Protein & Peptide Science*, 7 (1), pp.47-56.
- Sainte Beuve, C., Allen, P.D., Dambrin, G., Rannou, F., Marty, I., Trouvé, P., Bors, V., Pavie, A., Gandgjbakch, I. & Charlemagne, D. (1997) Cardiac calcium release channel (ryanodine receptor) in control and cardiomyopathic human hearts: mRNA and protein contents are differentially regulated. *Journal of Molecular and Cellular Cardiology*, 29 (4), pp.1237-46.
- Saito, A., Inui, M., Radermacher, M., Frank, J. & Fleischer, S. (1988) Ultrastructure of the calcium release channel of sarcoplasmic reticulum. *The Journal of Cell Biology*, 107 (1), pp.211-9.
- Sambrook, J. & Russell, D.W. (2001) *Molecular Cloning: A Laboratory Manual*, CSHL Press.
- Samsó, M. & Wagenknecht, T. (1998) Contributions of electron microscopy and single-particle techniques to the determination of the ryanodine receptor three-dimensional structure. *Journal of Structural Biology*, 121, pp.172-180.
- Samsó, M., Wagenknecht, T. & Allen, P.D. (2005) Internal structure and visualization of transmembrane domains of the RyR1 calcium release channel by cryo-EM. *Nature Structural & Molecular Biology*, 12 (6), pp.539-44.
- Santana, L.F., Gómez, A.M. & Lederer, W.J. (1998) Ca<sup>2+</sup> flux through promiscuous cardiac Na<sup>+</sup> channels: slip-mode conductance. *Science*, 279 (5353), pp.1027-33.
- Sato, C., Hamada, K., Ogura, T., Miyazawa, A., Iwasaki, K., Hiroaki, Y., Tani, K., Terauchi, A., Fujiyoshi, Y. & Mikoshiba, K. (2004) Inositol 1,4,5-trisphosphate receptor contains multiple cavities and L-shaped ligand-binding domains. *Journal of Molecular Biology*, 336 (1), pp.155-64.
- Sato, Y., Ferguson, D.G., Sako, H., Dorn, G.W., Kadambi, V.J., Yatani, A., Hoit, B.D., Walsh, R.A. & Kranias, E.G. (1998) Cardiac-specific overexpression of mouse cardiac calsequestrin is associated with depressed cardiovascular function and hypertrophy in transgenic mice. *The Journal of Biological Chemistry*, 273 (43), pp.28470-7.
- Schmitt, J.P., Kamisago, M., Asahi, M., Li, G.H., Ahmad, F., Mende, U., Kranias, E.G., MacLennan, D.H., Seidman, J.G. & Seidman, C.E. (2003) Dilated cardiomyopathy and heart failure caused by a mutation in phospholamban. *Science*, 299 (5611), pp.1410-3.
- Schoner, W. (2001) Endogenous cardiotonic steroids. *Cellular and Molecular Biology (Noisy-Le-Grand, France)*, 47 (2), pp.273-80.
- Schoner, W. (2000) Ouabain, a new steroid hormone of adrenal gland and hypothalamus. *Experimental and Clinical Endocrinology & Diabetes: Official Journal, German Society of Endocrinology [and] German Diabetes Association*, 108 (7), pp.449-54.
- Schoner, W. & Scheiner-Bobis, G. (2007) Endogenous and exogenous cardiac glycosides:

Their roles in hypertension, salt metabolism, and cell growth. *American Journal of Physiology. Cell Physiology*, 293 (2), pp.C509-36.

- Schwarz, D., Klammt, C., Koglin, A., Löhr, F., Schneider, B., Dötsch, V. & Bernhard, F. (2007) Preparative scale cell-free expression systems: New tools for the large scale preparation of integral membrane proteins for functional and structural studies. *Methods*, 41 (4), pp.355-369.
- Scote, M. & Williams, A.J. (2002) The cardiac ryanodine receptor (calcium release channel): emerging role in heart failure and arrhythmia pathogenesis. *Cardiovascular Research*, 56 (3), pp.359-72.
- Scote, M. & Williams, A.J. (2004) Myocardial calcium signalling and arrhythmia pathogenesis. *Biochemical and Biophysical Research Communications*, 322 (4), pp.1286-1309.
- Serysheva, I.I., Bare, D.J., Ludtke, S.J., Kettlun, C.S., Chiu, W. & Mignery, G.A. (2003) Structure of the type 1 inositol 1,4,5-trisphosphate receptor revealed by electron cryomicroscopy. *The Journal of Biological Chemistry*, 278 (24), pp.21319-22.
- Serysheva, I.I., Hamilton, S.L., Chiu, W. & Ludtke, S.J. (2005) Structure of Ca<sup>2+</sup> release channel at 14 Å resolution. *Journal of Molecular Biology*, 345 (3), pp.427-31.
- Serysheva, I.I., Ludtke, S.J., Baker, M.L., Cong, Y., Topf, M., Eramian, D., Sali, A., Hamilton, S.L. & Chiu, W. (2008) Subnanometer-resolution electron cryomicroscopy-based domain models for the cytoplasmic region of skeletal muscle RyR channel. *Proceedings of the National Academy of Sciences of the United States of America*, 105 (28), pp.9610-5.
- Serysheva, I.I., Chiu, W. & Ludtke, S.J. (1995) Single-Particle Electron Cryomicroscopy of the Ion Channels in the Excitation–Contraction Coupling Junction. *Methods in Cell Biology*, 79, pp.407-435.
- Severs, N.J. (2000) The cardiac muscle cell. *BioEssays: News and Reviews in Molecular, Cellular and Developmental Biology*, 22 (2), pp.188-99.
- Shao, C., Furusawa, Y., Aoki, M. & Ando, K. (2003) Role of gap junctional intercellular communication in radiation-induced bystander effects in human fibroblasts. *Radiation Research*, 160 (3), pp.318-23.
- Sharma, M.R., Jeyakumar, L.H., Fleischer, S. & Wagenknecht, T. (2000) Three-dimensional structure of ryanodine receptor isoform three in two conformational states as visualized by cryo-electron microscopy. *The Journal of Biological Chemistry*, 275 (13), pp.9485-91.
- Silvester, N.C., Barberini-Jammaers, S.R., Ashton, P.M., Jayanthi, A., Yeung, W.Y., Jundi, H., Kotecha, A., Lai, F.A. & George, C.H. (2009) Investigating the Ca<sup>2+</sup>-cycling basis of rhythmicity and synchronicity in coupled cardiomyocyte monolayers. *Biophysical Journal Supplement*.
- Sitsapesan, R. & Williams, A.J. (1994) Regulation of the gating of the sheep cardiac sarcoplasmic reticulum Ca<sup>2+</sup>-release channel by luminal Ca<sup>2+</sup>. *The Journal of Membrane Biology*, 137 (3), pp.215-26.
- Sitsapesan, R. & Williams, A.J. (1995) The gating of the sheep skeletal sarcoplasmic



reticulum  $\text{Ca}^{2+}$ -release channel is regulated by luminal  $\text{Ca}^{2+}$ . *The Journal of Membrane Biology*, 146 (2), pp.133-44.

Skerra, A. & Plückthun, A. (1991) Secretion and in vivo folding of the Fab fragment of the antibody McPC603 in *Escherichia coli*: influence of disulphides and cis-prolines. *Protein Engineering*, 4 (8), pp.971-9.

Somerville, J.E., Goshorn, S.C., Fell, H.P. & Darveau, R.P. (1994) Bacterial aspects associated with the expression of a single-chain antibody fragment in *Escherichia coli*. *Applied Microbiology and Biotechnology*, 42 (4), pp.595-603.

Song, L., Sobie, E.A., McCulle, S., Lederer, W.J., Balke, C.W. & Cheng, H. (2006) Orphaned ryanodine receptors in the failing heart. *Proceedings of the National Academy of Sciences of the United States of America*, 103 (11), pp.4305-10.

Sorrentino, V. & Volpe, P. (1993) Ryanodine receptors: how many, where and why? *Trends in Pharmacological Science*, 14, pp.98-103.

Splawski, I., Timothy, K.W., Sharpe, L.M., Decher, N., Kumar, P., Bloise, R., Napolitano, C., Schwartz, P.J., Joseph, R.M., Condouris, K., Tager-Flusberg, H., Priori, S.G., Sanguinetti, M.C. & Keating, M.T. (2004)  $\text{Ca}_v1.2$  calcium channel dysfunction causes a multisystem disorder including arrhythmia and autism. *Cell*, 119 (1), pp.19-31.

Stange, M., Xu, L., Balshaw, D., Yamaguchi, N. & Meissner, G. (2003) Characterization of recombinant skeletal muscle (Ser-2843) and cardiac muscle (Ser-2809) ryanodine receptor phosphorylation mutants. *The Journal of Biological Chemistry*, 278 (51), pp.51693-702.

Stern, M.D., Pizarro, G. & Rios, E. (1997) Local Control Model of Excitation-Contraction Coupling in Skeletal Muscle. *Journal of General Physiology*, 110 (4), pp.415-440.

Stern, M.D., Song, L., Cheng, H., Sham, J.S., Yang, H.T., Boheler, K.R. & Rios, E. (1999) Local Control Models of Cardiac Excitation-Contraction Coupling . A Possible Role for Allosteric Interactions between Ryanodine Receptors. *Journal of General Physiology*, 113 (3), pp.469-489.

Stewart, R., Zissimopoulos, S. & Lai, F.A. (2003) Oligomerization of the cardiac ryanodine receptor C-terminal tail. *The Biochemical Journal*, 376 (Pt 3), pp.795-9.

Studier, F.W. (2005) Protein production by auto-induction in high density shaking cultures. *Protein Expression and Purification*, 41 (1), pp.207-34.

Surek, B., Wilhelm, M. & Hillen, W. (1991) Optimizing the promoter and ribosome binding sequence for expression of human single chain urokinase-like plasminogen activator in *Escherichia coli* and stabilization of the product by avoiding heat shock response. *Applied Microbiology and Biotechnology*, 34 (4), pp.488-94.

Sutko, J.L. & Airey, J.A. (1996) Ryanodine receptor  $\text{Ca}^{2+}$  release channels: does diversity in form equal diversity in function? *Physiological Reviews*, 76 (4), pp.1027-71.

Sutko, J.L., Airey, J.A., Welch, W. & Ruest, L. (1997) The pharmacology of ryanodine and related compounds. *Pharmacological Reviews*, 49 (1), pp.53-98.

Sutko, J.L. & Willerson, J.T. (1980) Ryanodine alteration of the contractile state of rat

- ventricular myocardium. Comparison with dog, cat, and rabbit ventricular tissues. *Circulation Research*, 46 (3), pp.332-43.
- Suzuki, Y.J. (2003) Stress-induced activation of GATA-4 in cardiac muscle cells. *Free Radical Biology & Medicine*, 34 (12), pp.1589-98.
- Swan, H., Piippo, K., Viitasalo, M., Heikkilä, P., Paavonen, T., Kainulainen, K., Kere, J., Keto, P., Kontula, K. & Toivonen, L. (1999) Arrhythmic disorder mapped to chromosome 1q42-q43 causes malignant polymorphic ventricular tachycardia in structurally normal hearts. *Journal of the American College of Cardiology*, 34 (7), pp.2035-42.
- Takasago, T., Imagawa, T., Furukawa, K., Ogurusu, T. & Shigekawa, M. (1991) Regulation of the cardiac ryanodine receptor by protein kinase-dependent phosphorylation. *Journal of Biochemistry*, 109 (1), pp.163-70.
- Takekura, H., Takeshima, H., Nishimura, S., Takahashi, M., Tanabe, T., Flockerzi, V., Hofmann, F. & Franzini-Armstrong, C. (1995) Co-expression in CHO cells of two muscle proteins involved in excitation-contraction coupling. *Journal of Muscle Research and Cell Motility*, 16 (5), pp.465-80.
- Takeshima, H., Nishi, M., Iwabe, N., Miyata, T., Hosoya, T., Masai, I. & Hotta, Y. (1994) Isolation and characterization of a gene for a ryanodine receptor/calcium release channel in *Drosophila melanogaster*. *Federation of Biochemical Societies Letters*, 337 (1), pp.81-7.
- Takeshima, H., Nishimura, S., Matsumoto, T., Ishida, H., Kangawa, K., Minamoto, N., Matsuo, H., Ueda, M., Hanaoka, M., Hirose, T. & Numa, S. (1989) Primary structure and expression from complementary DNA of skeletal muscle ryanodine receptor. *Nature*, 339, pp.439-445.
- Taylor, C.W. (1998) Inositol trisphosphate receptors:  $Ca^{2+}$ -modulated intracellular  $Ca^{2+}$  channels. *Biochimica Et Biophysica Acta*, 1436 (1-2), pp.19-33.
- Terentyev, D., Nori, A., Santoro, M., Viatchenko-Karpinski, S., Kubalova, Z., Gyorke, I., Terentyeva, R., Vedamoorthyrao, S., Blom, N.A., Valle, G., Napolitano, C., Williams, S.C., Volpe, P., Priori, S.G. & Gyorke, S. (2006) Abnormal interactions of calsequestrin with the ryanodine receptor calcium release channel complex linked to exercise-induced sudden cardiac death. *Circulation Research*, 98 (9), pp.1151-8.
- Terentyev, D., Viatchenko-Karpinski, S., Gyorke, I., Terentyeva, R. & Gyorke, S. (2003b) Protein phosphatases decrease sarcoplasmic reticulum calcium content by stimulating calcium release in cardiac myocytes. *The Journal of Physiology*, 552 (Pt 1), pp.109-18.
- Terentyev, D., Viatchenko-Karpinski, S., Györke, I., Volpe, P., Williams, S.C. & Györke, S. (2003a) Calsequestrin determines the functional size and stability of cardiac intracellular calcium stores: Mechanism for hereditary arrhythmia. *Proceedings of the National Academy of Sciences of the United States of America*, 100 (20), pp.11759-64.
- Thomas, N.L., George, C.H. & Lai, F.A. (2004) Functional heterogeneity of ryanodine receptor mutations associated with sudden cardiac death. *Cardiovascular Research*, 64 (1), pp.52-60.

- Thomas, P. & Smart, T.G. (2005) HEK293 cell line: a vehicle for the expression of recombinant proteins. *Journal of Pharmacological and Toxicological Methods*, 51 (3), pp.187-200.
- Timerman, A.P., Jayaraman, T., Wiederrecht, G., Onoue, H., Marks, A.R. & Fleischer, S. (1994) The ryanodine receptor from canine heart sarcoplasmic reticulum is associated with a novel FK-506 binding protein. *Biochemical and Biophysical Research Communications*, 198 (2), pp.701-6.
- Timerman, A.P., Ogunbumni, E., Freund, E., Wiederrecht, G., Marks, A.R. & Fleischer, S. (1993) The calcium release channel of sarcoplasmic reticulum is modulated by FK-506-binding protein. Dissociation and reconstitution of FKBP-12 to the calcium release channel of skeletal muscle sarcoplasmic reticulum. *The Journal of Biological Chemistry*, 268 (31), pp.22992-9.
- Timerman, A.P., Onoue, H., Xin, H.B., Barg, S., Copello, J., Wiederrecht, G. & Fleischer, S. (1996) Selective binding of FKBP12.6 by the cardiac ryanodine receptor. *The Journal of Biological Chemistry*, 271 (34), pp.20385-91.
- Tompers, D.M. & Labosky, P.A. (2004) Electroporation of murine embryonic stem cells: a step-by-step guide. *Stem Cells*, 22 (3), pp.243-9.
- Torizawa, T., Shimizu, M., Taoka, M., Miyano, H. & Kainosho, M. (2004) Efficient production of isotopically labeled proteins by cell-free synthesis: a practical protocol. *Journal of Biomolecular NMR*, 30 (3), pp.311-25.
- Tsien, R.W., Bean, B.P., Hess, P., Lansman, J.B., Nilius, B. & Nowycky, M.C. (1986) Mechanisms of calcium channel modulation by beta-adrenergic agents and dihydropyridine calcium agonists. *Journal of Molecular and Cellular Cardiology*, 18 (7), pp.691-710.
- Tunwell, R.E., Wickenden, C., Bertrand, B.M., Shevchenko, V.I., Walsh, M.B., Allen, P.D. & Lai, F.A. (1996) The human cardiac muscle ryanodine receptor-calcium release channel: identification, primary structure and topological analysis. *The Biochemical journal*, 318 ( Pt 2), pp.477-87.
- Uhlén, P. (2004) Spectral analysis of calcium oscillations. *Science's STKE: Signal Transduction Knowledge Environment*, 2004 (258), p.pl15.
- Valdivia, H.H., Kaplan, J.H., Ellis-Davies, G.C. & Lederer, W.J. (1995) Rapid adaptation of cardiac ryanodine receptors: modulation by Mg<sup>2+</sup> and phosphorylation. *Science*, 267 (5206), pp.1997-2000.
- Vanderheiden, G.J., Fairchild, A.C. & Jago, G.R. (1970) Construction of a Laboratory Press for Use with the French Pressure Cell. *Applied Microbiology*, 19 (5), pp.875-7.
- Vatner, D.E., Sato, N., Kiuchi, K., Shannon, R.P. & Vatner, S.F. (1994) Decrease in myocardial ryanodine receptors and altered excitation-contraction coupling early in the development of heart failure. *Circulation*, 90 (3), pp.1423-30.
- Vinarov, D.A., Loushin Newman, C.L. & Markley, J.L. (2006) Wheat germ cell-free platform for eukaryotic protein production. *The Federation of Biochemical Societies Journal*, 273 (18), pp.4160-9.
- Wagenknecht, T. & Radermacher, M. (1995) Three-dimensional architecture of the skeletal

- muscle ryanodine receptor. *Federation of Biochemical Societies Letters*, 369 (1), pp.43-6.
- Wagenknecht, T., Radermacher, M., Grassucci, R., Berkowitz, J., Xin, H.B. & Fleischer, S. (1997) Locations of calmodulin and FK506-binding protein on the three-dimensional architecture of the skeletal muscle ryanodine receptor. *The Journal of Biological Chemistry*, 272 (51), pp.32463-71.
- Wagenknecht, T., Grassucci, R., Frank, J., Saito, A., Inui, M. & Fleischer, S. (1989) Three dimensional architecture of the calcium channel/foot structure of sarcoplasmic reticulum. *Nature*, 338, pp.167-170.
- Wang, S.Q., Stern, M.D., Ríos, E. & Cheng, H. (2004) The quantal nature of Ca<sup>2+</sup> sparks and in situ operation of the ryanodine receptor array in cardiac cells. *Proceedings of the National Academy of Sciences of the United States of America*, 101 (11), pp.3979-84.
- Watkins, H., McKenna, W.J., Thierfelder, L., Suk, H.J., Anan, R., O'Donoghue, A., Spirito, P., Matsumori, A., Moravec, C.S. & Seidman, J.G. (1995) Mutations in the genes for cardiac troponin T and alpha-tropomyosin in hypertrophic cardiomyopathy. *The New England Journal of Medicine*, 332 (16), pp.1058-64.
- Wehrens, X.H.T., Lehnart, S.E., Huang, F., Vest, J.A., Reiken, S.R., Mohler, P.J., Sun, J., Guatimosim, S., Song, L.S., Roseblit, N., D'Armiento, J.M., Napolitano, C., Memmi, M., Priori, S.G., Lederer, W.J. & Marks, A.R. (2003) FKBP12.6 deficiency and defective calcium release channel (ryanodine receptor) function linked to exercise-induced sudden cardiac death. *Cell*, 113 (7), pp.829-40.
- Wehrens, X.H.T., Lehnart, S.E. & Marks, A.R. (2005) Intracellular calcium release and cardiac disease. *Annual Review of Physiology*, 67, pp.69-98.
- Wehrens, X.H.T., Lehnart, S.E., Reiken, S., Vest, J.A., Wronska, A. & Marks, A.R. (2006) Ryanodine receptor/calcium release channel PKA phosphorylation: a critical mediator of heart failure progression. *Proceedings of the National Academy of Sciences of the United States of America*, 103 (3), pp.511-8.
- Wehrens, X.H.T., Lehnart, S.E., Reiken, S.R. & Marks, A.R. (2004a) Ca<sup>2+</sup>/calmodulin-dependent protein kinase II phosphorylation regulates the cardiac ryanodine receptor. *Circulation Research*, 94 (6), pp.e61-70.
- Wehrens, X.H.T. & Marks, A.R. (2004b) Novel therapeutic approaches for heart failure by normalizing calcium cycling. *Nature Reviews Drug Discovery*, 3 (7), pp.565-574.
- White, S.M., Constantin, P.E. & Claycomb, W.C. (2004) Cardiac physiology at the cellular level: use of cultured HL-1 cardiomyocytes for studies of cardiac muscle cell structure and function. *American Journal of Physiology. Heart and Circulatory Physiology*, 286 (3), pp.H823-9.
- Whitney, G.K., Glick, B.R. & Robinson, C.W. (1989) Induction of T4 DNA ligase in a recombinant strain of *Escherichia coli*. *Biotechnology and Bioengineering*, 33 (8), pp.991-8.
- Williams, A.J., West, D.J. & Sitsapesan, R. (2001) Light at the end of the Ca<sup>2+</sup>-release

channel tunnel: structures and mechanisms involved in ion translocation in ryanodine receptor channels. *Quarterly Reviews of Biophysics*, 34 (1), pp.61-104.

- Winograd, E., Pulido, M.A. & Wasserman, M. (1993) Production of DNA-recombinant polypeptides by tac-inducible vectors using micromolar concentrations of IPTG. *BioTechniques*, 14 (6), pp.886, 890.
- Wit, A.L. & Rosen, M.R. (1983) Pathophysiologic mechanisms of cardiac arrhythmias. *American Heart Journal*, 106 (4 Pt 2), pp.798-811.
- Witcher, D.R., Kovacs, R.J., Schulman, H., Cefali, D.C. & Jones, L.R. (1991) Unique phosphorylation site on the cardiac ryanodine receptor regulates calcium channel activity. *The Journal of Biological Chemistry*, 266 (17), pp.11144-52.
- Woodcock, E.A., Arthur, J.F. & Matkovich, S.J. (2000) Inositol 1,4,5-trisphosphate and reperfusion arrhythmias. *Clinical and Experimental Pharmacology & Physiology*, 27 (9), pp.734-7.
- Xiao, B., Masumiya, H., Jiang, D., Wang, R., Sei, Y., Zhang, L., Muryama, T., Ogawa, Y., Lai, F.A., Wagenknecht, T. & W, C.S.R. (2002) Isoform-dependent formation of heteromeric  $Ca^{2+}$  release channels (ryanodine receptors). *Journal of Biological Chemistry*, 277 (44), pp.41778-41785.
- Xiao, B., Jiang, M.T., Zhao, M., Yang, D., Sutherland, C., Lai, F.A., Walsh, M.P., Wartier, D.C., Cheng, H. & Chen, S.R.W. (2005) Characterization of a novel PKA phosphorylation site, serine-2030, reveals no PKA hyperphosphorylation of the cardiac ryanodine receptor in canine heart failure. *Circulation Research*, 96 (8), pp.847-55.
- Xiao, B., Zhong, G., Obayashi, M., Yang, D., Chen, K., Walsh, M.P., Shimoni, Y., Cheng, H., Ter Keurs, H. & Chen, S.R.W. (2006) Ser-2030, but not Ser-2808, is the major phosphorylation site in cardiac ryanodine receptors responding to protein kinase A activation upon beta-adrenergic stimulation in normal and failing hearts. *The Biochemical Journal*, 396 (1), pp.7-16.
- Xiao, R.P., Valdivia, H.H., Bogdanov, K., Valdivia, C., Lakatta, E.G. & Cheng, H. (1997) The immunophilin FK506-binding protein modulates  $Ca^{2+}$  release channel closure in rat heart. *The Journal of Physiology*, 500 ( Pt 2), pp.343-54.
- Xin, H., Senbonmatsu, T., Cheng, D., Wang, Y., Copello, J.A., Ji, G., Collier, M.L., Deng, K., Jeyakumar, L.H., Magnuson, M.A., Inagami, T., Kotlikoff, M.I. & Fleischer, S. (2002) Oestrogen protects FKBP12.6 null mice from cardiac hypertrophy. *Nature*, 416 (6878), pp.334-8.
- Yabuta, M., Onai-Miura, S. & Ohsuye, K. (1995) Thermo-inducible expression of a recombinant fusion protein by *Escherichia coli* lac repressor mutants. *Journal of Biotechnology*, 39 (1), pp.67-73.
- Yamada, M., Ikeda, Y., Yano, M., Yoshimura, K., Nishino, S., Aoyama, H., Wang, L., Aoki, H. & Matsuzaki, M. (2006) Inhibition of protein phosphatase 1 by inhibitor-2 gene delivery ameliorates heart failure progression in genetic cardiomyopathy. *The FASEB Journal: Official Publication of the Federation of American Societies for Experimental Biology*, 20 (8), pp.1197-9.
- Yamada, N., Makino, Y., Clark, R.A., Pearson, D.W., Mattei, M.G., Guénet, J.L., Ohama, E.,

- Fujino, I., Miyawaki, A. & Furuichi, T. (1994) Human inositol 1,4,5-trisphosphate type-1 receptor, InsP3R1: structure, function, regulation of expression and chromosomal localization. *The Biochemical Journal*, 302 ( Pt 3), pp.781-90.
- Yamamoto, T., El-Hayek, R. & Ikemoto, N. (2000) Postulated role of interdomain interaction within the ryanodine receptor in Ca<sup>2+</sup> channel regulation. *The Journal of Biological Chemistry*, 275 (16), pp.11618-25.
- Yamamoto, T., Yano, M., Kohno, M., Hisaoka, T., Ono, K., Tanigawa, T., Saiki, Y., Hisamatsu, Y., Ohkusa, T. & Matsuzaki, M. (1999) Abnormal Ca<sup>2+</sup> release from cardiac sarcoplasmic reticulum in tachycardia-induced heart failure. *Cardiovascular Research*, 44 (1), pp.146-55.
- Yamamoto, T. & Ikemoto, N. (2002) Peptide probe study of the critical regulatory domain of the cardiac ryanodine receptor. *Biochemical and Biophysical Research Communications*, 291 (4), pp.1102-1108.
- Yamamoto-Hino, M., Sugiyama, T., Hikichi, K., Mattei, M.G., Hasegawa, K., Sekine, S., Sakurada, K., Miyawaki, A., Furuichi, T. & Hasegawa, M. (1994) Cloning and characterization of human type 2 and type 3 inositol 1,4,5-trisphosphate receptors. *Receptors & Channels*, 2 (1), pp.9-22.
- Yang, Z., Ikemoto, N., Lamb, G.D. & Steele, D.S. (2006) The RyR2 central domain peptide DPc10 lowers the threshold for spontaneous Ca<sup>2+</sup> release in permeabilized cardiomyocytes. *Cardiovascular Research*, 70 (3), pp.475-85.
- Yano, K. & Zarain-Herzberg, A. (1994) Sarcoplasmic reticulum calsequestrins: structural and functional properties. *Molecular and Cellular Biochemistry*, 135 (1), pp.61-70.
- Yano, M., Ono, K., Ohkusa, T., Suetsugu, M., Kohno, M., Hisaoka, T., Kobayashi, S., Hisamatsu, Y., Yamamoto, T., Kohno, M., Noguchi, N., Takasawa, S., Okamoto, H. & Matsuzaki, M. (2000) Altered stoichiometry of FKBP12.6 versus ryanodine receptor as a cause of abnormal Ca<sup>2+</sup> leak through ryanodine receptor in heart failure. *Circulation*, 102 (17), pp.2131-6.
- Yano, M., Kobayashi, S., Kohono, M., Doi, M., Tokuhisa, T., Okuda, S., Suetsugu, M., Hisaoka, T., Obayashi, M., Ohkusa, T., Kohno, M. & Matsuzaki, M. (2003) FKBP12.6-mediated stabilization of calcium release channel (ryanodine receptor) as a novel therapeutic strategy against heart failure. *Circulation*, 107, pp.477-484.
- Yano, M. (2008) Ryanodine receptor as a new therapeutic target of heart failure and lethal arrhythmia. *Circulation Journal: Official Journal of the Japanese Circulation Society*, 72 (4), pp.509-14.
- Yano, M., Ikeda, Y. & Matsuzaki, M. (2005a) Altered intracellular Ca<sup>2+</sup> handling in heart failure. *The Journal of Clinical Investigation*, 115 (3), pp.556-64.
- Yano, M., Okuda, S., Oda, T., Tokuhisa, T., Tateishi, H., Mochizuki, M., Noma, T., Doi, M., Kobayashi, S., Yamamoto, T., Ikeda, Y., Ohkusa, T., Ikemoto, N. & Matsuzaki, M. (2005b) Correction of defective interdomain interaction within ryanodine receptor by antioxidant is a new therapeutic strategy against heart failure. *Circulation*, 112 (23), pp.3633-43.
- Yano, M., Yamamoto, T., Ikeda, Y. & Matsuzaki, M. (2006) Mechanisms of Disease:

ryanodine receptor defects in heart failure and fatal arrhythmia. *Nature Clinical Practice. Cardiovascular Medicine*, 3 (1), pp.43-52.

- Yin, C. & Lai, F.A. (2000) Intrinsic lattice formation by the ryanodine receptor calcium-release channel. *Nature Cell Biology*, 2 (9), pp.669-71.
- Yin, C., Blayney, L.M. & Lai, F.A. (2005a) Physical Coupling between Ryanodine Receptor–Calcium Release Channels. *Journal of Molecular Biology*, 349 (3), pp.538-546.
- Yin, C., D'Cruz, L.G. & Lai, F.A. (2008) Ryanodine receptor arrays: not just a pretty pattern? *Trends in Cell Biology*, 18 (4), pp.149-56.
- Yin, C., Han, H., Wei, R. & Lai, F.A. (2005b) Two-dimensional crystallization of the ryanodine receptor  $Ca^{2+}$  release channel on lipid membranes. *Journal of Structural Biology*, 149 (2), pp.219-224.
- Zandstra, P.W., Bauwens, C., Yin, T., Liu, Q., Schiller, H., Zweigerdt, R., Pasumarthi, K.B.S. & Field, L.J. (2003) Scalable production of embryonic stem cell-derived cardiomyocytes. *Tissue Engineering*, 9 (4), pp.767-78.
- Zhang, J., Liu, Z., Masumiya, H., Wang, R., Jiang, D., Li, F., Wagenknecht, T. & Chen, S.R.W. (2003a) Three-dimensional localization of divergent region 3 of the ryanodine receptor to the clamp-shaped structures adjacent to the FKBP binding sites. *The Journal of Biological Chemistry*, 278 (16), pp.14211-8.
- Zhang, L., Kelley, J., Schmeisser, G., Kobayashi, Y.M. & Jones, L.R. (1997) Complex formation between junctin, triadin, calsequestrin, and the ryanodine receptor. Proteins of the cardiac junctional sarcoplasmic reticulum membrane. *The Journal of Biological Chemistry*, 272 (37), pp.23389-97.
- Zhang, T., Maier, L.S., Dalton, N.D., Miyamoto, S., Ross, J., Bers, D.M. & Brown, J.H. (2003b) The deltaC isoform of CaMKII is activated in cardiac hypertrophy and induces dilated cardiomyopathy and heart failure. *Circulation Research*, 92 (8), pp.912-9.
- Zhang, Y. & Yu, L. (2008) Single-cell microinjection technology in cell biology. *BioEssays: News and Reviews in Molecular, Cellular and Developmental Biology*, 30 (6), pp.606-10.
- Zhao, K., Hurst, R., Slater, M. & Bulleit, R. (2007) Functional protein expression from a DNA based wheat germ cell-free system. *Journal of structural and functional genomics*, 8 (4), pp.199-208.
- Zhu, Y. & Nosek, T.M. (1991) Inositol trisphosphate enhances  $Ca^{2+}$  oscillations but not  $Ca^{2+}$ -induced  $Ca^{2+}$  release from cardiac sarcoplasmic reticulum. *Pflügers Archiv: European Journal of Physiology*, 418 (1-2), pp.1-6.
- Zissimopoulos, S. & Lai, F.A. (2006) Redox regulation of the ryanodine receptor/calcium release channel. *Biochemical Society Transactions*, 34 (Pt 5), pp.919-21.
- Zissimopoulos, S. & Lai, F.A. (2005) Interaction of FKBP12.6 with the cardiac ryanodine receptor C-terminal domain. *The Journal of Biological Chemistry*, 280 (7), pp.5475-85.
- Zorzato, F., Fujii, J., Otsu, K., Phillips, M., Green, N.M., Lai, F.A., Meissner, G. &

MacLennan, D.H. (1990) Molecular cloning of cDNA encoding human and rabbit forms of the Ca<sup>2+</sup> release channel (ryanodine receptor) of skeletal muscle sarcoplasmic reticulum. *Journal of Biological Chemistry*, 265 (4), pp.2244-2256.



## ***Appendices***

---

**Appendix I – List of Primers**

All of the oligonucleotides used were designed to incorporate a 5' *Eco*RI and a 3' *Xho*I restriction site (underlined), and had a  $T_m$  of 58-60°C.

**Full length I-Domain (aa 3722-4610)**Forward – 5'-GGCCGAATTCTGAGCTTCTATACCAGCAAGCCCGA-3'Reverse – 5'-GGCTCGAGTTCCAATTTCCGTGCCACTTCCTTTTC-3'**ID<sup>A</sup> (aa 3722-4353)**Forward – 5'-GGCCGAATTCTGAGCTTCTATACCAGCAAGCCCGA-3'Reverse – 5'-CGGCTCGAGGGGTTTCTCTCTCCCTCCTC-3'**ID<sup>B</sup> (aa 4353-4499)**Forward – 5'-GGCCGAATTCTCCCCTGGAAGCCGCCCTGCCC-3'Reverse – 5'-CGGCTCGAGGTTGCGAGCAAATAGTTTAG-3'**ID<sup>C</sup> (aa 4353-4610)**Forward – 5'-GGCCGAATTCTCCCCTGGAAGCCGCCCTGCCC-3'Reverse – 5'-GGCTCGAGTTCCAATTTCCGTGCCACTTCCTTTTC-3'

**Appendix II – Bioinformatic analysis of RyR2 and IP3R I-domains**

	$\alpha$ -helix (%)	$\beta$ -turn (%)	Extended strand (%)	Coil (%)
<b>RyR2</b>				
ID	59.96	5.62	9.45	24.97
IDA	63.33	5.08	7.62	23.97
IDB	57.14	3.4	6.12	33.33
IDC	57.53	3.09	10.81	28.57
<b>IP3R-1</b>				
IDA-like	54.54	4.25	11.15	30.05
IDB-like	51.82	3.64	10.93	33.60
IDC-like	56.90	5.08	11.14	26.88
<b>IP3R-2</b>				
IDA-like	54.21	3.95	11.45	30.39
IDB-like	48.39	4.44	12.90	34.27
IDC-like	56.14	5.06	12.29	26.51

**Table ii. Predicted structural motifs in RyR2 I-Domains and the I-Domain-like regions in IP<sub>3</sub>R.**

Motifs were predicted using the SOPMA algorithm as described in Table i. The detailed organisation of these motifs within the RyR2 and IP<sub>3</sub>R is shown in Figure iii to v.

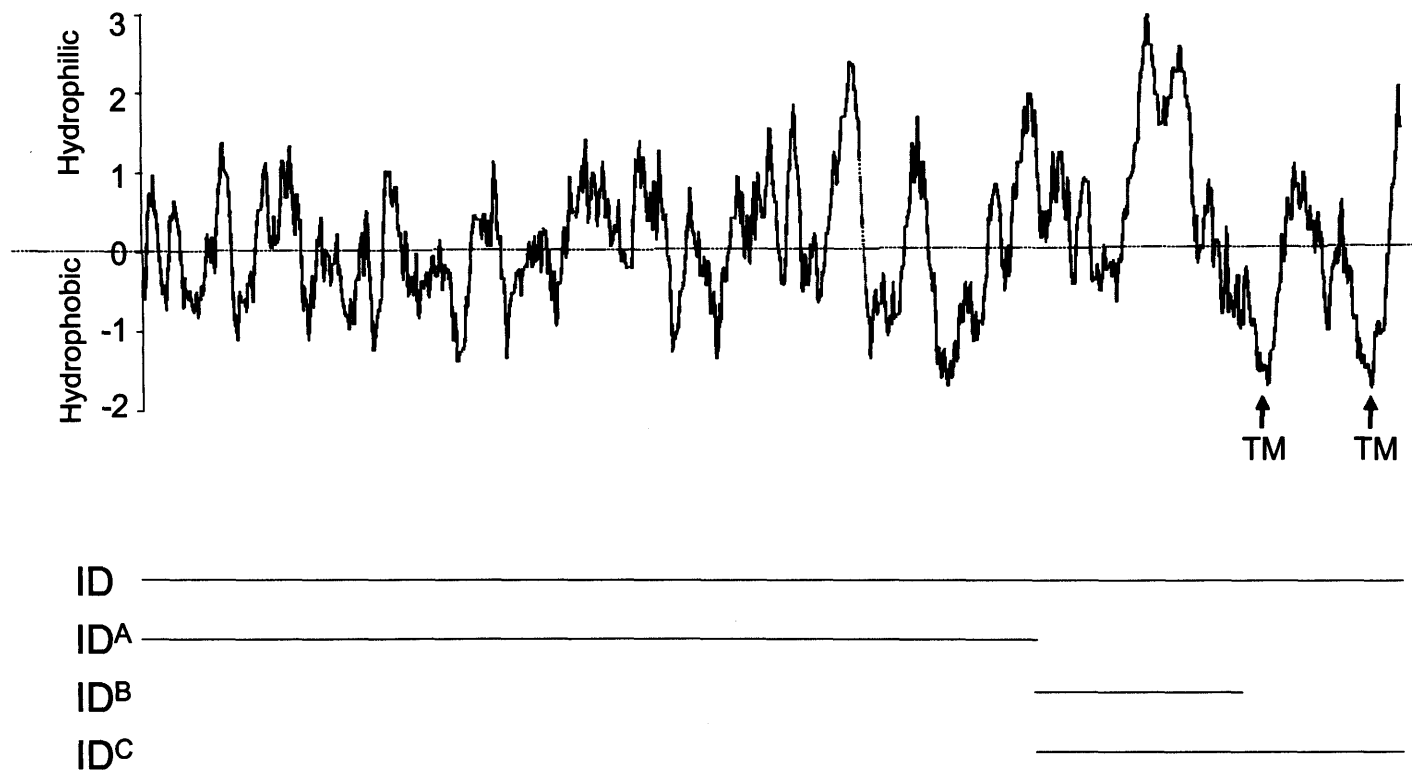


**Figure i. Hydropathy analysis of the human RyR2 I-Domain**

Hydropathy analysis of the human RyR2 I-domain (residues 3722-4610) was performed using the Hopp-Woods algorithm as described in Table i. The hydrophobic scale is given in Figure ii. Positive and negative ranges correspond to hydrophilic and hydrophobic residues, respectively. The two TM regions (arrowed) correspond to TM1 and 2 according to the model of Tunwell *et al.*

Using the scale Hphob. / Hopp & Woods, the individual values for the 20 amino acids are:

Ala:	-0.500
Arg:	3.000
Asn:	0.200
Asp:	3.000
Cys:	-1.000
Gln:	0.200
Glu:	3.000
Gly:	0.000
His:	-0.500
Ile:	-1.800
Leu:	-1.800
Lys:	3.000
Met:	-1.300
Phe:	-2.500
Pro:	0.000
Ser:	0.300
Thr:	-0.400
Trp:	-3.400
Tyr:	-2.300
Val:	-1.500

**Figure ii. Hydrophobicity scale**

H= alpha helix / T= beta turn / E= extended strand / C=coil

- Homology between RyR2 and IP<sub>3</sub>R-1 / IP<sub>3</sub>R-2
- Homology between RyR2 and IP<sub>3</sub>R-1
- Homology between RyR2 and IP<sub>3</sub>R-2

Figure iii- IDA-like region homology

